UNIVERSITAT POLITÈCNICA DE VALÈNCIA

ICITECH
CIENCIA Y TECNOLOGÍA DEL HORMIGÓN

Experimental assessment of the shear resistant behaviour of precast concrete beams with top cast-in-place concrete slab

Evaluación experimental del comportamiento resistente a cortante de vigas prefabricadas de hormigón con losa superior de hormigón in situ

DOCTORAL THESIS

Submitted to attain the degree of Doctor by the Universitat Politècnica de València

PRESENTED BY

LISBEL RUEDA GARCÍA

Thesis directors:

Dr. José Luis Bonet Senach

Dr. Pedro Fco. Miguel Sosa

Valencia, May 2022

Acknowledgements

After almost five years since I started my doctoral thesis, I look back and only remember how happy I have been at this period of my life. Maybe I only remember the good things because these last months of the thesis have been very beautiful, as you start to understand everything and see the results materialised in the form of journal articles and this doctoral thesis. Of course, there have been many hard moments when you do not understand anything and do not know how to go on, but those moments have been less bad thanks to the people who have accompanied me on this journey.

First of all, I must thank my thesis directors, José Luis Bonet and Pedro Miguel, for the opportunity they gave me and their support. José Luis, whom I have known for almost ten years, as he says, has long since ceased to be my tutor. Thank you for all the hours you spent helping me and listening to me. And thanks also to Pedro for all the time he has given me to get me unstuck in complicated moments of the thesis and for the support I have felt he was giving me.

Secondly, I would like to thank my laboratory technician and friend, Lino Martinez. We made the time in the lab as enjoyable as possible, with some bets in between, arguments, *almuerzos*, but above all a lot of laughs. Thanks also to my colleague Celia Traver for becoming a good friend and introducing me to the social life of ICITECH with such great people. Later the group grew to become "The Tranquis", whom I greatly appreciate. I also thank my colleague from the beginning Andrea Monserrat for listening to me and helping me in difficult moments. I'm sure I'm leaving out many people who have also helped me. To all of them thank you very much.

I would also like to say a big thank you to Jaime Mata and Walter Kaufmann for the opportunity they gave me to stay at ETH Zurich in pandemic times. Despite having the most disastrous of starts, the adventure ended beautifully, and I take with me great memories and great colleagues who know I will be back for recording the next video.

And last but not least, I would like to thank my family, my boyfriend and my friends for their support, especially my sister Ada. But this thanks goes mainly to my parents, Antonio and Amparo, who have taken every step in the last 30 years to make my life the best possible and I owe everything to them. I love you.

In addition, the present doctoral thesis would not have been possible without the financial support of the *Ministerio de Ciencia e Innovación* (MCIN) and the *Agencia Estatal de Investigación* (AEI) through Grants BIA2015-64672-C4-4-R and RTI2018-099091-B-C21-AR, both funded by MCIN/AEI/10.13039/501100011033 and by the "ERDF A way of making Europe". I am thankful as well for their support through Grant BES-2016-078010 funded by MCIN/AEI/10.13039/501100011033 and by the "ESF Investing in your future". The project was also supported by the Regional Government of Valencia through Project AICO/2018/250. And finally, thanks to the Concrete Science and Technology University Institute (ICITECH) of the Universitat Politècnica de València (UPV; Spain) in which this research project has been developed, and to our concrete supplier Caplansa.

Abstract

Construction with precast concrete elements is a booming sector due to the acceleration of the construction process, the saving of costs arising from the on-site construction and the quality and finish improvement, among others. Precast concrete beams are frequently used in the precast construction of civil engineering structures such as bridges and buildings. Construction with these beams requires the pouring of a cast-in-place concrete layer on top of the beams after their placement, which works as a unifying element to ensure structural integrity. Structural elements obtained in this way are known as concrete composite beams.

In composite beams, some aspects such as the shear strength of the interface between concretes have been studied in multiple publications. However, their shear behaviour has not yet been analysed in depth. Consequently, there is very little information, both in the existing literature and in current design codes, about the shear strength of these elements, how the presence of an interface between the concretes influences the shear strength or how the cast-in-place concrete slab contributes to the shear strength.

The aim of this doctoral thesis is to study the shear strength of concrete composite beams. For this purpose, an extensive experimental programme is developed, consisting of monolithic and composite beams with and without transverse reinforcement, with rectangular or T-shaped cross-section and with concretes of different qualities in the precast beam and in the slab. A total of 69 reinforced concrete beams are tested under shear forces in order to analyse the different variables of interest in shear strength.

Based on the experimental results, a mechanical model for predicting the shear strength of concrete composite beams with rectangular and T-shaped cross-section is proposed, which is also applicable to monolithic T-beams.

In addition, to support the experimental study and the mechanical model, some specimens of the experimental programme are numerically modelled.

All in all, the aim is to improve the current state of knowledge in this field by providing a large number of experimental results and analysing the design parameters, as well as to lay the foundations for the development of a formulation for the design of existing structures and the assessment of existing ones that is globally accepted by the scientific community.

Resumen

La construcción con elementos prefabricados de hormigón es un sector en alza por la aceleración del proceso constructivo, el ahorro de costes derivados de la obra *in situ* y la mejora de la calidad y acabados, entre otros. En la construcción prefabricada de estructuras de ingeniería civil como puentes y edificios es frecuente el empleo de vigas prefabricadas de hormigón. La construcción con estas vigas requiere el vertido de una capa de hormigón *in situ* sobre las mismas tras su emplazamiento, que sirve como elemento integrador para garantizar la unidad estructural. Los elementos estructurales que se obtienen de esta forma son conocidos como vigas compuestas de hormigón.

En vigas compuestas, aspectos como la resistencia a rasante de la interfaz entre hormigones han sido estudiados en numerosas publicaciones. No obstante, su comportamiento a cortante no ha sido, por el momento, analizado en profundidad. En consecuencia, existe muy poca información, tanto en la literatura existente como en los códigos de diseño actuales, acerca de la resistencia a cortante de estos elementos, de cómo influye la presencia de una interfaz entre los hormigones en la resistencia a cortante o de cómo contribuye la losa hormigonada *in situ* a dicha resistencia.

La presente tesis doctoral tiene como objetivo estudiar la resistencia a cortante de vigas compuestas de hormigón. Para ello, se desarrolla un extenso programa experimental compuesto por vigas monolíticas y compuestas con y sin armadura transversal, con sección transversal rectangular o en forma de T y con hormigones de diferentes calidades en la viga prefabricada y en la losa hormigonada *in situ*. Se ensaya a cortante un total de 69 vigas de hormigón armado con el fin de analizar las diferentes variables de interés en la resistencia a cortante.

A partir de los resultados experimentales, se propone un modelo mecánico de predicción de la resistencia a cortante de vigas compuestas de hormigón con sección transversal rectangular y en forma de T, que también es de aplicación a vigas monolíticas en T.

Además, como apoyo al estudio experimental y al modelo mecánico, se modelan numéricamente algunos especímenes del programa experimental.

Con todo ello, se busca incrementar el estado actual del conocimiento en este campo, mediante el aporte de un gran número de resultados experimentales y el análisis de los parámetros de diseño, así como sentar las bases para el desarrollo de una formulación de diseño de estructuras compuestas y de evaluación de las ya existentes globalmente aceptada por la comunidad científica.

Resum

La construcció amb elements prefabricats de formigó és un sector en alça per l'acceleració del procés constructiu, l'estalvi de costos derivats de l'obra *in situ* i la millora de la qualitat i acabats, entre altres. En la construcció prefabricada d'estructures d'enginyeria civil com a ponts i edificis és freqüent l'ús de bigues prefabricades de formigó. La construcció amb aquestes bigues requereix l'abocament d'una capa de formigó in situ sobre les bigues després del seu emplaçament, que serveix com a element integrador per a garantir la unitat estructural. Els elements estructurals que s'obtenen d'aquesta forma són coneguts com a bigues compostes de formigó.

En bigues compostes, aspectes com la resistència a rasant de la interfície entre formigons han sigut estudiats en nombroses publicacions. No obstant això, el seu comportament a tallant no ha sigut, de moment, analitzat en profunditat. En conseqüència, existeix molt poca informació, tant en la literatura existent com en els codis de disseny actuals, sobre la resistència a tallant d'aquests elements, de com influeix la presència d'una interfície entre els formigons en la resistència a tallant o de com contribueix la llosa formigonada *in situ* a aquesta resistència.

La present tesi doctoral té com a objectiu estudiar la resistència a tallant de bigues compostes de formigó. Per a això, es desenvolupa un extens programa experimental compost per bigues monolítiques i compostes amb armadura transversal i sense, amb secció transversal rectangular o en forma de T i amb formigons de diferents qualitats en la biga prefabricada i en la llosa formigonada *in situ*. S'assaja a tallant un total de 69 bigues de formigó armat amb la finalitat d'analitzar les diferents variables d'interés en la resistència a tallant.

A partir dels resultats experimentals, es proposa un model mecànic de predicció de la resistència a tallant de bigues compostes de formigó amb secció transversal rectangular i en forma de T, que també és aplicable a bigues monolítiques en T.

A més, com a suport a l'estudi experimental i al model mecànic, es modelen numèricament alguns espècimens del programa experimental.

Amb tot això, es pretén incrementar l'estat actual del coneixement en aquest camp, mitjançant l'aportació d'un gran nombre de resultats experimentals i l'anàlisi dels paràmetres de disseny, així com establir les bases per al desenvolupament d'una formulació de disseny d'estructures compostes i d'avaluació de les ja existents globalment acceptada per la comunitat científica.

Thesis structure

This doctoral thesis is presented as a compilation of six published articles and two articles ready for their future publication. The thesis is divided into eight chapters in which those articles are included. The references of the articles, in order of appearance, are:

- 1st paper: Rueda-García L, Bonet Senach JL, Miguel Sosa PF. Experimental study of concrete composite beams subjected to shear. Proceedings of the fib Symposium 2019: Concrete - Innovations in Materials, Design and Structures, 2019, p. 1779–86.
- 2nd paper: Rueda-García L, Bonet Senach JL, Miguel Sosa PF. Influence of interface roughness and shear reinforcement ratio in vertical shear strength of composite reinforced concrete beams. Hormigón y Acero 2022; 72.
- 3rd paper: Rueda-García L, Bonet Senach JL, Miguel Sosa PF, Fernández Prada MÁ. Experimental analysis of the shear strength of composite concrete beams without web reinforcement. Engineering Structures 2021;229:111664. https://doi.org/10.1016/j.engstruct.2020.111664.
- 4th paper: Rueda-García L, Bonet JL, Miguel Sosa PF, Fernández Prada MÁ. Safety assessment of shear strength current formulations for composite concrete beams without web reinforcement. In: Fédération Internationale du Béton (fib), editor. Proceedings for the 2021 fib Symposium. Concrete Structures: New Trends for Eco-Efficiency and Performance, Lisbon: 2021, p. 2305–14.
- 5th paper: Rueda-García L, Bonet Senach JL, Miguel Sosa PF, Fernández Prada MÁ. Analysis of the shear strength mechanism of slender precast concrete

beams with cast-in-place slab and web reinforcement. Engineering Structures 2021;246:113043. https://doi.org/10.1016/j.engstruct.2021.113043.

- 6th paper: Rueda-García L, Bonet Senach JL, Miguel Sosa PF, Fernández Prada MÁ. Experimental study on the shear strength of reinforced concrete composite T-shaped beams with web reinforcement. Engineering Structures 2022;255:113921. https://doi.org/10.1016/j.engstruct.2022.113921.
- 7th paper: Rueda-García L, Bonet Senach JL, Miguel Sosa PF, Fernández Prada MÁ. Experimental analysis of the shear resistance of precast concrete T-beams with a top cast-in-place slab. 2022. (Ready for submission to a scientific journal).
- 8th paper: Rueda-García L, Bonet Senach JL, Miguel Sosa PF, Fernández Prada MÁ. Shear strength prediction of slender reinforced concrete composite beams and monolithic T- and I-shaped beams with web reinforcement. 2022. (Ready for submission to a scientific journal).

Table of contents

Chapter 1. Introduction

This chapter describes the problem that gives rise to this thesis. The objective and scope of the thesis are also specified. Besides, it explains the structure of the document, where the content of each chapter of the thesis is defined.

1. Problem statement

Concrete bridges, which are key elements of transportation infrastructures, must carry increasing loads whilst suffering deterioration along their service life. In Spain, there are more than 27,000 concrete bridges just on the National Road Network, for which, according to PIARC [1], the Spanish government allocates an annual maintenance budget of approximately €30 million, which means an average maintenance cost of approximately €1,000 per bridge. Besides, around 60% of the Spanish bridges are more than 40 years old [1]. It is therefore expected that many of the existing bridges will need to be structurally assessed in the short to medium term.

On the other hand, the current codes are oriented towards the design of new structures and therefore, in some respects, subordinate accuracy to ease of use and, in addition, adopt partial safety factors that are not appropriate for existing structures. As a result, many bridges currently in service could theoretically become obsolete if assessed with the design codes, and their replacement would entail exorbitant costs. In the last decade, some countries, such as Canada, USA, UK, Denmark and Switzerland, have developed codes to evaluate existing bridges that have allowed bridges to be kept in service that do not meet current design requirements, but have proven their capacity to safely resist applied loads [2]. In this same direction, the articles of the future Eurocode 2, part 1-1 [3], will consider the evaluation of existent structures, and will include an annexe in which this subject will be presented in depth.

In this context, the project HORVITAL was born, in which this doctoral thesis is included through subproject BIA2015-64672-C4-4-R. The main objective of this project was to contribute to the development of a suitable methodology for the structural assessment and reinforcement of bridge decks and other concrete structures, by focusing on the rigorous calculation of their resistance to tangential forces, which is still little-known.

A very common deck typology of the bridges built since the mid-20th century consists of precast beams with cast-in-place slab on top, namely concrete composite beams. Given the vast number of existing bridges of this typology, studying their structural behaviour is especially important. Moreover, there is currently a clear trend towards precast construction with reinforced concrete elements, so that this type of construction is not only observed in bridges but also in many other structures such as beam-and-block floors, rib-and-slab floors with precast reinforced concrete beams or connections of precast floor slabs (e.g., hollow-core slabs) supported by precast beams, where the free space is filled with cast-in-place concrete [4,5]. Some examples are shown in Fig. 1.

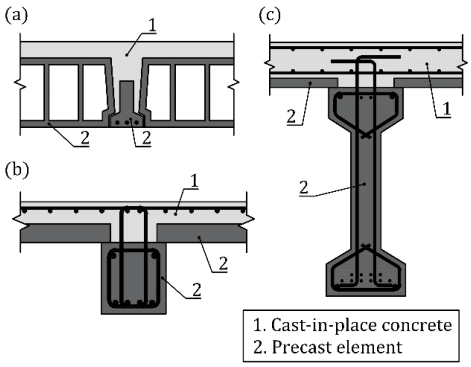

Fig. 1. Examples of concrete composite beams in precast construction: (a) beam-and-block floor; (b) connection of precast beam and hollow-core slab filled with cast-in-place concrete; (c) precast bridge girder with cast-in-place slab.

While interface shear strength has been widely studied in concrete composite beams [6–11], their vertical shear strength has not been analysed in depth [12]. In the literature, there are experimental analyses of full-scale composite specimens with web reinforcement [13–21], but they do not analyse either the contribution of the slab to shear strength or the influence of the interface between concretes on shear strength. Very few publications have studied those issues, the most important being those by Halicka *et al.* [4,22,23] and Kim *et al.* [12,24]. In fact, Halicka [22], who performed an experimental study on the influence of interface quality on concrete composite beams' shear strength, points out there are few research works regarding the influence of the interface cracking on the composite element's shear resistance. Kim *et al.* [12,24] ran an experimental programme about the shear strength of rectangular composite beams. Their study focused mainly on analysing the existence of different quality concretes (high-strength and low-strength concrete) at the beam and slab. However, the interface between concretes did not influence the specimens' behaviour, which behaved similarly to monolithic specimens. Their study, therefore, did not analyse how the existence of an interface influences shear strength.

Current codes (like EC2 [25] and MC-10 [26]) do not clarify how to account for the slab in the shear strength of composite elements. Only ACI 318-19 [27] specifies how composite specimens' shear strength can be calculated: using the properties of the element (precast beam or cast-in-place slab) that result in the most critical shear strength value or the properties of individual elements. Nevertheless, relevant experimental and theoretical evidence are still needed to support the validity of these considerations for composite specimens [12,24].

The gap in the knowledge of concrete composite structures shown above motivates the present research, since there is a limited number of experimental tests that

analyse the influence of the interface between concretes on shear strength and none that study the contribution of the slab to shear strength. In addition, current design codes have little information on the structural calculation of the shear strength of concrete composite elements.

2. Objective and scope

The objective of this doctoral thesis is to experimentally analyse the vertical shear behaviour of concrete composite beams. The purpose is to know how bridge girders with cast-in-place slab on top behave when they are subjected to shear forces. To this aim, the analysis process starts with simpler composite elements, such as elements without web reinforcement, and from there on, additional variables are included in the problem.

The scope of this thesis covers specimens that show a structural failure influenced by the existence of an interface between concretes. A pure horizontal shear failure, as well as a monolithic behaviour of the beams, are not included in the project scope. These two failure modes are avoided as they have already been much more studied in the existing literature.

As a result of the experimental study, the development of a predictive model of the shear strength based on a mechanical model is sought. The numerical modelling is used to support the above studies.

All in all, the aim is to improve the current state of knowledge in this field and to lay the foundations for a mechanical model for calculating the shear strength of composite elements that is accepted by the scientific community.

3. Structure of the document

This doctoral thesis is presented as a compilation of articles. The thesis is divided into eight chapters in which those articles are included following the structure described below.

In Chapter 1, the problem statement, the objective and scope of the thesis and the content of the document are described.

Chapter 2 shows the preliminary experimental programme for the characterisation of the interface between concretes. This chapter consists of two conference papers that describe the state of the art, the experimental tests, their analysis and conclusions.

In Chapter 3, the experimental study on the shear strength of concrete composite beams without web reinforcement is explained. Two papers describe this study. First, a journal article shows the experimental programme and its results and analysis. Second, a conference paper goes deeply in the safety analysis of the shear strength current formulations for beams without web reinforcement.

Chapter 4 shows the biggest part of the experimental programme, which is the experimental study on the shear strength of concrete composite beams with web reinforcement. This experimental programme is described by means of three journal articles. The first article details the results obtained from the study of composite rectangular specimens. The second one describes the results for composite T-shaped specimens. The third one shows the research carried out on T-beams with cast-in-place slab.

Chapter 5 describes the proposed mechanical model for the shear strength prediction of composite beams with web reinforcement. The content of this chapter is also explained through a journal article.

In Chapter 6 the numerical model developed for the specimens of this experimental programme with the software IDEA StatiCa Detail during a stay abroad at ETH Zurich (Switzerland) of the doctoral student is described.

In Chapter 7 a general discussion of the results is presented, in which the most relevant information from the previous chapters and the main findings are described and analysed from a critical point of view.

Finally, in Chapter 8 the main conclusions of the doctoral thesis are listed and some recommendations for future research are given.

4. References

[1] PIARC. World Road Association 2021. http://www.piarc.org.

[2] Wiśniewski DF, Casas JR, Ghosn M. Codes for safety assessment of existing bridges-current state and further development. Struct Eng Int J Int Assoc Bridg Struct Eng 2012;22:552–61. https://doi.org/10.2749/101686612X13363929517857.

[3] CEN. prEN 1992-1-1-D7:2020 Eurocode 2: Design of Concrete Structures – Part 1-1: General rules – Rules for buildings, bridges and civil engineering structures. 2020.

[4] Halicka A, Jabłoński Ł. Shear failure mechanism of composite concrete T-shaped beams. Proc Inst Civ Eng Struct Build 2016;169:67–75.

[5] Ribas González CR, Fernández Ruiz M. Influence of flanges on the shear-carrying capacity of reinforced concrete beams without web reinforcement. Struct Concr 2017. https://doi.org/10.1002/suco.201600172.

[6] Loov RE, Patnaik AK. Horizontal Shear Strength of Composite Concrete Beams With a Rough Interface. PCI J 1994;39:48–69.

[7] Saemann JC, Washa GW. Horizontal Shear Connections between Precast Beams and Cast-in-Place Slabs. ACI J Proc 1964;61:1383–409.

[8] Kahn LF, Slapkus A. Interface Shear in High Strength Composite T-Beams. PCI J 2004;49:102–10.

[9] Kovach J, Naito C. Horizontal Shear Capacity of Composite Concrete Beams without Interface Ties. ATLSS Report No. 05-09: 2008.

[10] Tan KH, Guan LW, Lu X, Lim TY. Horizontal shear strength of indirectly loaded composite concrete beams. ACI Struct J 1999;96:533–8.

[11] Fang Z, Jiang H, Liu A, Feng J, Chen Y. Horizontal Shear Behaviors of Normal Weight and Lightweight Concrete Composite T-Beams. Int J Concr Struct Mater 2018;12. https://doi.org/10.1186/s40069-018-0274-3.

[12] Kim C-G, Park H-G, Hong G-H, Kang S-M. Shear strength of composite beams with dual concrete strengths. ACI Struct J 2016;113:263–74.

[13] Hartmann DL, Breen JE, Kreger ME. Shear capacity of high strength prestressed concrete girders. Austin: 1988.

[14] Shahawy MA, Batchelor B deV. Shear Behavior of Full-Scale Prestressed Concrete Girders: Comparison Between AASHTO Specifications and LRFD Code. PCI J 1996;41:48–62. https://doi.org/10.15554/pcij.05011996.48.62.

[15] Ross BE, Ansley MH, Hamilton III HR. Load testing of 30-year-old AASHTO Type III highway bridge girders. PCI J 2011;56.

[16] Hamilton III HR, Llanos G, Ross BE. Shear performance of existing prestressed concrete bridge girders. 2009.

[17] Runzell B, Shield C, French C. Shear Capacity of Prestressed Concrete Beams. 2007.

[18] Cumming, A David., Shield, Carol K., French CE. Shear Capacity of High-Strength Concrete Pre-stressed Girders. 1998.

[19] Hawkins NM, Kuchma DA. Application of LRFD Bridge Design Specifications to High- Strength Structural Concrete: Shear Provisions. 2007.

[20] Avendaño AR, Bayrak O. Shear strength and behaviour of prestressed concrete beams. Technical Report: IAC-88-5DD1A003-3, Texas Department of Transportation: 2008.

[21] Ruiz MF, Muttoni A. Shear strength of thin-webbed post tensioned beams. ACI Struct J 2009;106.

[22] Halicka A. Influence new-to-old concrete interface qualities on the behaviour of support zones of composite concrete beams. Constr Build Mater 2011:4072–8.

[23] Jabłoński Ł, Halicka A. Influence of the interface reinforcement on static performance of concrete composite T-shaped beams. Bud i Archit 2020;19:063–76. https://doi.org/10.35784/bud-arch.2170.

[24] Kim C-G, Park H-G, Hong G-H, Kang S-M, Lee H. Shear Strength of Concrete Composite Beams with Shear Reinforcements. ACI Struct J 2017;114:827–37.

[25] CEN. EN 1992-1-1:2004. Eurocode 2: Design of concrete structures - Part 1-1: General rules and rules for buildings. 2004.

[26] Fédération International du Béton (fib). Model Code 2010. Ernst & Sohn; 2012.

[27] ACI Committee 318. Building code requirements for structural concrete (ACI 318-19); and commentary (ACI 318R-19). Farmington Hills: American Concrete Institute; 2019.

Chapter 2. Characterisation of the interface between concretes

A preliminary experimental programme for the characterisation of the interface between concretes in composite specimens with and without shear reinforcement was found necessary to define the appropriate interface roughness and ratio of reinforcement crossing the interface for the rest of the composite specimens of the thesis.

This characterisation tests are described in this chapter by means of two conference papers. The first paper describes the experimental tests carried out in four specimens with web reinforcement, their analysis, and conclusions. The second paper includes the three specimens tested without web reinforcement and gives a more detailed analysis of the seven specimens.

1st PAPER

Details:

Type of paper	Conference paper
Title	*Experimental study of concrete composite beams subjected to shear*
Authors	Lisbel Rueda García José Luis Bonet Senach Pedro Francisco Miguel Sosa
Congress	*fib* Symposium 2019: Concrete - Innovations in Materials, Design and Structures
Date	27th-29th May, 2019
City	Krakow (Poland)
Status	Accepted and presented
Full reference	Rueda-García L, Bonet Senach JL, Miguel Sosa PF. Experimental study of concrete composite beams subjected to shear. Proceedings of the fib Symposium 2019: Concrete - Innovations in Materials, Design and Structures, 2019, p. 1779–86.

Experimental study of concrete composite beams subjected to shear

Lisbel Rueda García[1], José Luis Bonet Senach[1] and Pedro Francisco Miguel Sosa[1]

[1]Concrete Science and Technology University Institute ICITECH, Universitat Politècnica de València, Valencia, Spain

Abstract

The present study tested the shear strengths of four reinforced concrete composite beams, simply supported and with two point loads. Each beam had a different treatment of the interface between the two concretes casted at different times in order to resist the horizontal shear at the interfaces: smooth surface or very rough surface, with or without additional shear connectors. Some parameters were fixed, such as the length and geometry of cross sections, longitudinal reinforcement ratios, shear reinforcement ratios and shear span-depth ratios of specimens. The nominal compressive strength of concretes (30 MPa) was the same for the two concretes used in the composite beams and for all the specimens. The aim of these tests was to analyse the influence of horizontal shear on the behaviour of reinforced concrete composite beams subjected to vertical shear stresses. This communication shows the results of these tests, in particular: the horizontal shear stresses and loads and shear forces reached during the tests, comparing them with those calculated according to design codes *fib* MC, EC2 and ACI 318. While horizontal shear failure was expected in three of the beams, they all failed due to vertical shear, which was also theoretically underestimated. It was observed that an interface existing between two concretes casted at different times influences the shear strength mechanism developed by the structural element and, therefore, the reached strength.

Keywords: reinforced concrete, composite beam, horizontal shear, shear strength, interface roughness.

1. Introduction

In the last decade, some countries (Canada, USA, UK, Denmark and Switzerland) have developed codes to evaluate existent bridges that have allowed to keep in service bridges that do not meet current design requirements, but have proven their capacity to safely resist applied loads. In this same direction, the articles of the future Eurocode 2, part 1-1, will consider the evaluation of existent structures, and will include an annexe in which this subject will be presented in depth. Particularly in Spain, only the State's road network has 33,000 bridges, of which 44% are made of reinforced concrete and 20% of prestressed concrete [1]. Many of these concrete

bridges have a very common typology of a deck constructed since the mid-20th century, consisting in precast beams with an *in situ* slab on top, namely composite concrete beams. Given the vast number of existent bridges of this typology, studying their structural behaviour is especially important.

Among the diverse aspects associated with a proper structural evaluation of existent bridges, the determination of its resistance to tangential solicitations is an essential aspect that is yet to be adequately solved. In fact codes *fib* Model Code (2010) [2], EN 1992 Eurocode 2 (2004) [3] and ACI 318 (2014) [4] provide semi-empirical expressions to evaluate the shear strength of beams that are conservative and excessively scattered (Reineck et al. (2014) [5] and Moore et al. (2015) [6]). Furthermore, no agreement has been reached on structural shear design by the different codes. This situation reflects the absence of an accepted universal formulation for analysing shear or a physical model that explains the real shear phenomenon.

In the design of precast beams decks with an *in situ* slab, it is common to omit the contribution of the slab to shear strength by staying on the safety side. This seems reasonable as shear strength is a phenomenon that still has many unknowns. However, that contribution does exist and it could be relevant when evaluating the strength of existent precast beams decks with an *in situ* slab. Only ACI 318-14 (Section 22.5.4.1) considers the strength evaluation of composite beams. Nonetheless, its accuracy is not clear as the current design equation was developed in line with monolithic beams test results (Kim et al. 2016 [7]).

The strength of composite beams made of two concretes and subjected to vertical shear forces has not been studied in-depth. Most studies that bring up experimental programmes to analyse composite beams focus on the horizontal shear strength of the interface between the two concretes, instead of on the evaluation of vertical shear strength. This is due to the critical importance of the adherence between concretes for the appropriate behaviour of composite beams. Of all these studies, we find Saemann & Washa (1964) [8], Loov & Patnaik (1994) [9] and Kahn & Slapkus (2004) [10], who analyse the effect of interface roughness, the shear span-depth ratio and shear reinforcement.

Recently, Kim et al. (2016 and 2017) [7,11] developed an experimental programme of composite beams made of conventional concrete and high-strength concrete, in beams with or without shear reinforcement, with rectangular cross sections, and subjected to tangential forces. They pointed out that the total number of experimental tests carried out to analyse the shear strength of composite beams is still insufficient. Hence, the development of new strength evaluation models for composite beams subjected to shear is limited.

Recent research works have noticed that the inclination and shape of critical shear cracks are modified by the existence of an interface between two concretes (Halicka & Jablonski (2016) [12] and Kim et al. (2016 and 2017)) [7,11]. Both the shape of the critical crack and its possible variable inclination condition the composite beam's strength because a more inclined crack involves more stirrups.

The present experimental programme intends to study the shear behaviour of reinforced concrete composite beams made of two concretes of different ages, with distinct interface roughness and different shear reinforcement ratios. Moreover, the shear strength mechanism developed in the tested beams is analysed, as is the validity of current design methods.

2. Test programme

2.1. Test specimens design

This series of experimental tests was designed to analyse the following two parameters that influence the shear strength of composite reinforced concrete beams: the roughness of the interface between the two concretes of different ages and the shear reinforcement ratio of the interface. Four four-point bending tests were run on reinforced concrete beams with a rectangular cross section made of two concretes of similar compression strength.

The fixed parameters in this series were: longitudinal reinforcement ratio (ρ_l = 4.08%); vertical shear reinforcement ratio (ρ_w = 0.223%); the shear span-depth ratio (a/d = 4.0); cross section geometry; nominal compression strength of the used concretes (f_c = 30 MPa). Furthermore, in order to avoid the influence of differential shrinkage and other long-term phenomena, the time between pouring the concrete of beams and that of slabs was reduced.

Four beams of 2.74 m length between supports were tested (3.44 m total length), in which two-point non-centred vertical loading was applied, with a distance of 0.40 m between loads, to obtain a 1.34-metre span in which failure was expected, plus another span of 1.00 m. The 1.00-metre span was reinforced to avoid its shear failure (Fig. 1). The depth of beams and length were adjusted to obtain the fixed shear span-depth ratio (a/d) of 4.0 in order to study a shear failure not affected by the arch effect (Kani et al. 1979 [13]).

Beams had two layers of concretes of different ages. The first layer, 0.30 m high, represented the precast beam of the composite beam. The second layer, 0.10 m high, was cast on the previous one and represented the *in situ* concrete slab.

The beams' longitudinal reinforcement was chosen to avoid the bending failure of beams. Shear reinforcement was calculated according to codes *fib* MC, EC2 and ACI

318. Specimens S1 and S2 had the same shear reinforcement ratio crossing the interface between concretes (Ø8 stirrups @250 mm), which was the code-based maximum spacing requirement for vertical shear reinforcement. Specimens S3 and S4 had additional connectors for resisting a higher horizontal shear (Ø8 stirrups @250 mm + Ø8 connectors @250 mm). These connectors had their corresponding anchor length. Connectors were not completely closed (Fig. 1) to avoid them to behave the same as a common shear stirrup.

Beams S1 and S3 had the same roughness of the interface between concretes: smooth (also known as "as cast"), commonly used in the construction of precast reinforced concrete beams with *in situ* concrete slabs. Beams S2 and S4 had a very rough interface to study the behaviour of composite beams subjected to tangential forces when the adherence between concretes is improved. Table 1 summarises the main characteristics of the specimens.

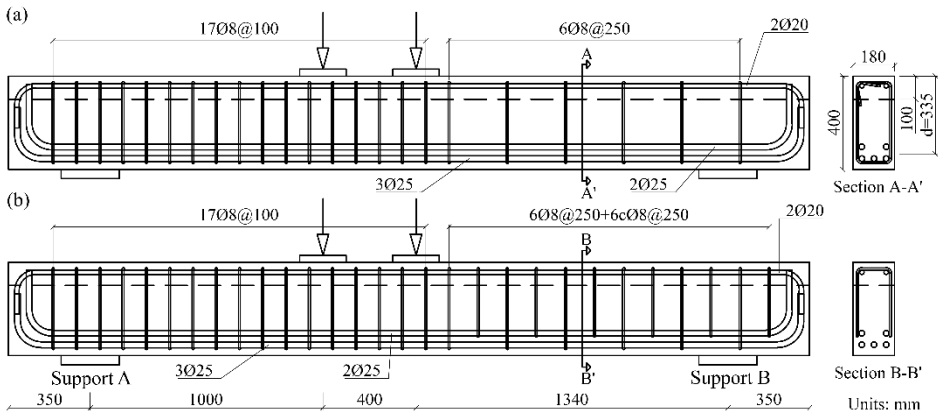

Fig. 1. Geometry and reinforcement of the specimens: (a) Specimens S1 and S2; (b) Specimens S3 and S4.

Table 1. Characteristics of the specimens.

Specimen	Surface	Vertical shear reinforcement	Horizontal shear connectors
S1	As cast	Ø8@250	-
S2	Very rough	Ø8@250	-
S3	As cast	Ø8@250	Ø8@250
S4	Very rough	Ø8@250	Ø8@250

2.2. Test setup and instrumentation

Beams were laid on two supports equipped with a steel balls bed each to eliminate the horizontal reaction. A steel beam was designed to divide the load of the actuator into two point loads. It was connected to a joint to keep load vertical all the time.

Three load cells were used to measure the actuator load and reactions at the supports. Vertical displacement transducers (LVDTs) were placed at the supports and below the central point load to measure vertical displacements. LVDTs were also placed on two cross sections to measure the opening of beams due to web cracks, interface cracks or cracks in the slab. Four horizontal LVDTs were placed at the interface to measure the slip between the two concrete layers. Strain gauges in tension longitudinal reinforcement were placed to know the strain of this reinforcement in five different beam sections and to check if it yielded due to bending. Strain gauges were also placed on the connectors and stirrups. Four pairs of strain gauges were placed on the concrete slab, on the same cross sections as the gauges of longitudinal reinforcement. Three cameras took pictures every 2 seconds. All this instrumentation was placed at the 1.34-metre long span.

2.3. Fabrication of specimens and material properties

The slab's concrete was poured 24 h after the beam's concrete to avoid differential shrinkage. In the 1.34-metre span of specimens S2 and S4, the interface was roughened before concrete hardened to obtain a very rough interface with dents of approximately 6-10 mm deep (from peak to valley) and a maximum spacing of 40 mm between peaks. In the reinforced spans of the four beams (the 1.00-metre long span), the interface roughness was smooth or as cast. Concrete was cured for 7 days before moving away the formworks.

Beams were tested approximately 40 days after being fabricated. The day the tests were done, the average nominal strengths of the concretes for beams S1 and S2 were 32.9 MPa for the beam's concrete and 31.9 MPa for the slab's concrete; and for beams S3 and S4, 32.8 MPa for the beam's concrete and 31.1 MPa for the slab's concrete. Three different diameters of B500SD steel-reinforcing bars were used. The Ø8 mm rebars had a yield strength of f_y = 534 MPa and a Young's modulus of E_s = 189 GPa. The Ø20 mm rebars had f_y = 534 MPa and E_s = 206 GPa. The Ø25 mm rebars had f_y = 556 MPa and E_s = 197 GPa.

2.4. Predicted results by design codes

The predicted strengths of the specimens were calculated based on the specifications of codes *fib* MC, EC2 and ACI 318 at their different approximation levels. The results are shown in Table 2. The calculations were done with the actual properties of the materials used in the tests. As mentioned before, beams S3 and S4 had additional connectors to resist a higher horizontal shear force. However, it was not possible to know in advance the contribution of those connectors to the vertical shear strength. That was why two strength values were calculated for those beams. The first one was a lower bound for strength, which corresponded to not treating connectors as vertical shear reinforcement at all; the second one was an upper bound, which corresponded to treating connectors as vertical shear reinforcement.

Only EC2, when connectors contributed to shear strength (cases S3.B and S4.B), gave a higher shear strength than the beams' bending strength because this code allows the highest inclination of the compression field to be contemplated. Regarding horizontal shear strength, both stirrups and connectors were treated as shear reinforcement as they had enough anchor length.

According to the strength predictions in Table 2, horizontal shear failure was expected in at least three of the beams: S1, S2 and S3. That was why beam S4 was designed, with a higher predicted horizontal shear strength, in order to obtain vertical shear failure and to find the limit between horizontal shear failure and vertical shear failure.

Table 2. Predictions of horizontal and vertical shear strengths and test results.

Specimen	Ultimate load predictions										Actual ultimate loads
	Bending	Horizontal shear $F_{u,H}$			Vertical shear $F_{u,V}$						
		fib MC	EC2	ACI 318	*fib* MC			EC2	ACI 318		
	$F_{u,M}$ (kN)	$F_{u,H,MC}$ (kN)	$F_{u,H,EC2}$ (kN)	$F_{u,H,ACI}$ (kN)	Level I $F_{u,V,LI}$ (kN)	Level II $F_{u,V,LII}$ (kN)	Level III $F_{u,V,LIII}$ (kN)	$F_{u,V,EC2}$ (kN)	Approx 1 $F_{u,V,ACI1}$ (kN)	Approx 2 $F_{u,V,ACI2}$ (kN)	$F_{u,T}$ (kN)
S1	557	84	140	68	256	286	345	369	298	314	464
S2	557	169	207	311	256	286	345	369	298	314	408
S3.A(1)	559	167	229	68	256	286	345	369	298	314	581
S3.B(2)					-	471	505	736	462	478	
S4.A(1)	559	261	310	400	256	286	345	369	298	314	571
S4.B(2)					-	471	505	736	462	478	
S4.C(3)					-	460	481	628	424	443	

(1) Connectors not treated as vertical shear reinforcement in the vertical shear ultimate load calculation.
(2) Connectors treated as vertical shear reinforcement in the vertical shear ultimate load calculation.
(3) Vertical shear ultimate load calculated for 1.00-metre span, where failure took place.

3. Test results

3.1. Failure description

Despite the predictions, no beam failed due to horizontal shear. They all displayed vertical shear failure. The actual ultimate loads of the tests are shown in Table 2.

Specimen S1, with smooth roughness and stirrups at a spacing of 250 mm, reached an ultimate load of 464 kN. The first web diagonal cracks appeared at a load between 180 and 230 kN. As load increased, diagonal cracks were connected through a

horizontal crack, which appeared at the interface between concretes. Specimen failure was sudden and took place on the slab of the 1.34 m span.

Beam S2, with the same reinforcement as beam S1 and a very rough interface, reached an ultimate load of 408 kN. During the test, diagonal cracks at the web spread to the slab, and displayed an almost monolithic behaviour. Finally, the beam failed due to one of the cracks that appeared on the slab.

Beam S3, with a smooth interface, stirrups at a spacing of 250 mm and connectors at a spacing of 250 mm, displayed much more distributed diagonal cracking than the previous beams, and reached failure at a load of 581 kN. Failure occurred due to a crack spreading through the interface between concretes, which made the compression chord fail.

Specimen S4, with the same reinforcement as beam S3, but with a very rough interface, failed at a load of 571 kN. Nonetheless, this fail took place at the reinforced span (the 1.00-metre long span) instead of the span in which failure was expected, this being the 1.34-metre span. Cracking was similar to that of the other beams with a smooth interface (S1 and S3): the crack spread along the interface before compression slab failure took place. It should be noted that in the reinforced span, although the beams had greater reinforcement, the interface roughness was as cast.

Fig. 2 shows a photo of each beam's moment of failure and the reinforcement inside them. Note that the image belongs to the reinforced span for beam S4. In the photos, critical cracks are highlighted. As seen, the crack clearly spreads along the interface between concretes in beams S1, S3 and S4. The cracks cross the interface into the compression chord with a reduced crack inclination angle.

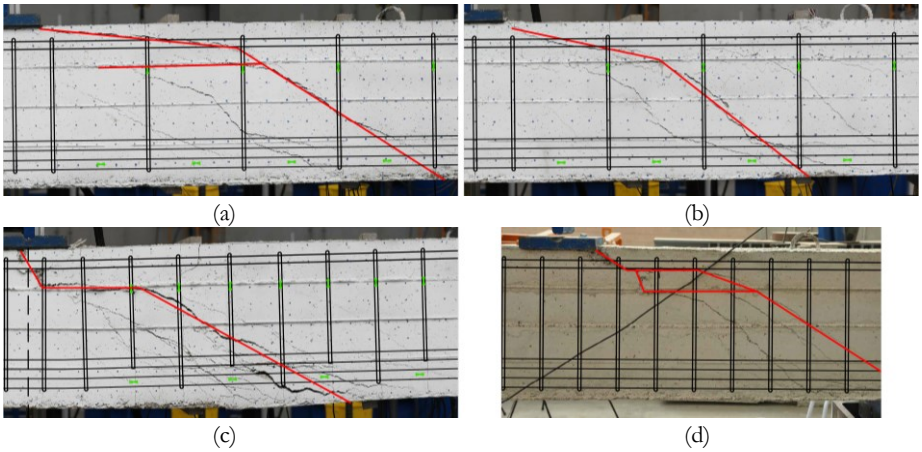

Fig. 2. Internal reinforcement on photos of the failure: (a) beam S1; (b) beam S2; (c) beam S3; (d) beam S4.

3.2. Experimental strength

Fig. 3 shows the relationship between vertical load and deflection below the central point load of the four tested beams (Fig. 3a). It also shows for each beam the strain of the strain gauges placed at the longitudinal reinforcement on the cross section of the central point load, which is the section of the highest bending moment (Fig. 3b).

Fig. 3.b shows that a yield strain was reached in beams S3 and S4, or came close to it, in tension longitudinal reinforcement (approx. 2.8‰). This approach to bending failure was due to the shear overstrength that beams reached compared to the predicted shear strengths. However, beams finally failed in shear.

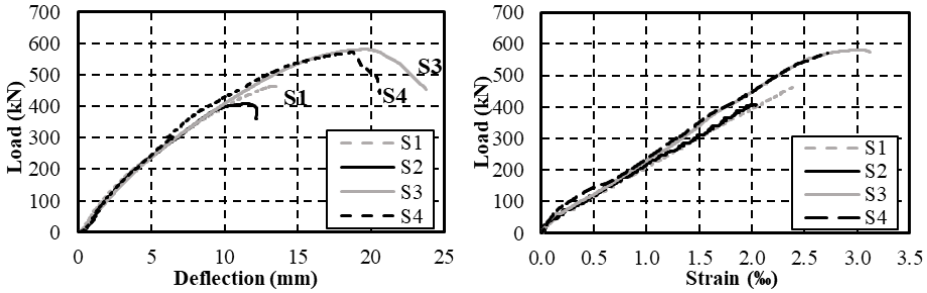

Fig. 3. Comparison between the instrumentation results of the four specimens at the central point load: (a) vertical load-deflection relationship; (b) vertical load-strain of the longitudinal reinforcement relationship.

The average horizontal shear stress of each beam is shown in Fig. 4, obtained from the results of the instrumentation placed on the 1.34-metre span. The global force equilibrium method was followed to calculate it. The strains plane was obtained on four cross sections of the beam at each test moment using the data of tension longitudinal reinforcement strain gauges and the two concrete strain gauges located on the slab. With the strains plane at the cross section, the stresses on that section were calculated. In this case, a Sargin's concrete constitutive curve was used, as described in EC2. By integrating stresses into the slab, compression force C can be obtained for all four instrumented sections. Horizontal shear stress τ_{Rd} at stretch i was calculated by dividing the difference of compression forces between two consecutive cross sections by distance x between both sections and width b of the beam (1). Despite this stress being theoretically constant along the span, in experimental terms some stretches had a higher horizontal shear stress than other stretches. In this case, showing the average value was considered appropriate, despite there being a higher value in some beam stretches.

$$\tau_{Rd,i} = \frac{C_i - C_{i-1}}{(x_i - x_{i-1}) \cdot b} \tag{1}$$

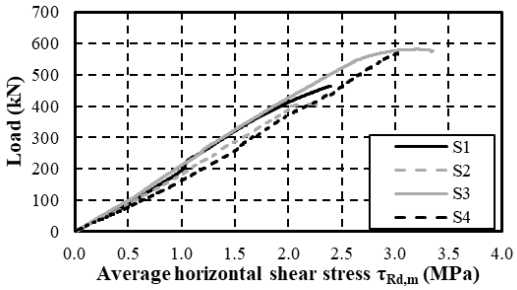

Fig. 4. Average horizontal shear reached in the four tested specimens.

4. Analysis of the test results

4.1. Interface roughness

In Table 3, the maximum experimental values of the average horizontal shear stress in the 1.34-metre spans are compared with the ultimate horizontal shear stresses predicted by the codes. Experimental horizontal shear stress is a safe estimation of the beams' horizontal shear strength as all the beams failed in vertical shear and none showed typical horizontal shear failure, in which a clear slip of the slab over the beam is observed.

In the beams with a smooth-roughness interface, Specimens S1 and S3, the horizontal shear stress reached at the interface was much higher than that predicted by the three codes, approximately 3-fold higher. In the beams with a very rough interface, Specimens S2 and S4, the predicted strengths came closer to the experimental values.

In view of the experimental results, codes safely estimate horizontal shear strength for the interface between concretes that is smooth or as cast. In the design phase, this could mean placing a higher connectors ratio than needed or, when evaluating existent structures, considering a structural element to be obsolete that actually has a higher strength than expected. However, it would be advisable to verify this observation by running more tests and to consider other influence factors, such as long-term effects.

Additionally, when comparing the failure modes of the beams with different interface roughness, the beams with a very rough interface displayed a similar behaviour to a monolithic beam: the diagonal cracks on the web crossed the interface and entered the compression chord without developing along the interface. However in the beams with smooth roughness, the crack developed along the interface (beams S1, S3 and S4), so it reached more stirrups or connectors than if

the diagonal crack directly crossed to the compression chord. This could be the reason why beam S1 had a higher shear strength than beam S2.

Table 3. Comparison between the experimental and predicted horizontal shear stresses.

Specimen	Actual average stress at failure $\tau_{Rd,T}$ (MPa)	Ultimate horizontal shear stress predictions $\tau_{Rd,H}$ (MPa)						Average error $\tau_{Rd,T}/\tau_{Rd,H}$
		fib MC		EC2		ACI 318		
		$\tau_{Rd,H,MC}$ (MPa)	$\tau_{Rd,T}/\tau_{Rd,H,MC}$	$\tau_{Rd,H,EC2}$ (MPa)	$\tau_{Rd,T}/\tau_{Rd,H,EC2}$	$\tau_{Rd,H,ACI}$ (MPa)	$\tau_{Rd,T}/\tau_{Rd,H,ACI}$	
S1	2.395	0.676	3.5	1.134	2.1	0.550	4.4	3.3
S2	2.266	1.368	1.7	1.671	1.4	2.516	0.9	1.3
S3	3.356	1.352	2.5	1.850	1.8	0.550	6.1	3.5
S4	3.073	2.106	1.5	2.506	1.2	3.232	1.0	1.2

One could think *a priori* that a beam with a very rough interface would reach higher shear strength than a beam with a smooth interface as the influence of having an interface between two different aged concretes would be lower. Nonetheless, it was observed that interface roughness affected the beam's cracking pattern by modifying the shear strength mechanism of the beam with a smooth interface and, therefore, its ultimate strength.

4.2. Shear reinforcement

Table 2 shows the large difference among the shear strength code predictions for shear reinforced concrete beams and the experimental results. For beams S1 and S2, the codes substantially underestimated the actual shear strength, although they considered a smaller compression field angle than that observed in the cracks in the tests. Beam S1 reached a 34% higher strength than that predicted by Level III approximation of *fib* MC, and beam S2 reached an 18% higher strength. In beam S4, with a smooth interface at the 1.00-metre long span where failure took place, the reached strength was 19% higher. In this last case, there was no beam with the same reinforcement, but a very rough interface to compare the effect of interface roughness.

In beams S3 and S4, additional connectors were placed with their proper anchor length to avoid at least one of the beams (beam S4) failing in horizontal shear, according to the codes' predictions. Although the shape of these connectors was not that of a closed stirrup, they clearly influenced the vertical shear strength as beams S3 and S4 reached a significantly higher shear strength than the same beams without connectors (beams S1 and S2, respectively). Even when connectors were treated as vertical shear reinforcement, codes *fib* MC and ACI 318 underestimated strength. The strength of beam S3 was 15% higher than the value predicted by *fib* MC.

However, EC2 overestimated shear strength. This is further proof of the wide dispersion between the different codes as regards the shear strength calculation.

It should be pointed out that the anchor length of the horizontal shear connectors in the tested beams almost covered the entire beam depth. If the beam had had a greater depth, connectors would not have covered the entire web, and thus would not have behaved as vertical shear reinforcement.

5. Conclusions

The objective of this experimental programme was to analyse in composite concrete beams, the influence of the surface roughness between concretes and the shear reinforcement ratio of the interface. The major findings of the study are:

1. For the beams of these tests, the codes used (*fib* MC, EC2 and ACI 318) safely estimated the horizontal shear strength reached at the interface, especially when the interface was smooth or as cast.
2. The beam with a very rough interface similarly behaved to a monolithic beam. In beams with a smooth interface, the crack developed horizontally along the interface, so its crossing to the compression chord was postponed.
3. The development of a crack along the interface allowed it to reach more stirrups or connectors and, hence, possibly greater strength. That is, roughness modified the beam's cracking pattern and, therefore, the shear strength mechanism that it developed.
4. The shear strength predictions of the codes for beams with shear reinforcement showed big differences among the codes and with respect to the experimental strengths.

In the future, a more detailed study of these observations will be necessary by testing a larger number of specimens, and by including, for example, monolithic beams, and even taking into account other influencing phenomena such as long-term effects.

Acknowledgements

This article forms part of the research conducted at the Concrete Science and Technology University Institute (ICITECH) of the Universitat Politècnica de València (UPV). This work has been supported by the Spanish Ministry of Economy and Business through Project BIA2015-64672-C4-4-R, by the Regional Government of Valencia through Project AICO/2018/250, and by the European Union with FEDER funds. The authors thank the Spanish Ministry of Economy and Business for Grant BES-2016-078010.

References

[1] Comité technique 4.3 - Ponts routiers Technical Committee 4.3 - Road Bridges, Estimation of load carrying capacity of bridges based on damage and deficiency, PIARC World Road Association, 2016.

[2] Fédération International du Béton (fib), Model Code 2010, Ernst & Sohn, 2012.

[3] CEN, EN 1992-1-1:2004. Eurocode 2: Design of concrete structures - Part 1-1: General rules and rules for buildings, 2004.

[4] ACI Committee 318, Building code requirements for structural concrete (ACI 318-14); and commentary (ACI 318R-14)., Farmington Hills: American Concrete Institute, 2014.

[5] K.-H. Reineck, E. Bentz, B. Fitik, D.A. Kuchma, O. Bayrak, ACI-DAfStb databases for shear tests on slender reinforced concrete beams with stirrups, ACI Struct. J. 111 (2014). https://doi.org/10.14359/51686819.

[6] A. Moore, C. Williams, D. Al-Tarafany, J. Felan, J. Massey, T. Nguyen, K. Schmidt, D. Wald, O. Bayrak, J. Jirsa, W. Ghannoum, Shear Behavior of Spliced Post-Tensioned Girders, Austin, 2015.

[7] C.-G. Kim, H.-G. Park, G.-H. Hong, S.-M. Kang, Shear strength of composite beams with dual concrete strengths, ACI Struct. J. 113 (2016) 263–274.

[8] J.C. Saemann, G.W. Washa, Horizontal Shear Connections between Precast Beams and Cast-in-Place Slabs, ACI J. Proc. 61 (1964) 1383–1409.

[9] R.E. Loov, A.K. Patnaik, Horizontal Shear Strength of Composite Concrete Beams With a Rough Interface, PCI J. 39 (1994) 48–69.

[10] L.F. Kahn, A. Slapkus, Interface Shear in High Strength Composite T-Beams, PCI J. 49 (2004) 102–110.

[11] C.-G. Kim, H.-G. Park, G.-H. Hong, S.-M. Kang, H. Lee, Shear Strength of Concrete Composite Beams with Shear Reinforcements, ACI Struct. J. 114 (2017) 827–837.

[12] A. Halicka, Ł. Jabłoński, Shear failure mechanism of composite concrete T-shaped beams, Proc. Inst. Civ. Eng. Struct. Build. 169 (2016) 67–75.

[13] M.W. Kani, Mark W. Huggins, Rudi R. Wittkopp, Kani on shear in reinforced concrete, University of Toronto, Dept. of Civil Engineering, Toronto, 1979.

2nd PAPER

Details:

Type of paper	Conference paper
Title EN	*Influence of interface roughness and shear reinforcement ratio in vertical shear strength of composite reinforced concrete beams*
Title ES (original)	*Influencia de la rugosidad de la interfaz y de la cuantía de armadura transversal en la resistencia a cortante de vigas compuestas de hormigón armado*
Authors	Lisbel Rueda García José Luis Bonet Senach Pedro Francisco Miguel Sosa
Congress	VIII Congreso de la Asociación Española de Ingeniería Estructural, ACHE
Date	24th-26th June, 2020. Postponed to 20th-22nd June 2022 due to the pandemic COVID-19
City	Santander (Spain)
Status	Accepted
Full reference	Rueda-García L, Bonet Senach JL, Miguel Sosa PF. Influence of interface roughness and shear reinforcement ratio in vertical shear strength of composite reinforced concrete beams. Hormigón y Acero 2022; 72.

NOTE: The original language of this conference paper is Spanish. The paper has been translated into English to unify the text of the thesis.

Influence of interface roughness and shear reinforcement ratio in vertical shear strength of composite reinforced concrete beams

Lisbel Rueda García[a], José Luis Bonet Senach[b] and Pedro Francisco Miguel Sosa[c]

[a] MSc Civil Engineering. Universitat Politècnica de València. Doctoral student. lisruega@cam.upv.es

[b] PhD Civil Engineer. Universitat Politècnica de València. University Professor. jlbonet@cst.upv.es

[c] PhD Civil Engineer. Universitat Politècnica de València. University Professor. pmiguel@cst.upv.es

Abstract

Shear behaviour of reinforced concrete composite beams, commonly used in civil engineering and building construction, has not been studied in depth. The objective of this work is to experimentally analyse the influence in shear strength of interface roughness between two concretes and horizontal shear reinforcement ratio, in composite beams with and without vertical shear reinforcement. The tests of seven composite beams show that an interface existing between two concretes and its characteristics modify failure mode of the element and, therefore, its strength, being necessary an adaptation of existing shear formulations to calculate this type of beams.

Keywords: reinforced concrete, composite beam, tangential forces, horizontal shear, vertical shear, interface roughness, shear reinforcement.

1. Introduction

In Spain alone, there are 33,000 bridges on the National Road Network. 44% of the bridges are made of reinforced concrete and 20% are made of prestressed concrete. 59% of the bridges are approximately 40 years old and 10% are more than 75 years old [1]. Many of these concrete bridges have a very common deck typology constructed since the mid-20th century, consisting of precast beams with an *in situ* slab on top, namely composite concrete beams. Given the large number of existing bridges of this typology and their age, it is particularly important to study their structural behaviour for a proper assessment of existing structures.

The calculation of the resistance to tangential forces is an essential aspect in the structural assessment of existing bridges that is not yet adequately solved. In fact, the current EHE-08 [2], EC2 (2004) [3], *fib* MC-2010 [4] and ACI 318-19 [5] provide

semi-empirical expressions for the shear strength of beams that are conservative and excessively scattered [6-8].

In the design of decks consisting of precast beams with top cast-in-place slab, it is common to disregard the contribution of the slab to shear strength, what stays on the safety side. However, such contribution does exist and may be relevant in the strength assessment of existing decks made of precast beams with top cast-in-place slab. Only the code ACI 318-19 [5] (Section 22.5.4) considers the shear assessment of beams consisting of a precast beam and a cast-in-place concrete slab by means of two methods: as the sum of the individual elements' shear strengths or as the shear strength of the entire composite section considering the lower strength of both concretes. However, it is not clear that the sum of the individual elements' shear strengths can ensure the safety of the composite beam [9].

The strength of beams composed of two concretes subjected to vertical shear forces has not been extensively studied. Most of the research proposes experimental programmes to analyse the behaviour of composite beams that focus their study on the shear strength at interfaces between concretes [10-12]. This is because the bond between the two concretes is critical for the proper behaviour of the composite beam.

Recently, Kim et al. (2016 and 2017) [9,13] have carried out an experimental programme in composite members with and without transverse reinforcement, with rectangular cross-sectional shape and subjected to tangential forces. Among their conclusions, they highlight that the design expressions proposed by the codes to assess the interface shear strength are very conservative. Furthermore, they point out that the total number of experimental tests that analyse the shear strength of composite members is still insufficient, and that the development of new models for assessing their resistance capacity is limited.

On the other hand, recent research has shown that the inclination and shape of the critical shear crack are modified by the existence of an interface between concretes [9,13,14]. The shape of the critical crack and its possible variable inclination influences the resistance capacity of the composite beam, since a more inclined crack affects a greater number of stirrups.

The present experimental programme aims to study the shear behaviour of composite beams made of two concretes, with different roughness of the interface between concretes and different ratios of transverse reinforcement crossing the interface, both for beams with and without shear reinforcement. Furthermore, the shear strength mechanism developed by the beams and the validity of the existing design methods are analysed.

2. Test programme

2.1. Characteristics of the beams designed

The beams of this experimental programme were designed with the aim of analysing two parameters that influence the shear strength of reinforced concrete composite beams: the roughness of the interface between concretes and the ratio of reinforcement crossing the interface, in beams with and without shear reinforcement.

Seven different composite beams were designed in order to define the boundary between an interface failure -debonding of the slab concrete from the beam concrete- and a shear failure -diagonal cracking failure of the beam web-.

They all consisted of four-point bending tests on 3.44 m long beams, on which two non-centred point loads were applied, spaced 0.40 m apart, forming a 1.00-metre span A and a 1.34-metre span B. Span A, identical for all beams, was reinforced to prevent its shear failure and had a smooth interface between concretes, i.e., it did not receive any treatment after the concrete casting. Span B is where the failure was expected, and the influence of the studied variables is analysed. The length of span B and the effective depth of the beams d = 0.335 m were adjusted to obtain a shear slenderness (a/d) of 4.0, in order to study a shear failure not affected by the arch effect [15].

The beams, with a 0.18 m wide rectangular cross-section, were made of two concretes of different ages. The concrete of the first phase, 0.30 m depth, represents the precast beam in a composite beam. The second phase concrete, 0.10 m depth, represents the cast-in-place slab.

The parameters fixed in this test series were: longitudinal reinforcement ratio (ρ_l = 4.08%); shear slenderness (a/d = 4.0); cross-section geometry; design compressive strength of the concretes used (f_c = 30 MPa).

The longitudinal reinforcement was calculated to avoid the bending failure of the beams, looking for a shear failure. The transverse shear reinforcement was calculated in accordance with the codes EHE-08 [2], EC2 (2004) [3], *fib* MC-2010 [4] and ACI 318-19 [5]. Three of the seven beams were designed without shear stirrups and the other four with Ø8 stirrups spaced every 250 mm, respecting the maximum spacing between stirrups defined by the codes used.

The beams without stirrups had a rough interface to resist the interface shear. In addition, two of the beams had different ratios of reinforcement crossing the interface in fork connector form with their corresponding anchorage length. In the beams with shear reinforcement, smooth and very rough interfaces were combined

with the use or not of fork connectors crossing the interface in addition to the shear stirrups (see Fig. 1).

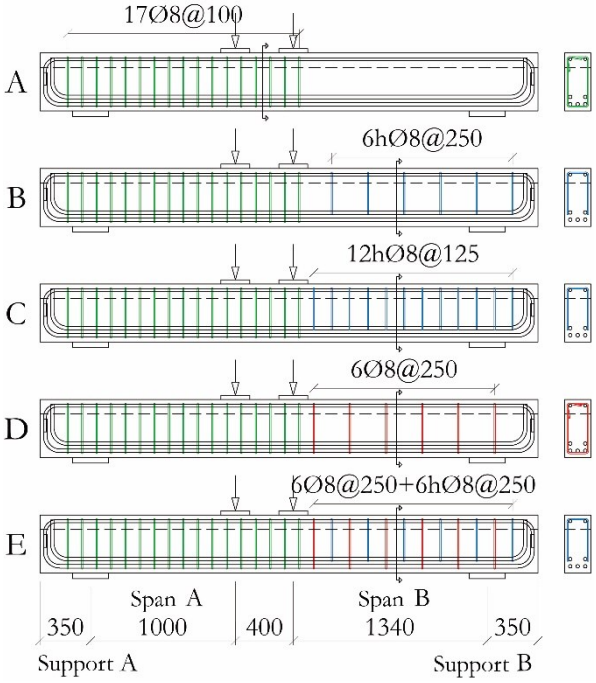

Fig. 1. Reinforcement layout of beams. Units: mm.

Table 1 summarises the characteristics of each specimen. The nomenclature used to identify the beams was as follows: shear reinforcement –SC, without stirrups, or CC, with stirrups–; interface roughness –R, very rough, or L, smooth–; and spacing between transverse reinforcement crossing the interface, in mm.

Table 1. Characteristics of span B of the beams designed. Units: mm.

Specimen ID	Interface roughness	Shear stirrups	Connectors (forks)	Reinforcement layout
SCR0	Very rough	-	-	A
SCR250	Very rough	-	hØ8@250	B
SCR125	Very rough	-	hØ8@125	C
CCL250	Smooth	Ø8@250	-	D
CCR250	Very rough	Ø8@250	-	D
CCL125	Smooth	Ø8@250	hØ8@250	E
CCR125	Very rough	Ø8@250	hØ8@250	E

Regarding the strength of the beams, the calculations according to the different codes indicated that the ultimate interface shear strength of beam SCR0, and possibly also SCR250, would be reached before its vertical shear strength. In contrast, beam SCR125 was expected to have a vertical shear failure.

For the elements with shear reinforcement –CCL250, CCR250, CCL125 and CCR125–, the beams with smooth interface were expected to have an interface shear failure, while the beams with rough interface were expected to possibly have a vertical shear failure.

2.2. Test setup and instrumentation

The beams were laid on two ball-bed supports to prevent horizontal reaction. A steel frame was designed to divide the actuator load into two point loads, with a pin connection to keep load vertical throughout the test (Fig. 2).

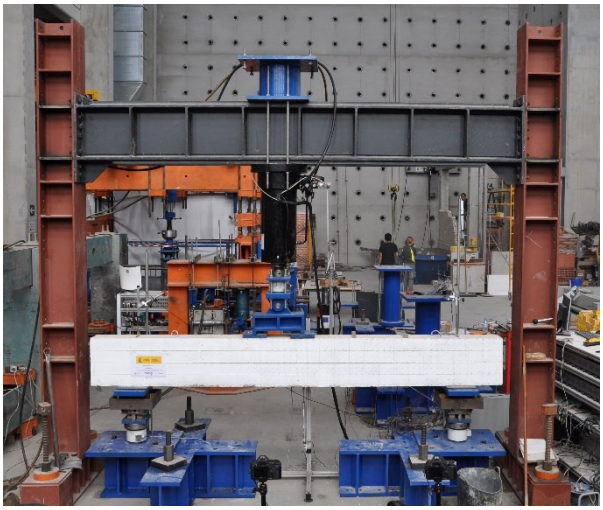

Fig. 2. Test setup.

Two load cells were used at the supports and one at the actuator. Vertical displacements were measured at the supports and under the actuator using displacement transducers (LVDTs). LVDTs were used in two sections of span B to measure the opening of the beams due to the formation of diagonal and horizontal cracks. Four horizontal LVDTs were placed in four sections to measure the slip between the slab and the beam.

Strain gauges were placed on the tension longitudinal reinforcement, on shear stirrups and on fork connectors, to measure reinforcement strains. Four pairs of strain gauges were also placed on the concrete surface in the same four cross-sections where gauges were placed on the longitudinal reinforcement.

In addition, three cameras with synchronised triggering took pictures every 2 seconds.

2.3. Material properties and fabrication

The beams were tested between 33 and 42 days after fabrication. The actual concrete strengths at the time of testing were 32 MPa for the beam and 31 MPa for the slab. Three different diameters of B500SD steel reinforcing bars were used. The Ø8 bars had a yield strength f_y = 534 MPa and a Young's modulus E_s = 189 GPa. The Ø20 bars had f_y = 534 MPa and E_s = 206 GPa. The Ø25 bars had f_y = 556 MPa and E_s = 197 GPa.

The slab concrete was poured 24 h after the beam concrete in order to avoid long-term effects such as differential shrinkage. In the beams that required it, the surface was raked before the first concrete hardened, resulting in a very rough surface consisting of grooves approximately 6 to 10 mm deep (peak-to-valley distance) and with a maximum peak-to-peak distance of 40 mm. The concrete cured for 7 days, at which time the formwork was removed.

3. Experimental results

3.1. Crack pattern and failure mode

The tested beams showed different strengths and failure modes depending on their transverse reinforcement and the roughness of the interface between concretes. Fig. 3 shows the crack patterns of the beams at the end of tests.

Beam SCR0, with a very rough interface and no transverse reinforcement, failed after reaching a shear force of 91 kN at span B. The shape of the critical crack was typical for beams without shear reinforcement, except for a small 80 mm long stretch where the crack became horizontal at the interface between concretes.

In the beam SCR250, with a very rough interface and fork connectors every 250 mm, shear cracks developed along the interface before penetrating the slab. The failure was caused by the failure of the compression chord, at a shear force of 161 kN.

Beam SCR125 reached a shear force of 175 kN. In this case, failure occurred when the crack closest to the point load reached the load distribution plate.

Beam CCL250, with shear stirrups every 250 mm and a smooth interface, showed a failure clearly affected by the existence of an interface between concretes. In this case, the shear cracks became horizontal as they reached the interface and prolonged until they connected with each other. The failure took place at a shear force of 206 kN, when the critical crack reached the top concrete layer.

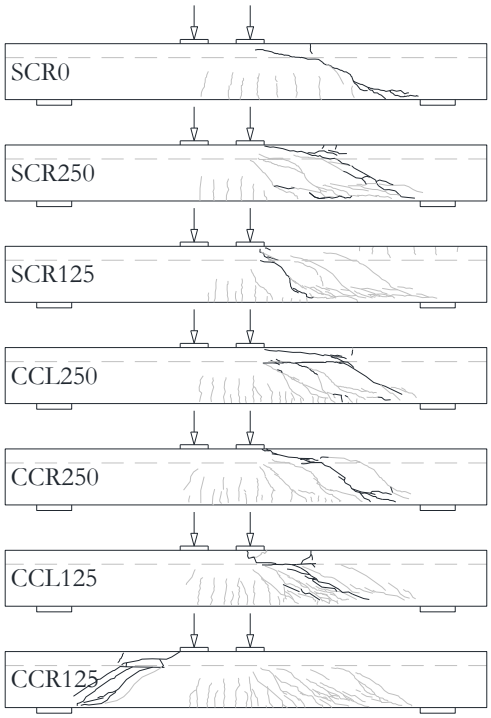

Fig. 3. Crack patterns of the tested beams.

In beam CCR250, like the previous one but with a rough interface, the cracks barely developed along the interface and failure was reached at 181 kN.

Beam CCL125, with smooth interface and shear stirrups and fork connectors, reached a shear force of 255 kN. In this beam, one of the diagonal cracks developed along the interface until finally failure occurred when this crack crossed the second concrete and reached the load distribution plate.

Beam CCR125, with a very rough interface and shear stirrups and fork connectors, reached a shear force in span B of 249 kN. However, the failure occurred in span A, with a shear force of 313 kN. In this span, diagonal cracks were observed which became horizontal at the interface and finally penetrated the second concrete layer towards the load.

It should be noted that in all the beams where there was a clear debonding of the second concrete with respect to the first concrete, a vertical crack appeared on top of the slab where the slope of the critical crack changes. Beams SCR0, SCR250, CCL250, CCL125 and CCR125 exhibited this crack. In contrast, beams SCR125 and CCR250 behaved similarly to a monolithic beam.

On the other hand, it can be seen that, when the transverse reinforcement spacing is small, failure occurs in a cross-section closer to the point load.

3.2. Resisted interface shear stress

The calculation of the interface shear stress with the instrumentation data is based on the global force equilibrium method. The strain plane is obtained in four cross-sections of span B throughout the test by using the strain data from the gauges of the tension longitudinal reinforcement and the gauges located on the slab concrete. From the strain plane in the cross-sections, the stresses are calculated using a Sargin-type constitutive curve, as described in EC2 (2004) [3]. The compressive force C in the slab is obtained by integrating the stresses in each instrumented cross-section. The interface shear stress in a stretch i between two cross-sections is calculated as:

$$\tau_{intshear,i} = \frac{C_i - C_{i-1}}{l \cdot b} \tag{1}$$

Where l is the distance between two consecutive cross-sections i and i-1, and b is the cross-section width.

Since no beam had a pure interface shear failure, the interface shear stress results are a lower bound of the interface shear stress that could be reached. Fig. 4 shows the average interface shear stress obtained from the instrumentation for each test as a function of the shear force in span B (V_B).

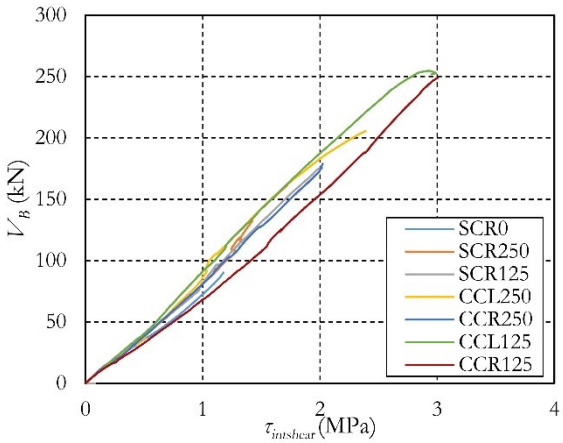

Fig. 4. Relationship between the interface shear stress and the shear force in span B in the tested beams.

3.3. Experimental shear force

Table 2 shows the results of the ultimate shear strength (V_{Rd}) for each beam in span B –except for beam CCR125, for which the shear strength of span A is given, where the failure occurred–. An estimation of the shear resisted by the transverse reinforcement ($V_{Rd,s}$) is also obtained. For this purpose, the photographs of each test are used, on which the reinforcement drawing is superimposed. In this way, the number of stirrups and/or fork connectors crossed by the critical crack is estimated. It is verified whether they have yielded at failure by means of the data from the strain gauges placed on the reinforcement crossing the interface. The shear component resisted by the concrete $V_{Rd,c}$, calculated as the difference between V_{Rd} and $V_{Rd,s}$, is also shown.

Table 2. Experimental shear strength.

Specimen ID	V_{Rd} (kN)	No. stirrups+ fork connectors	$V_{Rd,s}$ (kN)	$V_{Rd,c}$ (kN)
SCR0	91	-	-	91
SCR250	161	2	107	54
SCR125	175	2	107	68
CCL250	206	3	161	45
CCR250	181	3	161	20
CCL125	255	4	215	40
CCR125 Span A	313	5	268	45

4. Analysis of test results

4.1. Crack pattern and failure mode

As observed in Fig. 3, horizontal cracking at the interface between concretes is present in most of the tested beams. Despite this, none of the beams can be considered to have an interface shear failure. Hanson in 1960 [16] considered a limit slip between concretes of 0.13 mm after which the joint behaviour of beam and slab is lost (beam and slab work as different elements, resulting in pure interface shear failure). The maximum slip measured by the instrumentation of these tests was 0.05 mm in the beam CCL250, which is far from that limit. Consequently, in all tests the beam and slab can be considered as working together. However, the presence of an interface between concretes did influence the crack trajectory.

In the literature [9, 13] this type of cracking where the diagonal crack is affected by the interface between concretes is identified as diagonal tension combined with horizontal shear cracking at the interface (TD+FR).

Regarding the interface roughness, there was a clear difference between the beams with a smooth interface and the beams with a rough interface, even though all of them showed the TD+FR failure type. In beams CCL250, CCL125 and in span A of CCR125, all with smooth interface, the horizontal crack at the interface extended over a longer length than in the beams with rough interface (see Fig. 3).

In addition, in beam CCL250 the horizontal crack reaches a greater number of stirrups, which modifies the shear behaviour of the beam. On the contrary, in beam CCR250, the diagonal cracks do not find any difficulty at the interface to penetrate the compression chord. The critical crack inclination is greater in this beam than in its homologous beam with a smooth interface, CCL250, and reaches a lower shear force.

Regarding the reinforcement crossing the interface, both in fork connector and stirrup form, it is observed that the greater the transverse reinforcement ratio, the greater the number of diagonal cracks and the more vertical they are.

4.2. Resisted interface shear stress

Fig. 4 shows that the average interface shear stress is directly proportional to the resisted shear force. Therefore, the smooth interface beams, which resisted a higher shear force than the very rough interface beams, also reached a higher interface shear stress.

On the other hand, Fig. 4 shows that, as expected, the higher the ratio of reinforcement crossing the interface, the higher the interface shear stress resisted.

4.3. Shear strength

The experimental shear force shown in Table 2 indicates that the strength of the beams without transverse shear reinforcement was lower than that reached by the beams with transverse reinforcement, as expected.

On the other hand, the results showed that the beams with fork connectors reached a higher shear strength than expected. This indicated that the fork connectors not only contributed to resist the interface shear but also the vertical shear.

The reason given to this behaviour is that the anchorage length of the fork connectors' legs made them be close enough to the tension longitudinal reinforcement to produce a truss resistance mechanism. This is a phenomenon that would not take place on a full scale, i.e., on a beam with a greater depth. However, the shear strength reached was not the same as in a beam with closed stirrups, and an intermediate strength was reached.

Additionally, from the estimation of $V_{Rd,s}$ shown in Table 2, it is deduced that this shear component increases with the transverse reinforcement ratio, with the $V_{Rd,c}$ component becoming less and less important.

5. Comparison with codes

5.1. Interface shear stress

Fig. 5 shows the mechanical capacity of the transverse reinforcement crossing the interface per beam metre ("clamping stress") –transverse reinforcement ratio ϱ_w multiplied by f_y– in relation to the average interface shear stress concomitant with the ultimate shear force, for the tested beams and according to the different codes: EHE-08 [2], EC2 (2004) [3], EC2 (2017) [17] (not applicable yet), *fib* MC-2010 [4] and ACI 318-19 [5].

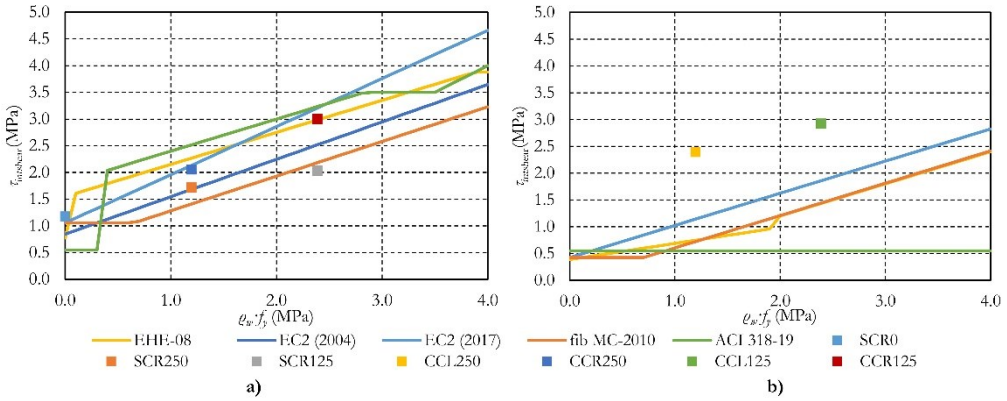

Fig. 5. Experimental and predicted by the codes relationship between the transverse reinforcement and the interface shear stress: a) Beams with a very rough interface, and b) Beams with a smooth interface.

Fig. 5.a corresponds to beams with a very rough interface. The plot shows that the experimental values are close to those estimated by the codes.

Fig. 5.b, which represents the behaviour of beams with a smooth interface, clearly shows how the two beams with a smooth interface reach a much higher strength than the calculated one. Thus, the codes give a very safe estimation of the shear strength of composite beams for the tested beams interface characteristics.

5.2. Shear strength

Table 3 shows the relationship between the experimental and the calculated shear strength $-V_{exp}/V_{code}$– for each of the tested beams and according to the different

codes: EHE-08 [2], EC2 (2004) [3], EC2 (2017) [17], *fib* MC-2010 [4] in its three approximation levels (LI, LII and LIII) and ACI 318-19 [5] with its two formulations (simplified –A1– and non-simplified –A2–). The values that do not appear in the table are those that, due to the beams' reinforcement characteristics, the codes do not allow their calculation.

Table 3. Relationship between the experimental shear strength and the codes' shear strength (V_{exp}/V_{code}).

	EHE-08	EC2 (2004)	EC2 (2017)	*fib* MC-2010 LI	*fib* MC-2010 LII	*fib* MC-2010 LIII	ACI 318-19 A1	ACI 318-19 A2
SCR0.A	0.94	0.94	1.12	2.29	1.28	-	1.27	1.27
SCR0.B	1.09	1.09	1.41	2.99	1.69	-	1.49	1.49
SCR250.A1	1.67	1.67	1.98	4.07	2.28	-	2.25	2.25
SCR250.B1	1.94	1.94	2.50	5.30	3.00	-	2.64	2.64
SCR250.A2	1.25	1.00	1.00	1.44	1.29	1.08	1.26	1.08
SCR250.B2	1.78	1.42	1.42	2.06	1.82	1.51	1.80	1.45
SCR125.A1	1.81	1.81	2.15	4.42	2.47	-	2.45	2.45
SCR125.B1	2.11	2.11	2.72	5.76	3.26	-	2.87	2.87
SCR125.A2	0.68	0.56	0.57	-	0.85	0.80	0.88	0.79
SCR125.B2	0.97	0.79	0.82	-	1.19	1.11	1.25	1.08
CCL250.A	1.59	1.27	1.27	1.84	1.64	1.36	1.59	1.37
CCL250.B	2.27	1.81	1.81	2.62	2.31	1.91	2.27	1.82
CCR250.A	1.40	1.12	1.12	1.62	1.45	1.20	1.41	1.20
CCR250.B	2.00	1.60	1.60	2.31	2.04	1.69	2.00	1.61
CCL125.A1	1.97	1.58	1.58	2.27	2.04	1.69	1.98	1.69
CCL125.B1	2.81	2.25	2.25	3.24	2.87	2.37	2.81	2.26
CCL125.A2	0.98	0.80	0.82	-	1.24	1.15	1.27	1.15
CCL125.B2	1.40	1.13	1.16	-	1.73	1.61	1.81	1.56
CCR125.A	0.97	0.89	0.92	-	1.21	1.16	1.32	1.21
CCR125.B	1.38	1.27	1.30	-	1.69	1.62	1.88	1.66

The table shows the calculations for different cases: assuming that the shear force is resisted by the entire rectangular cross-section (beam and slab) –case A– and assuming that only the beam resists shear –case B–, the latter being the method considered in all the codes except for ACI 318-19 [5]. On the other hand, the strength is calculated assuming that the reinforcement crossing the interface in fork connector form does not contribute to resisting shear –case 1– and assuming that it does –case 2–.

Beams SCR0, CCL250 and CCR250, all without fork connectors, show results very close to those estimated by the codes in case A. In case B the estimations are very much on the safety side. The same applies to beam CCR125, whose span A shear strength is presented. In general, EC2 2017 [17] is the code that best approximates the results. However, it should be noted that in some cases –SCR0.A and CCR125.A– the experimental shear strength was lower than the estimated one, thus

some codes gave unsafe predictions when the strengths of beam and slab were considered. This may be due to the possible strength reduction given by the existence of an interface between concretes. It should be noted that this strength underestimation does not occur with ACI 318-19 [5] –the only code that considers the shear strength assessment of composite beams–.

Regarding the presence of the fork connectors as reinforcement crossing the interface, the shear strength of beam SCR250 is well above the calculated one if the transverse reinforcement is considered to not contribute to resist shear, but it is close to the calculated one if it is considered to contribute. On the contrary, the actual strength of beam SCR125 is far from the estimated one if the fork connectors are taken as shear reinforcement. Something similar occurs with beam CCL125.

6. Conclusions

The aim of this experimental programme was to analyse the influence of the interface strength characteristics on the shear strength of concrete composite beams. The most relevant conclusions are:

- The existence of an interface between concretes modified the critical shear crack trajectory and, therefore, the strength of the tested element. In particular, the crack development along the interface reached a higher number of transverse reinforcements and, consequently, gave a higher shear strength.
- The code formulations for the shear strength of the interface between two concretes underestimate the resistant capacity of the beams. This dispersion was particularly relevant for beams with a smooth interface (with no further treatment after the first concrete pouring).
- Giving the interface a very rough roughness made the beam behave similarly to a monolithic beam.
- For the tested beams, with diagonal tension failure combined with horizontal shear cracking at the interface, the codes give unsafe results if the joint shear strength of the beam and slab is considered, and well above the experimental shear strength if only the beam is considered. It would be important to adjust the formulations both for the design of precast beams with cast-in-place slab and for the assessment of this type of existing structures.

Given the small number of experimental tests in this field, an experimental programme to study the behaviour of reinforced concrete composite beams failing in diagonal tension combined with horizontal shear cracking at the interface should be developed for different cross-sectional geometries.

Acknowledgements

This work has been carried out thanks to the support of the Spanish *Ministerio de Economía y Empresa* through Project BIA2015-64672-C4-4-R; the *Generalitat Valenciana* through Project AICO/2018/250, and the European Union through ERDF funds. The authors would like to thank the Spanish *Ministerio de Economía y Empresa* for the pre-doctoral grant BES-2016-078010.

References

[1] Comité technique 4.3 - Ponts routiers Technical Committee 4.3 - Road Bridges. Estimation of load carrying capacity of bridges based on damage and deficiency. PIARC World Road Association: 2016.

[2] Comisión Permanente del Hormigón. EHE-2008. Instrucción de Hormigón Estructural. Ministerio de Fomento. Madrid: 2008.

[3] CEN. EN 1992-1-1:2004. Eurocode 2: Design of concrete structures - Part 1-1: General rules and rules for buildings. 2004.

[4] Fédération International du Béton (fib). Model Code 2010. Ernst & Sohn; 2012.

[5] ACI Committee 318. Building code requirements for structural concrete (ACI 318-19); and commentary (ACI 318R-19). Farmington Hills: American Concrete Institute; 2019.

[6] Reineck K-H, Bentz EC, Fitik B, Kuchma DA, Bayrak O. ACI-DAfStb database of shear tests on slender reinforced concrete beams without stirrups. ACI Struct J 2013;110.

[7] Reineck K-H, Bentz E, Fitik B, Kuchma DA, Bayrak O. ACI-DAfStb databases for shear tests on slender reinforced concrete beams with stirrups. ACI Struct J 2014;111. https://doi.org/10.14359/51686819.

[8] Moore A, Williams C, Al-Tarafany D, Felan J, Massey J, Nguyen T, et al. Shear Behavior of Spliced Post-Tensioned Girders. Austin: 2015.

[9] Kim C-G, Park H-G, Hong G-H, Kang S-M. Shear strength of composite beams with dual concrete strengths. ACI Struct J 2016;113:263–74.

[10] Saemann JC, Washa GW. Horizontal Shear Connections between Precast Beams and Cast-in-Place Slabs. ACI J Proc 1964;61:1383–409.

[11] Loov RE, Patnaik AK. Horizontal Shear Strength of Composite Concrete Beams With a Rough Interface. PCI J 1994;39:48–69.

[12] Kahn LF, Slapkus A. Interface Shear in High Strength Composite T-Beams. PCI J 2004;49:102–10.

[13] Kim C-G, Park H-G, Hong G-H, Kang S-M, Lee H. Shear Strength of Concrete Composite Beams with Shear Reinforcements. ACI Struct J 2017;114:827–37.

[14] Halicka A, Jabłoński Ł. Shear failure mechanism of composite concrete T-shaped beams. Proc Inst Civ Eng Struct Build 2016;169:67–75.

[15] Kani MW, Mark W. Huggins, Rudi R. Wittkopp. Kani on shear in reinforced concrete. Toronto: University of Toronto, Dept. of Civil Engineering; 1979.

[16] Hanson NW. Precast-Prestressed Concrete Bridges – 2. Horizontal Shear Connections. J PCA Res Dev Lab 1960;2:38–58.

[17] CEN. PT1 prEN 1992-1-1/D2 Eurocode 2: Design of concrete structures - Part 1-1: General rules, rules for buildings, bridges and civil engineering structures. 2017.

Chapter 3. Experimental study on the shear strength of concrete composite beams without web reinforcement

The objective of this research is to analyse the shear behaviour of precast concrete beams commonly used in civil engineering, such as those used in the construction of road bridges, covered by a cast-in-place concrete slab. To achieve this goal, it is necessary to start from a simpler approach before analysing more complex cases. Therefore, in the second phase of the experimental programme the shear behaviour of composite beams without web reinforcement is studied. To that aim, this chapter analyses the shear resistant behaviour of 21 monolithic and composite specimens with different cross-sectional shapes.

Two papers describe this study. First, a journal article shows the experimental programme and its results and analysis. Second, a conference paper goes deeply in the safety analysis of the shear strength current formulations for beams without web reinforcement.

3rd PAPER

Details:

Type of paper	Journal article
Title	*Experimental analysis of the shear strength of composite concrete beams without web reinforcement*
Authors	Lisbel Rueda García José Luis Bonet Senach Pedro Francisco Miguel Sosa Miguel Ángel Fernández Prada
Journal	Engineering Structures
Publisher	Elsevier
ISSN	0141-0296
JIF	4.471 (2020)
JIF Quartile	Q1 (20/137) ENGINEERING, CIVIL
Status	Published
Date	Accepted: 23rd November 2020 Available online: 18th December 2020
Full reference	Rueda-García L, Bonet Senach JL, Miguel Sosa PF, Fernández Prada MÁ. Experimental analysis of the shear strength of composite concrete beams without web reinforcement. Engineering Structures 2021;229:111664. https://doi.org/10.1016/j.engstruct.2020.111664.

Experimental analysis of the shear strength of composite concrete beams without web reinforcement

Lisbel Rueda García, lisruega@cam.upv.es

José Luis Bonet Senach, jlbonet@cst.upv.es

Pedro Fco. Miguel Sosa, pmiguel@cst.upv.es

Miguel Ángel Fernández Prada, mafernan@cst.upv.es

Universitat Politècnica de València, Camí de Vera s/n, 46022 Valencia, Spain

Abstract

Composite concrete members without web reinforcement are often used in precast construction. The contribution of the cast-in-place concrete topping slab to vertical shear strength has been traditionally disregarded. However, significant cost savings can result from designing and assessing these structures if this contribution is considered. This paper presents the experimental study of a series of 21 monolithic and composite (precast beam and cast-in-place slab) specimens without web reinforcement, and with rectangular and T-shaped cross-sections, failing in shear. The vertical shear strength was analysed by the following test variables: cross-section shape, the existence of an interface between different aged concretes, strengths of the two concretes and the differential shrinkage effect. From these experimental tests, it was concluded that the slab contributed to shear strength, the use of high-strength concrete slightly increased specimens' shear strength and the differential shrinkage did not reduce shear strength. Specimens' failure modes were analysed based on their shear transfer mechanisms, noticing that the arching action in the slab was considerable after critical shear crack formation. The vertical shear strength experimental results were well predicted by the codes' formulations (Eurocode 2, Model Code 2010 and ACI 318-19) when composite beam depth was taken for the calculations instead of beam depth. Codes significantly underestimated the horizontal shear strengths of the composite specimens.

Keywords: reinforced concrete, composite beam, T-shaped beam, precast construction, vertical shear strength, horizontal shear strength, differential shrinkage.

Highlights

Shear in monolithic and composite concrete beams without stirrups was studied

Slab width, interface, concrete strength and differential shrinkage were analysed

The interface between concretes modified the critical shear crack direction

The slab contributed to increase the shear strength of the composite specimen

An over-strength of the T-shaped composite beams due to arching action was noted

Nomenclature

a	shear span
b	concrete section width
C	compression force at the slab
c	concrete cover
c_a	coefficient for the adhesive bond
d	effective depth
d_g	maximum size of the aggregate
E_c	modulus of elasticity of concrete
E_s	modulus of elasticity of reinforcement
f_c	compressive strength of the concrete measured in cylinder
$f_{c,28}$	compressive strength of the concrete measured in cylinder at the age of 28 days
$f_{c,min}$	minimum compressive strength of the two concretes of the composite beam
$f_{c,wa}$	weighted average of the beam's and slab's concrete compressive strengths estimated from the area ratio
f_{ct}	tensile strength of concrete
f_u	tensile strength of reinforcement
f_y	yield strength of reinforcement
h	overall height of member
M_{Ed}	design value of the applied bending moment
V_{Ed}	design shear force in the section considered
$V_{R,code}$	shear strength predicted by the design code
$V_{R,max1}$	experimental first local maximum of the shear-deflection relation
$V_{R,max2}$	experimental second local maximum of the shear-deflection relation

x	distance between a beam's instrumented cross-sections
z	internal lever arm
γ_c	partial safety factor for concrete material properties
γ_s	partial safety factor for steel material properties
ε_u	reinforcement strain at maximum load
ε_x	longitudinal strain at the mid-depth of the effective shear depth at the control section
ρ_l	reinforcement ratio of tension longitudinal reinforcement
σ_n	the lowest expected compressive stress resulting from an eventual normal force acting on the interface
$\tau_{R,code}$	horizontal shear stress predicted by the design code
$\tau_{R,exp}$	average experimental horizontal shear stress
$Ø$	nominal diameter of a reinforcing bar

1. Introduction

Cast-in-place concrete is frequently used in precast concrete construction to integrate structural elements. Precast concrete beams, together with cast-in-place concrete over them, form what is commonly known as a composite concrete beam. This type of construction has been widely used for decades and its employment is still growing. Given the many existing constructions involving this construction system, ranging from structural floors to concrete beams bridges, studying their structural behaviour is especially relevant. In particular, the study of composite reinforced concrete beams without shear reinforcement is important because of its applicability to building construction [1].

Traditionally, research on composite beams has focused on their horizontal shear strength [2] given the critical importance of adherence between concretes so that composite beams appropriately behave. Among these studies, Loov and Patnaik [3], Kovach and Naito [4] or Fang *et al.* [5] analysed the effect of interface roughness, the shear span-depth ratio, properties of concretes and shear reinforcement. One of the conclusions was that the current codes, especially ACI 318-19 [6], underestimate the horizontal shear strength of the composite beams' interface between concretes, almost always requiring the presence of interface reinforcement.

In the last century, vertical shear strength in monolithic beams has been widely studied, but no agreement about structural shear design has yet been reached

between the existent codes, which provide semi-empirical expressions to evaluate the shear strength of concrete beams that are excessively scattered [7]. Nonetheless, the determination of composite beams' resistance to vertical shear solicitations has not been studied in-depth [2]. Indeed, in both the design and assessment of composite beams' shear strength, the contribution of the slab to shear strength is commonly omitted to stay on the safety side. This omission seems reasonable because shear strength is a phenomenon that still involves many unknowns. However, that contribution does exist and, therefore, it should be considered in calculations for economical designs [2]. In the scientific literature, some publications on the experimental analysis of full-scale composite concrete beams can be found [8,9]. They show their structural behaviour, focusing analyses on verifying their shear strength according to design codes. However, no studies have analysed the contribution of the cast-in-place slab to the composite beam's shear strength.

Regarding the different codes' vertical shear strength considerations in composite beams, some codes, like MC-10 [10], do not refer to such elements. Other codes, like EC2 [11] (Section 10.9.3(8)) and ACI 318-19 [6] (Section 22.5.4), allow the possibility of considering the whole composite beam to resist shear as long as the horizontal shear at the interface between the two concretes is verified. Only ACI 318-19 [6] specifies how this composite beams can be calculated: using the properties of the individual elements or the properties of the element that result in the most critical value.

Nowadays, it is well-known that the existence of an interface between two concretes varies the pattern of shear cracks in relation to monolithic beams [2,12,13]. Notwithstanding, Halicka [14] revealed that few experimental tests done with composite concrete beams subjected to vertical shear actually consider the influence of interface cracking on the composite element's vertical shear behaviour. In fact the latest studies in composite beams [2] have neither analysed the influence of the interface on vertical shear strength nor compared this behaviour to that of monolithic beams.

Recently, Kim *et al.* [2,12] carried out an experimental programme of the vertical shear strength of rectangular composite beams made of normal-strength concrete and high-strength concrete in beams with and without web reinforcement. Regarding the beams without web reinforcement [2], they observed that the use of high-strength concrete on the precast beam did not significantly increase the shear strength of the composite element, that a greater longitudinal reinforcement ratio increased the shear strength of the beams, and that the shear strength decreased with increasing the shear span-effective depth ratio. Kim *et al.* [2] evaluated the shear strength of the composite elements using the average concrete strength obtained from the area ratio of the two concretes used in the cross-section, and observed that current design codes safely estimated the shear strength of the composite beams.

They remarked that the total number of existent experimental tests that analyse composite beams' shear strength is still insufficient. The shape of beams and other parameters need to be considered. Consequently, the development of new shear strength evaluation models for composite beams is limited.

Extending studies to new cross-sectional shapes is important because the behaviour of the structural elements compound of a precast beam with a cast-in-place slab on top could resemble in that of a composite T-shaped beam in some cases. Examples of actual structural elements with this cross-sectional shape and without web reinforcement are shown in Fig. 1. Furthermore, the inclination and shape of critical shear cracks vary when section width undergoes abrupt variations [15,16]. It has also been long since known [17] that T-shaped beams fail in shear instead of bending in a wider range of shear span-effective depth ratios (a/d). All this proves the importance of studying shear in T-shaped composite elements.

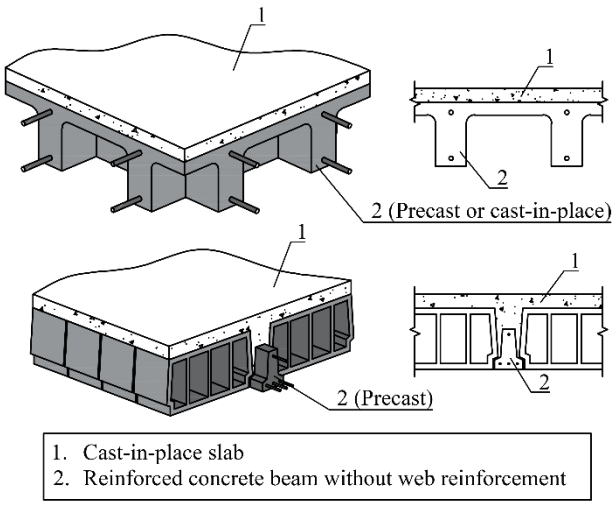

Fig. 1. Examples of structural elements compound of a reinforced concrete beam without web reinforcement and a cast-in-place slab.

The present research work intends to study the contribution of the cast-in-place slab's depth and width to the vertical shear strength in composite reinforced concrete beams without web reinforcement. This objective is experimentally studied in rectangular and T-shaped monolithic and composite beams by analysing the effect of the cross-section shape, the existence of an interface between two different aged concretes, the strengths of the two concretes and the effect of differential shrinkage between concretes. Moreover, the shear transfer mechanisms developed in the more relevant loading stages while running tests are analysed. The validity of the current design methods is also studied.

This research work is especially significant in the precast construction field as it intends to increase the number of existent experimental tests, and contribute with them to the extension of current codes with a more economical perspective when both designing new construction and assessing existent structures.

2. Test programme

2.1. Test parameters

Twenty-one experimental tests were designed to analyse the influence of the following four variables on the shear strength of composite reinforced concrete beams without web reinforcement:

- The cross-sectional shape (Fig. 2). It was firstly considered a reference rectangular section type A that equals that of the precast beams used in composite specimens. Secondly, three different sections with the same depth and web width, but with different flange widths, were adopted: section B, without flanges; section C with flange width that equals slab depth, which is frequently assumed in the literature [1,15]; section D, whose flange width was twice the slab depth.
- The existence of an interface between two different aged concretes. Specimens A1, B1 and C1 were fabricated with one concrete (monolithic beams) and specimens B2, C2 and D2 with two concretes (composite beams).
- The strengths of the two concretes of the composite beam. Two types of concretes were used: normal-strength concrete (NSC), with a nominal compressive strength of 30 MPa; and high-strength concrete (HSC), with a nominal compressive strength of 60 MPa. NSC represented a concrete commonly used in cast-in-place elements, while HSC was representative of a concrete usually poured for fabricating precast beams.
- The differential shrinkage between concretes. In a composite structure, differential shrinkage is a loading case itself, since it generates shrinkage stresses in the structure that are mainly compressive in the base layer and tensile in the overlay, as Silfwerbrand stated [18]. In 10 of the 12 composite specimens, the slab's concrete was poured 24 h after the beam's concrete. This way, the construction process was faster and the differential shrinkage between the beam's and the slab's concretes was reduced. This fabrication timeline was already carried out in previous experimental studies on vertical and horizontal shear strength of composite beams [2–4,12]. However, the described tests reflect the difference between concrete classes at the beam and the slab, but not the influence of different aged concretes at the beam and the slab. Hence, in order to analyse if different ages between concretes had a significant influence on vertical shear strength in this experimental

programme, the fabrication process was modified in two of the specimens, where the slab's concrete was poured when the beam's concrete shrinkage had stabilised.

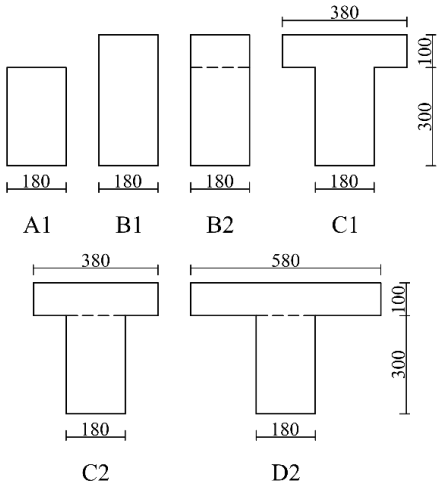

Fig. 2. Cross-section types (dimensions in mm).

The number of specimens of each series is shown in Table 1. Specimens were named using the notation *xOPyzk(j)*, where:

- "*xO*" denoted the series of beams without web reinforcement: NO for the specimens in which the beam's concrete was NSC, HO for specimens in which the beam's concrete was HSC, and DO for the beams fabricated with differential shrinkage between concretes.
- "*Py*" for the fabrication batch (from P1 to P5 as the beams fabrication process of pouring beam's and slab's concretes was conducted 5 times).
- "*z*" denoted the cross-sectional shape (A, B, C, or D) (Fig. 2).
- "*k*" denoted the number of different concretes used to fabricate the specimen (1 for monolithic beams, 2 for composite beams).
- "*j*" was used only when more than one specimen was fabricated with identical previous characteristics ("a" or "b").

Table 1. Characteristics of beams' series.

Series	Type of beam's concrete	Type of slab's concrete	Number of specimens for each cross-sectional type					
			A1	B1	B2	C1	C2	D2
NO	NSC	NSC	2	2	3	2	2	2
HO	HSC	NSC	1	1	1	1	1	1
DO	NSC	NSC	0	0	2	0	0	0

The fixed parameters in all the beams were: longitudinal reinforcement ratio (ρ_l = 4.0%), shear span-effective depth ratio (a/d = 4.0), relative concrete cover (c/h = 0.16) and interface roughness (very rough interface). Longitudinal reinforcement was designed to avoid bending failure. The shear span-effective depth ratio was fixed in order to foster a shear failure in both the rectangular and T-shaped beams based on the observations of Kani's valley [17]. Concrete cover and spacing between rebars were chosen according to the code provisions. A very rough interface treatment was used between concretes based on the conclusions of a previous study carried out by the authors [19]. According to the classification of failure mechanisms of composite concrete beams shown in Halicka [14], horizontal shear failure occurs when interface cracking appears prior to diagonal cracking. In Rueda-García *et al.* [19], beams with the same characteristics as those of this research work presented interface cracking after the diagonal cracking, thus proving the effectiveness of the given interface treatment for not failing in horizontal shear nor showing a monolithic behaviour. The interface reinforcement turned out to be unnecessary, even though the code calculations predicted horizontal shear failure.

Beam and slab were fabricated on the same formwork, without lifting the beam after the first concrete pouring. Thus in this experimental study, both the beam and slab were simultaneously loaded.

2.2. Test specimens

All the specimens' dimensions and reinforcements are specified in Fig. 3. Specimens type B, C and D had a total length of 3.50 m (2.74 m between supports). Two-point non-centred vertical loading was applied, with a 0.40-metre space between loads, to obtain a weak 1.34-metre shear span without shear reinforcement in which failure was expected. The other 1.00-metre span was reinforced to avoid its shear failure and induce the failure at the 1.34-metre span. Specimens type A were 3.16 m long (2.40 m between supports) to obtain the fixed shear span-effective depth ratio value (a/d = 4.0).

Some of these beams were composite beams with two layers of different aged concretes. The first layer, 0.30 m high, represented the precast beam of the composite beam. The second layer, 0.10 m high, was cast on the previous one and represented the cast-in-place concrete slab.

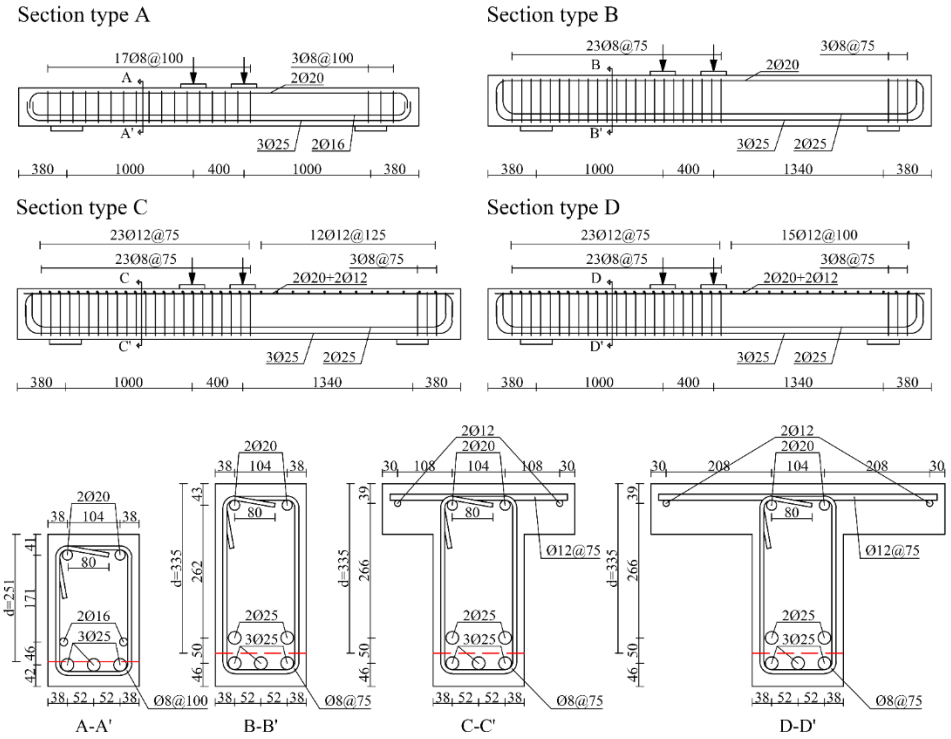

Fig. 3. Dimensions and reinforcement of beams with section types A, B, C and D (dimensions in mm).

2.3. Fabrication of specimens

Concrete casting was done by dividing the 21 specimens into five fabrication batches (P1 to P5 in Table 2) to eliminate the variable concrete strength when comparing the test results of the specimens in the same batch. In series NO and HO, concrete casting was performed in two phases. In the first phase, the beam's concrete was poured and the surface was raked before concrete hardened to obtain a very rough interface with dents of approximately 6 mm deep (from peak to valley) and a maximum spacing of 40 mm between peaks (dimensions defined in current design codes [6,10,11]). An example of this roughness is shown in Fig. 4. In the second phase done 24 h later, the slab's concrete was poured over the beam's concrete. Concrete was cured for 7 days before moving away the formworks.

In series DO, concrete shrinkage was measured after pouring the beam's concrete and raking the surface. After 134 days when the data revealed that concrete shrinkage had stabilised, the slab's concrete was poured.

Table 1. Summary of the test results.

Series	Fabri-cation batch	Specimen	$f_{c,28}$ beam (MPa)	$f_{c,28}$ slab (MPa)	f_c beam (MPa)	f_c slab (MPa)	E_c beam (MPa)	E_c slab (MPa)	f_{ct} beam (MPa)	f_{ct} slab (MPa)	$V_{R,max1}$ (kN)	$V_{R,max2}$ (kN)	$\tau_{R,exp}$ (MPa)	Cracking mode (*)
NO	P1	NOP1B2	32	31	32	31	35228	31848	2.41	2.72	91	(**)	1.48	DC+HC
	P2	NOP2A1	36	33	39	-	32294	-	1.86	-	75	84	-	DC
		NOP2B1			40	-	31507	-	2.39	-	88	62	-	DC
		NOP2C1			40	-	31507	-	2.39	-	72	90	-	DC+HC
		NOP2C2			39	34	34732	25789	2.29	2.77	94	83	2.59	DC+HC
		NOP2D2			39	34	34732	25789	2.29	2.77	84	80	1.99	DC+HC
	P3	NOP3A1	30	37	33	-	25329	-	2.93	-	62	72	-	DC
		NOP3B1			30	-	28717	-	2.41	-	81	57	-	DC
		NOP3B2a			31	38	26604	29635	2.45	1.77	70	41	-	DC
		NOP3B2b			31	38	26604	29635	2.45	1.77	86	92	2.04	DC+HC
		NOP3C1			30	-	28717	-	2.41	-	79	83	-	DC+HC
		NOP3C2			29	38	28403	32502	2.37	3.02	86	79	1.90	DC+HC
		NOP3D2			29	38	28403	32502	2.37	3.02	85	130	(***)	DC+HC
HO	P4	HOP4A1	61	31	61	-	36655	-	3.29	-	86	81	-	DC
		HOP4B1			63	-	36492	-	3.34	-	93	67	-	DC
		HOP4B2			63	31	36655	29521	3.70	2.36	101	71	-	DC
		HOP4C1			63	-	36492	-	3.34	-	90	88	-	DC+HC
		HOP4C2			63	31	36655	29521	3.70	2.36	86	97	2.01	DC+HC
		HOP4D2			63	31	36655	29521	3.70	2.36	99	116	1.54	DC+HC
DO	P5	DOP5B2a	24	36	29	37	24939	31243	2.44	2.82	88	72	2.04	DC+HC
		DOP5B2b			29	37	24939	31243	2.44	2.82	89	97	1.91	DC+HC

(*) Cracking mode at $V_{R,max1}$: DC is diagonal cracking; HC is horizontal cracking (at the interface in composite beams or at the plane in which the section width changes in T-shaped beams).
(**) Loading process was finished after first load drop.
(***) Calculation was not possible due to gauges failure.

Fig. 4. Very rough interface conditions.

2.4. Material properties

The properties of concrete were measured according to UNE-EN 12390 [20–22] and were calculated as the average of two tested concrete cylinders (300 mm high, 150 mm diameter) at the age of 28 days and each day a specimen was tested. Specimens were tested approximately 30 days after being fabricated. The compressive strength range of concrete at the testing age was between 29 and 40 MPa for NSC, and between 61 and 63 MPa for HSC. The modulus of elasticity of concretes varied from 25 to 35 GPa for NSCs and from 36 to 37 GPa for HSC. The tensile strength of concretes varied from 1.77 to 3.02 MPa for NSCs and from 3.29 to 3.70 MPa for HSC. Table 2 shows the nominal compressive strengths f_c of both the beam's and slab's concretes measured for each specimen the day it was tested and at the age of 28 days ($f_{c,28}$). The moduli of elasticity E_c and the tensile concrete strength f_{ct} measured the day the specimen was tested are also shown in Table 2.

For NSCs, the amount of Portland cement, the water-cement ratio and the maximum aggregate size (d_g) were 325 kg/m^3, 0.52 and 10 mm, respectively. For HSC, these same properties were 500 kg/m^3, 0.44 and 10 mm, respectively.

The steel type used for reinforcement was C class (according to EC2 [11]). Table 3 offers the results of the characterisation tests carried out according to UNE-EN ISO 6892 [23]. To determine the average values of the steel mechanical properties, two pieces of reinforcing steel were tested for each nominal diameter.

Table 3. Average values of the flexural and transversal reinforcement properties.

Series	NOP1			NOP2, NOP3, HOP4, DOP5				
Ø (mm)	8	20	25	8	12	16	20	25
f_y (MPa)	534	534	556	538	533	561	585	557
E_s (GPa)	189	206	197	203	207	240	192	199
f_u (MPa)	662	639	670	658	638	675	673	666
ε_u (%)	10.1	10.5	9.7	12.0	13.3	31.9	41.0	48.3

2.5. Instrumentation

Three 1000 kN load cells were used to take continuous measurements of the force in the hydraulic jack and the reactions at the bearing points.

As shown in Fig. 5a, lineal variable displacement transformers (LVDTs) were used to measure the displacements on the concrete surface. Five vertical LVDTs (V1 to V5) were placed at the supports and below three beam sections to measure vertical displacements. Four horizontal LVDTs (H1 to H4) were used to record the possible slips between the slab and beam along the interface, to analyse the influence of the interface in the behaviour of the specimen under vertical shear. Two vertical LVDTs (O1 and O2) were connected to the upper and bottom parts of two cross-sections to detect the beginning of the crack opening of either the web or the interface.

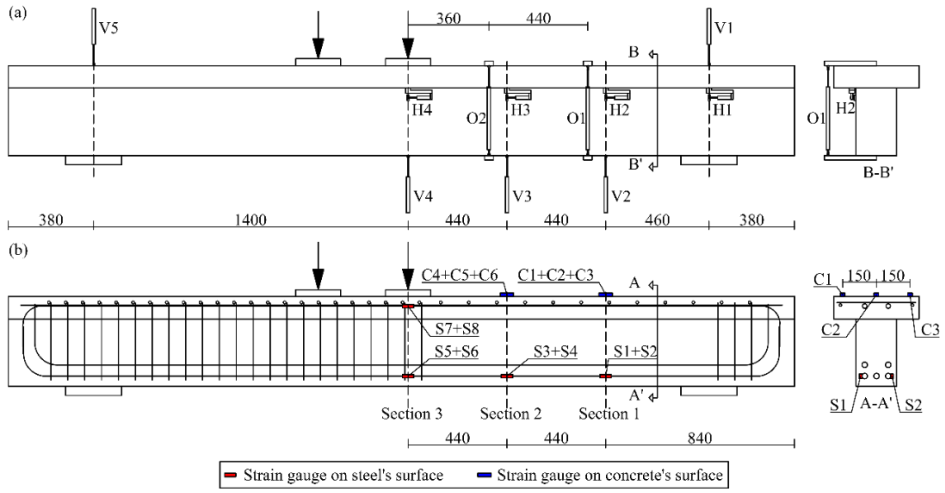

Fig. 5. Instrumentation for the shear test of a beam with section type C: (a) LVDTs; (b) strain gauges (dimensions in mm).

As shown in Fig. 5b, six strain gauges of 120 Ω resistance and 2 mm measuring length (S1 to S6) were used to measure the strains of the tension longitudinal reinforcement steel in three sections (Sections 1, 2 and 3). A pair of strain gauges (S7 and S8) was also placed on the compression longitudinal reinforcement below the central point load. Strain gauges of 120 Ω resistance and 60 mm measuring length were used to measure the strains on the concrete surface. Two (in rectangular beams) or three (in T-shaped beams) strain gauges were placed on top of the concrete slab in two sections (C1 to C6 in Fig. 5b). The distance between strain gauges on the concrete surface was 100 mm in beams with section type B, 150 mm in section type C and 250 mm in section type D.

While testing, two digital cameras took pictures of the principal span at a rate of 0.5 Hz. A high-speed camera was used to record brittle failures and to detect the beginning of failure.

Additionally, the shrinkage of the two beams of series DO was monitored for almost 4 months starting from day 2 after pouring concrete. Different techniques were used: continuous measurements of two LVDTs placed horizontally to each beam's end (H1 and H2 in Fig. 6a), one strain gauge placed on the concrete surface (C1 in Fig. 6a) and three internal gauges placed on longitudinal reinforcement (S1, S6 and S7 in Fig. 6b). In addition, a 3x3 mesh of discs was glued on the beam's lateral surface to measure deformations with a demountable mechanical strain gauge (DEMEC). Measurements with DEMEC were taken twice weekly.

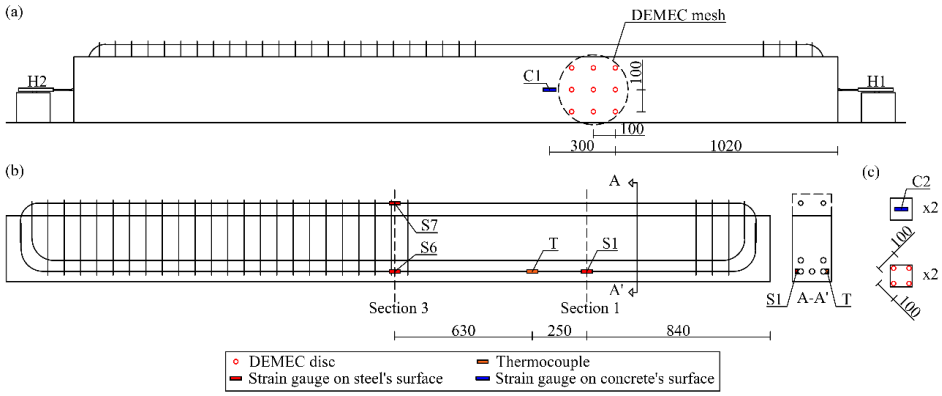

Fig. 6. Instrumentation for the shrinkage measurement of a beam of series DO: (a) external instrumentation; (b) internal instrumentation; (c) instrumentation of a concrete cube (dimensions in mm).

To measure internal temperature, a thermocouple was placed inside each beam (T in Fig. 6b). Ambient temperature and humidity were constantly measured.

Two concrete cubes (100x100x100 mm) were fabricated while casting the beam's concrete to measure free shrinkage by means of two strain gauges and two 2x2 meshes of DEMEC discs on each cube (see Fig. 6c).

2.6. Test setup and procedure

A steel-loading frame with a 1200 kN hydraulic actuator was used to perform the shear tests (Fig. 7a). Beams were laid on two supports (250 mm width) equipped with a steel balls bed each to eliminate the horizontal reaction, as shown in Fig. 7c. Both bearing points allowed rotations on the frame's plane. A steel beam was designed to divide the load of the actuator into two point loads (Fig. 7b). It was connected to a hinge joint for the load to remain vertical all the time. This steel beam

transmitted load to specimens through 200x200x30 mm steel load plates. Load was applied with the displacement control (0.02 mm/s).

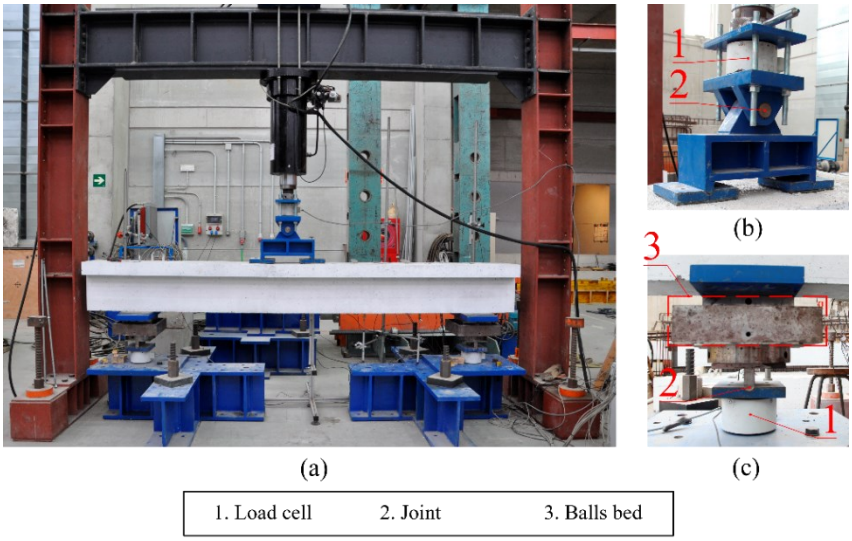

Fig. 7. Experimental setup and testing frame: (a) general view; (b) two-point loading system; (c) bearing points system.

3. Test results and discussion

3.1. Shear-deflection relation

The shear at the non-reinforced span (principal span) and the deflection below the point load closest to that span (LVDT V4 in Fig. 5a) were measured. Fig. 8 shows the shear-deflection relation measured in all the test specimens, except specimens NOP3B1 and NOP3C1 due to a failure of the LVDTs during tests. As seen in Fig. 8b-d, composite beams' curves are presented together with their homologous monolithic beams' curves. In order to facilitate the reading of the graphs, series DO beams are represented separately in Fig. 8e. Most of the beams tested in this test programme, both monolithic and composite, underwent two local maximums in shear, as seen in the graphs. The first local maximum corresponded to the critical shear crack appearing. After the load drop, the load-carrying capacity of most tested specimens continued to increase, which gave a second local maximum in the shear-deflection relation. In some cases, this second maximum was higher than the first one.

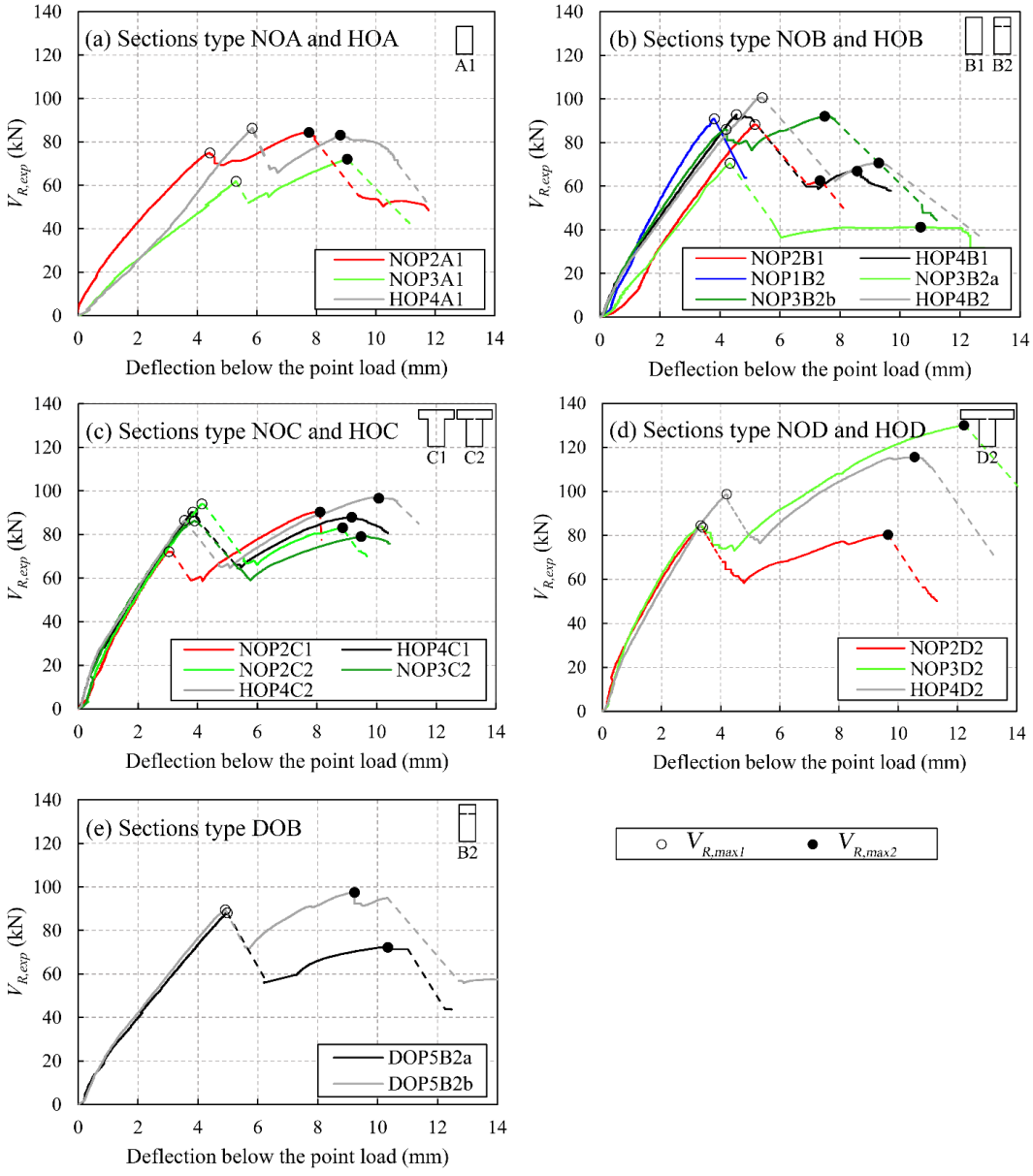

Fig. 8. Shear-deflection relation of all the test specimens: (a) sections type A; (b) sections type B from series NO and HO; (c) sections type C; (d) sections type D; (e) sections type B from series DO. (Specimens NOP3B1 and NOP3C1 not included: failure of LVDTs).

3.2. Shear strength

3.2.1. Vertical shear strength

Table 2 shows the shear values for the first and second local maximums ($V_{R,max1}$ and $V_{R,max2}$) of the shear-deflection curves.

All specimens failed in shear. The maximum strains measured along the tension longitudinal reinforcement (1.4‰) were far from the yield strain (2.8‰).

3.2.2. Interface horizontal shear stresses

The average horizontal shear stress at the interface $\tau_{R,exp}$ concurrent with $V_{R,max1}$ was obtained experimentally from the strains provided by the gauges located on both the concrete surface and the longitudinal reinforcement at Sections 1, 2 and 3 (see Fig. 5). For each section, a plane distribution of strains was defined by the compression strain on the concrete surface (or the strain at the compression longitudinal reinforcement in Section 3) and the strain on the tension reinforcement. The three strains measured on top of the concrete slabs of the specimens with flanges were similar in all the T-shaped specimens; that is, no evidence for shear lag was detected until shear's first local maximum was reached. Nevertheless, only the strains measured by the central strain gauges were used in the obtaining of the strains plane (gauges C2 and C5 in Fig. 5b). The strains plane was turned into a distribution of stresses using the Sargin's concrete constitutive curve and the steel constitutive curve described in EC2 [11]. By integrating only the compression stresses above the interface, or above the neutral axis if it was located over the interface, and including the stresses at compression longitudinal reinforcement, compression force C was obtained for all three instrumented sections. Tension stresses of concrete below the neutral axis were neglected. The horizontal shear stress at the interface between the beam's and the slab's concretes of a stretch i of the composite beam ($\tau_{R,exp,i}$) was calculated by dividing the difference of the compression forces between two consecutive cross-sections by distance x between both sections and beam width b (1). Table 2 shows the average value of the horizontal shear stress of the three stretches ($\tau_{R,exp}$) for those composite specimens in which horizontal cracking at the interface occurred at $V_{R,max1}$ (see the "Cracking mode" column at Table 2).

$$\tau_{R,exp,i} = \frac{C_i - C_{i-1}}{x_{i,i-1} \cdot b} \tag{1}$$

The method to calculate the horizontal shear stress is only valid if there is no slip between concretes at the interface. This slip was controlled by the horizontal LVDTs described in Fig. 5. It was verified that the slips recorded by horizontal LVDTs were almost negligible in all the specimens until $V_{R,max1}$ was reached. After the formation of the critical shear crack, the interface between concretes was usually cracked, what

caused a discontinuity in the strains plane. Thus the calculation of horizontal shear by this method was not possible after $V_{R,max1}$.

3.3. Crack pattern observations

Fig. 9 shows the crack patterns of the tested beams grouped according to section type. In this figure, the cracks observed until shear's first local maximum $V_{R,max1}$ are represented by a thin black line; those cracks that appeared immediately after $V_{R,max1}$ are denoted by a thick black line; orange depicts the cracks observed until shear's second local maximum $V_{R,max2}$; blue indicates the cracks that appeared after $V_{R,max2}$ with definitive specimen collapse.

3.3.1. Cracking at $V_{R,max1}$

The first cracks noted in all the specimens, regardless of their cross-sectional shape, were bending cracks, which rose from the bottom of the beam (see A in Fig. 10a). As load increased, some of these vertical cracks extended to the neutral axis (B in Fig. 10a) by roughly following a quasi-vertical direction, just as Fernández *et al.* stated [24]. These cracks became flatter on a second branch of the crack above the neutral axis [1] to thus form diagonal shear cracks (branch C in Fig. 10a). This behaviour occurred similarly for the rectangular and T-shaped beams until the crack reached the plane where the cross-sectional width increased. When shear's first local maximum was reached, the specimens' crack pattern was similar to that shown in Fig. 10a.

3.3.2. Cracking after $V_{R,max1}$

Once shear's first local maximum had been reached, load drop took place due to entire diagonal critical crack tip development (D in Fig. 10b). The shape of the critical crack in the compression chord showed differences from one beam to another.

In monolithic beams with rectangular cross-sections, two different behaviours were observed in critical crack tip development. In some specimens, the critical crack crossed the beam depth and left a very tight compression chord, or even crossed it completely until the extreme compression fibre of the cross-section was reached (described by Zararis as the splitting of concrete in the compression chord [25]). An example of this crack pattern was observed in specimen NOP3A1 (Fig. 9a). In other specimens, the critical crack finished well below the load plate, and left uncracked a considerable depth of the compression chord, as seen in specimen NOP2A1 (Fig. 9a). In the rectangular composite beams, an interface existed between concretes that could deviate the direction of the critical crack by forcing it to develop through the interface before accessing the slab (see Fig. 9c and the "Cracking mode" column of Table 2).

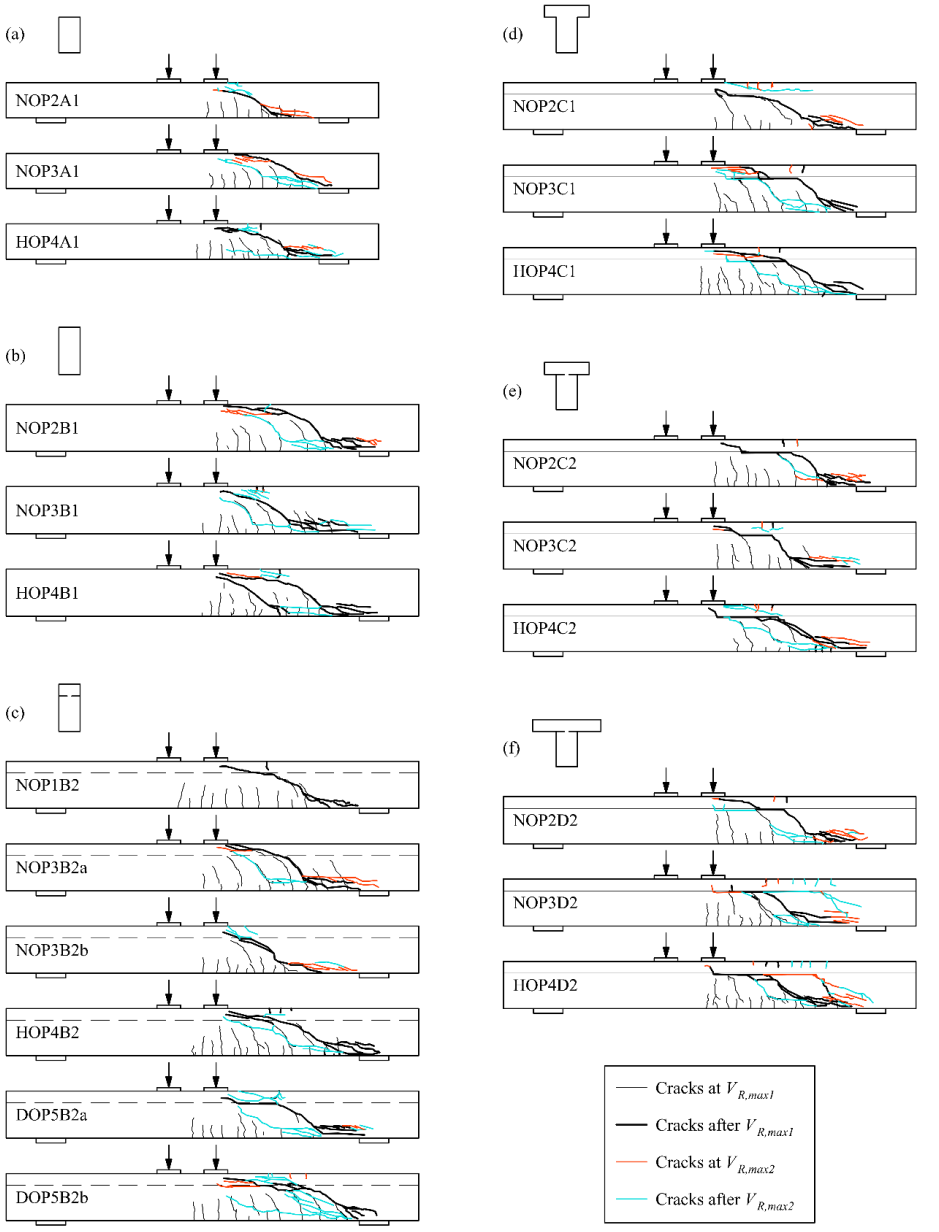

Fig. 9. Crack patterns of the test specimens in different test stages grouped according to section type: (a) A1; (b) B1; (c) B2; (d) C1; (e) C2; (f) D2.

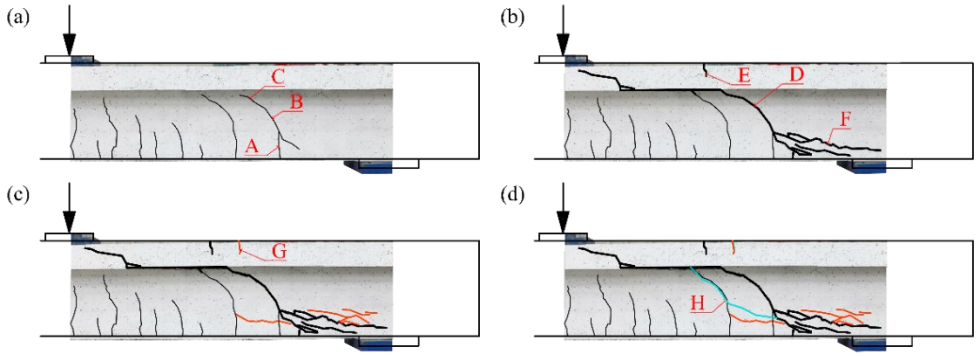

Fig. 10. Example of crack pattern of specimen NOP2C2 at different load stages: (a) at $V_{R,max1}$; (b) after $V_{R,max1}$; (c) at $V_{R,max2}$; (d) after $V_{R,max2}$.

In the T-shaped monolithic beams, a discontinuity in the cross-section width modified the direction of the critical crack by forcing it to develop along the plane in which the section width changed. This behaviour has been already observed in previous research works with T-shaped monolithic beams without web reinforcement [1], where the two following crack pattern types were noted. Firstly, the crack pattern with a delamination crack [16], in which the critical crack developed horizontally when reaching the plane in which the beam width changed and developed along it over a long stretch before accessing the T-shaped beam head. For example, specimen NOP2C1 displayed this crack pattern (Fig. 9d). Secondly, the crack pattern with a diagonal crack at the head [15,16], in which the critical crack at the web crossed the plane in which beam width changed and continued as an inclined crack in the head, as seen in specimen HOP4C1 (Fig. 9d). In both crack patterns, the appearance of vertical cracks starting from the starting on top of the head was observed, which indicates head bending (E in Fig. 10b). In the T-shaped composite beams, the interface forced the critical crack to develop along the plane in which the section width changed at a longer distance (Fig. 9e-f).

In all the specimens, the formation of different longitudinal cracks was observed at the level of the tension longitudinal reinforcement after the entire critical shear crack had developed. These cracks developed from the end of the critical crack to the support of the element (see F at Fig. 10b).

3.3.3. Cracking at $V_{R,max2}$

Critical shear crack development did not lead to the collapse of all the specimens. Some beams underwent increased load, with a second local maximum in shear. The gradual formation of new cracks took place (Fig. 10c).

Having reached shear's second local maximum, almost all the beams presented new longitudinal cracks at the tension longitudinal reinforcement level and the length of

the existent ones grew (see Fig. 9). In some specimens, the length of the diagonal critical crack tip increased.

In all the T-shaped beams, new bending vertical cracks appeared at the top of the slab (G in Fig. 10c). This was also observed in the rectangular composite beams in which the interface substantially modified the direction of the critical shear crack, as seen in specimen DOP5B2b (Fig. 9c).

In the beams whose shear's second local maximum was very high, such as specimens NOP3D2 and HOP4D2 (Fig. 8d), a new crack developed along the interface in the direction towards the support (Fig. 9f).

3.3.4. Cracking after $V_{R,max2}$

After reaching the shear's second local maximum, specimens collapsed. In many tested beams, an already existent diagonal shear crack opened, which differed from the critical crack and was closer to the point load than the latter (H in Fig. 10d), and multiple longitudinal cracks formed at the tension longitudinal reinforcement level. By way of example, see beam NOP2B1 in (Fig. 9b). In other specimens, the crushing of concrete at the compression chord was observed. This happened in those beams in which the compression chord had remained almost intact after critical shear crack had formed (e.g. beams NOP2A1, HOP4A1 and NOP3B2b). In other specimens like NOP2C1 and HOP4C2, diagonal slab cracking occurred. A combination of these crack patterns was also observed in some beams; that is, the opening of another diagonal crack and the crushing of concrete in the compression chord, as seen in beams NOP3B1 and DOP5B2a. All these crack patterns are observed at Fig. 9.

Specimens NOP3D2 and HOP4D2 collapsed with the opening of the crack that appeared at the interface in the direction towards the support (see Fig. 9f).

3.4. Failure modes

The potential shear-carrying mechanisms that can be run to transfer shear force in the beams without stirrups were described by Fernández Ruiz, Muttoni and Sagaseta [24,26] among others. By considering the crack pattern observed in the beams herein tested, three phases were identified depending on the main shear-carrying mechanisms that resisted shear force: phase 1, until $V_{R,max1}$ was reached; phase 2, between $V_{R,max1}$ and $V_{R,max2}$; phase 3, after $V_{R,max2}$. Fig. 11 shows the three schematic strut-and-tie representations associated with these three phases.

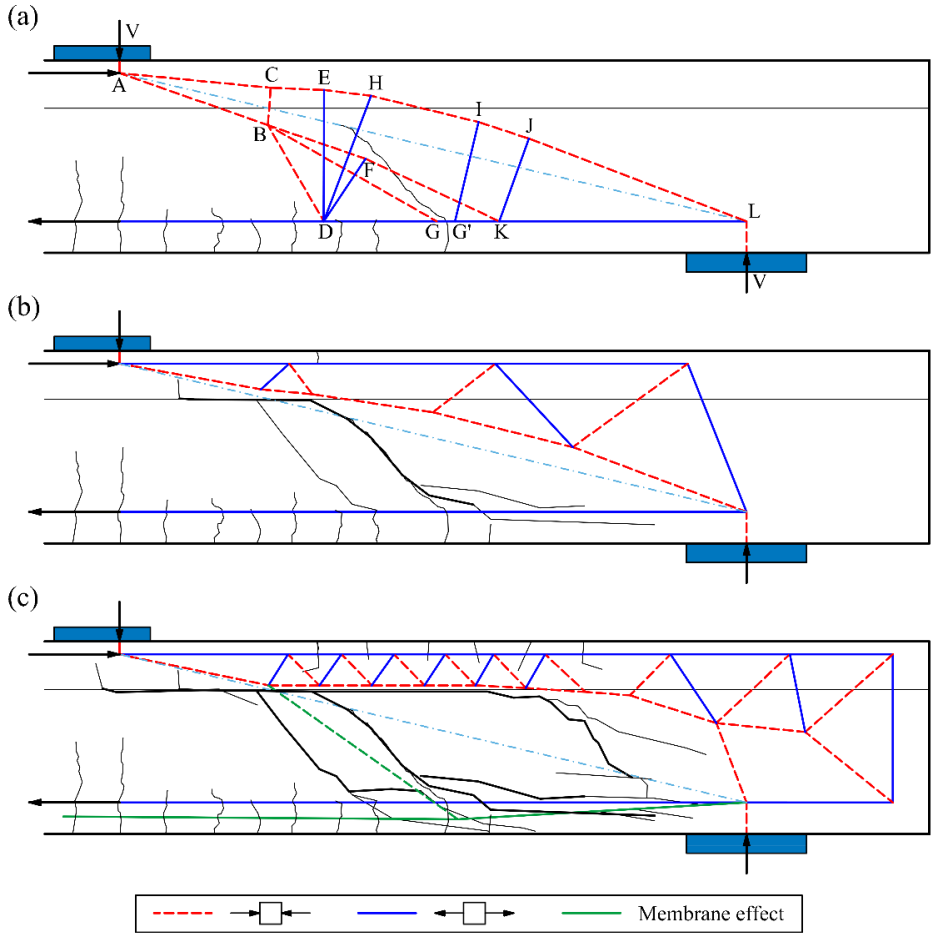

Fig. 11. Strut-and-tie models of the shear transfer mechanisms observed, drawn on specimen NOP3D2: (a) development of diagonal cracks; (b) after critical shear crack formation; (c) collapse.

3.4.1. First phase: development of diagonal cracks

A first phase was observed until shear's first local maximum was reached, when the crack pattern was like that of specimen NOP3D2 shown in Fig. 11a, with a shear-deflection relation depicted in Fig. 8d.

Fig. 11a shows the strut-and-tie model that explains the load paths in this phase. A portion of shear force was transferred across the critical shear crack, mainly by aggregate interlock (strut FK), residual tensile stresses (tie DH) and dowel action (G-G'). The remaining shear force was transferred by the inclination of the compression strut (strut EH) above the critical shear crack tip.

The behaviour of all the tested specimens in this first phase was similar, regardless of them having a rectangular cross-section or a T-shaped section.

In this phase, the strain gauges located on top of beams showed compression strain. Immediately before the shear's first local maximum was reached, these gauges showed a slight compression strain reduction at the same time as the new diagonal cracks appeared on the beam's web. This indicates a change towards other shear-carrying mechanisms.

3.4.2. Second phase: after critical shear crack formation

After reaching shear's first local maximum, the critical shear crack extended towards the applied load (Fig. 11b) and its width increased. A major load drop was recorded. Critical shear crack development disabled the cantilever action of the "tooth" (strut BD and tie DE in Fig. 11a) and the increasing crack width reduced the residual tension stress (tie DH in Fig. 11a), which made these shear-carrying mechanisms negligible.

In the T-shaped monolithic beams, the critical shear crack developed along the horizontal plane connecting the web and head of the beam (see Fig. 9d). In the rectangular composite beams, the interface between concretes could become a weak plane and, consequently, deviate crack development along that plane (e.g. in specimens NOP3B2b and DOP5B2a shown in Fig. 9c). In the T-shaped composite beams, the interface between concretes always deviated the critical crack direction (see Fig. 10b and Fig. 11b).

The increase in the critical crack width reduced the aggregate-interlock action, but increased the dowel action of the tension longitudinal reinforcement. However, the potential dowel action increment was truncated by the appearance of the longitudinal cracks at this longitudinal reinforcement level (Fig. 11b). Furthermore, the aggregate interlock and dowel actions reduced as new cracks (Fig. 11b) appeared in the tension zone above the shear critical crack (concrete ties G'I and KJ in Fig. 11a).

In this second phase, vertical cracks starting from the top of the slab appeared and the strain gauges placed on the upper side of the slab recorded tensile strains, which indicated the existence of tension stresses on the element's upper side. These observations evidenced the existence of an upper strut-and-tie system (Fig. 11b), which made the arching action over the critical shear crack possible. As Swamy *et al.* observed [16], specimens acted as a tied arch. This mechanism allowed shear force to increase until the shear's second local maximum $V_{R,max2}$ was reached.

3.4.3. Third phase: collapse

This phase is identified as specimens' failure after reaching the shear's second local maximum. Different behaviours were observed in this phase depending on the

critical shear crack shape. Nonetheless, they can all be described by loss of the shear transfer mechanisms' capacity due to the arching action, with a clear loss of dowel action. However, the great deflection of the longitudinal tie allowed a membrane effect to resist a portion of shear force (Fig. 11c).

The specimens' shear resistance capacity in this phase was governed mainly by the capacity of the arching action, which depended on the degradation level of the compression chord. In some specimens, the critical shear crack caused the splitting of concrete in the compression chord: it crossed almost its entire depth or narrowed it. This happened, for example, in specimens NOP2B1 and NOP2D2 (Fig. 9). In such cases, the arching action did not allow high shear's second local maximum values to be obtained.

Conversely in other specimens, load could flow over the critical shear crack in the direction to the support. The collapse of these beams was due to the crushing (i.e. DOP5B2b) or splitting (i.e. HOP4C2) of the concrete of the compression chord after major aching action took place thanks to the large enough depth of the compression chord that left the critical shear crack. These beams showed high over-strengths at shear's second local maximum. This behaviour was observed in, for example, specimens NOP2A1 and NOP2C1 (Fig. 9).

Specimens NOP3D2 and HOP4D2 had the highest over-strengths of the tested beams (Fig. 8d). In these cases, the compression chord was almost intact and a crack developed along the interface in the direction to the support. This effect forced the elbow-shaped strut to move towards the support, and to occupy a position at which it was unable to resist the existing shear force at the span. This led these elements to fail (see Fig. 11c).

As seen above, the existence, or not, of a shear's second local maximum greater than the shear's first local maximum in the beams of this experimental programme depended on: the critical shear crack shape, mainly at the compression chord; the presence of an interface between concretes; the existence of a geometrical discontinuity at the section width. However, not all the specimens with the same cross-section characteristics developed a second local maximum greater than the first one. Consequently, as no behaviour pattern could be defined, it was unsafe to take the absolute maximum as the element's shear strength. This measure was also adopted by Kim *et al.* in those specimens presenting an over-strength after diagonal tension cracking [2].

In the present study, in order to verify the design models, and based on structural safety criteria, specimens' shear strength was defined as the first shear's local maximum.

3.5. Influence of test parameters on shear strength

3.5.1. Contribution of a cast-in-place concrete slab

To study the contribution to shear strength of the cast-in-place concrete slab on top of the beams, the elements with section type A1 were compared to those with section type B2. This comparison was made by fabrication batches to avoid the influence of concrete strength variable. In Fig. 12, the experimental shear strength results are classified by section type and distinguishing the beams according to the fabrication batches.

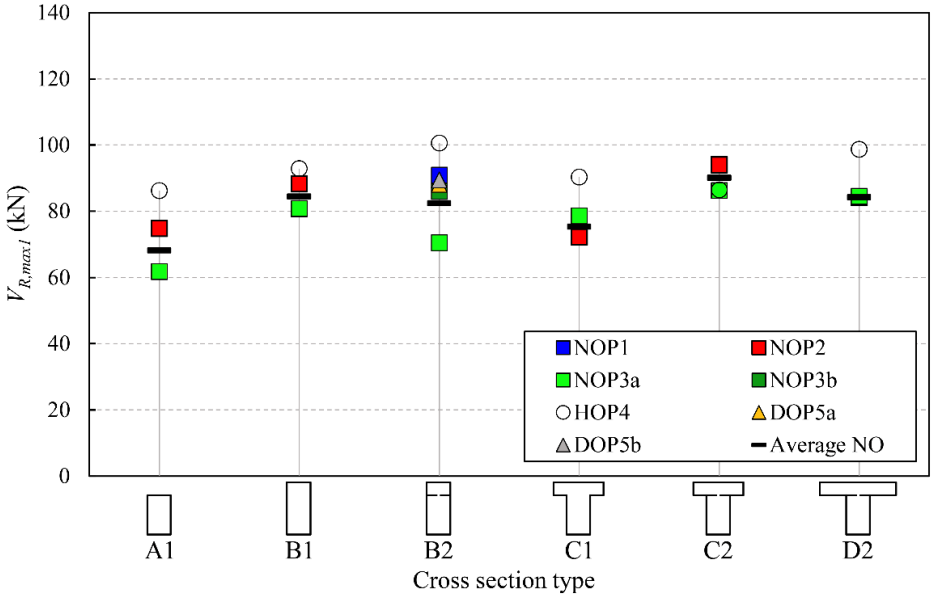

Fig. 12. Experimental shear strength of all the tested specimens corresponding to shear's first local maximum.

The shear strength of the B2 beams was, on average, 23% higher than that of the A1 beams of the same batch. This result was similar to that of the B1 beams compared to the A1 beams (19%). This increase in both cases was less than that of their respective effective depths (33%). Consequently, the slab did not increase the shear strength of the element in the same quantity as the effective depth increased. This minor shear strength increment in monolithic beams can be explained exclusively by the size effect, as the other parameters were identical. Since B1 and B2 beams' shear strengths were similar, the size effect could be also the main cause of this minor increment of the shear strengths of the B2 composite beams with

respect to the A1 beams and not the weakness of the bond on the interface plane between concretes.

As Halicka pointed out [14], if the shear force that initiates interface cracking is lower than the shear force that leads to diagonal cracks appearing, the delamination of the interface and thus, the horizontal shear failure, will take place prior to shear failure. As specimens were designed to avoid horizontal shear failure (Rueda *et al.* [19]), the cast-in-place concrete slab had the same effect as adding depth to the shear area, although interface cracking occurred.

3.5.2. Existence of an interface between concretes

The influence of an interface between concretes in specimens' shear strength was studied by comparing the behaviour of the B1 beams with the B2 beams of the same fabrication batch, and the C1 beams with the C2 beams of the same batch.

The B2 beams were expected to have intermediate shear strength between those of beams A1 and B1 because of the weakness of the interface between both concretes. However on average, the shear strength of beams B1 and B2 was similar (Fig. 12). In particular, specimens NOP3B2b and HOP4B2 had higher shear strengths than specimens NOP3B1 and HOP4B1, respectively. On the contrary, beam NOP3B2a presented lower shear strength than beam NOP3B1. Regarding the T-shaped beams, the specimens made of two concretes, C2, had a slightly higher shear strength than monolithic beams C1 when the average values of $V_{R,max1}$ for sections C1 and C2 were compared. However, this was not a regular behaviour. In particular, this over-strength was observed in the beams of batches NOP2 and NOP3, whereas a slightly decreased strength was noted in batch HOP4 (Fig. 12).

In the rectangular composite beams, the over-strength of the composite specimens was associated with the modification of the critical shear crack path, which spread along the interface plane because of its weakness. This modification changed the contribution of shear-transfer mechanisms and, as a result, shear resistance capacity increased. However, specimens NOP3B2a and NOP3B2b were assumedly identical, but had different crack patterns (Fig. 9), which evidences the uncertainty of the critical shear crack path shape.

In the T-shaped beams, the critical shear crack path always deviated due to the geometrical discontinuity in section width. In the composite T-shaped beams, the crack spread along the interface over a longer length.

It can be generally concluded that if a portion of the critical shear crack path developed along the interface, the composite beam had a higher shear strength than the monolithic beam. This could be due to the greater compression chord depth as the existence of an interface postponed the crack entering the slab, what left a wider concrete chord in both the rectangular and T-shaped beams.

3.5.3. Flange width

In order to study the influence of flange width on shear strength, the beams with section type B were compared to their homologous beams with sections C and D. From these comparisons, the following findings were drawn:

a) The flanges of the T-shaped monolithic and composite beams with section type C did not entail any increased shear strength compared to their homologous rectangular beams, neither when comparing shear's first local maximum nor its second one (see Table 2).
b) Shear's first local maximums of beams type D2 were comparable to those of sections B2 and C2 (Fig. 12). However, they showed higher shear's second local maximums because the critical shear crack path allowed a considerable arching action mechanism to develop. Thus specimen NOP3D2 showed an over-strength higher than 40% compared to sections B2 and C2 of the same batch, and specimen HOP4D2 displayed an over-strength over 15%.
c) Regarding crack patterns, a great similarity was observed between the beams with section types C2 and D2 (Fig. 9). When comparing fabrication batches, the critical crack of both beams had the same inclination and position in the principal span, regardless of flange width. The only difference between them laid in the critical crack developing in the compression chord: in some beams, it completely crossed it, but did not in other beams, which allowed the subsequent arching action mechanism to develop.

In view of the observed behaviours, it was verified that shear's first local maximum, which corresponded to diagonal beam cracking, was governed principally by the shear transfer actions that occurred at the beam's web: aggregate-interlock action and dowel action. The compression chord-related actions were not so relevant in this stage. Hence the rectangular and the T-shaped beams had similar shear strength upon the first local maximum. Consistently with Kani's predictions [17], high tension longitudinal reinforcement ratio ρ_l brought about a marked increase in dowel action, as well as increased aggregate-interlock action due to a crack widths reduction. This could imply a reduction in the contribution of flanges to shear strength, as Ayensa *et al.* observed [27].

At collapse, behaviour was almost entirely governed by the arching action (cantilever mechanism). The specimens in this experimental programme showed that the development, or not, of an over-strength thanks to flanges depended on how the critical shear crack altered the compression force path, as explained in Section 3.4 of this paper. For example, after critical shear crack formation, the strength of specimen NOP2C1 could increase, but HOP4C1 could not, existing clear differences in the shape of their shear critical cracks (Fig. 9). Swamy and Qureshi [28] also observed the possibility of having a second stage in the shear strength of the T-shaped beams that may, or may not surpass, that at shear cracking.

Different results are found in the literature about the comparison of the shear strengths between the rectangular and T-shaped beams without web reinforcement. Authors like Placas and Swamy *et al.* [15,16] observed the same failure type and at the same load of T-shaped beams and their homologous rectangular beams in beams with a similar shear span-effective depth ratio to that in this programme. In Placas [15], beams with a/d = 3.4 and ϱ_l = 1.46% were tested, while in Swamy *et al.* [16], beams with a/d = 4.0 and ϱ_l = 1.70% for rectangular beams or ϱ_l = 2.67% for T-shaped beams were used. Other authors like Kotsovos [29] obtained higher strengths in T-shaped beams, apparently in a second local maximum after diagonal cracking in beams with a/d = 3.3 and ϱ_l = 5.20%.

In this experimental programme, the T-shaped beams that had an over-strength in shear capacity showed that the flange width in beam type C (once the slab depth) was not wide enough to develop a considerable over-strength by arching action, as their shear strength was similar to that one in the rectangular beams. However, flange width in beam type D (twice the slab depth) was wide enough. It should be highlighted that this over-strength was possible thanks to the transverse reinforcement provided in the slab, which allowed shear transfer through flanges. Without this mesh, failures caused by the shear between web and flanges would have been observed [17].

3.5.4. Concrete strength

In the composite beams, the series HO specimens were compared to their series NO homologous specimen to analyse the influence on shear strength of using different compressive concrete strengths for both beam and slab.

In most cases, the specimens with a high-strength concrete (HSC) in the beam displayed slightly more shear strength (4% on average) than the beams made of normal-strength concrete (NSC), as seen in Fig. 12. The monolithic beams made of HSC had higher strength than the beams made of NSC. In these cases, as HSC was present over the entire concrete section, it was not possible to conclude whether this higher strength was due to the presence of HSC in the beam's web or at the compression chord. With the composite beams, the HO beams also showed higher strength than those of series NO (except HOP4C2, with a similar strength to NOP2C2 and NOP3C2, what could only be explained by the variability associated to concrete's shear behaviour uncertainties). As NSC was present in the slabs of both series, it was deduced that, for the specimens of this experimental programme, diagonal tension cracking was governed mostly by the web's concrete strength. Hence the greater the web's concrete strength, the higher the shear at which the diagonal cracking occurs.

Shear's second local maximum was analysed by studying the beams in which shear's second local maximum was higher than the first one. When normalising specimens'

shear strength by the square root of the compressive strength of the slab's concrete, the beams with the same cross-section type had the same ratio. The beams D2 were particularly remarkable, as the dispersion of shear's second local maximum was considerable. This result is shown in Fig. 13. It was deduced, therefore, that the arching action mechanism was governed mostly by the slab's concrete strength, as previous authors have stated [2]: shear capacity increases with the slab's concrete strength.

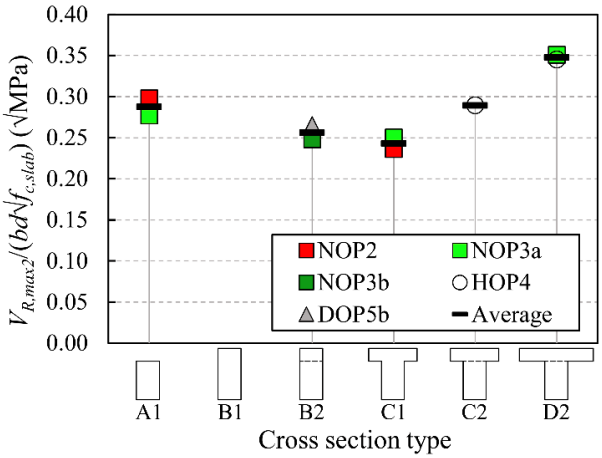

Fig. 13. Normalised shear strength of specimens in which shear's second local maximum was higher than shear's first local maximum.

3.5.5. Differential shrinkage

As explained in Section 2.3, the slab's concrete of the specimens in series DO was cast when the beam's shrinkage was considered stabilised. After approximately 70 testing days, the measurements taken by the instrumentation started to achieve an asymptotic behaviour in relation to time, after which time shrinkage was limited. This asymptote was reached at an average strain of concrete gauges of 0.7‰ and an average strain of internal steel gauges of 0.12‰. The ambient temperature and that measured by the internal thermocouples was around 26ºC throughout testing. The average ambient humidity was 64%.

The beams of series DO were compared to their homologous beams in series NO to study how the differential shrinkage between different aged concretes would influence shear strength.

In the series DO specimens, the interface between concretes clearly modified the direction of the critical crack by forcing it to propagate along the interface over a considerably long stretch (see Fig. 9c). In fact this behaviour allowed specimen

DOP5B2b to display a subsequent over-strength by the arching action mechanism. On the contrary in the beams of series NO, the interface deviated the critical shear crack over a short stretch (specimens NOP1B2 and NOP3B2b) or it even did not modified it (specimen NOP3B2a). This observed behaviour in the beams of series DO can be explained by the shrinkage stresses that generate when there is a difference in the shrinkage of the composite beam's concretes [18].

Regarding specimens' shear capacity, when shear's first local maximums were observed (see Fig. 12), the shear strength of series DO was similar to the shear strengths obtained in the beams B2 of series NO.

As a result of these observations, it was deduced that the use of different aged concretes at the beam and the slab modified the cracking pattern of the composite beams, but did not significantly change the vertical shear strength of the specimens. However, it is not possible to generalize this conclusion to other beam geometries and weather conditions. A more detailed experimental study should be conducted in that case.

4. Comparison of test results with existing code provisions

4.1. Vertical shear strength

Fig. 14 shows the relation between the experimental shear's first local maximum, and the shear strength predicted by design codes ($V_{R,max1}/V_{R,code}$) for the monolithic (A1, B1 and C1) and composite (B2, C2 and D2) specimens. The considered codes were EC2 [11] (Fig. 14a), ACI 318-19 [6] (Fig. 14b), and MC-10 [10] at its two approximation levels for the beams without web reinforcement: Level I (Fig. 14c) and Level II (Fig. 14d). The different codes' shear formulations are gathered in Table 4. The tested average values of the materials were used. In all cases, the partial safety factor for concrete γ_c and steel material properties γ_s was 1.0, and the used concrete section width (b) was the web's width for all the cross-sectional shapes as codes disregard the contribution of flanges.

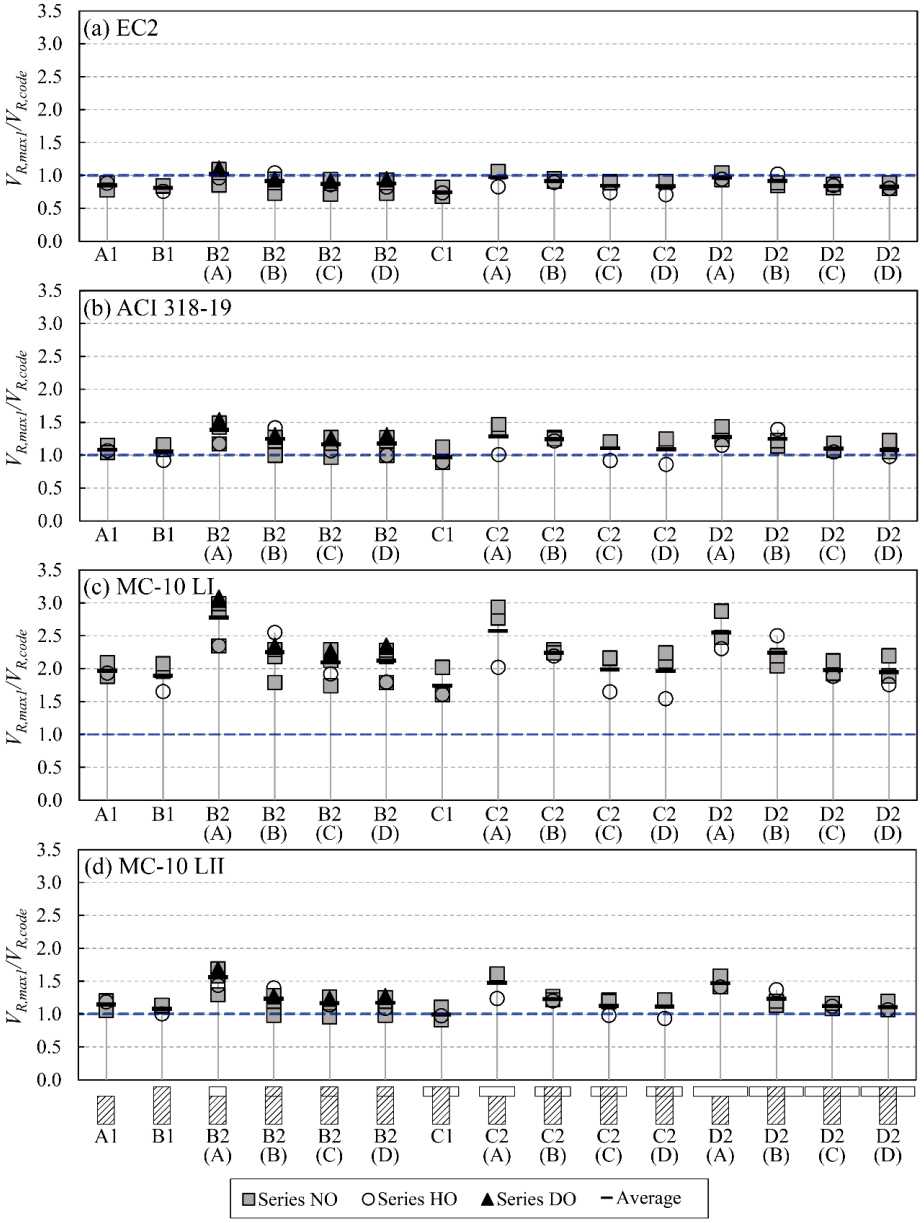

Fig. 14. Relation between the experimental shear strength and the predicted shear strength by design codes for all the tested specimens: (a) EC2 [11]; (b) ACI 318-19 [6]; (c) MC-10 Level I [10]; (d) MC-10 Level II [10].

Table 4. Codes' shear capacity formulations for beams without web or interface reinforcement.

Code	Vertical shear strength equations (kN)	Horizontal shear strength equations (MPa)
EC2 [11]	$V_{R,code} = C_{R,c}k(100\rho_l f_c)^{1/3}bd10^3 \geq \nu_{min}bd10^3$ where $C_{R,c} = 0.18$; $k = 1 + \sqrt{\frac{200}{1000d}} \leq 2.0$; $\nu_{min} = 0.035k^{3/2}f_c^{1/2}$	$\tau_{R,code} = c_a f_{ct} + \mu\sigma_n \leq 0.5\nu f_c$ where $\nu = 0.6\left(1 - \frac{f_c}{250}\right)$ See c_a and μ values at section 6.2.5(2) [11]
ACI 318-19 [6]	$V_{R,code} = 664.3\lambda_s\lambda\rho_l^{1/3}\sqrt{f_c}bd \leq 415.2\lambda\sqrt{f_c}bd$ where $\lambda_s = \sqrt{\frac{2}{1+3.94d}} \leq 1.0$; λ=1.0 for normalweight concrete	$\tau_{R,code} = 0.55$
MC-10 Level I [10]	$V_{R,code} = k_v\sqrt{f_c}zb10^3$ (if $f_c \leq 70$ and $d_g \geq 0.010$) where $\sqrt{f_c} \leq 8$; $k_v = \frac{0.18}{1+1.25z}$	$\tau_{R,code} = c_a f_{ct} + \mu\sigma_n \leq 0.5\nu f_c$ where $\nu = 0.55\left(\frac{30}{f_c}\right)^{1/3} < 0.55$ See c_a and μ values at tables 7.3-1 and 7.3-2 [10]
MC-10 Level II [10]	$V_{R,code} = k_v\sqrt{f_c}zb10^3$ where $\sqrt{f_c} \leq 8$; $k_v = \frac{0.4}{1+1500\varepsilon_x}\frac{1.3}{1+k_{dg}z}$; $\varepsilon_x = \frac{1}{2E_s\rho_l bd}\left(\frac{M_{Ed}}{z} + V_{Ed}\right)$; $k_{dg} = 1$ (if $f_c \leq 70$ and $d_g \geq 0.016$); $k_{dg} = \frac{32}{16+1000d_g}$ (if $f_c \leq 70$ and $d_g < 0.016$); $k_{dg} = 2$ (if $f_c > 70$);	
All variables but f_c, f_{ct} and σ_n in SI units (f_c, f_{ct} and σ_n in MPa).		

In all the specimens the horizontal shear limit state was experimentally verified because all the failures were brought about diagonal cracking. Therefore, according to the indications of EC2 and ACI 318-19 about composite beams' shear strength, it was possible to evaluate the composite beams as elements in which the slab's depth formed part of the shear strength area. Nonetheless, in this Section, the composite specimens' shear strength was calculated considering that only the beam contributed to resist shear (Case A), in order to compare this result with the entire composite member's shear strength. To calculate the composite specimen's shear strength, considering the contribution of the slab's depth, the two calculation methods that ACI 318-19 proposes for composite members where the specified concrete compressive strength, unit weight, or other properties of different elements vary were used: using the properties of the element that result in the most critical value of shear strength, in which case $f_{c,min}$ was used (Case B); or using the properties of the individual elements, in which case the weighted average of the concrete strengths of the beam and the slab $f_{c,wa}$ was used (Case C), as it was observed in Kim *et al.* [2]. Additionally, the entire composite specimen's effective depth and the compressive strength of the beam's concrete were used (Case D). The four cases were calculated

with all the considered codes (EC2, ACI 318-19 and MC-10) for comparison (see Fig. 14).

Table 5 shows the following statistical indicators of the relation $V_{R,max1}/V_{R,code}$ calculated with each code for the 9 monolithic beams of this experimental programme: mean value, coefficient of variation CV (calculated as the ratio of the population standard deviation to the mean), minimum and maximum values, and number of unsafe results of 9 beams. Table 6 shows the same statistical indicators for each code and for Cases A, B, C and D of the 12 composite specimens.

Table 5. Statistical indicators of the relation $V_{R,max1}/V_{R,code}$ for the 9 monolithic specimens.

Code	EC2	ACI 318-19	MC-10 LI	MC-10 LII
Mean	0.81	1.03	1.87	1.08
CV (%)	8.06	9.84	9.97	8.57
Minimum	0.69	0.89	1.60	0.91
Maximum	0.89	1.15	2.09	1.20
No.unsafe	9	3	0	2

Table 6. Statistical indicators of the relation $V_{R,max1}/V_{R,code}$ for the 12 composite specimens.

Code	EC2				ACI 318-19				MC-10 LI				MC-10 LII			
Case	A	B	C	D	A	B	C	D	A	B	C	D	A	B	C	D
Mean	1.00	0.92	0.86	0.86	1.33	1.25	1.13	1.13	2.67	2.25	2.04	2.04	1.52	1.23	1.15	1.15
CV (%)	9.04	8.40	7.81	9.04	12.67	8.49	9.94	12.67	12.67	8.49	9.94	12.67	9.67	8.45	8.07	9.52
Minimum	0.83	0.73	0.72	0.71	1.01	0.99	0.91	0.86	2.02	1.79	1.65	1.54	1.24	0.98	0.96	0.94
Maximum	1.11	1.04	0.94	0.95	1.54	1.41	1.27	1.31	3.09	2.55	2.29	2.36	1.69	1.40	1.26	1.28
No.unsafe	5	10	12	12	0	1	2	4	0	0	0	0	0	1	2	2

As seen in Table 5, ACI 318-19 and MC-10 LII gave quite accurate estimations of the monolithic elements' shear strength (mean values of 1.03 and 1.08, respectively). When comparing the results for monolithic and composite specimens (Table 5 and Table 6), the codes better estimated the shear strength of the monolithic beams; thus, the composite specimens' shear strength was underestimated by the codes' formulations using the four perspectives A, B, C and D (except for EC2, that gave, in most cases, unsafe results).

For the composite beams of series NO and DO, the models gave results that lay more on the safety side when only the beam was used to calculate shear strength (Case A) instead of using both the beam and slab (Cases B, C and D), as seen in Fig. 14. In the composite beams of series HO, Case B gave safer results than Cases A, C and D when codes EC2, ACI 318-19 and MC-10 LI were employed given the use of the lower f_c of the slab in the calculations. Cases C and D gave the same mean values for all the codes, but with a higher coefficient of variation in Case D.

EC2 gave a very unsafe shear strength estimation in the monolithic beams. In the composite specimens, only Case A gave a good estimation, although with several unsafe results (see Table 6). Thus, using the entire depth of the composite beam gave an unsafe estimation in Cases B, C and D. It should be noted that EC2 is currently undergoing a revision process in which the shear strength formulation for members not requiring design shear reinforcement is particularly being revised.

ACI 318-19 well estimated the monolithic specimens' results with a low coefficient of variation (9.84%). For composite specimens, Case B gave a better estimation than Case A, with almost none unsafe results (1 beam). When using the $f_{c,wa}$ in the calculations (Case C) the estimation was even better (the mean value of $V_{R,max1}/V_{R,code}$ was 1.13) and still with few unsafe results (see Table 6). Case D, that is using the beam's f_c, gave the same mean value as Case C, but more scattered and with more unsafe results. This code showed the best approximation of the shear strengths to the actual ones, staying on the safety side.

MC-10 LI provided a very simple formulation, but gave very safe results for both monolithic and composite specimens. MC-10 LII fitted the results much better than LI. The monolithic beams' shear strength prediction by MC-10 LII was quite accurate. For composite specimens, Case C gave a good estimation with a low coefficient of variation (8.07%) and a few unsafe results (2 beams).

4.2. Horizontal shear strength

Table 7 shows the statistical indicators of the relation between the experimental horizontal shear stress at the interface $\tau_{R,exp}$ concurrent with $V_{R,max1}$ and the predicted horizontal shear stress by design codes $\tau_{R,code}$ for the composite beams of this experimental programme. Just the composite beams in which interface cracking took place at $V_{R,max1}$ were included in this analysis. Thus, beams NOP3B2a and HOP4B2 were excluded (see the "Cracking mode" column of Table 2). Specimen NOP3D2 was not included as the strain gauges for calculating the experimental horizontal shear stress failed. The used codes were: EC2 [11], ACI 318-19 [6] and MC-10 [10]. Their horizontal shear strength equations for interfaces without reinforcement crossing it are presented in Table 4. No unsafe results were obtained with any employed code.

Table 7. Statistical indicators of the relation $\tau_{R,exp}/\tau_{R,code}$ for the composite beams of this experimental programme with interface cracking (9 specimen. NOP3D2 not included: failure of strain gauges).

Code	EC2	ACI 318-19	MC-10
Mean	2.36	3.54	1.88
CV (%)	14.95	16.37	14.95
Minimum	1.81	2.70	1.45
Maximum	2.96	4.70	2.36

Codes EC2 and MC-10 have a similar formulation based on the Mohr-Coulomb failure criterion. This criterion considers an increase in horizontal shear strength provided by the lowest expected compressive stress resulting from an eventual normal force acting on the interface (σ_n), normally applicable to confined elements (see Table 4). In this case, the normal stresses acting on the interface were neglected, staying on the safety side, although it was known that compression struts crossed the interface along the span. The existence of normal compressive stresses at the interface could increase the horizontal shear strength of the composite beams [2].

The ACI 318-19 formulation has an experimental basis which, for the beams without the minimum interface reinforcement defined by this code, limits the horizontal shear strength at the interface to 0.55 MPa.

In view of the results presented in Table 7, all the models gave a very safe result. When looking at the coefficient of variation, the three used codes presented a similar dispersion for the beams in this experimental programme. EC2 gave more restrictive results than MC-10 because its coefficient for adhesive bond c_a for very rough interfaces is lower. ACI 318-19 presented the greatest dispersion of the used codes: the experimental horizontal shear stresses obtained in the beams were between 1.48 and 2.59 MPa (see Table 2); that is, between 2.7- and 4.7-fold the ACI 318-19 prediction. Therefore, as Kim *et al.* already observed in their composite beams [2], ACI 318-19 underestimates the horizontal shear stress in beams with a very rough interface.

Consequently, it can be stated that codes underestimated the horizontal shear capacity of the concrete at the interface of the composite beams in this experimental programme. Therefore, the codes overestimate the required interface reinforcement to prevent horizontal shear failure. However, the interface's properties can be very different, although the same roughness is sought, as many variables take part: maximum aggregate size, concrete workability at casting, cleanliness of the interface, presence of laitance, concrete curing, differential shrinkage, etc. For this reason, it is justifiable that codes provide very safe expressions.

5. Summary and conclusions

The influence of a cast-in-place slab on the shear strength of composite reinforced concrete beams without web reinforcement was analysed in the present study. For this purpose, an experimental programme with 21 monolithic and composite beams subjected to shear was presented. The failure modes, the influence of an interface between different aged concretes, the cross-section shape, the strengths of the two concretes and the effect of differential shrinkage were analysed. The main conclusions were the following:

1. Most of the tested beams in this test programme underwent two local maximums in shear. The first corresponded to critical shear crack formation. The second local maximum, sometimes higher than the first, was due to the deviation of the compression strut over the critical crack by the arching action mechanism.
2. The arching action's capacity depended on the degradation level of the compression chord after entire critical shear crack formation. In those specimens in which the critical shear crack caused the splitting of concrete in the compression chord, the arching action mechanism was unable to generally reach high second local maximums in shear strength. Conversely, the specimens in which the critical shear crack left intact a wide enough depth of the compression chord developed major arching action.
3. According to the analysed variables, no behaviour pattern was observed on the degradation of the compression chord after critical shear crack formation. Thus it was unsafe to take shear's absolute maximum as the element's shear strength.
4. For the beams in this experimental programme, it was demonstrated that, if the horizontal shear at the interface in the composite beams was verified, the cast-in-place concrete slab would increase the element's shear strength compared to the shear strength of only the beam as the slab was seen to add depth to the shear area.
5. In the composite rectangular beams, the interface between concretes was able to deviate the direction of the critical shear crack by forcing it to propagate along the interface before accessing the slab. In the T-shaped monolithic beams, the geometrical discontinuity in section width also deviated the direction of the critical crack along this weakness plane. In the T-shaped composite beams, the interface was a plane of weakness that always deviated the direction of the critical crack, normally by a longer length than in the T-shaped monolithic beams before entering the slab.
6. Both the rectangular beams and T-shaped beams had a similar shear's first local maximum as shear strength was governed by the shear transfer actions that occurred at the beam's web. Afterwards, some beams developed an over-strength at shear's second local maximum. It was observed that the flange width of beams type C (once the slab's depth) was not enough to develop a high over-strength by the arching action, but did suffice in beams type D, where flange width was twice the slab's depth. These latter beams achieved the highest over-strengths.
7. In most cases, the specimens with HSC in the beam had slightly greater shear strength than the beams made of NSC in both the monolithic and composite beams. This proved that critical shear cracking was governed mostly by the web's concrete strength. Based on the experimental results, it was deduced

that the arching action mechanism was governed mostly by the slab's concrete strength.

8. Differential shrinkage in series DO did not have a significant influence on the vertical shear capacity of the composite beams without shear reinforcement. It influenced, however, the observed cracking pattern, as the critical shear crack developed along the interface in a longer stretch than in the beams with a reduced differential shrinkage, what can be explained by the shrinkage stresses that generate when there is a difference in the shrinkage of the composite beam's concretes. However, this conclusion can not be generalized to other beam geometries and weather conditions, for which a more detailed study should be conducted.
9. As the compliance of the horizontal shear limit state in all the composite specimens was experimentally demonstrated, the shear strength of the composite beams without shear reinforcement was assessed with the codes' formulations in four ways: considering only the beam's shear strength and considering the entire composite beam's shear strength using $f_{c,min}$, the shear strength of the individual elements or the beam's f_c. Except for EC2 [11], which only provided a safe result when only the beam's shear strength was considered, the other codes showed a more accurate result when using the entire composite beam depth. Level I Approximation of the MC-10 [10] presented a simple but very safe formulation. Level II Approximation of the MC-10 [10] and ACI 318-19 [6] gave good results, especially when the sum of the individual elements' shear strengths was used. They were slightly conservative and gave only a few unsafe results. The four considered perspectives in calculating composite elements' shear strength, underestimated the actual shear strengths in comparison with the estimations made for monolithic beams, which were more accurate (except for EC2 [11] that provided very unsafe results for monolithic beams).
10. The codes underestimated the horizontal shear capacity at the interface of the composite beams without reinforcement crossing the interface. Therefore, the required interface reinforcement to prevent horizontal shear failure is overestimated. The codes whose formulation is based on the Mohr-Coulomb failure criterion (EC2 [11] and MC-10 [10]) presented better results than ACI 318-19 [6], but were still far from the actual horizontal shear strength.

The experimental programme carried out in this research work contributes to increase the number of existent experimental tests of composite beams, which are necessary to improve current codes. However, in order to delve into the precast concrete construction field and the cast-in-place slab contribution to shear strength, further research in precast beams with web reinforcement and different cross-sectional shapes should be conducted.

Acknowledgements

This research has been supported by: the Spanish Ministry of Science and Innovation through Research Project BIA2015-64672-C4-4-R and RTI2018-099091-B-C21-AR; the Regional Government of Valencia through Project AICO/2018/250; the European Union with FEDER funds. The experimental programme was developed in the Laboratory of Concrete of the Institute of Concrete Science and Technology (ICITECH) of the Universitat Politècnica de València (UPV) with concrete supplied by Caplansa. The Spanish Ministry of Science and Innovation supported Lisbel Rueda through grant BES-2016-078010.

References

[1] Ribas González CR, Fernández Ruiz M. Influence of flanges on the shear-carrying capacity of reinforced concrete beams without web reinforcement. Struct Concr 2017. https://doi.org/10.1002/suco.201600172.

[2] Kim C-G, Park H-G, Hong G-H, Kang S-M. Shear Strength of Composite Beams with Dual Concrete Strengths. ACI Struct J 2016;113:263–74.

[3] Loov RE, Patnaik AK. Horizontal Shear Strength of Composite Concrete Beams With a Rough Interface. PCI J 1994;39:48–69.

[4] Kovach J, Naito C. Horizontal Shear Capacity of Composite Concrete Beams without Interface Ties. ATLSS Report No. 05-09: 2008.

[5] Fang Z, Jiang H, Liu A, Feng J, Chen Y. Horizontal Shear Behaviors of Normal Weight and Lightweight Concrete Composite T-Beams. Int J Concr Struct Mater 2018;12. https://doi.org/10.1186/s40069-018-0274-3.

[6] ACI Committee 318. Building code requirements for structural concrete (ACI 318-19); and commentary (ACI 318R-19). Farmington Hills: American Concrete Institute; 2019.

[7] Marí A, Cladera A, Bairán J, Oller E, Ribas C. Shear-flexural strength mechanical model for the design and assessment of reinforced concrete beams subjected to point or distributed loads. Front Struct Civ Eng 2014;8. https://doi.org/10.1007/s11709-014-0081-0.

[8] Avendaño AR, Bayrak O. Shear strength and behaviour of prestressed concrete beams. Technical Report: IAC-88-5DD1A003-3, Texas Department of Transportation: 2008.

[9] Shahawy MA, Batchelor B deV. Shear behavior of full-scale prestressed concrete girders: Comparison between AASHTO specifications and LRFD

code. PCI J 1996;41.

[10] Fédération International du Béton (fib). Model Code 2010. Ernst & Sohn; 2012.

[11] CEN. EN 1992-1-1:2004. Eurocode 2: Design of concrete structures - Part 1-1: General rules and rules for buildings. 2004.

[12] Kim C-G, Park H-G, Hong G-H, Kang S-M, Lee H. Shear Strength of Concrete Composite Beams with Shear Reinforcements. ACI Struct J 2017;114:827–37.

[13] Halicka A, Jabłoński Ł. Shear failure mechanism of composite concrete T-shaped beams. Proc Inst Civ Eng Struct Build 2016;169:67–75.

[14] Halicka A. Influence new-to-old concrete interface qualities on the behaviour of support zones of composite concrete beams. Constr Build Mater 2011:4072–8.

[15] Placas A. Shear failure of reinforced concrete beams. Faculty of Engineering of the University of London. Imperial College of Science and Technology, 1969.

[16] Swamy R, Andriopoulos A, Adepegba D. Arch action and bond in concrete shear failures. J Struct Div 1970;96:1069–91.

[17] Kani MW, Mark W. Huggins, Rudi R. Wittkopp. Kani on shear in reinforced concrete. Toronto: University of Toronto, Dept. of Civil Engineering; 1979.

[18] Silfwerbrand J. Stresses and strains in composite concrete beams subjected to differential shrinkage. ACI Struct J 1997;94:347–53.

[19] Rueda-García L, Bonet Senach JL, Miguel Sosa PF. Influence of interface roughness and shear reinforcement ratio in vertical shear strength of composite concrete beams. In: ACHE, editor. VIII Congr. la Asoc. Española Ing. Estructural, ACHE, Santander: 2020.

[20] UNE-EN 12390-3:2020. Testing hardened concrete - Part 3: Compressive strength of test specimens. 2020.

[21] UNE-EN 12390-6:2010. Testing hardened concrete - Part 6: Tensile splitting strength of test specimens. 2010.

[22] UNE-EN 12390-13:2014. Testing hardened concrete - Part 13: Determination of secant modulus of elasticity in compression. 2014.

[23] UNE-EN ISO 6892-1:2017. Metallic materials - Tensile testing - Part 1: Method of test at room temperature. 2017.

[24] Fernández Ruiz M, Muttoni A, Sagaseta J. Shear strength of concrete members without transverse reinforcement: A mechanical approach to consistently account for size and strain effects. Eng Struct 2015;99:360–72. https://doi.org/10.1016/j.engstruct.2015.05.007.

[25] Zararis IP, Karaveziroglou MK, Zararis PD. Shear strength of reinforced concrete T-beams. ACI Struct J 2006;103:693–700.

[26] Muttoni A, Fernández Ruiz M. Shear strength of members without transverse reinforcement as function of critical shear crack width. ACI Struct J 2008;105.

[27] Ayensa A, Oller E, Beltrán B, Ibarz E, Marí A, Gracia L. Influence of the flanges width and thickness on the shear strength of reinforced concrete beams with T-shaped cross section. Eng Struct 2019;188:506–18. https://doi.org/10.1016/j.engstruct.2019.03.057.

[28] Swamy RN, Qureshi SA. An ultimate shear strength theory for reinforced concrete T-beams without web reinforcement. Matériaux Constr 1974;7:181–9. https://doi.org/10.1007/BF02473833.

[29] Kotsovos MD, Bobrowski J, Eibl J. Behaviour of reinforced concrete T-beams in shear. Struct Eng Part B R&D Q 1987;65 B:1–10.

4th PAPER

Details:

Type of paper	Conference paper
Title	*Safety assessment of shear strength current formulations for composite concrete beams without web reinforcement*
Authors	Lisbel Rueda García José Luis Bonet Senach Pedro Francisco Miguel Sosa Miguel Ángel Fernández Prada
Congress	*fib* Symposium 2021: Concrete Structures: New Trends for Eco-Efficiency and Performance
Date	14th-16th June, 2021
City	Lisbon (Portugal)
Status	Accepted and presented
Full reference	Rueda-García L, Bonet JL, Miguel Sosa PF, Fernández Prada MÁ. Safety assessment of shear strength current formulations for composite concrete beams without web reinforcement. In: Fédération Internationale du Béton (fib), editor. Proceedings for the 2021 fib Symposium. Concrete Structures: New Trends for Eco-Efficiency and Performance, Lisbon: 2021, p. 2305–14.

Safety assessment of shear strength current formulations for composite concrete beams without web reinforcement

Lisbel Rueda-García [1, *], José Luis Bonet Senach [2], Pedro Francisco Miguel Sosa [2], Miguel Ángel Fernández Prada [2]

1. Concrete Science and Technology University Institute ICITECH, Universitat Politècnica de València, Valencia, Spain

2. Department of Construction Engineering and Civil Engineering Projects, Concrete Science and Technology University Institute ICITECH, Universitat Politècnica de València, Valencia, Spain

[*]Corresponding author email: lisruega@cam.upv.es

Abstract

Construction with precast concrete elements without web reinforcement and cast-in-place concrete on them to enhance the overall structure's integrity is a widespread practice in building construction. However as these composite elements' vertical shear strength has not been studied in-depth, a clear criterion about cast-in-place concrete's contribution to shear resistance is still a pending matter. The present study intends to reach practical conclusions about the shear strength assessment of composite concrete elements without web reinforcement. To do so, the shear strengths of 36 specimens, provided by existing shear formulations, were compared: 19 specimens tested by the authors, in which the existence of an interface between concretes, the cross-sectional shape and the concrete compressive strengths of the beam and slab were studied; and 17 specimens taken from a previous study about composite elements by Kim et al. (2016). The applied shear formulations were those of EC2-04, Draft 7 of EC2-20, *fib* MC-10, ACI 318-19 and the model proposed by Kim et al. (2016). Firstly, specimens' shear strength was calculated by considering that only the beam resisted shear. Secondly according to ACI 318-19 indications about assessing composite elements' shear strength, the entire composite element's effective depth was used considering the lower of the compressive strengths of the beam's and slab's concretes and the weighted average of the compressive strengths. Additionally, the entire effective depth and the beam's concrete compressive strength were used. Codes formulations were more precise when estimating the monolithic specimens' shear strengths than those of composites. Therefore, the development of an adapted methodology to assess these elements' shear strengths is needed. EC2-20 obtained the most accurate results and gave quite good estimations for composite elements when the entire effective depth and weighted average of the concretes compressive strengths were considered.

Keywords: reinforced concrete, composite beam, precast construction, vertical shear strength, codes' shear formulations.

1. Introduction

Ever since the first prestressed joists began to be manufactured halfway through the last century, the use of precast elements without transverse reinforcement on which a layer of cast-in-place concrete is poured has spread worldwide in the construction world. Given the widespread use of composite elements, the study of their structural behaviour is most important.

In the composite elements field, studies about the horizontal shear strength of the interface between concretes are common (e.g., Loov and Patnaik 1994 [1] or Kovach and Naito 2008 [2]) because reaching the potential bending and shear strength of a composite beam is not possible if the interface strength has been exceeded (Halicka 2011 [3]). However, as the behaviour of these elements subjected to vertical shear forces has not been studied in-depth, a clear criterion about the contribution of the cast-in-place concrete to shear resistance is still a pending matter. This contribution in design is often omitted to, thus, stay on the safety side because shear is a phenomenon with many unknowns. Nonetheless, this contribution exists (Rueda-García et al. 2021 [4]) and its consideration could be favourable for assessing the shear strength of existing structures.

Some current design codes like *fib* Model Code (2010) [5] do not refer to the shear strength treatment of composite elements. Other codes, such as EN 1992 Eurocode 2 (2004) [6] in Section 10.9.3(8) and Draft 7 of the prEN 1992 Eurocode 2 (2020) [7] in Section 13.6.1(5), allow the design of concrete elements with a topping at least 40 mm thick as composite elements if the shear at the interface is verified. ACI 318 (2019) [8] in Section 22.5.4, apart for requiring the horizontal shear strength of the interface to be verified, it also indicates how the shear strength of these composite elements can be calculated: using the properties of the individual elements or the properties of the element that result in the most critical value.

Of all existing experimental studies on composite beams subjected to shear, that carried out by Kim et al. (2016) [9] should be mentioned. It is an experimental study that was performed with 22 monolithic and composite rectangular concrete beams without web reinforcement, with a cross-section of 0.26x0.40 m, shear span-depth ratios a/d of 2.5 and 4.0, and different longitudinal reinforcement ratios (ρ_l = 1.31%, 1.75% and 2.87%). In both monolithic and composite beams, the authors used different concrete classes, e.g. normal-strength concrete (NSC) and high-strength concrete (HSC), with a nominal compressive strength of 24 MPa and 60 MPa, respectively. In composite beams, they studied different area ratios of HSC to NSC. Their study analysed the existence of different concrete classes, but not distinct

concrete ages (in composite specimens, the upper layer concrete casting was carried out 24 h after the lower layer concrete casting). For the assessment of composite beams' shear strengths with existing formulations, they used the weighted average of the beam and slab's concrete compressive strengths $f_{c,wa}$, according to the ACI 318 proposal about employing properties of individual elements. These authors observed how design codes formulations underestimated shear strength, except for the beams with $f_{c,wa} \geq 50$ MPa and $\varrho_l \leq 1.75\%$, in which strength was overestimated. Consequently, they proposed a shear strength calculation method for composite beams, which is also applicable to monolithic beams, and is based on using the compressive strengths of each element, which well fitted the shear strength of the beams in their experimental programme.

When paying attention to the geometric characteristics of the composite elements typically employed in building constructions (for example, beam-and-block floors, one-way ribbed slabs or two-way ribbed slabs), the behaviour of these elements could resemble that of a T-shaped composite beam more than that of a rectangular composite beam. As T-shaped monolithic beams behave differently to rectangular beams due to the section width change, the study of T-shaped composite beams is considered to be of interest. Therefore, the authors of the present communication recently developed an experimental programme in 21 monolithic and composite beams with rectangular and T-shaped cross-sections without web reinforcement, and with $a/d = 4.0$, $\varrho_l = 4.08\%$ using concretes of different compressive strengths (NSC and HSC of 30 and 60 MPa nominal strength, respectively), where the concretes in the composite beams were cast with a 24-hour difference, except for two specimens in which the influence on the shear strength of a large age difference between concretes was studied (Rueda-García et al. 2021). The main characteristics and results of this study are explained in the next section.

The present study aims to analyse the accuracy of existing shear formulations in composite concrete elements without web reinforcement to reach practical conclusions about their shear strength assessment. For this purpose, the shear strength of a selection of monolithic and composite beams from the studies of Rueda-García et al. (2021) [4] and Kim et al. (2016) [9] was calculated with formulations of EC2-04, EC2-20 D7, MC-10, ACI 318-19 and Kim et al. (2016) using different criteria to assess shear strength in composite beams. In particular, those specimens with $a/d = 4.0$ and with a 24-hour age difference between concretes in composite beams were herein included. There were, thus, 36 specimens with different: longitudinal reinforcement ratios ($\varrho_l = 1.31\%$, 1.75%, 2.87% and 4.08%); concrete classes (NSCs of 24 or 30 MPa nominal compressive strength and HSCs of 60 MPa nominal compressive strength); cross-sectional geometries (rectangular or T-shaped); slab to beam area ratios.

2. The authors' test programme

In this communication, the experimental results of 19 of the 21 specimens tested by the authors in Rueda-García et al. (2021) were compared to the shear strengths predicted by different formulations. The main characteristics of these tests, as well as the obtained results and relevant observations, are explained below.

2.1. Test specimens

Nineteen monolithic and composite simply-supported beams without web reinforcement were fabricated and tested under two point loads. The variables analysed to study their influence on shear strength were: cross-sectional shape, the existence of an interface between concretes and the concrete compressive strengths of both the beam and slab.

The fixed parameters in all the specimens were: shear span-effective depth ratio (a/d = 4.0) of the principal span (the non-reinforced span in shear in which failure was expected); longitudinal reinforcement ratio (ρ_l = 4.08%); relative concrete cover (c/h = 0.16); roughness of the interface in composite beams (very rough interface according to design codes EC2-04, EC2-20, MC-10 and ACI 318-19). Fig. 1 shows the geometry and reinforcement of the test specimens.

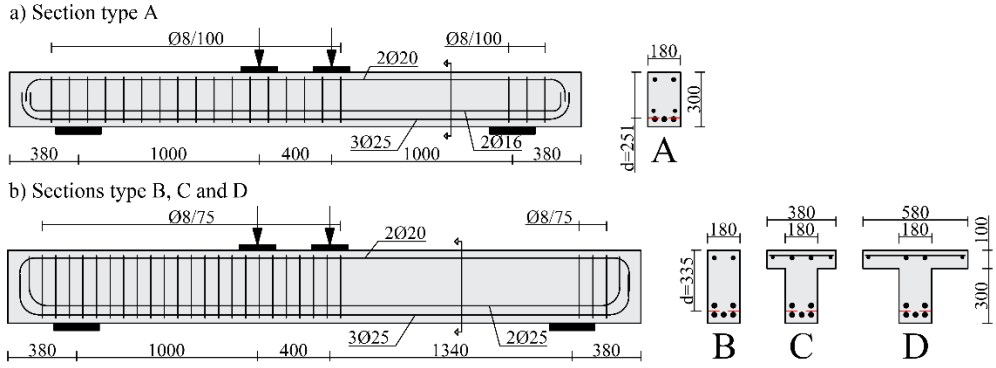

Fig. 1. Geometry and reinforcement of the test specimens: a) specimens with section type A; b) specimens with sections type B, C and D (units: mm).

Regarding the cross-section shape, specimens with rectangular cross-sections were fabricated (sections A and B in Fig. 1) and with T-shape sections (sections C and D in Fig. 1) to study the influence of flange width on the shear strength of composite beams without web reinforcement.

In order to study how the existence of an interface between concretes influences shear strength, specimens of one concrete or monolithic (A1, B1 and C1 in Table 1)

and of two concretes or composite (B2, C2 and D2 in Table 1) were fabricated. In the composite specimens, the lower 3/4 area of the cross-section (0.30 m) corresponded to the concrete of the precast beam and the upper 1/4 area (0.10 m) corresponded to the concrete of the cast-in-place slab on top of the beam.

Table 1. Summary of specimens and test results.

Series	Fabrication batch	Specimen	Section type	f_c beam (MPa)	f_c slab (MPa)	V_{exp} (kN)
NO	P1	NOP1B2	B2	32	31	91
	P2	NOP2A1	A1	39	-	75
		NOP2B1	B1	40	-	88
		NOP2C1	C1	40	-	72
		NOP2C2	C2	39	34	94
		NOP2D2	D2	39	34	84
	P3	NOP3A1	A1	33	-	62
		NOP3B1	B1	30	-	81
		NOP3B2a	B2	31	38	70
		NOP3B2b	B2	31	38	86
		NOP3C1	C1	30	-	79
		NOP3C2	C2	29	38	86
		NOP3D2	D2	29	38	85
HO	P4	HOP4A1	A1	61	-	86
		HOP4B1	B1	63	-	93
		HOP4B2	B2	63	31	101
		HOP4C1	C1	63	-	90
		HOP4C2	C2	63	31	86
		HOP4D2	D2	63	31	99

The analysis of the influence of the compressive strengths of the beam's and slab's concretes was carried out by manufacturing a series of specimens in which both the beam and slab were fabricated with a normal-strength concrete NSC of 30 MPa nominal compressive strength (series NO in Table 1), and by producing series of specimens in which the beam had a high-strength concrete HSC of 60 MPa and the slab had an NSC of 30 MPa (series HO in Table 1).

The specimens' fabrication was divided into four fabrication batches (P1 to P4 in Table 1). In them all, firstly the concrete of the monolithic specimens and the beam's concrete of the composite specimens were poured. Before concrete hardened, composite beams' surface was raked to obtain a very rough interface. After 24 h, the slab's concrete of the composite elements was poured.

Specimens were tested approximately 30 days after being fabricated. The compressive strengths of concretes on the day specimens were tested are shown in Table 1 (f_c). The maximum aggregate size d_g of concretes was 10 mm. For the steel properties of the longitudinal reinforcement, a yield strength f_y of 557 MPa and a modulus of elasticity E_s of 199 GPa were measured.

2.2. Test results

All the specimens showed diagonal cracking failure. In most of the T-shaped monolithic specimens and the rectangular and T-shaped composite specimens, the diagonal critical shear crack deviated horizontally along the interface between concretes or on the plane in which the section width changed. No specimen underwent pure horizontal shear failure. Crack patterns representative examples of rectangular and T-shaped monolithic and composite specimens are shown in Fig. 2. Specimens' experimental shear strength is shown in Table 1 as V_{exp}.

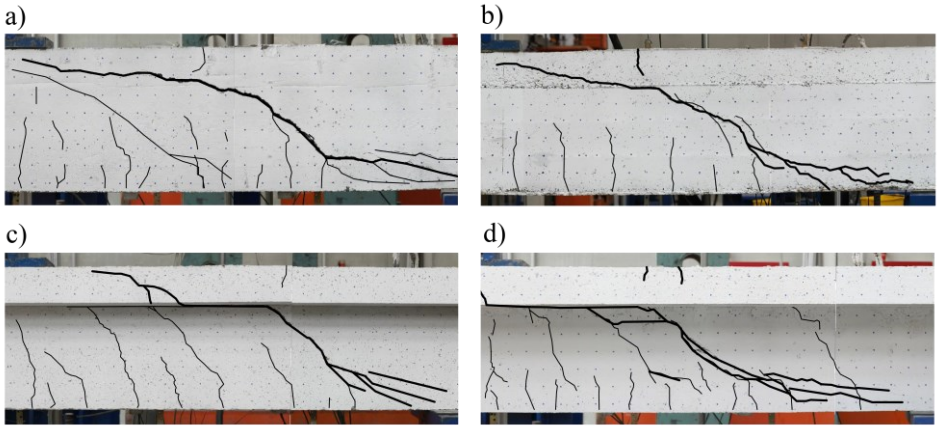

Fig. 2. Examples of the test specimens crack patterns: a) rectangular monolithic beam HOP4B1; b) rectangular composite beam NOP1B2; T-shaped monolithic beam NOP3C1; d) T-shaped composite beam HOP4D2.

By comparing beams A1 with beams B2, it was concluded that the cast-in-place slab contributed to resist shear in the specimens of this experimental programme. It was observed that the V_{exp} in the rectangular and T-shaped specimens was similar, thus it was concluded that shear strength was governed by the shear transfer actions that occurred on the beams' web. On average, the HO series specimens showed slightly higher shear strength than those of the NO series, which once again proves the importance of the beam's web concrete in the shear strength of beams without web reinforcement. In most cases, it was also noted that the composite specimens displayed slightly higher shear strength than their homologous monolithic specimens, which was possibly due to the critical shear crack propagating along the

interface, which could increase compression chord depth and, thus, its shear strength.

3. Vertical shear strength predictions

In order to carry out this comparative study between shear formulations to assess their precision in calculating the shear strength of composite elements without web reinforcement, the results of the 19 specimens described in Section 3 and the results of 17 of the specimens tested by Kim et al. (2016) were used.

In the study by Kim et al. (2016), four beam series were fabricated, of which only the three series with a/d = 4.0 were taken for this study in order to avoid possible overstrengths by the arching action of the series with a/d = 2.5. Each series had a different longitudinal reinforcement ratio (ρ_l = 1.31%, 1.75% and 2.87%). In this communication, only the influence of using different concrete classes in the beam and slab (NSC and HSC), the location of these concretes in the beam or slab, and the relation between the depth of both the beam and slab, were analysed. In each series, five cross-section types were studied, all of which were rectangular (0.26x0.40 m): sections A and B, both monolithic, were fabricated with NSC and HSC, respectively; composite sections C and D, in which NSC was used in the upper 3/8 and 5/8 areas of the cross-section, respectively, and HSC in the lower area; composite section E, where HSC was employed in the upper 3/8 and NSC in the lower area.

For calculations, the shear formulations for elements without web reinforcement of the following current design codes were used: EC2-04, MC-10 at its two approximation levels and ACI 318-19. Additionally, the new formulation of the future EC2-20 presented in Draft 7, based on the Critical Shear Crack Theory (CSCT), was applied, as was the method proposed by Kim et al. (2016) for monolithic and composite beams, in which the effective depths of the tension and compression zones, and their respective concrete compressive strengths, are used.

When predicting the shear strength of composite beams with the codes' formulations, four different perspectives were employed. On the one hand, it was considered that only the beam resisted shear. Thus the beam's effective depth d_b and the compressive strength of the beam's concrete $f_{c,b}$ were used. On the other hand, the entire composite beam's effective depth d_c was employed. In this case, the minimum of the beam's and slab's compressive strengths ($f_{c,min}$), the weighted average of the beams' and slab's compressive strengths ($f_{c,wa}$), obtained from the area ratio of both concretes, or the beam's concrete compressive strength ($f_{c,b}$), were used. Although only ACI 318-19 proposes utilising d_c and $f_{c,min}$ or $f_{c,wa}$, the four perspectives were calculated with all the considered codes' formulations for comparison purposes.

Firstly, the precision of formulations was analysed in the 16 monolithic beams selected from the studies of Rueda-García et al. (2021) (9 tests) and Kim et al. (2016) (7 tests). Table 2 provides the mean value and coefficient of variation (CV) of the relation between the experimental shear strength V_{exp} and the shear strength predicted by the different formulations V_{pred} for the nine monolithic beams fabricated with NSC and the seven monolithic beams produced with HSC.

Table 2. Statistical indicators of the V_{exp}/V_{pred} ratio for the 16 monolithic beams without web reinforcement.

Concrete type	EC2-04		EC2-20 D7		MC-10 LI		MC-10 LII		ACI 318-19		Kim et al. 2016	
	Mean	CV (%)	Mean	CV (%)	Mean	CV (%)	Mean	CV (%)	Mean	CV (%)	Mean	CV (%)
NSC	0.89	14.50	1.06	9.20	1.99	11.62	1.16	10.87	1.21	17.77	0.92	12.36
HSC	0.85	12.00	0.99	9.46	1.61	18.07	1.07	10.72	1.03	13.01	0.91	11.48

The results in Table 2 show that EC2-04 gave a very unsafe V_{pred} for the monolithic specimens in this study. On the contrary, the formulation proposed in the new EC2-20 D7 gave the highest precision values of all the employed formulations, plus a low CV. Although the MC-10 Level I has a simple formulation, it was very much on the safety side. Level II showed more accurate results and little dispersion. Unlike the other applied formulations, it was observed that both ACI 318-19 and MC-10 LI gave a very different result between the specimens with NSC and those with HSC. The method proposed by Kim et al. (2016) led to unsafe results in monolithic beams.

Table 3 shows the mean value and CV of the V_{exp}/V_{pred} ratio for the seven composite specimens fabricated with NSC in the beam and slab, which all come from Rueda-García et al. (2021), and the 13 composite beams fabricated with HSC and NSC (3 from Rueda-García et al. (2021) and 10 from Kim et al. (2016)) for the four described calculation perspectives. Regarding the different studied cross-section types, those whose result did not differ significantly from the rest were included in the analysis. For this reason, the three specimens from Kim et al. (2016) with section type D (NSC in the upper 5/8 area of the cross-section and HSC in the lower area), were separated from the population in the d_b, $f_{c,b}$ method for the HSC-NSC beams, because, as the beam's depth was much lower than the slab's depth, the V_{pred} was very much on the safety side. Therefore, if these specimens were analysed with the other specimens, they would increase the safety of the method's mean value. Similarly in the d_c, $f_{c,b}$ method for the HSC-NSC beams, the three specimens of Kim et al. (2016) with section type E (HSC in the upper 3/8 and NSC in the lower area) were separated from the rest because, as the HSC was in the slab and not in the beam, the V_{pred} was very much on the safety side, which would also increase the safety of the method's mean value.

Table 3. Statistical indicators of the V_{exp}/V_{pred} ratio for the 20 composite beams without web reinforcement.

Concrete types	Method	EC2-04		EC2-20 D7		MC-10 LI		MC-10 LII		ACI 318-19		Kim et al. (2016)	
		Mean	CV (%)	Mean	CV (%)	Mean	CV (%)	Mean	CV (%)	Mean	CV (%)	Mean	CV (%)
NSC-NSC	d_b, $f_{c,b}$	1.01	7.68	1.23	7.68	2.75	8.22	1.53	7.73	1.37	8.22	0.89	7.63
	d_c, $f_{c,min}$	0.88	7.82	1.11	7.82	2.15	7.84	1.18	7.82	1.19	7.84		
	d_c, $f_{c,wa}$	0.86	7.87	1.08	7.87	2.08	8.12	1.15	7.90	1.15	8.12		
	d_c, $f_{c,b}$	0.87	7.68	1.09	7.68	2.10	8.22	1.16	7.74	1.16	8.22		
HSC-NSC	d_b, $f_{c,b}$(1)	1.35	24.27	1.45	18.42	2.67	22.51	2.13	26.04	1.84	31.07	0.99	14.78
	d_b, $f_{c,b}$(2)	2.18	1.17	2.16	1.17	4.24	11.31	5.51	3.29	3.51	1.06		
	d_c, $f_{c,min}$	1.09	12.99	1.23	11.69	2.26	16.40	1.36	11.83	1.52	14.62		
	d_c, $f_{c,wa}$	0.93	11.03	1.05	8.79	1.77	13.75	1.16	9.48	1.20	12.38		
	d_c, $f_{c,b}$(3)	0.85	11.66	0.97	10.49	1.56	15.32	1.06	10.54	1.04	12.00		
	d_c, $f_{c,b}$(4)	1.08	3.55	1.18	3.55	2.14	12.91	1.32	3.41	1.52	4.12		

(1) The three specimens with section type D of Kim et al. (2016) are not included.
(2) Only the three specimens with section type D of Kim et al. (2016).
(3) The three specimens with section type E of Kim et al. (2016) are not included.
(4) Only the three specimens with section type E of Kim et al. (2016).

Fig. 3 depicts the results obtained for the seven composite specimens of Rueda-García et al. (2021) fabricated with NSC with the formulations showing the highest precision according to the observations in Table 3 (EC2-20 D7, MC-10 LII and ACI 318-19, and the calculation methods of d_c with $f_{c,min}$, $f_{c,wa}$ and $f_{c,b}$). Fig. 4 shows the results of these same formulations for the 13 composite specimens of Rueda-García et al. (2021) and Kim et al. (2016) fabricated with HSC and NSC, but excluding the three type E specimens of Kim et al. (2016) in the method with d_c and $f_{c,b}$.

Table 3, Fig. 3 and Fig. 4 show that, generally, considering that only the beam resisted shear gave results very much on the safety side with all the formulations in both specimens NSC-NSC (mean value of 1.58 on average for all the formulations) and HSC-NSC (1.89). As expected, for the NSC-NSC specimens the three methods that used d_c gave a similar mean value for each formulation and with similar dispersion (around 8%) because the compressive strengths of the beam's and slab's concretes were similar. If the results of each formulation for the composite beams are compared with those of the same formulation for the monolithic beams (Table 2), it is observed that the precision of formulations was higher for the monolithic beams, which proves that incorporating an adapted methodology into existing formulations to assess composite beams' shear strength would be needed. It was also found that if concrete's compressive strength was similar at both the beam and slab (NSC-NSC), the existence of an interface did not significantly change the dispersion of the calculation method (8% on average for all formulations and

methods), while for different class concretes at the beam and the slab (HSC-NSC), the dispersion of the results increased (15%).

Regarding the precision shown by the different formulations, EC2-04 gave unsafe results for the NSC-NSC specimens and for the HSC-NSC specimens when d_c and $f_{c,wa}$ or $f_{c,b}$ were used. EC2-20 D7 was generally the most accurate formulation with the least dispersion in the specimens made with NSC, especially when d_c and $f_{c,wa}$ or $f_{c,b}$ were used. In the HSC-NSC beams, while the use of d_c and $f_{c,min}$ gave a very safe result, that of d_c and $f_{c,wa}$ showed the highest precision and lowest dispersion (Fig. 3). However, the use of d_c and $f_{c,b}$ (excluding type E beams) gave a slightly unsafe result. MC-10 LI obtained a very safe results compared to the other codes, and had the highest dispersion in the HSC-NSC beams. MC-10 LII and ACI 318-19 showed better precision, with similar results and on the safety side, but ACI 318-19 gave higher dispersion. The model of Kim et al. (2016) was greatly adjusted to the results of beams with different strength concretes, which was characteristic of their experimental programme, but was unsafe for the NSC-NSC beams.

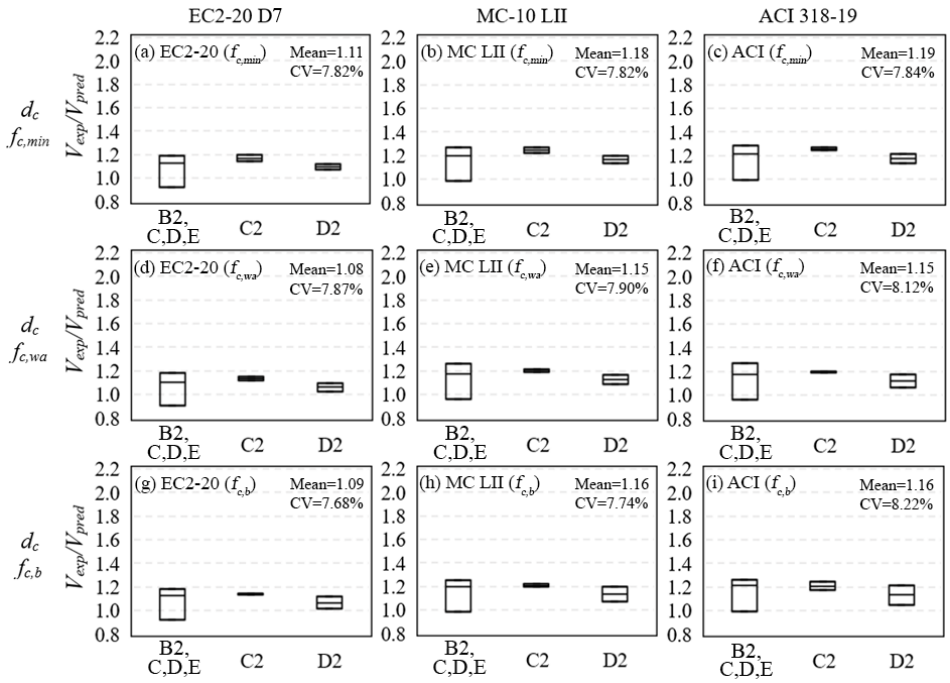

Fig. 3. Shear strengths predicted by the codes for the 7 composite beams without web reinforcement made of NSC.

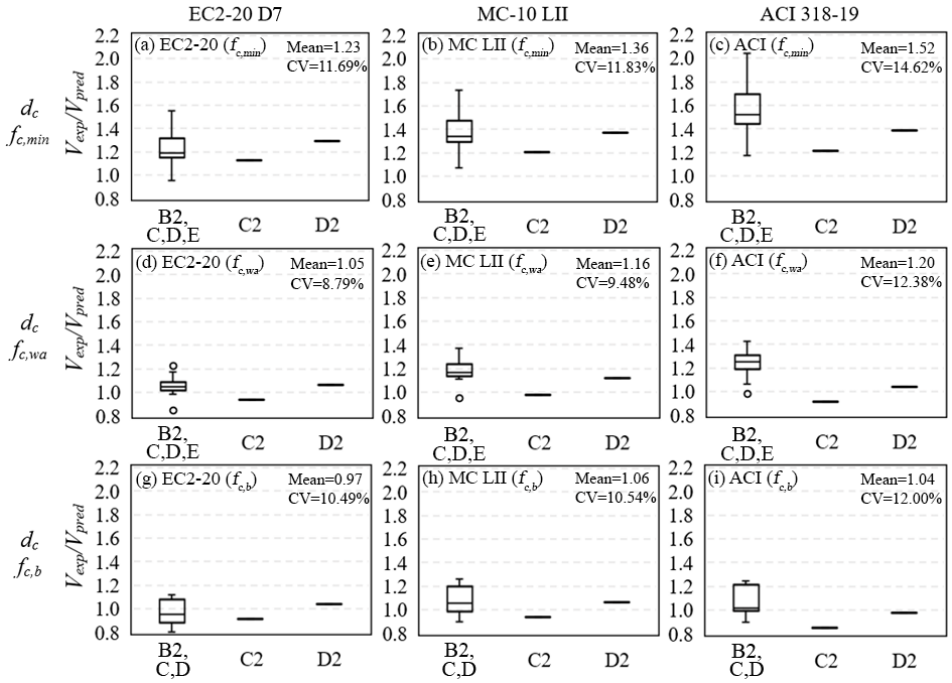

Fig. 4. Shear strengths predicted by the codes for the 13 composite beams without web reinforcement made of HSC and NSC (10 specimens in method d_c, $f_{c,b}$).

Fig. 4 shows the differences in the three methods that used d_c in beams with different concretes at both the beam and slab. This case is especially important because the use of different concretes is more widespread in composite construction. On the one hand, the use of $f_{c,min}$ was much safer than that of $f_{c,wa}$ and $f_{c,b}$ because of the large difference in the compressive strengths of both the beam and slab concretes in this series. The use of $f_{c,min}$ in beams with different concretes gave a mean value of 1.49 on average for all the formulations, while the beams with equal strength concretes gave, on average, 1.30. The smallest dispersions in the results were obtained when $f_{c,wa}$ was used (10% on average for all the formulations, with a mean value of 1.24) as the method's precision is independent of where HSC and NSC are in the composite beam and the relation between their effective depths. Although the use of d_c and $f_{c,b}$ is commonplace for calculating shear strength (Runzell et al. 2007 [10] or Avendaño and Bayrak 2008 [11], among others), and may be on the safety side if the beam's depth is much higher than that of the slab, this method proved slightly unsafe for the beams in this analysis when they were assessed with EC2-20 D7. The result came quite close to the actual one when MC-10 LII and ACI 318-19 were used, albeit with considerable dispersion because, in this case, the method's precision depends on the relation between the effective depths of both the beam and slab. A mean value of

1.17 was obtained by this method for all the composite specimens and formulations (1.28 for equal strength concretes and 1.10 for different strength concretes).

By way of conclusion, it can be deduced that the calculation of the shear strength of the composite beams without web reinforcement, fabricated with two concretes of equal or different compressive strengths using the entire depth of composite beam d_c and the weighted average of the beam's and slab's concrete compressive strengths estimated from the area ratio ($f_{c,wa}$), gave a precise value that was on the safety side with little dispersion when the EC2-20 D7 formulation was applied.

4. Conclusions

The objective of this communication was to reach practical conclusions for the assessment of the shear strength of composite concrete beams without web reinforcement by means of a safety analysis of the existing shear formulations. The major findings of the study were:

1. Existing formulations were more accurate when assessing the shear strength of the monolithic specimens than the composite specimens. Therefore, the need to incorporate a calculation methodology into design codes that adapts to composite concrete elements without web reinforcement was found.
2. Formulations showed greater dispersion for the composite specimens made of different compressive strength concretes (coefficient of variation of 15%, on average for all the formulations) than for those made with equal compressive strength concretes (8%).
3. Of all the calculation methods herein used, the assessment of the composite beams' shear strength when considering that only the beam resisted shear gave a very safe result (1.58 and 1.89 for the beams with equal and different compressive strength concretes, respectively, on average for all the formulations). Employing the entire depth of composite element d_c and the minimum compressive strength of the beam's and slab's concretes increased safety in the beams with different compressive strengths at the beam and the slab (1.30 for equal compressive strengths vs. 1.49 for different compressive strengths). The use of d_c and the weighted average of the compressive strengths of the beam's and slab's concretes generally gave the best results (1.24 on average for all the formulations). Employing d_c and the compressive strength of the beam's concrete provided good results (1.17), but they were unsafe in some cases.
4. The formulation of Draft 7 of EC2-20, using the entire depth of the composite element and the weighted average of the compressive strengths of the beam's and slab's concretes, gave the most accurate results, which

remained on the safety side (mean value of 1.08 for the composite beams with equal strength concretes and 1.05 for different strength concretes).

However, the number of experimental specimens is still limited and, thus, further studies are required to verify the shear strength of composite concrete elements without web reinforcement. In the future, a detailed study of the existing formulations, paying attention to their theoretical basis in order to specify how the beam's and slab's concretes contribute to shear strength, would be of great interest.

Acknowledgements

This study forms part of the research conducted at the Concrete Science and Technology University Institute (ICITECH) of the Universitat Politècnica de València (UPV, Spain) with concrete supplied by Caplansa. The project has been supported by the Spanish Ministry of Science and Innovation through Projects BIA2015-64672-C4-4-R and RTI2018-099091-B-C21-AR; the Regional Government of Valencia through Project AICO/2018/250, and the European Union with FEDER funds. The authors thank the Spanish Ministry of Economy and Business for Grant BES-2016-078010.

References

[1] Loov RE, Patnaik AK. Horizontal Shear Strength of Composite Concrete Beams With a Rough Interface. PCI J 1994;39:48–69.

[2] Kovach J, Naito C. Horizontal Shear Capacity of Composite Concrete Beams without Interface Ties. ATLSS Report No. 05-09: 2008.

[3] Halicka A. Influence new-to-old concrete interface qualities on the behaviour of support zones of composite concrete beams. Constr Build Mater 2011:4072–8.

[4] Rueda-García L, Bonet Senach JL, Miguel Sosa PF, Fernández Prada MÁ. Experimental analysis of the shear strength of composite concrete beams without web reinforcement. Eng Struct 2021;229:111664. https://doi.org/10.1016/j.engstruct.2020.111664.

[5] Fédération International du Béton (fib). Model Code 2010. Ernst & Sohn; 2012.

[6] CEN. EN 1992-1-1:2004. Eurocode 2: Design of concrete structures - Part 1-1: General rules and rules for buildings. 2004.

[7] CEN. prEN 1992-1-1-D7:2020 Eurocode 2: Design of Concrete Structures

– Part 1-1: General rules – Rules for buildings, bridges and civil engineering structures. 2020.

[8] ACI Committee 318. Building code requirements for structural concrete (ACI 318-19); and commentary (ACI 318R-19). Farmington Hills: American Concrete Institute; 2019.

[9] Kim C-G, Park H-G, Hong G-H, Kang S-M. Shear strength of composite beams with dual concrete strengths. ACI Struct J 2016;113:263–74.

[10] Runzell B, Shield C, French C. Shear Capacity of Prestressed Concrete Beams. 2007.

[11] Avendaño AR, Bayrak O. Shear strength and behaviour of prestressed concrete beams. Technical Report: IAC-88-5DD1A003-3, Texas Department of Transportation: 2008.

Chapter 4. Experimental study on the shear strength of concrete composite beams with web reinforcement

In this third phase of the experimental programme, which is the biggest in number of experimental tests and variables studied, composite specimens with web reinforcement are analysed.

The experimental study of this chapter is described by means of three journal articles. The first article details the results obtained from the study of composite rectangular specimens, for which 18 monolithic and composite rectangular beams are analysed. The second article studies composite T-shaped specimens consisting of a rectangular concrete beam with a top cast-in-place slab. The article describes and analyses the results of 19 monolithic and composite T-shaped specimens. The third article shows the research conducted to study the shear resistant behaviour of T-beams with cast-in-place slab by testing 6 specimens with different characteristics.

The three articles explain the test programme, analyse the crack patterns and instrumentation results, and describe the shear strength mechanisms. In the first article a mechanical model for interpreting the experimental results is proposed, which is extended to T-shaped specimens in the second and third articles. Also, the test results are compared to the codes' provisions.

5th PAPER

Details:

Type of paper	Journal article
Title	*Analysis of the shear strength mechanism of slender precast concrete beams with cast-in-place slab and web reinforcement*
Authors	Lisbel Rueda García José Luis Bonet Senach Pedro Francisco Miguel Sosa Miguel Ángel Fernández Prada
Journal	Engineering Structures
Publisher	Elsevier
ISSN	0141-0296
JIF	4.471 (2020)
JIF Quartile	Q1 (20/137) ENGINEERING, CIVIL
Status	Published
Date	Accepted: 13th August 2021 Available online: 25h August 2021
Full reference	Rueda-García L, Bonet Senach JL, Miguel Sosa PF, Fernández Prada MÁ. Analysis of the shear strength mechanism of slender precast concrete beams with cast-in-place slab and web reinforcement. Engineering Structures 2021;246:113043. https://doi.org/10.1016/j.engstruct.2021.113043.

Analysis of the shear strength mechanism of slender precast concrete beams with cast-in-place slab and web reinforcement

Lisbel Rueda García, lisruega@cam.upv.es

José Luis Bonet Senach, jlbonet@cst.upv.es

Pedro Fco. Miguel Sosa, pmiguel@cst.upv.es

Miguel Ángel Fernández Prada, mafernan@cst.upv.es

Universitat Politècnica de València, Camí de Vera s/n, 46022, Valencia, Spain

Abstract

Precast concrete beams with cast-in-place slabs on top, namely concrete composite beams are frequently used for building concrete bridge decks. In designs, the contribution of cast-in-place slabs to shear strength tends to be omitted. However, given the vast number of existent bridges with this deck typology, significant cost savings could be made when assessing these structures if the slab's shear strength is considered. This paper analyses how cast-in-place slab influences the shear behaviour of concrete composite beams with web reinforcement. For this purpose, an experimental programme of 18 concrete specimens with web reinforcement and rectangular cross-sections was run, in which the following parameters varied: cross-sectional depth; existence of an interface between concretes; compressive strengths of the concrete of beams and slabs; differential shrinkage between concretes. It was observed that: the slab contributed to resist shear; the existence of an interface between concretes led to a crack appearing along it that caused the transmitted shear to be divided into two load paths: one through the precast beam and another one through the slab; the slab's concrete strength was that which mainly influenced the element's shear strength; differential shrinkage did not reduce shear strength. Based on experimental observations, a mechanical model is proposed in this paper to assess the composite elements' shear strength, which considers the yielding of both stirrups and the slab's longitudinal reinforcement to be a failure criterion, which well predicted the experimental results. The shear formulations of Eurocode 2, the Level III Approximation of Model Code 2010 and the (b) Formula of ACI 318-19 offered a similar result to the herein proposed method when using the entire composite element effective depth and the weighted average of the concrete strengths of both the beam and slab estimated from the area ratio. Codes significantly underestimated specimens' interface shear.

Keywords: precast construction, reinforced concrete, composite beam, shear strength, shear failure, mechanical model, design, assessment.

Highlights

Shear in monolithic and composite beams with stirrups was experimentally tested

Slab contributed to increase composite specimens' shear strength

The interface between concretes modified the shear strength mechanism

A mechanical model of composite specimens' shear strength is proposed

The proposed model well fits this test programme's experimental results

1. Introduction

The report conducted by the Technical Committee 4.3 "Road bridges" of PIARC in 2016 [1] revealed that at least 50% of the participating countries' bridges are made of reinforced or prestressed concrete; particularly in Europe, this percentage is more than 80% on average. To construct these concrete bridges, a very common deck typology has often been used since the mid-20th century, which consists in precast concrete beams with a cast-in-place slab on top, commonly known as concrete composite beams (Fig. 1). Given the considerable number of existent decks with this typology, it is especially important to study their structural behaviour.

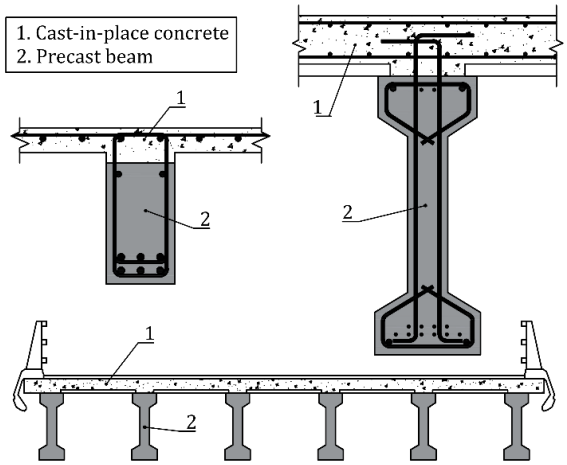

Fig. 1. Examples of the cross-sections of precast beams with cast-in-place slabs frequently used in concrete composite beams decks.

The interface between concretes in concrete composite beams is a weakness plane whose premature failure may limit both the element's vertical and horizontal shear

strengths [2]. The research work carried out on composite beams has traditionally focused on analysing the interface shear [3–8], mainly to analyse the effect of interface roughness, the shear span-depth ratio, concretes' properties and the interface's shear reinforcement. However, a few experimental studies in the existent literature have analysed the vertical shear behaviour of reinforced concrete composite beams [9].

In vertical shear designs of reinforced concrete composite beams, the contribution of the cast-in-place slab to shear strength is usually neglected because it remains on the safety side. However, the slab's contribution could be significant to assess the shear strength of existing bridge decks made of precast concrete beams and cast-in-place slabs as increased shear strength due to cast-in-place slab's contribution can imply substantial maintenance cost savings in these infrastructures [9], which derive from reducing the need for their reinforcement, or even their replacement. Hence the importance of studying whether the cast-in-place concrete slab resists shear in composite beams, in which way and how much it can resist.

In general, current design codes' shear formulations do not describe the shear strength prediction when, as is common in composite beams, the concretes' compressive strengths of the precast beam and the cast-in-place slab differ. Only ACI 318-19 [10] in Section 22.5.4 specifies how this shear strength can be calculated: using the concrete compressive strength of the element (precast beam or cast-in-place slab) that results in the most critical shear strength value or the properties of the individual elements. However today, relevant experimental and theoretical evidence is not sufficient to support the validity of the design code for composite beams [9,11]. EC2 [12] in Section 10.9.3(8) allows the design of concrete elements with a topping of at least 40 mm thick as composite elements if the shear at the interface is verified. Other codes like MC-10 [13] do not refer to this type of structural elements.

In the scientific literature, several publications [14–23] are about the experimental analysis of full-scale concrete composite beams with web reinforcement. Most have focused on analysing the verification of these elements' shear capacity according to design code' formulations. However, these studies have not analysed either the contribution of the cast-in-place concrete slab to the composite beam's shear strength or how the existence of a joint between concretes of different ages can affect shear behaviour.

According to Halicka [2], there is little number of research works regarding the influence of the interface cracking on the composite unit's shear resistance. She performed an experimental study on the influence of interface quality on concrete composite beams' shear strength, in which she proposes a classification of failure mechanisms of concrete composite beams. According to this classification, interface shear failure will take place when the shear force that initiates interface cracking is

less than the shear force that results in diagonal cracking appearing, which will limit the element's ultimate vertical shear strength. On the contrary, if diagonal cracking occurs first, two situations can be observed: the shear that produces interface cracking is lower than the element's ultimate shear strength, in which case the trajectory of diagonal cracks will be modified along the interface before penetrating the upper chord; the shear that produces interface cracking is higher than the element's ultimate shear strength, in which case the composite beam will behave like a monolithic beam. The second failure mode will be the structurally desired behaviour as the interface is not a weakness plane for shear strength. However, the first failure mode can be common, especially in elements with either significant differential shrinkage between the concrete of the beam and that of the slab, or changes in the section width (T-shaped beams) [24,25], and deserves to be studied.

Kim *et al.* [11] ran an experimental programme about the shear strength of rectangular composite beams with shear reinforcements. Their study focused mainly on analysing the existence of different class concretes (high-strength and low-strength concretes) at the beam and slab. They obtained results on the relation between the shear strength of composite beams and the compressive strengths of the beam and slab's concretes and the beam and the slab's depth. This provided information about the extent to which each composite beam part contributes to shear strength. However, both transverse reinforcement and interface roughness in these experimental tests meant that the interface shear strength was high. Thus the failure mode was barely affected generally by the existence of an interface, and the behaviour of these specimens was similar to the monolithic one according to the Halicka classification [2]. Their study, therefore, did not analyse how the existence of an interface would influence shear strength.

In a previous study carried out by the authors [26], the shear strength of 21 monolithic and concrete composite beams, with rectangular and T-shaped cross-sections and with no web reinforcement, was analysed. The main findings of the rectangular composite specimens were that: 1) the existence of a slab on top of the beam improved its shear strength; 2) the interface between concretes could modify the critical shear crack shape, consequently, the shear strength mechanism; 3) the use of high-strength concrete in the precast beam slightly increased its shear strength; 4) the differential shrinkage between the concretes of the precast beam and the cast-in-place slab did not significantly influence composite specimens' vertical shear capacity; 5) the design codes generally provided better estimations of actual strengths when the entire composite beam depth and individual elements' shear strengths were used, and gave results on the interface shear that were very much on the safety side.

Following these previous studies, the present research work studies how the cast-in-place slab influences the shear behaviour of concrete composite beams with web

reinforcement. The specific aim is to analyse the shear strength mechanism of rectangular reinforced concrete composite beams with web reinforcement, particularly in those composite beams in which the existence of an interface between concretes substantially modifies the shear strength mechanism, unlike what happens when beams display monolithic behaviour. To this end, 18 monolithic and composite rectangular specimens, with equal and different cross-sectional depths, compressive strengths of the beam and slab's concretes, and different concrete ages, were experimentally tested. The obtained results, as well as the different introduced variables, are analysed. Based on the experimental results, a mechanical model for assessing the shear strength of the composite beams in the experimental programme is proposed, which can be used as a reference for the future development of a method to assess composite beams' shear strength. Both the proposed model and the formulations for calculating the shear strength of current design codes are verified with the experimental programme results.

The main contributions of this research work are, on the one hand, to increase the number of available experimental tests in this field and, on the other hand, to provide a better understanding of the shear transfer mechanism in composite beams whose elements have different quality concretes. This will allow researchers to propose mechanical-based design and assessment formulations for such elements to improve their safety and prolong their service life.

2. Test programme

2.1. Test parameters

In order to analyse the contribution of cast-in-place concrete slabs to the shear strength of a rectangular composite beam with web reinforcement, and how the existence of an interface between concretes can affect its shear behaviour, the following four variables were studied:

(a) Cross-sectional depth. Firstly, a reference section type A, which represented the precast beam used in composite elements. Secondly, a section type B with an increased depth compared to section A (see Fig. 2)
(b) The existence of an interface between concretes. Beams were fabricated with one concrete (monolithic beams A1 and B1 in Fig. 2) or two concretes (composite beams, compound of a beam with a cast-in-place slab on top: B2 in Fig. 2)
(c) Strengths of the beam and slab's concretes. Two types of concretes were used to fabricate specimens: normal-strength concrete (NSC) with a design compressive strength of 30 MPa, which represented a concrete traditionally used in cast-in-place construction; a concrete with higher compressive

strength (HCS), with a design compressive strength of 50 MPa, which represented a concrete often used in precast concrete plants. In the composite specimens, the influence of the beam's concrete compressive strength was studied using NSC or HCS on the beam, while the slab's concrete compressive strength was fixed to a conventional concrete (NSC)

(d) Differential shrinkage between concretes. Most composite specimens were fabricated with concretes of similar ages (24-hour difference) for a faster construction process and to reduce the differential shrinkage between the beam and slab's concretes. However, in order to analyse if the use of different ages concretes, common in precast construction, had a significant influence on the shear strength of the composite specimens in this experimental programme, the slab's concrete was poured later into two composite beams once the beam's concrete shrinkage stabilised.

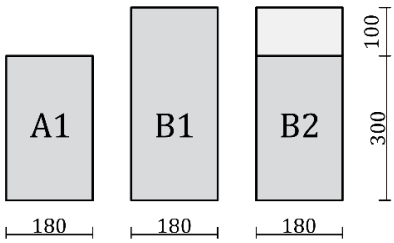

Fig. 2. Cross-section types (dimensions: mm).

The following parameters were fixed to avoid their influence on the study:

- Interface roughness ("smooth" or "as-cast"). The beam's concrete underwent no further treatment after vibration, so the interface between beam and slab's concretes was "smooth" or "as cast", as described in current design codes [12,13]
- Longitudinal reinforcement ratio (ρ_l = 4.0%). Longitudinal reinforcement was designed to avoid the bending failure of all beams
- Shear reinforcement ratio (ρ_w = 0.22%). The web reinforcement design met the most restrictive minimum spacing requirements between stirrups of all the codes used to design these beams [10,12,13]
- The shear span-effective depth ratio (a/d = 4.0). a/d was chosen based on the observations of Kani's valley [27] to foster shear failure
- Relative concrete cover (c/h = 0.16). The concrete cover met the design codes' specified minimums

Both interface roughness and the shear reinforcement ratio were chosen based on the observations made by a previous research work carried out by the authors [28], in which beams with the same characteristics as those in this experimental

programme showed that the smooth interface, together with vertical shear reinforcement, were enough to obtain the beam's diagonal cracking prior to interface cracking. This proved the interface treatment's effectiveness in neither failing in interface shear nor showing monolithic behaviour, even though the code calculations predicted interface shear failure. Smooth interface roughness is also the roughness that is often left in precast concrete plants.

This experimental programme fabricated 18 reinforced concrete beams with web reinforcement, divided into three series: NW, HW and DW. The beam and slab's concrete types employed in the series, the number of days that elapsed between the beam's concrete pouring and the slab's concrete pouring in the composite specimens, and the number of specimens per series, are shown in Table 1. In the composite specimens of series NW and DW, the compressive strengths of the beam and slab's concretes were similar (NSC in both), while different concrete compressive strengths were used in series HW (HCS on the beam and NSC on the slab).

Table 1. Series of the experimental programme.

Series	Type of beam's concrete	Type of slab's concrete	Days between beam and slab's concrete pouring	Number of specimens per cross-sectional type		
				A1	B1	B2
NW	NSC	NSC	1	3	3	4
HW	HCS	NSC	1	2	2	2
DW	NSC	NSC	134	0	0	2

Specimen designation was carried out using *xWPyzk(j)*, where: "*xW*" denoted the name of the series (NW for the specimens with NSC on the beam, HW for the specimens with HCS on the beam and DW for the specimens fabricated with different aged concretes); "*Py*" was the batch of concrete pouring (from P1 to P7 as the fabrication process was conducted 7 times); "*z*" denoted the cross-sectional shape (A or B in Fig. 2); "*k*" was the number of concretes that formed the specimen (1 for monolithic beams, 2 for composite beams); "*j*" ("a" or "b") was used when more than one specimen with the same previously described characteristics was fabricated.

2.2. Test specimens

Fig. 3 shows specimens' dimensions and reinforcement. The total length of the beams with section B was 3.50 m, with a distance of 2.74 m between supports. Two-point non-centred vertical loading was applied, with a 0.40 m distance between loads, which formed two spans: a 1.34-metre principal span, in which failure was expected, and resulted in fixed parameter $a/d = 4.0$, and a 1.00-metre span, reinforced to avoid its shear failure. The beams with section type A were designed with a 3.16 m length

(2.40 m between supports) to obtain fixed parameter a/d = 4.0, with 1.00-metre principal and reinforced spans.

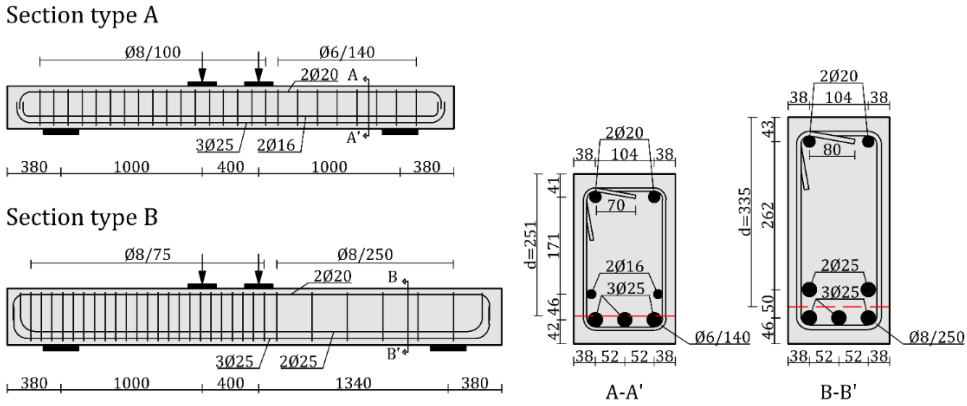

Fig. 3. Dimensions and reinforcement of beams type A and B (dimensions in mm).

In the composite beams (sections B2), two concrete layers were used. The first layer, 0.30 m high, represented the precast beam. The second layer, 0.10 m high and cast on top of the previous one, represented the cast-in-place concrete slab.

2.3. Fabrication of specimens

Beams were fabricated in seven batches (P1 to P7 in Table 2), which allowed a comparison to be made between the beams of the same batch without influencing the concrete strength variable. The beam fabrication process was carried out in two phases. The first phase consisted in beam's concrete pouring (concrete of the monolithic specimens and the precast beam's concrete in the composite specimens). In all the composite beams, at the principal span, where failure was expected, no surface treatment was performed after concrete pouring. So the surface was "smooth" or "as-cast", according to current code definitions [10,12,13]. The concrete surface of the reinforced span was raked before concrete hardened to increase the interface shear strength. Dents of approximately 6 mm deep (from peak to valley) and a maximum spacing of 40 mm between peaks were made. A "very rough" interface was created in this way as defined in the codes. Good workability conditions for the concrete casting were sought. Table 2 shows the measured slump of the first phase concretes because their consistency can influence surface roughness. The slump test was done in accordance with UNE-EN 12350-2 [29].

Table 2. Summary of the test results.

Series	Fabrication batch	Specimen	$f_{c28,b}$ (MPa)	$f_{c28,s}$ (MPa)	f_{cb} (MPa)	f_{cs} (MPa)	E_{cb} (MPa)	E_{cs} (MPa)	f_{tb} (MPa)	f_{ts} (MPa)	Slump beam (cm)	V_{exp} (kN)	$\tau_{b,exp}$ (MPa)
NW	P1	NWP1B2	32	32	33	32	33535	37689	2.61	2.27	6.0	206	3.79
	P2	NWP2A1	37	-	37	-	33421	-	2.99	-	17.5	158	-
		NWP2B1		-	37	-	33421	-	2.99	-		181	-
		NWP2B2		34	39	34	31961	30428	2.58	2.50		186	3.43
	P3	NWP3A1	32	-	33	-	32927	-	2.58	-	22.5	128	-
		NWP3B1		-	31	-	32927	-	2.58	-		174	-
		NWP3B2		38	32	37	32927	33854	2.58	3.21		169	3.12
	P4	NWP4A1	39	-	39	-	28652	-	2.79	-	18.0	153	-
		NWP4B1		-	39	-	28300	-	2.86	-		168	-
		NWP4B2		33	40	33	26413	28715	3.04	2.48		191	3.53
HW	P5	HWP5A1	43	-	43	-	24633	-	2.58	-	20.0	144	-
		HWP5B1		-	42	-	24662	-	2.40	-		207	-
		HWP5B2		22	43	22	24633	20098	2.58	2.01		172	3.17
	P6	HWP6A1	52	-	52	-	28651	-	2.86	-	24.0	(*)	-
		HWP6B1		-	52	-	28395	-	2.86	-		199	-
		HWP6B2		36	52	36	28395	29458	2.86	3.01		186	3.44
DW	P7	DWP7B2a	24	36	29	37	24939	31243	2.44	2.82	15.0	167	3.09
		DWP7B2b			29	37	24939	31243	2.44	2.82		179	3.30

Notation:
Suffix "b" refers to beam's concrete.
Suffix "s" refers to slab's concrete.
(*) V_{exp} could not be measured because of failure detected during the test process.

The second fabrication phase consisted in the slab's concrete being poured on the composite specimens and subsequent concrete curing for the next 7 days. In beams NW and HW, this phase was carried out 24 h after the first phase to, thus, reduce differential shrinkage between concretes as much as possible. In beams DW, this second phase took place 134 days after the first phase when the beam's concrete shrinkage measurements indicated that it was stabilised.

In all the fabricated specimens, the entire length of beam was laid on the floor when the slab's concrete was being poured. Hence in this experimental programme, both the beam and slab were loaded at the same time.

2.4. Material properties

The mechanical characterisation of the used concretes was carried out according to UNE-EN 12390 [30–32]. The results obtained were the average of two concrete cylinders (300 mm high, 150 mm diameter), tested at the age of 28 days and every day a specimen was tested. Beams were tested approximately 28 days after the fabrication process. The average values of the compressive strengths of the beam and slab's concretes measured at the age of 28 days ($f_{c,28}$) are offered in Table 2, which also shows the average values of the compressive strengths of the beam and slab's concretes ($f_{c,b}$ and $f_{c,s}$, respectively), the moduli of elasticity E_c and the tensile concrete strengths f_{ct} (calculated as the 90% of the tensile splitting strength of concrete, according to [33]) measured on the day when each specimen was tested. The average coefficients of variation of these measurements were 2, 3 and 7% for the compressive strength, the modulus of elasticity and the tensile strength of concretes, respectively.

For concrete dosage, the water-cement ratio, the amount of Portland cement and the maximum aggregate size were 0.52, 325 kg/m^3 and 10 mm for NSC, and 0.44, 500 kg/m^3 and 10 mm for HCS, both respectively.

The mechanical properties of reinforcing steel were obtained according to UNE-EN ISO 6892 [34]. Steel type was C class according to classification of EC2-04 [12]. Two pieces of reinforcing steel of each nominal diameter were tested to obtain the average values of the steel mechanical properties shown in Table 3. It should be noted that the stirrups used in all the specimens (except the specimens of series NWP1) were made of the same steel so that the comparison of beams' shear strength provided by stirrups did not depend on steel properties.

Table 3. Average values of the reinforcing steel properties.

	Series	Ø (mm)	f_y (MPa)	E_s (GPa)	ε_y (‰)	f_u (MPa)	ε_u (%)
Stirrups	NWP1	8	534	189	2.8	662	10.1
	Rest of series	6	534	227	2.4	666	11.0
		8	538	203	2.7	658	12.0
Longitudinal reinforcement	NWP1	20	534	206	2.6	639	10.5
		25	556	197	2.8	670	9.7
	NWP2, NWP3, NWP4, DWP7	16	561	240	2.3	675	31.9
		20	585	192	3.0	673	41.0
		25	557	199	2.8	666	48.3
	HWP5	16	545	230	2.4	655	31.7
		20	541	194	2.8	654	26.7
		25	548	235	2.3	658	21.6
	HWP6	16	531	231	2.3	641	33.2
		20	560	190	2.9	675	22.0
		25	574	237	2.4	687	19.2

2.5. Instrumentation

Three 1000 kN load cells were used to measure the hydraulic jack force and the reactions at the two bearing points.

Strain gauges (120 Ω resistance and 2 mm measuring length) were placed on some steel reinforcing bars surface to measure strains. As shown in Fig. 4a, three pairs of strain gauges (G1 to G6) were placed at three different cross-sections upon tension longitudinal reinforcement (Sections A, B and C). Below the central point load, a pair of strain gauges was placed on compression longitudinal reinforcement (G7 and G8). Pairs of strain gauges were glued in the middle of the two legs of four stirrups (stirrups w1 to w4 in Fig. 4a) of the principal span (five stirrups for beams type A) (gauges G9 to G16 in Fig. 4a).

On the concrete surface of beams type B, two strain gauges (120 Ω resistance and 60 mm measuring length), separated from one another by 100 mm, were placed at Sections A and B in Fig. 4a (gauges C1 to C4 in Fig. 4a).

While testing, linear variable displacement transformers (LVDTs) were used. They took continuous measurements of displacements on concrete surfaces. As shown in Fig. 4b, four LVDTs were placed horizontally to measure the slip at the interface in the composite beams (H1 to H4). Five LVDTs (V1 to V5) measured vertical displacements at the supports and at Sections A, B and C. Two more vertical LVDTs, O1 and O2, were connected to the top and bottom of beams to detect the beginning of cracking at either the interface or the web.

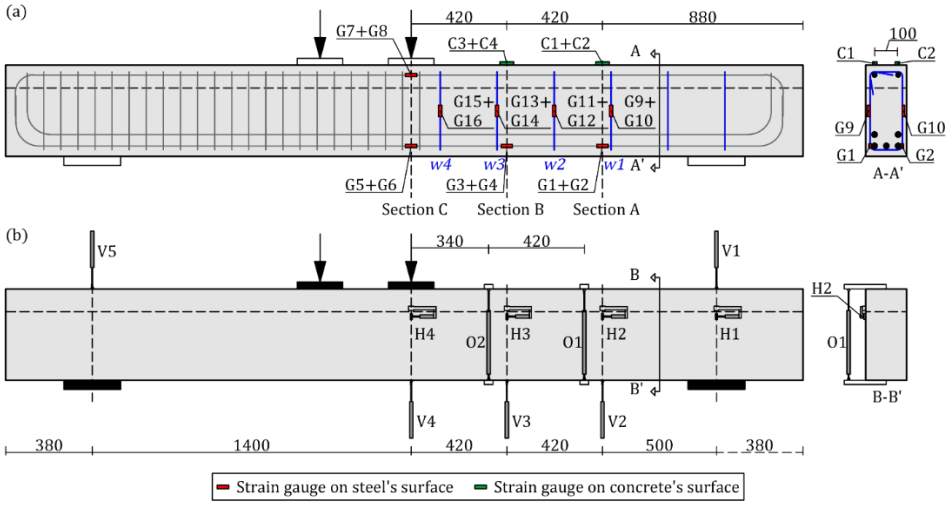

Fig. 4. Instrumentation of a type B2 beam for the shear test: (a) strain gauges; (b) LVDTs (dimensions in mm).

Two digital cameras took pictures during testing at a rate of 0.5 Hz and a high-speed camera recorded brittle failures.

In the two beams of series DW, concrete's shrinkage was monitored for 4 months starting from day 2 after beam's concrete pouring. As shown in Fig. 5, five strain gauges glued to the steel surface (G1, G6, G7, G9 and G13 in Fig. 5a), and one strain gauge glued to the concrete lateral surface (C5 in Fig. 5b), were connected to a data acquisition system to take continuous strain measurements during the shrinkage test. A 3x3 discs mesh was placed on the concrete lateral surface (Fig. 5b) to measure deformations twice weekly by a demountable mechanical strain gauge (DEMEC). Two horizontal LVDTs were placed at the beam's ends to take continuous beam length shortening measurements (H1 and H2 in Fig. 5b). A thermocouple glued to the steel surface (T in Fig. 5a) measured internal temperature, while a digital thermo-hygrometer recorded the ambient temperature and humidity throughout the shrinkage test. Additionally, two control concrete cubes (100x100x100 mm), like that represented in Fig. 5c, were fabricated with the beam's concrete of series DW. Free shrinkage was measured by placing two strain gauges on the surface of each cube, and two 2x2 discs meshes for the DEMEC measurements. The shrinkage test lasted 112 days.

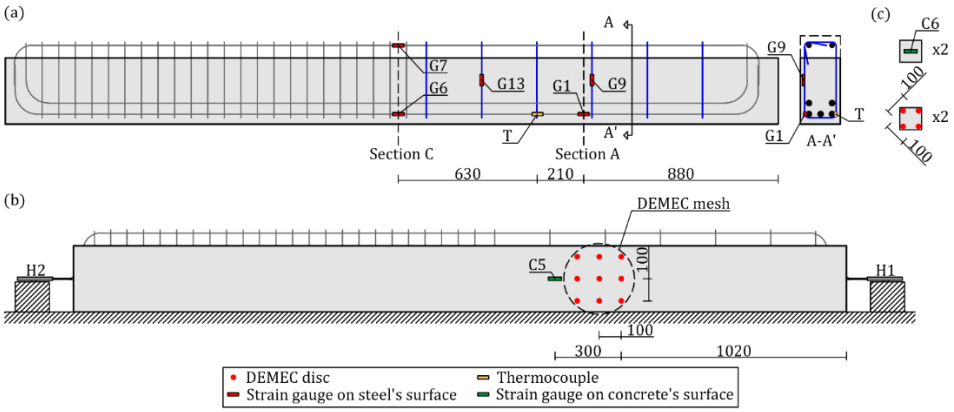

Fig. 5. Instrumentation of a DW beam for the shrinkage test: (a) internal instrumentation; (b) external instrumentation; (c) concrete cube instrumentation (dimensions in mm).

2.6. Test setup and procedure

A steel-loading frame was used to perform shear tests (Fig. 6a). The vertical load was applied by means of a 1200 kN hydraulic jack with displacement control (0.02 mm/s). The hydraulic actuator load was divided into two point loads by means of a steel frame with a joint to keep the load vertical (Fig. 6b). Load was transmitted to beams through two steel plates (200x200x30 mm). Beams were laid on two bearing points. As shown in Fig. 6c, they were made of a steel plate (250 mm width), a steel balls bed to eliminate the horizontal reaction and a joint to allow rotations on the plane of the steel-loading frame.

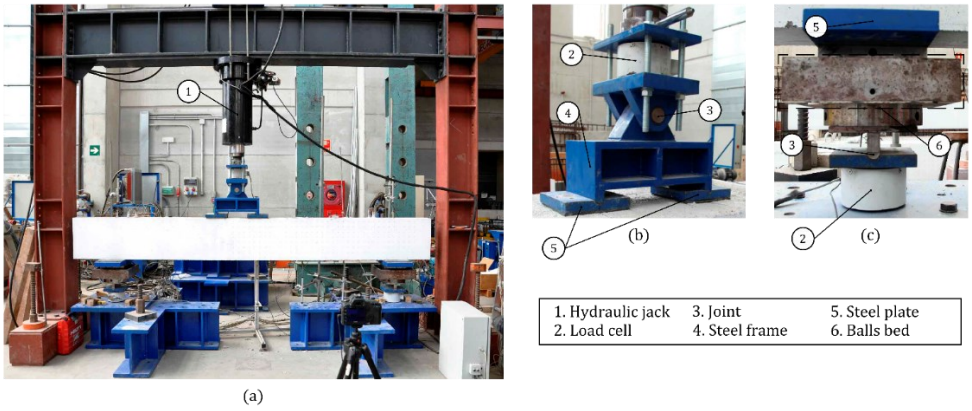

Fig. 6. Shear test experimental setup: (a) global view; (b) loading system; (c) bearing points system.

3. Test results and Discussion

3.1. Shear-deflection relation

Fig. 7 shows the relation between the shear force at the principal span V and the deflection below the point load closest to that span (LVDT V4 in Fig. 4b) of all test specimens, except beam HWP6A1, due to failure during the test process. The maximum shear force reached during tests (V_{exp}) and the shear force correspondent to the first diagonal crack appearing ($V_{diag,crack}$) are highlighted on curves. The $V_{diag,crack}$ value was obtained from the instrumentation results as the shear force for which significant strains were recorded for the first time in one of the instrumented stirrups (Fig. 4a) or large displacements in LVDTs O1 or O2 (see Fig. 4b), and by verifying the results with the test pictures.

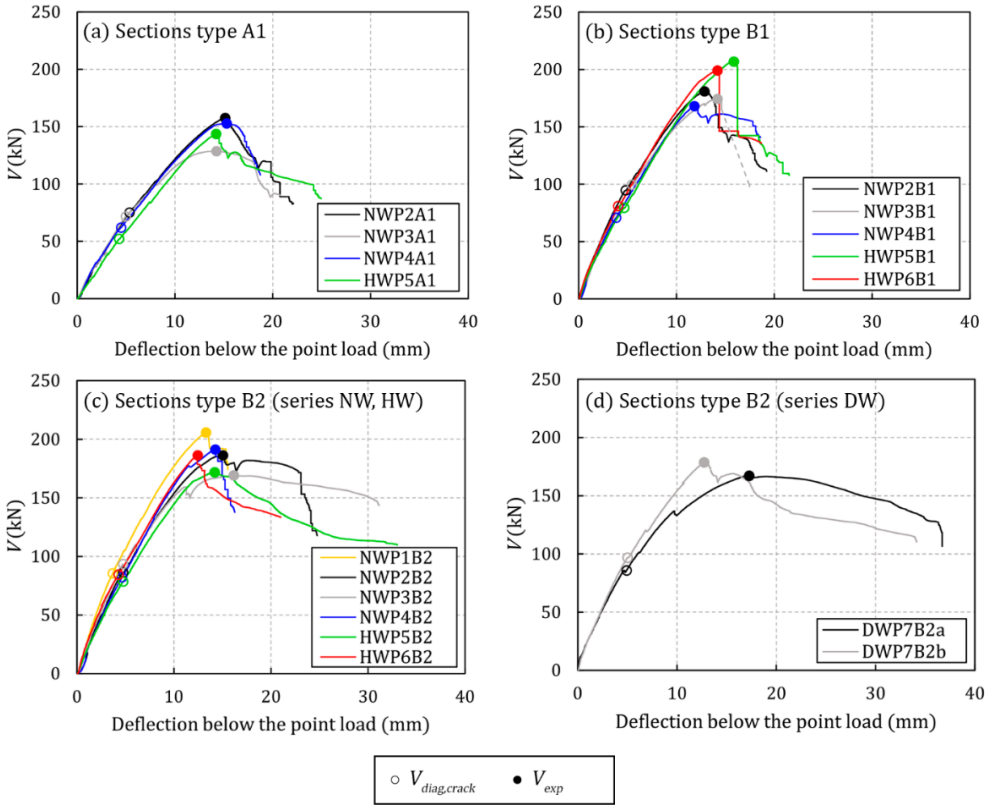

Fig. 7. Shear-deflection relation of test specimens: (a) sections type A1; (b) sections type B1; (c) sections type B2 from series NW and HW; (d) sections type B2 from series DW (specimen HWP6A1 not included: test process failure).

3.2. Shear strength

The vertical shear strength value of the test specimens (V_{exp}) is shown in Table 2. This table also indicates the interface shear stress concurrent with V_{exp} ($\tau_{h,exp}$), calculated as $V_{exp}/(0.9bd)$, as indicated in EC2 [12] and used by previous authors [11], based on equilibrium conditions, for the composite specimens of this experimental programme.

3.3. Crack pattern observations

The principal span crack patterns of all the beams in this experimental programme are shown in Fig. 8. The existent cracks when maximum shear V_{exp} was reached are represented, as are the cracks that occasionally appeared immediately after V_{exp} with a sudden load drop (e.g., see specimen HWP6B1 in Fig. 7), and the cracks observed at the end of tests.

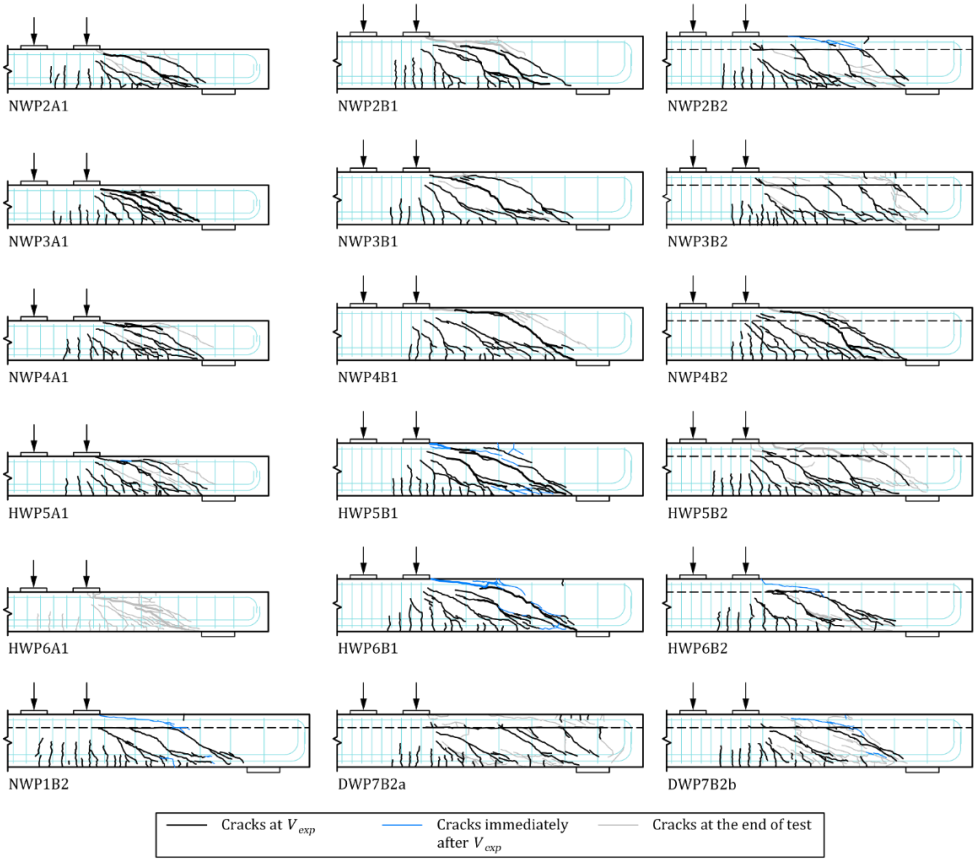

Fig. 8. Crack patterns of the test specimens in different test stages.

In the first load stages, all the specimens showed similar cracking propagation. The first observed cracks were bending cracks. These cracks appeared in the region of almost pure bending and extended vertically up to the beam's neutral axis (cracks observed in the area below the point load in Fig. 8), exactly as early research observed [35]. With increasing load, more bending cracks appeared along beams' principal span. The cracks in the zone below the load remained vertical, while the shear span cracks curved towards the point load after surpassing the tension longitudinal reinforcement level.

At a shear force between 36 and 57% of maximum shear, a diagonal crack opened during tests (see $V_{diag,crack}$ at Fig. 7). This opening was detected in the measurements of one of the vertical LVDTs (O1 or O2 in Fig. 4b). Consequently, the strain gauges located on the stirrups showed that the stirrup crossed by this crack underwent increased strain at that instant. As load increased, new diagonal cracks appeared on the principal span and an increase in the strain of the correspondent stirrup crossed by them took place.

When the diagonal cracks of the principal span exceeded the neutral axis depth, they became flatter on a second branch. After this load stage, major differences in beams' crack patterns were observed according to whether they were monolithic or composite.

3.3.1. Rectangular monolithic beams

In the rectangular monolithic beams (sections type A1 and B1), a variation in the inclination of diagonal cracks was observed on this second branch when they penetrated the compression chord (see Fig. 8). These diagonal cracks continued propagating through the compression chord in the point load direction and through the tension chord in the direction of the support as longitudinal cracks at the tension longitudinal reinforcement level until maximum shear force V_{exp} was reached.

After V_{exp}, a progressive load drop occurred during which the critical shear crack propagated towards the load plate (see NWP2A1 in Fig. 8). In some cases, the formation of a longitudinal crack at the compression longitudinal reinforcement level or splitting of the concrete cover along the compression longitudinal reinforcement was even observed (see NWP2B1 and NWP4A1 in Fig. 8). Diagonal cracks progressed further towards the support by means of cracks at the tension longitudinal reinforcement level.

3.3.2. Rectangular composite beams

In most of the tested beams with section type B2, while the inclination of the first branch of diagonal cracks was similar to that of the monolithic beams, the second branch of cracks took a horizontal direction, which was coincident with the interface between concretes. As seen in Fig. 8, the second branches of the diagonal cracks

spread until they connect to one another along the shear span. Specimens NWP1B2, NWP2B2, NWP3B2, HWP6B2, DWP7B2a and DWP7B2b displayed this behaviour. Vertical cracks at the top of the slab were observed above the point at which the diagonal cracks closest to the support reached the interface (e.g., see NWP3B2 in Fig. 8). The rest of the slab remained practically intact when beams reached V_{exp}. Immediately after V_{exp}, some specimens showed a small load drop in relation to a diagonal crack forming on the slab from the initial part of the interface crack closest to the support in the point load direction (see the shear-deflection relation of specimens NWP1B2, NWP2B2, HWP6B2 and DWP7B2b in Fig. 7 and their respective cracking patterns in Fig. 8). Other specimens displayed very ductile behaviour, with a very progressive load decrease, and without the formation of such a diagonal crack on the slab (see specimens NWP3B2 and DWP7B2a in Fig. 7 and their cracking patterns in Fig. 8).

In the other tested composite specimens, the influence of the interface between concretes on the trajectory of the diagonal cracks was less noticeable. Particularly in specimen HWP5B2, the drift of the diagonal cracks along the interface was limited and the connexion between the diagonal cracks at the interface did not take place at V_{exp} (see Fig. 8). After V_{exp}, some cracks on the slab appeared in specimen HWP5B2 during a gradual load decrease (see Fig. 7 and Fig. 8). Specimen NWP4B2 showed a similar crack pattern to that of the monolithic beams at both V_{exp} and the end of test. The critical shear crack did not change direction when it crossed the interface between concretes.

The horizontal splitting of the concrete cover along the tension longitudinal reinforcement was generally observed in all specimens.

3.4. Instrumentation results

Table 4 shows the main results obtained at V_{exp} from the strain gauges placed on the test specimens (see Fig. 4a). The stirrup stress at mid-length is shown for the instrumented stirrups of the principal span as $\sigma_{s,wi}$, where i is the number of stirrup (stirrups w1 to w4 in Fig. 4a), calculated as the average of the strains measured by the two strain gauges located at each stirrup multiplied by the material's modulus of elasticity. The result was limited to the steel yield strength. Note that in the specimens with section type A1, with more stirrups on the principal span, the result for the stirrup w5 is also shown, which corresponds to the stirrup closest to the load plate. The average strains measured by the two pairs of strain gauges located on the concrete's surface in Sections A and B of Fig. 4a are also shown respectively as $\varepsilon_{c,SA}$ and $\varepsilon_{c,SB}$. Finally, the average of the strains measured by the two strain gauges located at the tension longitudinal reinforcement below the point load (gauges G5 and G6 in Section C in Fig. 4a) is also shown in Table 4 as $\varepsilon_{s,l}$.

Table 4. Main results obtained from the instrumentation measurements at V_{exp} (specimen HWP6A1 not included: test process failure) (positive sign for compression).

Specimen	$\sigma_{s,w1}$[1] (MPa)	$\sigma_{s,w2}$[1] (MPa)	$\sigma_{s,w3}$[1] (MPa)	$\sigma_{s,w4}$[1] (MPa)	$\sigma_{s,w5}$[1] (MPa)	$\varepsilon_{c,SA}$ (‰)	$\varepsilon_{c,SB}$ (‰)	$\varepsilon_{s,l}$ (‰)
NWP1B2	-534	-534	-534	[2]	-	-	-	-2.39
NWP2A1	-534	-534	-534	-534	-532	-	-	-2.23
NWP2B1	-538	-538	-538	-511	-	-0.03	0.75	-1.85
NWP2B2	-502	-517	-451	-227	-	-4.06	1.40	-2.34
NWP3A1	-534	-534	-534	-534	-276	-	-	-1.83
NWP3B1	-538	-538	-538	-367	-	0.04	0.68	-1.89
NWP3B2	-538	-538	-538	-99	-	-0.15	1.63	-2.19
NWP4A1	[3]	-534	-534	-534	-354	-	-	-1.62
NWP4B1	-538	-538	-474	-168	-	0.36	1.43	-2.12
NWP4B2	-538	-538	-538	-359	-	-0.10	0.96	-2.21
HWP5A1	-534	-534	-534	-534	-365	-	-	-2.15
HWP5B1	-538	-538	-538	-538	-	-0.10	0.86	-2.53
HWP5B2	-538	-538	-538	-422	-	0.20	1.78	-2.03
HWP6B1	-538	-538	-538	-297	-	0.00	1.62	-2.14
HWP6B2	-538	-538	-538	-402	-	0.20	1.53	-2.11
DWP7B2a	-538	-532	-538	-54	-	0.16	1.11	-2.19
DWP7B2b	-538	-538	-538	-112	-	-0.18	1.10	-2.15

[1] Stresses calculated values with the strains measured by the strain gauges and the constitutive laws of the steel tested in laboratory.
[2] Non-instrumented stirrup in this test.
[3] The two strain gauges located on the stirrup failed.

Regarding the strain of the tension longitudinal reinforcement below the point load, it should be noted that in all the tests $\varepsilon_{s,l}$ was lower than the strain correspondent to the steel yield strength of the longitudinal reinforcement (approx. 2.8‰), which shows that specimens were far from the bending failure at V_{exp}.

On the other hand, on the DW series beams, it was observed that the value of the measurements taken by the instrumentation that controlled the beam's concrete shrinkage began to become asymptotic approximately 70 days after the shrinkage test started, which indicated that shrinkage had stabilised. The value of this asymptote for the free shrinkage measured by the gauges of the concrete control cubes (Fig. 5c) was an average strain of 0.7‰. In the concrete strain gauges located at beams (C5 in Fig. 5b), the asymptote was reached at an average strain of 0.2‰, and at an average strain of 0.1‰ in the internal steel gauges (Fig. 5a). The internal temperature of beams and ambient temperature were, on average, 26ºC, and the average ambient humidity was 64%.

3.5. Effect of test parameters on shear strength

Fig. 9 shows the shear strengths of the test specimens, including a summary table of the compressive strengths of the concretes used in both the beam and slab to facilitate finding differences due to the various introduced test parameters: the cross-sectional depth, the existence of an interface between concretes, the strength of the beam and slab's concretes and the differential shrinkage between concretes.

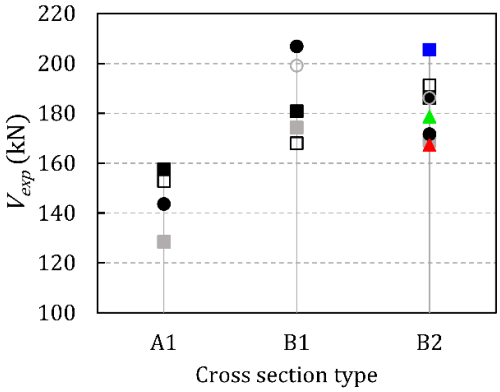

	$f_{c,b}$ (MPa)	$f_{c,s}$ (MPa)
NWP1	33	32
NWP2	37	34
NWP3	32	37
NWP4	39	33
HWP5	43	22
HWP6	52	36
DWP7B2a	29	37
DWP7B2b	29	37

Fig. 9. Experimental shear strength of test specimens and summary of compressive concrete strengths (specimen HWP6A1 not included: test process failure).

3.5.1. Cross-sectional depth

Regarding cross-sectional depth, the specimens with sections type A and B were compared to analyse the slab's contribution to shear strength. On average, the beams with sections type B1 and B2 had 26% and 24% higher shear strengths, respectively, than the A1 beams from the same fabrication batch. So it could be deduced that the cast-in-place slab contributed to resist shear.

When only analysing the NW series with concretes of similar compressive strengths in both the beam and slab, the depth enlargement in beams B1 and B2 increased shear strength in relation to the A1 beams at a similar percentage (20% and 25% on average, respectively). However, the depth increase of section B in relation to section A was 33%. The lesser increase in the shear strength of beams type B1 in relation to depth increase could only be explained by the size effect because the other parameters were identical. Therefore, as the increase in shear strength of the B2 beams was similar to that of the B1 beams, it was deduced that this lesser increase in the B2 beams' shear strength could also be due to the size effect, and not to an interface existing between concretes.

Furthermore, the relation between beam height increase and shear strength increase of NW specimens can be explained with coefficient k of equation 6.2 of EC2 [12],

which accounts for size effect. The relation between depth increase and shear strength increase was, on average, 1.108 for the B1 specimens and 1.064 for the B2 specimens, what came close to the relation between the k coefficients for A beams and B beams, which is 1.067.

In the beams with different compressive strength concretes at both the beam and slab (HW series), it was not appropriate to draw conclusions because of, on the one hand, the insufficient results obtained in the absence of the V_{exp} value of specimen HWP6A1 and, on the other hand, the apparent dispersion shown by the series HWP5 specimens as specimen HWP5A1 and specimen HWP5B1 acquired a lower and a higher shear strength than expected, respectively, in view of the compressive strengths of their concretes.

3.5.2. Existence of an interface between concretes

The existence of an interface between concretes affected specimens' crack pattern, as indicated in Section 3.3, causing in some cases cracks to develop along the interface. The degree of cracking at the interface was a phenomenon that showed some dispersion, what could be seen comparing the two composite specimens of series DW, which were manufactured under equal conditions but presented somewhat different cracking (see Fig. 8). This finding proved the dispersion that concrete elements subjected to tangential stresses (interface shear stresses in this case) display. However, certain variables that could influence the degree of interface cracking of the specimens in this experimental programme were found to exist. Regarding the specimens with reduced differential shrinkage between concretes (series NW and HW), greater or lesser interface cracking could have been related to the beam's concrete workability during casting (see the slump measurements in Table 2) and concrete's setting time (which depended on the water-cement ratio, being the setting faster in the concretes with a lower water-cement ratio). Thus we observed in the concretes with a higher degree of workability and a higher water-cement ratio that the interface with the "as-cast" roughness was smoother, which facilitated interface cracking during tests *versus* the concretes with a lower degree of workability and a lower water-cement ratio, whose interface was rougher. In the DW series beams, the previous variables could affect interface cracking, but mainly the shrinkage stresses generated at the interface when there is a difference in the shrinkage of the beam and slab's concretes [36] could be the cause of the extended interface cracking in both test specimens.

When comparing the shear strengths of the specimens from the same fabrication batch with section types B1 and B2 to analyse the influence of an existing interface, two behaviours were distinguished: that of series NW and that of series HW. In the NW series specimens, and regardless of the interface cracking type of specimens B2 (extended interface cracking or cracking like a monolithic beam), the maximum shear was similar in beam B1 and beam B2 from the same fabrication batch (see Fig.

9). Only in the NWP4 series did a major difference appear between the specimens with sections B1 and B2. However, this difference was attributed to the fact that the strength of specimen NWP4B1 was lower than expected. It was deduced for the composite specimens in this experimental programme that for equal concrete compressive strengths in both the beam and slab, the existence of an interface did not significantly influence the specimen's shear strength compared to the same specimen made with one concrete. Regarding the HW series specimens with different concrete compressive strengths in both the beam and slab, the specimens with section type B2 showed lower shear strength than the B1 specimens (Fig. 9). In both HWP5 and HWP6, the crack pattern of the beams type B2 at V_{exp} was scarcely affected by an interface existing between concretes (see Fig. 8). Consequently, it was deduced that the lower shear strength of the B2 specimens was due mainly to the existence of a lower compressive strength concrete at the slab.

3.5.3. Strengths of the beam and slab's concretes

When comparing series NW to series HW, the higher concrete strength of the HW series in the specimens with section type B1 provided higher shear strength, which was around 16% higher (see specimens B1 in Fig. 9). In the composite beams, no appreciable differences were observed in the V_{exp} of the series HW and NW beams, what could be due to the fact that specimens' shear strength depended mainly on the compressive strength of the slab's concrete which, in all the specimens of both series NW and HW, had a similar compressive strength (normal-strength concrete, as shown in Table 1). Only specimen NWP1B2 had a much higher V_{exp} than the average value recorded for the other composite specimens, despite showing greater interface cracking than other specimens (see Fig. 8) and a lower compressive strength of the slab's concrete than the other specimens did (see Fig. 9). Once again, this demonstrated the scattering that can be found in shear.

3.5.4. Differential shrinkage between concretes

The shear strengths of the series NW specimens were compared to those of the series DW specimens. The major differential shrinkage that took place between the beam and slab concretes had no significant influence on the shear strength of the composite specimens as similar shear strengths to those of the specimens with reduced differential shrinkage were obtained (see Fig. 9).

4. Shear strength mechanism

4.1. Failure mode description

Until the time the first diagonal crack appeared, all the monolithic and composite specimens showed the same shear strength mechanism as that observed in the

reinforced concrete beams with the same characteristics as those of this programme, and without web reinforcement [26], as previously described by several authors [37,38]. Until the first diagonal crack formed, shear was resisted by the combined action of the following shear transfer actions: cantilever action, dowel action, aggregate interlock, residual tensile strength of concrete, and the arching action or inclination of the compression strut above cracks.

Whereas diagonal crack (critical shear crack) development entailed a maximum shear strength of the element in the beams with no transverse reinforcement, the existence of transverse reinforcement allowed it to absorb the tension forces that were generated in concrete, and to vertically confine the compression chord and limit crack width to, thus, contribute to increase the shear strength of the beam's web. This allowed specimens to achieve higher shear strengths. Thus as new diagonal cracks developed from existing bending cracks, beams' stirrups were activated; that is, their strain significantly increased when they were crossed by a diagonal crack, as indicated in Section 3.3.

In monolithic specimens and in those composite specimens with quasimonolithic behaviour (NWP4B2 and HWP5B2), in which the existence of the interface did not significantly modify the crack pattern, it was observed that, as load increased, damage concentrated on one of the diagonal cracks, the critical shear crack (see Fig. 8). As load increased, crack opening also increased and, thus, the aggregate interlock, cantilever action and the residual tensile strength of concrete decreased, and the strength of other mechanisms increased, such as transverse reinforcement action, the dowel action of longitudinal reinforcement or arching action, until a maximum shear strength was reached (V_{exp}). Afterwards, failure occurred with sudden crack extension towards the loading point due to a shear failure of the compression chord.

However, in the remaining composite beams of this experimental programme (NWP1B2, NWP2B2, NWP3B2, HWP6B2, DWP7B2a, DWP7B2b), diagonal cracks developed along the interface and clearly separated the lower beam, or precast beam, from the top slab, which delayed the penetration of diagonal cracks into the compression chord. Fig. 8 shows that at V_{exp} the diagonal cracks of the indicated specimens did not penetrate the top slab, so it remained intact. Thus in the precast beam, with many diagonal cracks, the main shear strength mechanisms were web reinforcement, the dowel action of longitudinal reinforcement and the aggregate interlock. Interface cracking development cancelled mechanisms like cantilever action between cracks. The slab could behave as a compressed element that transmitted shear like an element with no shear reinforcements. The connection between both elements (precast beam and slab) took place through the activation of other shear strength mechanisms: the dowel action of transverse reinforcement when it was crossed by the interface crack or the aggregate interlock in the interface crack. After V_{exp}, sudden failure in some specimens occurred due to the formation

of a diagonal crack that crossed the slab (see specimens NWP1B2, NWP2B2, HWP6B2 and DWP7B2b in Fig. 8), which denoted the shear failure of the compression chord, while others displayed more ductile failure due to the slab's bending failure (see specimens NWP3B2 and DWP7B2a in Fig. 8).

4.2. Proposed shear strength mechanical model for the composite beams

Based on the failure mode observations, a mechanical model for assessing the shear strengths of the composite specimens of this experimental programme is proposed. The model for calculating the shear strength of the composite specimens with interface cracking is first described. After that, the experimental evidence that support the proposed model are presented. Finally, the application of the proposed model to the composite specimens of the experimental programme when the extension of the interface crack is unknown is described.

It should be noted that the proposed model was developed for its use in the shear strength assessment of this experimental programme's composite specimens, providing a better understanding of the shear strength mechanism developed by this type of elements that could be used as a reference for the future development of a method to assess composite beams' shear strength. To extend the scope of application of this mechanical model, further experimental tests are needed.

4.2.1. Proposed shear strength model for the composite beams with interface cracking of the experimental programme

Fig. 10a depicts a simplified representation of the observed shear strength mechanism by means of a strut-and-tie model for the specimen NWP3B2 test, which is an example of a test with more extended interface cracking. Fig. 10a represents the two shear transmission paths that were observed in the composite beams with interface cracking; one through the precast beam and another one through the cast-in-place slab.

The shear strength mechanism of the precast beam is explained by means of a strut-and-tie model composed of two superimposed trusses. In this model, the struts represent the compressive stresses carried by the beam's web and the aggregate interlock in the shear cracks. The finite-dimensional nodes at the level of the tension longitudinal reinforcement (see Fig. 10a) represent the dowel action of this reinforcement. The shear strength of the cast-in-place slab is modelled with a simple truss strut-and-tie model without shear reinforcement. Both triangulated bar structures are connected to one another by finite-dimensional nodes at the interface. There are mainly two considered horizontal forces that act at these nodes: the dowel action of transverse reinforcement in the interface crack and the force resulting from the aggregate interlock in the interface crack (Fig. 10b). The vertical forces that converge in nodes are considered self-balanced in each part independently (precast

beam on one side and slab on the other) so that the transmission of vertical forces between the beam and slab is neglected in this model.

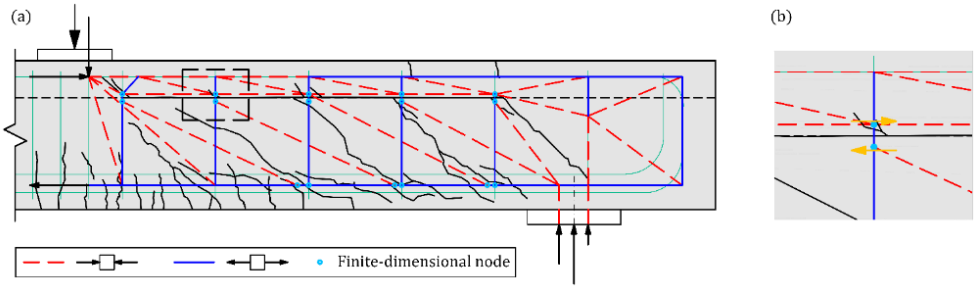

Fig. 10. Proposed strut-and-tie model of the shear strength mechanism developed by specimen NWP3B2: (a) precast beam and cast-in-place slab models; (b) forces at the finite-dimensional nodes of the interface crack.

In the composite beams of this experimental programme with an extended interface cracking (NWP1B2, NWP2B2, NWP3B2, HWP6B2, DWP7B2a, DWP7B2b), three different variants of the strut-and-tie model represented in Fig. 10 were observed which depend on the extension of the interface crack along the principal span. The calculation procedure of the shear strength of the specimens with those variants consists on obtaining separately the component of the total shear at the principal span that is resisted by the precast beam (V_{pb}) and the component of the total shear transmitted by the slab (V_s). Two possible failure modes were observed at the slab: bending failure ($V_{s,BF}$) or shear failure ($V_{s,SF}$). Thus, the shear strength of the composite element estimated with the proposed model (V_{pred}) is calculated as:

$$V_{pred} = V_{pb} + V_s = V_{pb} + min\{V_{s,BF}, V_{s,SF}\} \quad (1)$$

The proposed formulation for the calculation of those shear components is explained in Annex B.

The results of calculating the shear strength of the precast beam and the slab by means of the proposed calculation methodology are shown in Table 5.

The proposed model for the precast beam provided a similar V_{pb} result for all the studied specimens (Table 5). The obtained difference lay in the yield strength of stirrups' steel.

Table 5. Main results of the proposed shear strength model for the composite specimens of the experimental programme with extended interface cracking.

Specimen	V_{pb} (kN)	$V_{s,BF}$ (kN)	$V_{s,SF}$ (kN)	V_{pred} (kN)	V_{exp}/V_{pred}
NWP1B2	107.4	125.1	62.6	170.0	1.21
NWP2B2	108.2	75.1	70.1	178.3	1.04
NWP3B2	108.2	52.6	72.7	160.8	1.05
HWP6B2	116.6	133.8	69.0	185.6	1.00
DWP7B2a	108.2	52.6	72.4	160.8	1.04
DWP7B2b	108.2	75.1	74.9	183.1	0.98

In specimens NWP1B2, NWP2B2, HWP6B2 and DWP7B2b, the lowest shear strength calculated in the slab was obtained from the shear failure criterion ($V_{s,SF}$). Hence according to the proposed model, these specimens accomplished their shear strength after exceeding the slab's ultimate shear. On the contrary, specimens NWP3B2 and DWP7B2a had a lower slab shear strength when it was obtained from the bending failure criterion ($V_{s,BF}$), which indicated that their shear strength was given by the yielding of the slab's longitudinal reinforcement prior to the slab's shear failure.

Despite adapting the model to the crack pattern of specimen NWP1B2, the model showed a very safe approximation to the actual value (V_{exp}/V_{pred} = 1.21), which could be due to the anomalous result of this specimen, which presented overstrength compared to the other specimens with section type B2 (see Section 3.4). Even so, the described model offered a good approximation to the experimental results, with a mean V_{exp}/V_{pred} value of 1.05 and a 7.06% coefficient of variation for the six analysed specimens.

4.2.2. Experimental evidence for the proposed model

There are several experimental results that support the adequacy of the proposed model to the shear strength behaviour shown by the composite specimens with extended interface cracking.

The stress reached by the stirrups of the principal span at V_{exp} at their mid-length was yield strength, or it came close to it in most cases (see Table 4). In general, stirrup w4 (Fig. 4a) had a lower stress, which could be because it was not crossed by a diagonal crack near the strain gauge location, and also because it was located close to the point load area. However, it is considered acceptable for the model to adopt the simplification of this stirrup also achieving its yield strength because this assumption does not significantly affect the result.

Regarding the cast-in-place slab model, the strain gauges located on the concrete surface on top of the slab in Sections A and B (Fig. 4a) of the composite specimens

with extended interface cracking measured strains consistently with the tensile or compressive forces considered in the model. In Section B, strain gauges showed compression throughout the test ($\varepsilon_{c,SB}$ in Table 4). However in Section A, gauges measured compression strains in the first test stages, but then changed towards tension strains. At V_{exp} the strains measured in Section A ($\varepsilon_{c,SA}$ in Table 4) were mainly negative (tension). The model represented in Fig. 10 illustrates this change from the compression strains near Section B to the tension strains near Section A in the upper slab part.

Regarding the cast-in-place slab failure type, in the specimens in which the proposed model indicated shear failure (NWP1B2, NWP2B2, HWP6B2, DWP7B2b), a diagonal crack that crossed the slab in the direction to the point load appeared immediately after V_{exp} (see Fig. 8). That diagonal crack did not show any signs of starting from the bending cracks in the slab but originated from within the slab (see the crack located between nodes 4 and 15 of the slab in Fig. B.1b). This justifies using Kupfer failure criterion [39] described herein in Annex B to calculate the shear strength of the slab failing in shear $V_{s,SF}$. In these specimens, the appearance of this diagonal crack took place along with a marked drop in shear, as observed on the shear-deflection relation curves (Fig. 7), typical of brittle shear failures. The specimens in which the proposed model indicated a bending failure of the slab (NWP3B2 and DWP7B2a) showed a very gradual decrease in shear after V_{exp}, typical of ductile failures due to bending.

4.2.3. General application of the proposed model to the composite specimens

As observed in the formulation of the proposed model, the use of one strut-and-tie model or another of the depicted in Fig. B.1, depends on how far the interface crack extends along the principal span. This is difficult to know prior to testing, during the design or in strength assessment phases.

The model proposed for specimens NWP3B2 and DWP7B2a (Variant A in Fig. B.1), in which the interface crack length is maximum because it covers the entire principal span, provided the lowest V_{pred} values, which were achieved by the yielding of the slab's longitudinal reinforcement.

If the crack length at the interface is not known, adopting the Variant A of the proposed model (see Annex B) to calculate the shear strength of the composite specimens will give a result on the safety side, which will be a lower bound of the shear strength that these specimens can develop. This model is also the simplest of the three proposed variants since the slab's shear strength is given by the yielding of the slab's longitudinal reinforcement, so it does not require doing iterative calculations. Only the formulas of Table B.1 for Variant A and the equation B.1 would be used.

Section 5 analyses the extent to which the proposed model was on the safety side for the composite specimens in this experimental programme by assuming that the interface crack length was maximum in them all.

5. Comparison of test results with existing code provisions and the proposed model

5.1. Vertical shear strength

In order to assess the vertical shear strength of the test specimens, the formulations of the following current design codes for the elements with shear reinforcement were used: EC2 [12], MC-10 [13] at its three approximation levels, and the two formulations of ACI 318-19 [10] (named (a) and (b) in Section 22.5.5.1). The composite specimens were also assessed with the proposed model as herein indicated in Section 4.4; that is, considering that the interface crack extended along the entire principal span in all specimens. With all the formulations, the tested average values of the materials were used. The partial safety factors for concrete (γ_c) and steel material properties (γ_s) were 1.0.

Table 6 shows the mean value and the coefficient of variation (CV) of the V_{exp}/V_{pred} ratio for each set of specimens assessed by the different formulations. These statistical indicators were used to analyse the studied sample, bearing in mind that the number of elements in the sample should have been higher for these indicators to take a significant value. To analyse the accuracy of the formulations in predicting shear strength, the 17 experimental programme specimens (excluding HWP6A1 due to test process failure) were grouped into three sets: nine monolithic specimens; six composite specimens with concretes of similar compressive strengths in both the beam and slab (series NW and DW); two composite specimens with different compressive strength concretes in both the beam and slab (series HW). In the composite specimens, shear strength was calculated by different methods considering that: only the precast beam resisted shear, for which the effective beam depth (d_b) and the compressive strength of the beam's concrete ($f_{c,b}$) were used; and the entire composite beam resisted shear, for which the used parameters were the composite beam's effective depth (d_c) and the beam's concrete strength ($f_{c,b}$), the slab's concrete strength ($f_{c,s}$) or the weighted average of the concrete strengths of both the beam and slab estimated from the area ratio ($f_{c,wa}$). For the composite specimens of series NW and DW, Table 6 shows only the value calculated with $f_{c,wa}$, because it hardly differed from the values calculated with $f_{c,b}$ or $f_{c,s}$ as these specimens were made by concretes with similar compressive strengths. No formulation for any specimen offered unsafe results.

Table 6. Statistical indicators of the V_{exp}/V_{pred} ratio for the test specimens (specimen HWP6A1 not included: test process failure).

Specimens	No. of specimens	Method	EC2		MC-10 LI		MC-10 LII		MC-10 LIII		ACI 318-19 (a)		ACI 318-19 (b)		Proposed model	
			Mean	CV (%)	Mean	CV (%)	Mean	CV (%)	Mean	CV (%)	Mean	CV (%)	Mean	CV (%)	Mean	CV (%)
Monolithic	9	d_b, $f_{c,b}$	1.17	8.13	1.68	8.13	1.46	7.85	1.18	6.88	1.41	7.05	1.20	6.93	-	-
Composite (NW,DW)	6	d_b, $f_{c,b}$	1.46	20.23	2.10	20.23	2.02	7.89	1.67	7.22	1.81	18.99	1.47	16.35	-	-
		d_c, $f_{c,wa}$	1.13	7.42	1.63	7.42	1.44	7.91	1.19	7.62	1.40	6.92	1.20	6.88	1.14	7.84
Composite (HW)	2	d_b, $f_{c,b}$	1.57	4.06	2.26	4.06	1.97	4.06	1.55	2.55	1.81	1.55	1.43	1.00	-	-
		d_c, $f_{c,b}$	1.10	4.06	1.59	4.06	1.40	4.06	1.10	2.58	1.27	1.55	1.07	1.14	1.12	3.81
		d_c, $f_{c,s}$	1.10	4.06	1.59	4.06	1.40	4.06	1.19	0.52	1.42	0.86	1.23	1.78	1.12	3.81
		d_c, $f_{c,wa}$	1.10	4.06	1.59	4.06	1.40	4.06	1.12	2.31	1.30	1.11	1.10	0.62	1.12	3.81

In the monolithic specimens, EC2 gave the closest approximation to the actual strength, with adequate scattering (see Table 6). Its formulation was also easy to apply. The LI and LII of MC-10 offered very safe results. Nonetheless, MC-10 LIII gave a good approximation, which came close to that of EC2, but its application could prove more difficult given its iterative formulation. ACI 318-19 (a) gave a safe result, while (b) gave a more accurate value, like those of EC2 and MC-10 LIII, and was still easy to calculate.

In Section 10.9.3(8), EC2 offers the possibility of designing precast elements with a concrete topping as composite elements, but it does not indicate how. With the results in Table 6, and as expected, the result obtained when considering only the precast beam (d_b) laid very much on the safety side in all the composite specimens. However, when the composite beam depth (d_c) was considered, a result closer to the actual one was obtained with very little dispersion, and in both the specimens with the same concretes (mean value of 1.13) and different concretes (1.10). Note that the EC2 formulation did not depend on the compressive strength of the concrete for the specimens in this experimental programme.

As MC-10 does not mention the shear treatment that the composite elements must receive, its shear formulation for assessing monolithic elements' shear strength was used to predict the shear strength of the composite specimens in this experimental programme, and its accuracy was analysed. Firstly, a very safe result was observed if only the precast beam (d_b) was considered. If the entire composite beam's effective depth (d_c) was contemplated, both LI and LII, which do not depend on the concrete compressive strength, still gave very safe results. LIII, which is a function of concrete compressive strength, gave an adequate result for the specimens of series NW and DW (mean value of 1.19), similarly to that obtained for the monolithic specimens

(1.18). The most accurate result for the two specimens of series HW, with a higher concrete compressive strength in the beam than in the slab, was obtained when $f_{c,b}$ was used (1.10).

ACI 318-19 indicates in Section 22.5.4 that the composite specimens' shear strength can be calculated with the individual elements' properties, which would be comparable to using $f_{c,wa}$ [9,11], or the properties of the element that result in the most critical value; that is, employing the lowest value of $f_{c,b}$ and $f_{c,s}$. Formulation (a) offered results that were very much on the safety side compared to (b), and both were very simple to apply. In the beams of series NW and DW, formulation (b) showed a good result (mean value of 1.20), although it was less precise than that of EC2 (1.13). In the two specimens of series HW, $f_{c,wa}$ gave a very good mean value (1.10) with a very low CV (0.62%), while the use of the lower compressive strength of either the beam or slab, which was that of the slab in this experimental programme, gave a very safe result. As expected, the calculation done with $f_{c,b}$ gave a closer result to the actual one (1.07), but its use is not considered in ACI 318-19.

Finally, employing the model proposed in Section 4.4 of this paper for the composite elements led to good precision, on the safety side and with low dispersion for both specimens of similar concretes in the beam and the slab (mean value of 1.14) and for different concretes (1.12). The obtained results were very similar to those of EC2 in both cases (1.13 and 1.10, respectively) and to that of ACI 318-19 (b) for series HW (1.10). It should be noted from the proposed model that it is based on a composite beam mechanical model that is supported by the experimental results, in which the component of the shear resisted by the precast beam and the component resisted by the slab are calculated by assuming that interface cracking occurs. Furthermore, the model does not depend on the concrete compressive strength of both the beam and slab as the shear component resisted by the beam depends on the yield strength of stirrups' steel, while the shear component resisted by the slab depends on the yield strength of the steel of the slab's longitudinal reinforcement.

5.2. Interface shear

Table 7 offers the mean value and the coefficient of variation (CV) of the relation between the experimental interface shear stress $\tau_{h,exp}$ concurrent with V_{exp} (see Table 2), calculated as explained in Section 3.2, and the predicted interface shear stress by design codes $\tau_{h,pred}$ for the composite specimens. The formulations of the following design codes for shear at the interface between the concretes in the elements with reinforcement crossing the interface were used: EC2 [12], MC-10 [13] and ACI 318-19 [10]. The coefficients indicated in each code for smooth interfaces (free surface not intentionally roughened, left without further treatment after vibration) were considered. The materials' tested average values were employed with all the

formulations. Partial safety factors γ_c and γ_s were 1.0. All the codes used gave safe results for all the specimens.

Table 7. Statistical indicators of the $\tau_{h,exp}/\tau_{h,pred}$ ratio for the eight composite specimens in the experimental programme.

Code	EC2	MC-10	ACI 318-19
Mean	2.97	4.97	6.11
CV (%)	5.84	5.88	6.67

All the codes presented very conservative results for the interface shear of the specimens in this programme, whose $\tau_{h,exp}$ represented a lower bound of the specimen's interface shear, calculated for the maximum experimental vertical shear strength V_{exp} as specimens did not fail in interface shear. The EC2 formulation, based on the Mohr-Coulomb failure criterion, was that which most closely approximated the experimental result, which almost tripled $\tau_{h,pred}$ (see Table 7). The MC-10 formulation, which is very similar to that of EC2, gave a safer result with a similar CV. In both cases, the term of the formula that considers the existence of compressive stress resulting from an eventual normal force acting on the interface, multiplied by a friction coefficient, was neglected, which is usual in designs, given the difficulty to quantify this stress in such elements. If it had been considered, a higher $\tau_{h,pred}$ would have been obtained. For ACI 318-19, the formulation limits interface shear to 0.55 MPa when the interface is not intentionally roughened, regardless of the existence or nonexistence of reinforcement crossing the interface. Hence a very safe result was obtained.

6. Summary and Conclusions

The objective of this paper was to analyse the shear strength mechanism of composite reinforced concrete beams with web reinforcement. To do so, 18 specimens of rectangular cross-section were experimentally tested, in which the following parameters that influence shear strength varied: the cross-sectional depth, the existence of an interface between concretes, the strengths of both the beam and slab's concretes and differential shrinkage between concretes. A mechanical model was proposed to assess the shear strength of the composite elements in the experimental programme based on the experimental observations. Finally, the formulations to calculate the vertical and interface shear strengths of different current design codes were verified. The main conclusions were as follows:

1. Placing a cast-in-place slab on top of the precast beam increased the element's shear strength. The shear strength of the composite beam made with concretes of similar compressive strengths in both the precast beam and cast-

in-place slab was higher than the shear strength of only the precast beam, and was similar to the shear strength of a monolithic beam with the same depth as the composite beam, made of concrete whose compressive strength was similar to that of the composite beam.

2. In general, the existence of an interface between concretes modified the crack pattern of the composite beams *versus* that of monolithic beams by forcing diagonal cracks to develop along the interface.
3. In the composite beams with a similar concrete compressive strength in both the beam and slab, the existence of an interface did not significantly modify the element's shear strength, regardless of the interface presenting more or less cracking, while the composite beams with higher concrete compressive strength in the precast beam than in the slab showed lower shear strengths than their homologous monolithic specimens made with the same concrete as that of the precast beam. Consequently, the shear strength of the composite beams analysed in this experimental programme depended on the concrete compressive strength of the slab or the compression chord.
4. The major differential shrinkage between the concretes of both the beam and slab did not significantly modify the shear strength of the composite beams in this experimental programme in relation to that of those specimens with reduced differential shrinkage.
5. The experimental observations indicated that in the composite specimens with extended interface cracking, shear was transmitted through two load paths: one part through the precast beam and the other through the cast-in-place slab. Consequently, the total shear resisted by the composite beam had two components: the shear resisted by the precast beam and the shear resisted by the cast-in-place slab. The transmission of horizontal forces between both load paths occurred through the interface crack due to the aggregate interlock at the crack and the dowel action of the transverse reinforcement crossing the crack.
6. The mechanical model proposed to assess the shear strength of the composite elements in this experimental programme adapted to each specimen's crack pattern. The shear transmission through the precast beam was modelled using a double truss strut-and-tie model in which the failure criterion was the yielding of stirrups. The shear transmission through the cast-in-place slab was modelled by a simple truss strut-and-tie model without shear reinforcement in which two possible failures were considered: the slab's bending failure due to the yielding of the slab's longitudinal reinforcement or the slab's shear failure when its concrete stresses reached the Kupfer's failure surface. The models adopted for each specimen in the experimental programme offered a very accurate approximation of the actual shear strength with a low coefficient of variation.

7. If the interface crack extension is unknown, the mechanical model proposed to calculate shear strength is that formulated for the composite beams showing the greatest interface cracking, in which the slab's failure is due to the yielding of the slab's longitudinal reinforcement, because it predicts a safe result for the element's shear strength. This model does not depend on the concrete compressive strength of both the beam and slab.
8. While assessing the shear strength of the composite specimens with the different current design formulations, considering that only the precast beam resists shear gave a very safe result in all cases. When the entire composite beam depth was used, the EC2 formulation [12], which does not depend on the concrete compressive strength in the specimens in this experimental programme, gave very good results that were similar to those obtained by applying the model herein proposed; approximation levels I and II of MC-10 [13] provided very safe results, while level III presented a better approximation, especially when the compressive strength of the precast beam's concrete was used to assess the composite beams with different concretes. As for the two formulations of ACI 318-19 [10], formulation (a), which is simpler, was very much on the safety side in all cases, while (b) gave very good results when the weighted average of the beam and slab's concrete compressive strengths was used. The formulations for the interface shear offered very safe results with employing the three codes.

This research work has increased the number of experimental tests on reinforced concrete composite beams with transverse reinforcement and has contributed to the study of the shear strength mechanism developed by such elements. It should be noted that the above conclusions were drawn for a limited number of specimens and that more tests should be run to reach relevant conclusions. In order to delve into the analysis of the shear strength mechanism and to improve the proposed model, tests should be done on elements with different dimensions and cross-sectional shapes.

Acknowledgements

The experimental programme of this research work was undertaken at the Concrete Science and Technology University Institute (ICITECH) of the Universitat Politècnica de València (UPV; Spain) with concrete supplied by Caplansa. The project was supported by the Spanish Ministry of Science and Innovation through Projects BIA2015-64672-C4-4-R and RTI2018-099091-B-C21-AR; the Regional Government of Valencia through Project AICO/2018/250; the European Union with FEDER funds. The authors thank the Spanish Ministry of Economy and Business for Grant BES-2016-078010 that supported Lisbel Rueda-García.

References

[1] Comité technique 4.3 - Ponts routiers Technical Committee 4.3 - Road Bridges. Estimation of load carrying capacity of bridges based on damage and deficiency. PIARC World Road Association: 2016.

[2] Halicka A. Influence new-to-old concrete interface qualities on the behaviour of support zones of composite concrete beams. Constr Build Mater 2011:4072–8.

[3] Saemann and Washa, G. W. JC. Horizontal Shear Connections between Precast Beams and Cast-in-Place Slabs. ACI J Proc 1964;61:1383–409.

[4] Loov RE, Patnaik AK. Horizontal Shear Strength of Composite Concrete Beams With a Rough Interface. PCI J 1994;39:48–69.

[5] Kahn LF, Slapkus A. Interface Shear in High Strength Composite T-Beams. PCI J 2004;49:102–10.

[6] Kovach J, Naito C. Horizontal Shear Capacity of Composite Concrete Beams without Interface Ties. ATLSS Report No. 05-09: 2008.

[7] Fang Z, Jiang H, Liu A, Feng J, Chen Y. Horizontal Shear Behaviors of Normal Weight and Lightweight Concrete Composite T-Beams. Int J Concr Struct Mater 2018;12. https://doi.org/10.1186/s40069-018-0274-3.

[8] Mahmoud MA, Elafandy TH, Okail HO, Abdelrahman AA. Interfacial shear behavior of composite flanged concrete beams. HBRC J 2014;10:206–14.

[9] Kim C-G, Park H-G, Hong G-H, Kang S-M. Shear strength of composite beams with dual concrete strengths. ACI Struct J 2016;113:263–74.

[10] ACI Committee 318. Building code requirements for structural concrete (ACI 318-19); and commentary (ACI 318R-19). Farmington Hills: American Concrete Institute; 2019.

[11] Kim C-G, Park H-G, Hong G-H, Kang S-M, Lee H. Shear Strength of Concrete Composite Beams with Shear Reinforcements. ACI Struct J 2017;114:827–37.

[12] CEN. EN 1992-1-1:2004. Eurocode 2: Design of concrete structures - Part 1-1: General rules and rules for buildings. 2004.

[13] Fédération International du Béton (fib). Model Code 2010. Ernst & Sohn; 2012.

[14] Hernandez G. Strength of Prestressed Concrete Beams with Web Reinforcement. 1958.

[15] Olesen S, Sozen MA, Siess CP. Investigation of prestressed reinforced concrete for highway bridges, part IV, strength in shear of beams with web reinforcement. 1967.

[16] Hartmann DL, Breen JE, Kreger ME. Shear capacity of high strength prestressed concrete girders. Austin: 1988.

[17] Shahawy MA, Batchelor B deV. Shear Behavior of Full-Scale Prestressed Concrete Girders: Comparison Between AASHTO Specifications and LRFD Code. PCI J 1996;41:48–62. https://doi.org/10.15554/pcij.05011996.48.62.

[18] Cumming, A David., Shield, Carol K., French CE. Shear Capacity of High-Strength Concrete Pre-stressed Girders. 1998.

[19] Runzell B, Shield C, French C. Shear Capacity of Prestressed Concrete Beams. 2007.

[20] Hawkins NM, Kuchma DA. Application of LRFD Bridge Design Specifications to High- Strength Structural Concrete: Shear Provisions. 2007.

[21] Avendaño AR, Bayrak O. Shear strength and behaviour of prestressed concrete beams. Technical Report: IAC-88-5DD1A003-3, Texas Department of Transportation: 2008.

[22] Hamilton III HR, Llanos G, Ross BE. Shear performance of existing prestressed concrete bridge girders. 2009.

[23] Ross BE, Ansley MH, Hamilton III HR. Load testing of 30-year-old AASHTO Type III highway bridge girders. PCI J 2011;56.

[24] Halicka A, Jabłoński Ł. Shear failure mechanism of composite concrete T-shaped beams. Proc Inst Civ Eng Struct Build 2016;169:67–75.

[25] Jabłoński Ł, Halicka A. Influence of the interface reinforcement on static performance of concrete composite T-shaped beams. Bud i Archit 2020;19:063–76. https://doi.org/10.35784/bud-arch.2170.

[26] Rueda-García L, Bonet Senach JL, Miguel Sosa PF, Fernández Prada MÁ. Experimental analysis of the shear strength of composite concrete beams without web reinforcement. Eng Struct 2021;229:111664. https://doi.org/10.1016/j.engstruct.2020.111664.

[27] Kani MW, Mark W. Huggins, Rudi R. Wittkopp. Kani on shear in reinforced concrete. Toronto: University of Toronto, Dept. of Civil Engineering; 1979.

[28] Rueda-García L, Bonet Senach JL, Miguel Sosa PF. Experimental study of concrete composite beams subjected to shear. Proc. fib Symp. 2019 Concr.

- Innov. Mater. Des. Struct., 2019, p. 1779–86.

[29] UNE-EN 12350-2:2020. Testing fresh concrete - Part 2: Slump test. 2020.

[30] UNE-EN 12390-3:2020. Testing hardened concrete - Part 3: Compressive strength of test specimens. 2020.

[31] UNE-EN 12390-6:2010. Testing hardened concrete - Part 6: Tensile splitting strength of test specimens. 2010.

[32] UNE-EN 12390-13:2014. Testing hardened concrete - Part 13: Determination of secant modulus of elasticity in compression. 2014.

[33] Comisión Permanente del Hormigón. EHE-2008. Instrucción de Hormigón Estructural. Ministerio de Fomento. Madrid: 2008.

[34] UNE-EN ISO 6892-1:2017. Metallic materials - Tensile testing - Part 1: Method of test at room temperature. 2017.

[35] Palaskas MN, Attiogbe EK, Darwin D. Shear strength of lightly reinforced T-beams. J Am Concr Inst 1981;78:447–55.

[36] Silfwerbrand J. Stresses and strains in composite concrete beams subjected to differential shrinkage. ACI Struct J 1997;94:347–53.

[37] Fernández Ruiz M, Muttoni A, Sagaseta J. Shear strength of concrete members without transverse reinforcement: A mechanical approach to consistently account for size and strain effects. Eng Struct 2015;99:360–72. https://doi.org/10.1016/j.engstruct.2015.05.007.

[38] Marí A, Cladera A, Bairán J, Oller E, Ribas C. Shear-flexural strength mechanical model for the design and assessment of reinforced concrete beams subjected to point or distributed loads. Front Struct Civ Eng 2014;8. https://doi.org/10.1007/s11709-014-0081-0.

[39] Kupfer HB, Gerstle KH. Behavior of concrete under biaxial stresses. ASCE J Eng Mech Div 1973;99:853–66.

Appendix A. Nomenclature

These Appendixes contain additional information that is not provided in the main body of the paper for the sake of brevity.

a	shear span
A_{sl}	area of the cross-section of the slab's longitudinal reinforcement
A_{sw}	area of the cross-section of the two legs of a stirrup

b	width of concrete section
c	concrete cover
d	effective depth
d'	depth of the slab's longitudinal reinforcement
d_b	effective depth of the precast beam
d_c	effective depth of the entire composite beam
E_c	modulus of elasticity of concrete
E_s	modulus of elasticity of reinforcement
$f_{c,28}$	compressive strength of the concrete measured in cylinders at the age of 28 days
$f_{c,b}$	compressive strength of the beam's concrete measured in cylinders
$f_{c,s}$	compressive strength of the slab's concrete measured in cylinders
$f_{c,wa}$	weighted average of the beam and slab's concrete compressive strengths measured in cylinders estimated from the area ratio
f_{ct}	tensile strength of concrete
$F_{H,dow}$	experimental horizontal force transferred across the interface crack by web reinforcement
$F_{H,exp}$	overall experimental horizontal force at the interface crack of composite specimens
$F_{H,int}$	experimental horizontal force transferred across a stretch of the interface crack by means of the aggregate interlock
$F_{H,pred}$	overall predicted horizontal force at the interface crack of composite specimens
f_u	tensile strength of reinforcement
f_y	yield strength of reinforcement
h	overall member height
h_s	cast-in-place slab height
I	moment of inertia of section about the centroidal axis
n	number of legs of a stirrup
N_s	axial force in the slab

$Ø$	nominal diameter of a reinforcing bar
T_l	tension force of slab longitudinal reinforcement
T_w	tension force of web reinforcement
V	shear force
$V_{diag,crack}$	shear force corresponding to the first diagonal crack appearing
V_{exp}	experimental shear strength
V_{pb}	shear strength of the precast beam
V_{pred}	predicted value of shear strength
V_s	shear strength of the slab
$V_{s,BF}$	shear strength of the slab failing in bending
$V_{s,SF}$	shear strength of the slab failing in shear
γ_c	partial safety factor for concrete material properties
γ_s	partial safety factor for steel material properties
δ	crack sliding
$\varepsilon_{c,Si}$	strain on the concrete surface in section *i*
$\varepsilon_{s,l}$	strain of tension longitudinal reinforcement below the point load
ε_u	reinforcement strain at maximum load
ε_y	reinforcement strain at yield strength
θ	inclination angle of the strut to the horizontal
ρ_l	reinforcement ratio of tension longitudinal reinforcement
ρ_w	reinforcement ratio of web reinforcement
σ_1, σ_2	principal stresses
$\sigma_{s,wi}$	stress at the mid-length of stirrup *i*
σ_x	normal stress in the longitudinal direction
σ_y	normal stress in the transverse direction
τ	tangential stress
$\tau_{h,exp}$	experimental shear stress at the interface between concretes
$\tau_{h,pred}$	predicted value of the shear stress at the interface between concretes

ω crack opening

Appendix B. Formulation of the proposed shear strength model for the composite beams with interface cracking of this experimental programme

Depending on the extension of the interface crack along the principal span, three different variants of the presented model in Section 4.2 are distinguished. Due to the evident similarity in the crack pattern, Variant A represents the behaviour of the specimens with the more extended interface cracking (NWP3B2 and DWP7B2a), whose strut-and-tie model is represented in Fig. B.1a. Variant B represents the behaviour of the specimens NWP2B2 and DWP7B2b (Fig. B.1b) and Variant C represents the shear strength mechanism of the specimens NWP1B2 and HWP6B2 (Fig. B.1c).

B.1. Shear strength of the precast beam

Fig. B.1 shows the proposed strut-and-tie models for the precast beam and the slab, represented as isolated. The shear strength mechanism of the precast beam is explained by means of a strut-and-tie model composed of two superimposed trusses. Both precast beam trusses converge at node 7 (see Fig. B.1a). The inclination angle θ of the struts of both trusses is given by the effective depth of the precast beam (d_b in Fig. B.1a) and twice the stirrup spacing, except for the struts of both trusses that converge at the support.

Based on experimental observations, the shear that the precast beam can transmit is considered to be limited by the yielding of stirrups' steel. Thus, by using the equilibrium equations and, as the failure criterion, that the tension in stirrups equals $T_w = A_{sw} \cdot f_y$, where A_{sw} is the cross-sectional area of the two legs of a stirrup, V_{pb} is obtained (see Table B.1). The horizontal forces that balance the nodes i in Fig. B.1 (where i is the node identifier) represent the dowel action of the transverse reinforcement at the interface and the aggregate interlock at the interface. Thus, depending on the extension of the interface crack some of these horizontal forces are eliminated. The formulas for calculating these forces for each variant of the model are expressed in Table B.1.

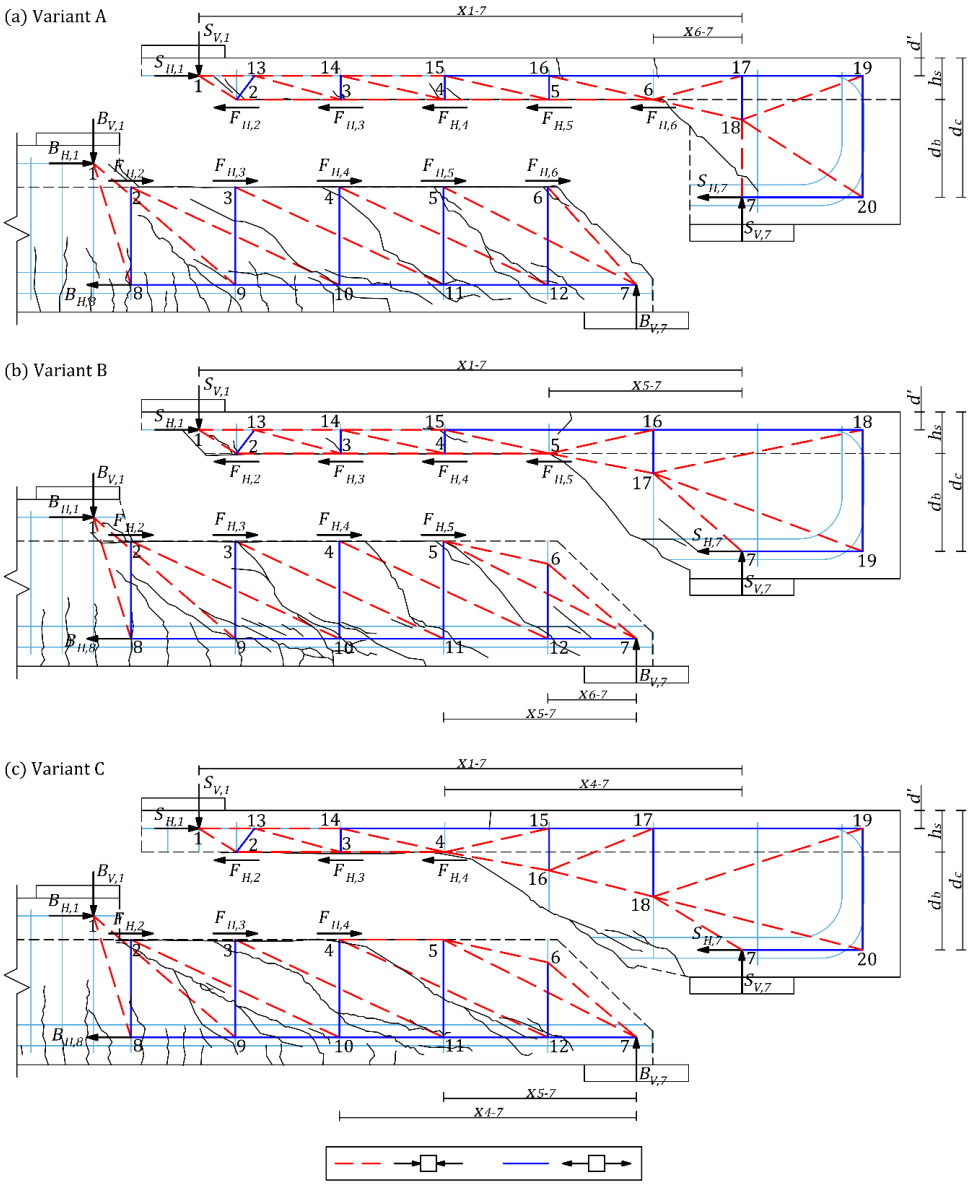

Fig. B.1. Proposed strut-and-tie models for the precast beam and the cast-in-place slab separately: (a) Variant A (specimen NWP3B2); (b) Variant B (specimen NWP2B2); (c) Variant C (specimen NWP1B2).

Table B.1. Formulation for the obtaining of the shear strength of the precast beam and the horizontal forces at the interface for the three variants of the proposed model.

Variant	V_{pb}	$F_{H,i}$
A	$V_{pb} = B_{V,7} = 2T_w$	$F_{H,i} = T_w \cdot \cot\theta_i$, where i = 2, 3, 4, 5, 6
B		$F_{H,i} = T_w \cdot \cot\theta_i$, where i = 2, 3, 4 $F_{H,5} = \frac{T_w(x_{5-7} + x_{6-7})}{d_b}$
C		$F_{H,i} = T_w \cdot \cot\theta_i$, where i = 2, 3 $F_{H,4} = \frac{T_w(x_{4-7}+x_{5-7})}{d_b}$

Notation:
$x_{j\text{-}k}$ is the horizontal distance between nodes j and k in Fig. B.1.
d_b is the effective depth of the precast beam.
θ_i is the angle formed by the strut that converges at node i with the horizontal.

B.2. Shear strength of the cast-in-place slab

The strut-and-tie model that explains the behaviour of the slab receives the horizontal forces $F_{H,i}$ calculated from the precast beam model, which have equal values and opposite directions (Fig. B.1). The component of the total shear transmitted by the slab (V_s) is represented in the strut-and-tie model by the vertical force at node 7 ($S_{V,7}$). Given the small slab depth and stirrups spacing, stirrups are not considered to contribute to resist shear, so the slab behaves like an element without shear reinforcement. The vertical ties of the truss represent the tension stresses resisted by concrete. The slab is assimilated to a beam with a positive bending moment on the left end (section of node 1 in Fig. B.1a) and a negative bending moment on the right end (section of node 6 in Fig. B.1a).

Two possible failure mechanisms in the slab are considered: bending failure of the slab due to yielding of the slab's longitudinal reinforcement or shear failure of the slab. The maximum $S_{V,7}$ that would be transmitted through each mechanism is calculated. The V_s of the model will be the lowest of the shear forces $S_{V,7}$ resisted by each mechanism.

B.2.1. Bending failure of the slab

The model represents the maximum tension force in the slab's longitudinal reinforcement at the slab's right end section. The used failure criterion is, therefore, the force in the horizontal tie (T_l) represented on the end section (ties 16-17, 15-16 and 14-15 in Variant A (Fig. B.1a), Variant B (Fig. B.1b) and Variant C (Fig. B.1c), respectively) is that which corresponds to the yielding of steel ($T_l = A_{sl} \cdot f_y$, where A_{sl} is the cross-section area of the slab's longitudinal reinforcement). Using the equilibrium equations in the slab's model and the failure criterion, force $S_{V,7}$ is

calculated. When the bending failure of the slab is achieved, force $S_{V,7}$ is identified as $V_{s,BF}$ and is calculated as:

$$V_{s,BF} = \frac{\left(\sum_{i=2}^{K} F_{H,i}\right) \cdot (h_s - d') \cdot d_b + T_l \cdot (h_s - d') \cdot (d_c - d')}{x_{1-7} \cdot d_b - x_{K-7} \cdot (d_c - d')} \quad \text{(B.1)}$$

where K is the identifier of the node located at the right end of the slab: 6 in Variant A, 5 in Variant B, 4 in Variant C; h_s is the slab's depth (see Fig. B.1); d' is the depth of the slab's longitudinal reinforcement; d_c is the composite beam's effective depth; d_b is the precast beam's effective depth, and x_{j-k} is the horizontal distance between nodes j and k of the slab's model. Forces $F_{H,i}$ are considered positive in the direction indicated in Fig. B.1.

B.2.2. Shear failure of the slab

The slab is considered to be subjected to a biaxial state of stresses. Failure occurs when concrete principal stresses reach the Kupfer's failure surface [39].

The principal tensile (σ_1) and compression (σ_2) stresses produced by a set of normal (σ_x and σ_y) and tangential (τ) stresses are calculated as:

$$\sigma_1 = \frac{\sigma_x + \sigma_y}{2} + \sqrt{\left(\frac{\sigma_x - \sigma_y}{2}\right)^2 + \tau^2} \quad \text{(B.2)}$$

$$\sigma_2 = \frac{\sigma_x + \sigma_y}{2} - \sqrt{\left(\frac{\sigma_x - \sigma_y}{2}\right)^2 + \tau^2} \quad \text{(B.3)}$$

where tensile stress is considered positive.

In the specimens of this programme, the normal stresses in the transverse direction to the slab directrix (σ_y) are considered negligible, and much lower than the normal compressive stresses parallel to the directrix (σ_x) produced by the axial force on the slab. Shear strength is calculated on the slab's cross-section with the lowest axial force and highest shear force, so a section located on the left of the slab's right end (see Fig. B.1) is taken. The axial force in slab N_s is obtained as a function of the shear calculated by the slab's shear failure ($V_{s,SF}$) using the horizontal forces obtained with the precast beam model:

$$N_s = F_{H,K} + \frac{V_{s,SF} \cdot x_{1-7} - (h_s - d') \cdot \sum_{i=2}^{K} F_{H,i}}{d_c - d'} \quad \text{(B.4)}$$

where K is the identifier of the node located on the right end of the slab: 6 in Variant A, 5 in Variant B, 4 in Variant C.

With the axial force in the slab, compression stress is calculated as $\sigma_x = -N_s/(b \cdot h_s)$.

In Kupfer's failure surface, by assuming the simplification around the corner of the uniaxial compression envelope as in [38], the relation between the principal stresses is:

$$\sigma_1 = |f_{ct}| + 0.8\frac{|f_{ct}|}{|f_{c,s}|}\sigma_2 \tag{B.5}$$

The tangential stress τ value is obtained by substituting (5) and (6) in (8). By assuming a parabolic distribution of tangential stresses on the slab's cross-section, the value of the shear resisted by the slab in the event of shear failure is obtained as $V_{s,SF} = 2/3 \cdot \tau \cdot b \cdot h_s$. It is also verified that $\sigma_1 \leq f_{ct}$ and $\sigma_2 \geq -f_{c,s}$. The f_{ct} of the slab's concrete is calculated from experimental $f_{c,s}$ using the formula provided by EC2 [12].

6th PAPER

Details:

Type of paper	Journal article
Title	*Experimental study on the shear strength of reinforced concrete composite T-shaped beams with web reinforcement*
Authors	Lisbel Rueda García José Luis Bonet Senach Pedro Francisco Miguel Sosa Miguel Ángel Fernández Prada
Journal	Engineering Structures
Publisher	Elsevier
ISSN	0141-0296
JIF	4.471 (2020)
JIF Quartile	Q1 (20/137) ENGINEERING, CIVIL
Status	Published
Date	Accepted: 18th January 2022 Available online: 1st February 2022
Full reference	Rueda-García L, Bonet Senach JL, Miguel Sosa PF, Fernández Prada MÁ. Experimental study on the shear strength of reinforced concrete composite T-shaped beams with web reinforcement. Engineering Structures 2022;255:113921. https://doi.org/10.1016/j.engstruct.2022.113921.

Experimental study on the shear strength of reinforced concrete composite T-shaped beams with web reinforcement

Lisbel Rueda García, lisruega@cam.upv.es

José Luis Bonet Senach, jlbonet@cst.upv.es

Pedro Fco. Miguel Sosa, pmiguel@cst.upv.es

Miguel Ángel Fernández Prada, mafernan@cst.upv.es

Universitat Politècnica de València, Camí de Vera s/n, 46022, Valencia, Spain

Abstract

The current increasing use of precast concrete elements and cast-in-place concrete slabs, namely concrete composite elements, in construction requires a better understanding of their behaviour in shear. In this work, 19 T-shaped composite and monolithic specimens failing in shear were experimentally tested. Their results were compared to study the influence on the shear strength of: the flange width, the presence of an interface between concretes and the strength of the concretes of both beam and slab. The shear transfer mechanisms were analysed by adapting to these specimens a mechanical model previously proposed by the authors for rectangular composite beams. It was concluded that: the composite specimens' shear strength did not increase with widening flange width when the specimens showed an extended interface cracking, but increased when their crack pattern was similar to that of the monolithic specimens; the presence of an interface decreased the shear strength; the slab's concrete compressive strength modified the composite specimens' shear strength when the slab failed in shear, but not when the slab failed in bending or when the interface failed. The shear formulations of EC2, MC-10 Level III and ACI 318-19 gave good estimations when using the weighted average of the compressive strengths of the beam and slab concretes, similarly to those obtained with the proposed model. From the experimental results, the improvement of the interface shear strength of composite beams is proposed as a practical recommendation for increasing their shear strength. At the same time, the slab width and the slab's concrete strength could be increased with the same purpose. This work experimental findings and the adaptation of the mechanical model to T-shaped beams lay the groundwork for a future development of a shear design and assessment formulation for concrete composite elements.

Keywords: precast construction, reinforced concrete, composite beam, T-shaped beam, shear strength, shear failure, mechanical behaviour, design, assessment.

Highlights

Monolithic and composite T-shaped beams with stirrups were tested in shear

The flange-web horizontal interface modified the shear strength mechanism

Flanges did not increase shear strength in beams with an extended interface cracking

Composite beams' shear strength decreased compared to monolithic beams

The proposed model well matches this test programme's experimental results

1. Introduction

Currently a clear trend towards prefabricated construction with reinforced concrete elements is seen. The use of precast concrete beams in building structures, bridges, etc., only requires employing a layer of cast-in-place concrete to ensure structural integrity [1], which results in structural elements known as concrete composite beams. This type of composite construction is present in many structures like building floors or bridge decks [2,3]. Given the vast number of these composite structures, it is important to study their structural behaviour to reduce design and maintenance costs. Currently, the contribution of cast-in-place slab to shear strength in composite beams is often neglected in the design and assessment of existing structures, but its consideration can imply substantial cost savings for these infrastructures [4,5].

While interface shear strength has been widely studied in composite beams [6–11], their vertical shear strength has not been analysed in depth [4]. Experimental analyses of full-scale composite specimens with web reinforcement can be found in the literature [12–20], but they do not analyse either the contribution of slab to shear strength or the influence of the interface between concretes on shear strength. Current codes (like EC2 [21] and MC-10 [22]) do not clarify how to account for the slab in the shear strength of composite elements. Only ACI 318-19 [23] specifies how composite specimens' shear strength can be calculated: using the properties of the element (precast beam or cast-in-place slab) that result in the most critical shear strength value or the properties of individual elements. Nevertheless, relevant experimental and theoretical evidence are still needed to support the validity of these considerations for composite specimens [1,4].

A previous study by the authors [24] analysed the contribution of cast-in-place slab to shear strength in concrete composite beams with rectangular cross-sections and web reinforcement. For the specimens of this experimental programme, it was concluded that slab increased shear strength. Thus, neglecting its contribution to shear strength was too conservative. Besides, the interface between concretes

significantly modified shear behaviour in comparison to monolithic specimens. This study of the shear strength mechanisms derived in the proposal of a mechanical model that analyses test specimens' behaviour.

In precast concrete structures, composite beams with T-shaped cross-sections are often employed, such as bridge decks consisting of precast concrete beams and cast-in-place slabs, beam-and-block floors, rib-and-slab floors with precast reinforced concrete beams or connections of precast floor slabs (e.g., hollow-core slabs) supported by precast beams, where the free space is filled with *in situ* concrete [2,3]. Some examples appear in Fig. 1.

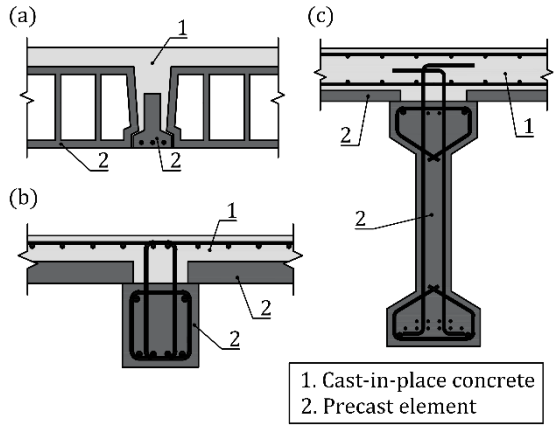

Fig. 1. Examples of reinforced concrete composite T-shaped elements in precast construction: (a) beam-and-block floor; (b) connection of precast beam and hollow-core slab filled with cast-in-place concrete; (c) precast bridge girder with cast-in-place slab.

Although the increased shear strength provided by flanges in monolithic T-shaped concrete beams has been traditionally and widely studied [25–32], and the literature offers several models for the distribution of tangential stresses in flanges [27,30,32–38], no experimental studies that analyse the influence of flanges on the shear strength of T-shaped concrete composite beams appear in the literature despite the many structural elements built with this typology in practice [2].

The aim of the present experimental programme is to study the shear strength of T-shaped reinforced concrete composite beams with shear reinforcement, consisting of a rectangular precast beam and a cast-in-place slab on top. For this purpose, 19 T-shaped reinforced concrete specimens were tested in shear with the following variable parameters: flange width, presence of an interface between concretes, and beam and slab's concrete strengths. An in-depth study of the shear strength mechanisms and failure modes of the specimens of this experimental programme was conducted by adapting to the specimens of this programme the lower-bound

plasticity-based model proposed in [24], which explained the results obtained on the influence of the studied parameters. Parameters were analysed by comparing specimens to one another, and also to the rectangular specimens of the previous study carried out by the authors in [24]. Current codes formulations for shear strength were also verified with the experimental results.

The present research work contributes to: increase the number of available experimental tests on concrete composite beams; study the contribution of the cast-in-place slab to concrete composite beams' shear strength by analysing different variables and mechanical behaviour; extend the mechanical model proposed by the authors to T-shaped composite elements; verify current codes' shear design provisions.

2. Materials and methods

2.1. Test parameters

The three variable parameters selected to analyse the shear behaviour of the T-shaped composite beams with web reinforcement are the following:

- Flange width. Two flange widths were studied in this work. First, the one of type C cross-section, that equalled flange depth, since multiple publications observed that the maximum contribution of flanges to shear strength is given by that width [25,32,33]. Second, the one of type D cross-section, whose flange width was twice the flange depth (Fig. 2), to verify in the specimens of this experimental programme that limit in the contribution of flanges observed by previous authors. Furthermore, the test results from these specimens can be compared to those provided by the authors in a previous work [24] for rectangular sections (type B series) as these specimens have the same web width and height as those of the type C and D series.
- Presence of an interface between concretes. The specimens of series C1 and D1 were monolithic (without interface), while the concretes of the beam and slab were cast at different times in the specimens of series C2 and D2 (with the interface) (Fig. 2).
- Beam and slab concretes' compressive strengths. Two different concrete strengths were used for the precast beams: normal-strength concrete (NSC), with a design compressive strength of 30 MPa, and concrete with higher compressive strength (HCS), with a design compressive strength of 50 MPa. For slabs, only an NSC with a design compressive strength of 30 MPa was used.

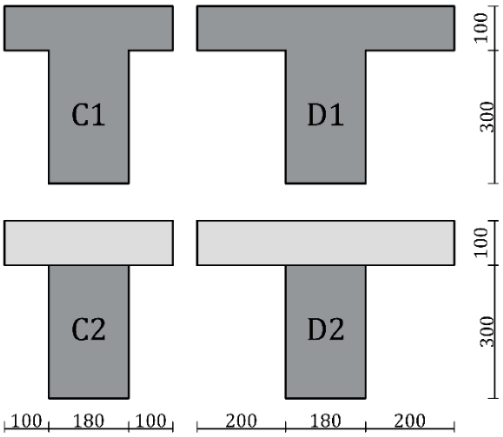

Fig. 2. Cross-section types (dimensions: mm).

2.2. Test specimens

This experimental programme consists of 19 T-shaped beams with web reinforcement. Table 1 shows the number of specimens of each cross-section type and the types of concrete used for the precast beam and the cast-in-place slab. The nomenclature of each specimen, *xWPyzk(j),* was analogous to that of a previous study performed by the authors for rectangular beams [24] to allow a comparison of specimens, where:

- "*xW*" refers to the name of the series: NW stands for the specimens with NSC in the precast beam and HW stands for the specimens with HCS in the precast beam.
- "*Py*" refers to the concrete pouring batch: from P2 to P7, as the fabrication process of these specimens was conducted 6 times. They were the same batches as in [24].
- "*z*" refers to the cross-section type (C or D in Fig. 2).
- "*k*" refers to the number of concretes that formed the specimen: 1 for monolithic beams, 2 for composite beams.
- "*j*" ("a" or "b") is used only when more than one specimen with the same previously described characteristics was fabricated.

Table 1. Series of the experimental programme.

Series	Type of beam's concrete	Type of slab's concrete	Number of specimens per cross-sectional type			
			C1	C2	D1	D2
NW	NSC	NSC	3	3	2	3
HW	HCS	NSC	2	2	2	2

The dimensions of specimens and their reinforcement are shown in Fig. 3. They were designed to emulate real precast beams with cast-in-place slabs used in practice, like those shown in Fig. 1b-c, but simplified to focus the test programme on the study of the test parameters defined in Section 2.1. All the specimens were 3.50 m long. The distance between supports was 2.74 m. Two-point loads with a 0.40 m distance between them were applied, which formed two spans: a 1.34-metre long principal span in which failure was expected; a 1.00-metre long span, which was reinforced to avoid its shear failure.

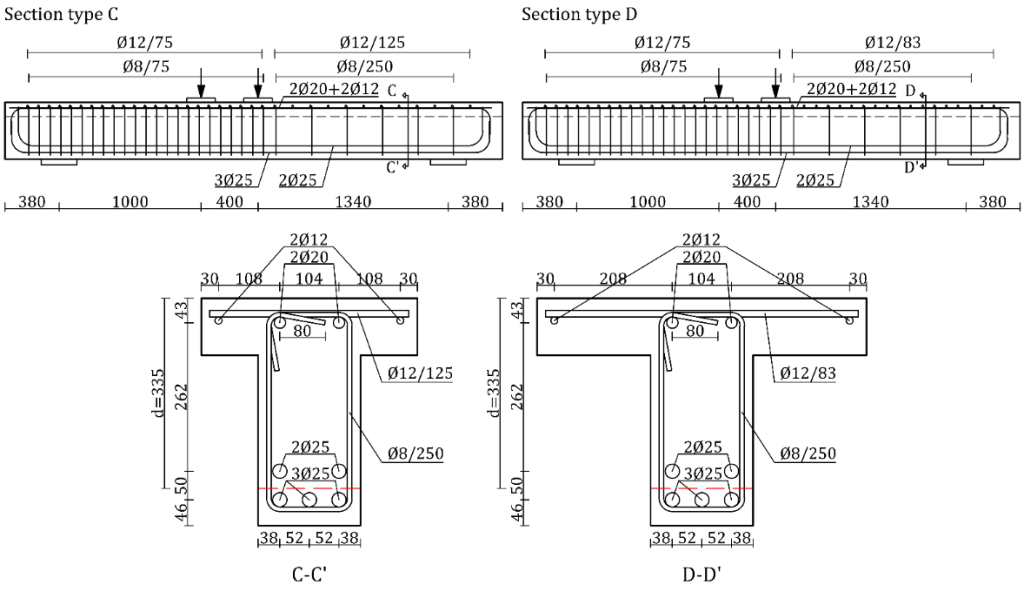

Fig. 3. Dimensions and reinforcement of beams type C and D (dimensions in mm).

In the composite specimens (C2 and D2), the precast beam was 0.30 m high (see Fig. 2) and the cast-in-place slab was 0.10 m high.

All the specimens had fixed the following characteristics to make them comparable between them: a 4.0% longitudinal reinforcement ratio (ρ_l) to avoid bending failure in all the specimens, including those with the widest flange; a shear reinforcement ratio (ρ_w) of 0.22%, which met the maximum spacing requirements between stirrups of all the design codes considered in this study [21–23]; a shear span-effective depth ratio (a/d) of 4.0, which was selected to foster shear failure governed mainly by beam shear-transfer actions [28,39]. The beam's concrete surface underwent no further treatment after vibration. The interface roughness and the shear reinforcement ratio were selected as a result of a previous study carried out by the authors [40], which showed that they were suitable for diagonal beam cracking to develop before interface cracking. Finally for the composite specimens, the time elapsed between

pouring the beam concrete and the slab concrete was 1 day. This time was set because a previous study by the authors [24] proved that, for the specimens of this experimental programme, marked differential shrinkage between the beam and slab concretes did not significantly change specimens' vertical shear strength.

2.3. Fabrication of specimens

Specimens were fabricated in six batches (fabrication batches P2 to P7 in Table 2) to compare the specimens from the same batch with identical concrete strength. The fabrication process of each batch was conducted on 2 consecutive days. On the first day, the concrete of the monolithic specimens and the precast beams of the composite specimens was poured. In the composite specimens, the interface between the concretes in the principal span, where failure was expected, was not further treated after vibration. Thus interface roughness was "as cast" or "smooth" according to current codes [21–23] (see Fig. 4). In the reinforced span, the interface was raked before concrete hardened to obtain a "very rough" interface as defined in the codes. The interface shear strength of the reinforced span was increased in this way. The measured slump of the beam's concrete, which can influence surface roughness [24], is shown in Table 2. The slump test was conducted in accordance with UNE-EN 12350-2 [41].

On the second day, the concrete of the composite specimens' slab was poured. The entire length of beams was laid on the floor during this concrete casting. Hence, in this experimental programme, the beam and slab of the composite specimens were loaded at the same time.

2.4. Material properties

Table 2 shows the 28-day compressive strength of concretes ($f_{c,28}$), and the compressive strength (f_c), modulus of elasticity (E_c) and tensile strength (f_{ct}) of the concretes at the testing age, which were obtained by averaging the test results over two cylindrical specimens (300 mm high, 150 mm diameter) according to UNE-EN 12390 [42–44]. Tensile concrete strength was obtained as 90% of concrete's tensile splitting strength, as described in [45]. The average coefficient of variation values of measurements are also indicated in Table 2.

Regarding concrete mixture composition, the NSC concretes had a water-cement ratio of 0.52, the amount of Portland cement was 325 kg/m^3 and a maximum aggregate size of 10 mm. The same parameters for HCS were 0.44, 500 kg/m^3 and 10 mm, respectively.

Table 3 shows the mechanical properties of reinforcing steel, which were obtained as indicated in UNE-EN ISO 6892 [46]. The results were the average of two tests for each nominal diameter. The steel used for all the bars was type C according to EC2 [21].

Table 2. Summary of the test results.

Series	Fabrication batch	Specimen	$f_{c,28,b}$ (MPa)	$f_{c,28,s}$ (MPa)	$f_{c,b}$ (MPa)	$f_{c,s}$ (MPa)	$E_{c,b}$ (MPa)	$E_{c,s}$ (MPa)	$f_{ct,b}$ (MPa)	$f_{ct,s}$ (MPa)	Slump beam (cm)	V_{exp} (kN)
NW	P2	NWP2C1	37	-	39	-	31961	-	2.83	-	17.5	221
		NWP2C2		34	38	34	33977	30756	3.02	2.88		177
		NWP2D2		34	38	34	33977	30756	3.02	2.88		216
	P3	NWP3C1	32	-	33	-	32927	-	2.58	-	22.5	187
		NWP3C2		38	32	37	32927	33854	2.58	3.21		172
		NWP3D2		38	31	38	32927	33854	2.58	3.21		176
	P4	NWP4C1	39	-	39	-	28300	-	2.86	-	18.0	200
		NWP4C2		33	39	33	28652	27606	2.79	2.80		197
		NWP4D2		33	40	33	28476	28715	3.04	2.48		229
	P7	NWP7D1a	24	-	24	-	22925	-	1.90	-	15.0	195
		NWP7D1b		-	24	-	22925	-	1.90	-		197
HW	P5	HWP5C1	43	-	42	-	24662	-	2.40	-	20.0	238
		HWP5C2		22	44	21	26936	20344	2.58	2.01		166
		HWP5D1		-	42	-	24662	-	2.40	-		200
		HWP5D2		22	44	21	26936	20344	2.58	2.01		173
	P6	HWP6C1	52	-	52	-	28395	-	2.86	-	24.0	231
		HWP6C2		36	52	36	28395	29458	2.86	3.01		222
		HWP6D1		-	52	-	28651	-	2.86	-		246
		HWP6D2		36	52	36	28395	29458	2.86	3.01		209

Notation: suffix "b" refers to the beam's concrete; suffix "s" refers to the slab's concrete.
Average coefficients of variation of measurements: 2% for $f_{c,28}$ and f_c; 3% for E_c; 7% for f_{ct}.

Fig. 4. "As cast" interface appearance before the cast-in-place slab's concrete casting.

Table 3. Average values of the transverse and longitudinal reinforcement properties.

	Series	Ø (mm)	f_y (MPa)	E_s (GPa)	ε_y (‰)	f_u (MPa)	ε_u (%)
Stirrups	All series	8	538	203	2.7	658	12.0
Longitudinal and slab's transverse reinforcement	NWP2, NWP3, NWP4	12	533	207	2.6	638	13.3
		20	585	192	3.1	673	41.0
		25	557	199	2.8	666	48.3
	NWP7, HWP5	12	529	196	2.7	651	30.3
		20	541	194	2.8	654	26.7
		25	548	235	2.3	658	21.6
	HWP6	12	527	201	2.6	657	29.9
		20	560	190	2.9	675	22.0
		25	574	237	2.4	687	19.2

2.5. Instrumentation

The instrumentation arranged in specimens consisted of: load cells, strain gauges and linear variable displacement transformers (LVDTs). Three 1000 kN load cells were used to measure the forces at the two bearing points and the hydraulic jack. Strain gauges of 2 mm measuring length and 120 Ω resistance were placed on some reinforcing bars: G1 to G6 (see Fig. 5a) on the tension longitudinal reinforcement at three different cross-sections (Sections A, B and C); G7 and G8 on the compression longitudinal reinforcement at Section C; G9 to G16 at the mid-length of the two legs of stirrups w3 to w6 (Fig. 5a). Three strain gauges of 60 mm measuring length and 120 Ω resistance were located on the top concrete surface at Sections A and B (gauges C1 to C6 in Fig. 5a). Their locations at type C and D cross-sections are shown in Fig. 5b. Finally, five LVDTs (V1 to V5 in Fig. 5c) were placed on the concrete surface to measure vertical displacements, two LVDTs (O1 and O2) were fixed to the top and bottom of beams to detect the beginning of cracking, and four LVDTs (H1 to H4) were fixed to the web and flange to measure the horizontal slip between them. In all the tests, two digital cameras took pictures at a rate of 0.5 Hz and a synchronised recording system was used so that each photogram was assigned to the corresponding applied load. A high-speed camera was employed to record brittle failures and to detect the beginning of cracking.

2.6. Test setup and procedure

Tests were performed in the same way as in the authors' previous studies [24,47], in which the steel loading frame shown in Fig. 6 was used. A 1200 kN hydraulic jack applied the vertical load with displacement control at a speed of 0.02 mm/s. Load was divided into two point loads by means of the steel frame shown in Fig. 6, which had a hinge to maintain load in a vertical direction, even if the upper beam plane was not horizontal due to its deformation. Two steel plates (200x200x30 mm) centred

on the slab width transmitted the load from the steel frame to specimens. The beam's two bearing points consisted of a steel plate 250 mm width, a ball bed to eliminate the horizontal reaction and a hinge to allow for rotations.

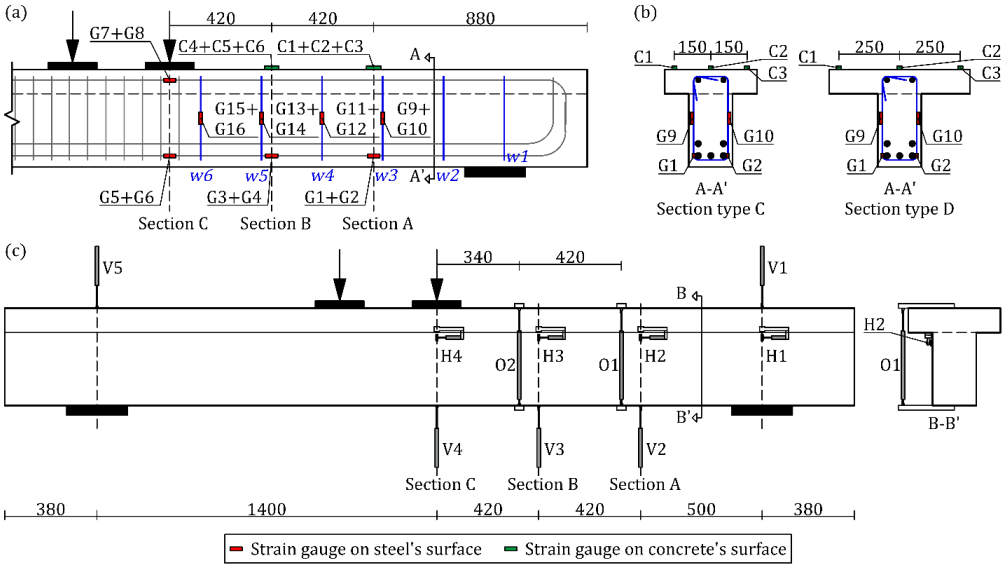

Fig. 5. Instrumentation of the test specimens: (a) strain gauges at the principal span; (b) strain gauges at section A-A' for beams type C and D; (c) LVDTs (dimensions in mm).

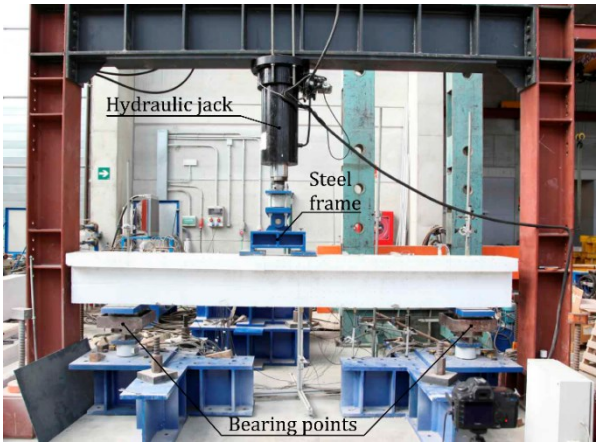

Fig. 6. Experimental setup.

3. Experimental results

3.1. Shear strength and shear-deflection relation

Table 2 shows the vertical shear strength of the test specimens (V_{exp}). The shear-deflection curves of all the test specimens are shown in Fig. 7. Shear force was measured at the principal span. Deflection was measured below the point load located at Section C (LVDT V4 in Fig. 5c). The maximum shear force (V_{exp}) is highlighted with a circle on each curve.

The specimens' self-weight is not included in any shear result since its effect was considered negligible.

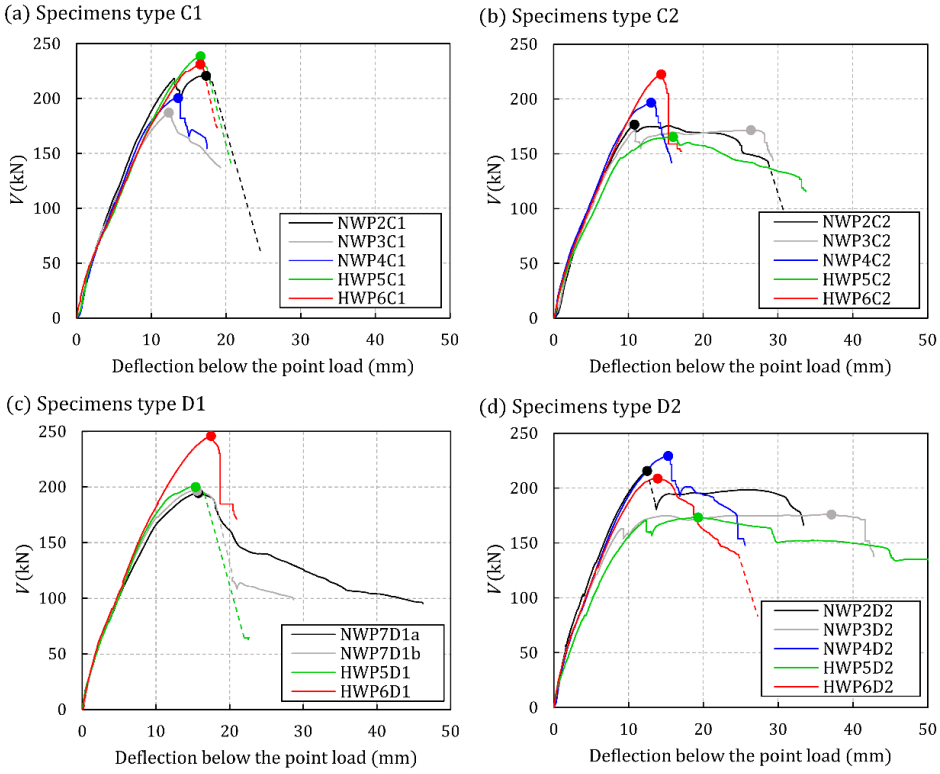

Fig. 7. Shear-deflection relation of the test specimens: (a) specimens with section type C1; (b) specimens with section type C2; (c) specimens with section type D1; (d) specimens with section type D2.

3.2. Crack patterns

Fig. 8 shows the principal span crack patterns of the test specimens in different load stages: at maximum shear force V_{exp}; immediately after V_{exp}, when some sudden

cracks appeared, which were normally accompanied by a load drop (e.g., see specimen HWP6C2 in Fig. 7b); at the end of testing.

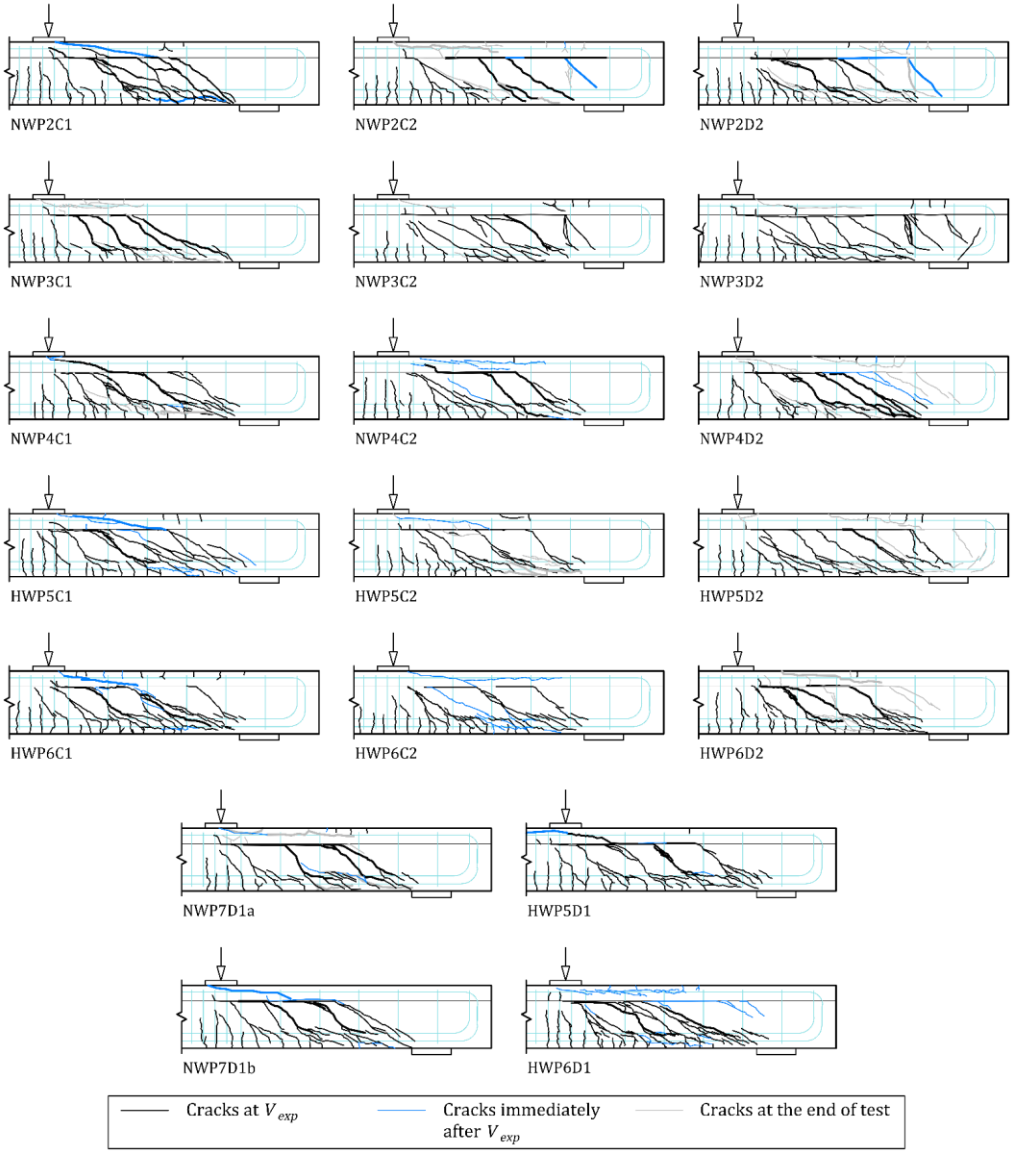

Fig. 8. Crack patterns of the test specimens in different test stages.

In all the test specimens, vertical bending cracks at the bottom of the principal span appeared in the first load stages. While the cracks in the area below the point load

remained vertical, some of the bending cracks at the shear span changed direction towards the point load as load increased, and formed the diagonal cracks, as observed in previous shear studies [1,2,25,29].

When diagonal cracks approached the plane in which the section width changed, in both the monolithic and composite specimens they deviated along this weakness plane (interface from now on) instead of penetrating the beam's head (slab from now on to refer to the flanges of the monolithic beams and the slab of the composite beams). This horizontal cracking at the flange-web interface (interface crack) has also been observed in multiple experimental studies on monolithic T-shaped beams with web reinforcement found in the literature [25,26,29,48], and also in composite T-shaped specimens with web reinforcement [2,6,10].

In most monolithic specimens, the diagonal cracks at the web were concentrated near the load (e.g., see specimen NWP3C1 in Fig. 8). In specimens C1 and D1, the interface crack extended from the loading plate to stirrups w3 or w4 (see Fig. 5a). Only in specimen HWP6D1 did this interface crack extend to a closer section to the support, stirrup w2, after the maximum load was reached (see Fig. 8). At the maximum load, V_{exp}, the slab of the monolithic specimens, remained mostly undamaged (except for that of specimens NWP4C1 and HWP5D1, where a diagonal crack had already penetrated the slab at V_{exp}). After V_{exp}, a diagonal crack ran through the slab towards the point load. Only in three of the nine monolithic specimens (NWP3C1, NWP7D1a and HWP6D1) did the slab show a different cracking pattern, in which a horizontal splitting crack appeared at the slab's longitudinal reinforcement level after the maximum load. The formation of the slab cracks was generally accompanied by the formation of horizontal cracks at the tension longitudinal reinforcement level [27,35].

In the composite specimens, web diagonal cracks were more distributed along the shear span than in the monolithic specimens (e.g., see specimen NWP3C2). The interface crack was also more extended and reached stirrup w2 in many specimens (see Fig. 5a) at V_{exp} (specimens NWP2C2, NWP3C2, NWP3D2 and HWP5D2). In other specimens, the interface crack extended to stirrup w2 after V_{exp} (NWP2D2, NWP4D2 and HWP6D2). The slab showed some bending cracks in all these specimens, which started at top of the area close to the end of interface cracking (see NWP3D2 at Fig. 8), and some horizontal cracks appeared at the slab long after the maximum load had occurred (see NWP2C2 in Fig. 8). In other composite specimens, the interface crack extended only to stirrup w3 (NWP4C2 and HWP5C2) or w4 (HWP6C2). In these specimens, a diagonal crack developed in the slab after V_{exp}, as observed in Fig. 8, also with the formation of horizontal cracks at the tension longitudinal reinforcement level.

3.3. Instrumentation results

The main results of the strain gauges located on the steel bars at V_{exp} were analysed. The strain gauges located at the mid-length of the two legs of instrumented stirrups w3 to w5 (see Fig. 5a) measured strains at V_{exp} which exceeded the steel yield strain in tension in all cases, which was 2.7‰ according to Table 3. The average strains of the two strain gauges located on stirrup w6 (Fig. 5a) were lower: 1.6‰ in tension on average for all the tested specimens. The average strain of the two strain gauges located on the bottom layer of the tension longitudinal reinforcement below the point load (gauges G5 and G6 in Fig. 5a) was generally below the steel yield strain (see Table 3), and gave 2.3‰ in tension on average for all the specimens. This confirmed that specimens were far from the bending failure at V_{exp}.

Fig. 9 shows the strains measured in four specimens, on one example for each cross-section type (see Fig. 2), by the strain gauges located on top of the slab: gauges C1, C2 and C3 at Section A and gauges C4, C5 and C6 at Section B (see Fig. 5a).

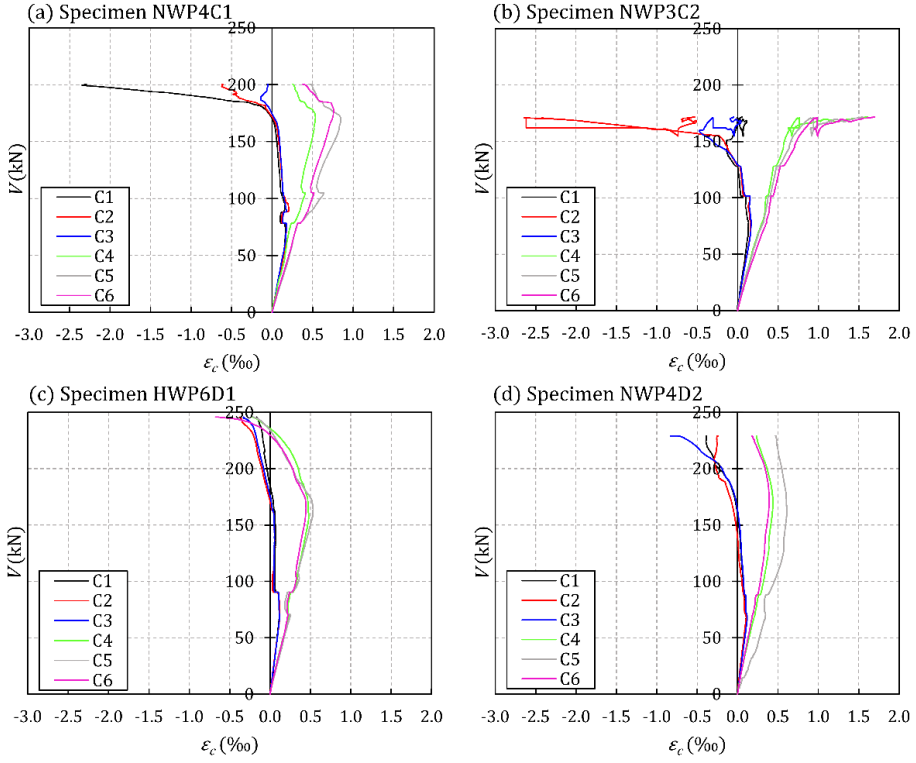

Fig. 9. Results of the strain gauges located on concrete's surface on top of the slab for different specimens: (a) specimen NWP4C1; (b) specimen NWP3C2; (c) specimen HWP6D1; (d) specimen NWP4D2 (positive ε_c for compression).

4. Analysis and discussion

4.1. Analysis of the shear strength mechanism

4.1.1. Shear strength mechanism description

Based on the observations of the crack patterns and the measurements of the strain gauges, the shear transfer actions (STAs) governing specimens' behaviour until the first diagonal cracks formed were identical in both the monolithic and composite beams, and the same as those observed in the rectangular beams studied in [24]: the combined action of the aggregate interlock in cracks, the cantilever action between cracks, the dowel action of the longitudinal reinforcement, the residual tensile strength of concrete and arching action [36,39]. After the diagonal cracks had formed, tensile forces developed in the shear reinforcement.

With increasing load, diagonal cracks continued to reach the plane where the section width changes and developed along this plane instead of penetrating the beam's head, because this was the weakest section in both the monolithic and composite beams. This behaviour was also observed in the rectangular composite specimens in [24]. Thus the shear strength mechanism was similar to that described in [24], in which this horizontal crack divided the shear transfer mechanisms into two paths: one through the beam's web (or the precast beam in the composite specimens) and one through the beam's head (or the slab in the composite beams). The shear transfer mechanism through the precast beam can be explained by a strut-and-tie model composed of two superimposed trusses (coloured in blue in Fig. 10). The shear transfer mechanism through the slab can be considered that of a member without shear reinforcement and modelled with a simple strut-and-tie model (coloured in green in Fig. 10), where transverse ties represent concrete in tension. Both shear transfer mechanisms are connected through the interface crack, where the dowel action of web reinforcement and aggregate interlock actions can take place. The connection between both triangulated bar structures is made by means of finite-dimensional nodes, in which only horizontal forces are considered to act. A more detailed explanation of this model is found in Appendix B.

The different beam web and slab widths result in a three-dimensional stress distribution in the slab. This was verified in the experimental tests by comparing the measures of the three strain gauges C1, C2 and C3 at Section A and C4, C5 and C6 at Section B (Fig. 5). As shown in Fig. 9, the strain measured by the central gauge did not significantly differ from that measured by the gauges at the flange ends. This meant that the effective width of the compression block in the slab equalled the total slab width in both the type C and D series. Note that high tensile strains for loads close to failure were recorded for some gauges (C1 in Fig. 9a and C2 in Fig. 9b),

which were consistent with the cracks observed at the top slab side around Section A.

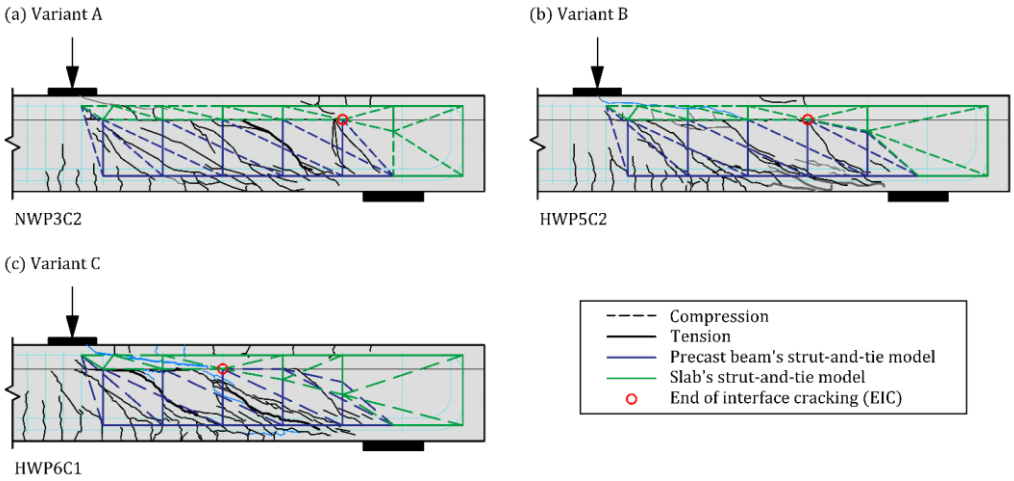

Fig. 10. Strut-and-tie model for the precast beam and the cast-in-place slab proposed in [24]: (a) Variant A (specimen NWP3C2); (b) Variant B (specimen HWP5C2); (c) Variant C (specimen HWP6C1).

Similarly to the rectangular composite beams with interface cracking, which were analysed by the authors in [24], the three variants of the proposed model in [24] (Variants A, B and C) can be identified in the beams of this experimental programme depending on interface crack length (see the examples of Fig. 10 for each variant). For sake of clarity, the point of the interface closest to the support where the interface crack ended (EIC) is marked. Table 4 shows the variant of the model that was attributed to each specimen. These were attributed according to the observed crack pattern. The measurements of the strain gauges located on the slab also indicated signs of the variant of the mechanical model adopted by specimens. For example, in the specimens showing a shear strength mechanism like that of Variant A, the strain gauges located at Section B (C4, C5 and C6 in Fig. 5a) showed a tendency towards compression throughout the test (see Fig. 9b) in accordance with the struts represented in the strut-and-tie model of the slab at that section (see Fig. B.1a). On the contrary in the specimens with Variant C, these gauges displayed a tension tendency about halfway through the test (see Fig. 9a, c and d), which proved that strain gauges were close to a tensile zone in concrete, as represented in the strut-and-tie model of Variant C (see Fig. B.1c).

Table 4. Estimated shear strength values of test specimens according to the extension of the model proposed in [24] to T-shaped specimens.

Specimen	Variant	Experimental failure mode	V_{exp} (kN)	V_{ph} (kN)	$V_{s,BF}$ (kN)	$V_{s,SF}$ (kN)	$V_{s,IF}$	V_{pred} (kN)	Predicted failure mode	V_{exp}/V_{pred}
NWP2C1	C	SF	221	108	152	104	-	212	SF	1.04
NWP3C1	C	SF	187	108	152	95	-	203	SF	0.92
NWP4C1	C	SF	200	108	152	109	-	218	SF	0.92
HWP5C1	C	SF	238	108	147	104	-	212	SF	1.12
HWP6C1	C	SF	231	108	149	126	-	235	SF	0.99
NWP7D1a	B	SF	195	108	84	71	-	179	SF	1.09
NWP7D1b	B	SF	197	108	84	71	-	179	SF	1.10
HWP5D1	C	SF	200	108	147	104	-	212	SF	0.94
HWP6D1	C	SF	246	108	149	126	-	234	SF	1.05
NWP2C2	A	BF	177	108	61	100	106	169	BF	1.05
NWP3C2	A	BF	172	108	61	111	106	169	BF	1.02
NWP4C2	B	SF	197	108	87	100	106	195	BF	1.01
HWP5C2	B	SF	166	108	83	68	106	176	SF	0.94
HWP6C2	C	SF	222	108	148	107	106	216	IF	1.03
NWP2D2	C	IF	216	108	152	102	106	210	SF	1.03
NWP3D2	A	BF	176	108	61	112	106	169	BF	1.04
NWP4D2	C	IF	229	108	152	94	106	202	SF	1.13
HWP5D2	A	BF	173	108	59	66	106	167	BF	1.04
HWP6D2	C	IF	209	108	148	107	106	216	IF	0.97

4.1.2. Failure modes

According to the above-described shear strength mechanism, the ultimate load of a T-beam with an interface crack is the sum of the shear resisted by the precast beam (given by the strut-and-tie model by considering that all stirrups had reached their yielding strength, as proved experimentally by the measurements of the stirrups' strain gauges at Section 3.3) and the shear strength transferred by the slab at failure. As the maximum shear resisted by the precast beam was reached before slab failure and it remained constant for increasing loads until the slab failed, the specimen's shear strength was reached when the slab failed. Depending on the interface crack length, three failure modes can occur in the slab or at the interface: slab bending failure (BF); slab shear failure (SF); interface failure (IF).

4.1.2.1. Slab bending failure (BF in Table 4)

This failure mode was identified in the specimens where a long interface crack was developed (Variant A in Fig. 10). The specimens that exhibited this failure mode showed shear-strain curves (Fig. 7) with no marked drop upon the maximum load.

In addition, vertical cracks were observed on the upper slab side (e.g., see NWP3C2 in Fig. 8) and tensile strains were measured in the slab strain gauges above the point EIC in Fig. 10 (see gauges C1, C2 and C3 in Fig. 9b). This denotes the existence of a negative bending moment resisted by the slab in this area.

4.1.2.2. Slab shear failure (SF in Table 4)

This failure mode was observed in some composite specimens and in all the monolithic specimens of this experimental programme. Upon maximum shear, a diagonal crack in the slab developed in direction to the point load (e.g., see NWP2C1 in Fig. 8) and, thus, a pronounced load drop in the shear-deflection curves took place (Fig. 7). This failure mode has also been described in previous studies on monolithic T-shaped beams [25,26,29].

4.1.2.3. Interface failure (IF in Table 4)

Three composite specimens (see NWP2D2, NWP4D2 and HWP6D2 in Fig. 8) showed a cracking pattern with a short interface crack before the peak load took place, that extended towards stirrup w2 (Fig. 5a) afterwards. In these three specimens, and unlike other composite specimens, after the load that led to crack interface extension, no new strength mechanism developed to increase this load. Therefore, the maximum load was determined by the load that produced crack prolongation. This failure mode has not been previously detected in rectangular composite specimens [24] and is identified in this paper as interface failure (IF).

From the Variant C of the proposed model (see Fig. 10), a new procedure for calculating experimental shear stress at the interface ($\tau_{i,exp}$) was developed (explained in detail in Appendix C). The horizontal shear force ($F_{i,nc}$) at the uncracked interface section was estimated by subtracting the horizontal forces ($F_{H,i}$) transferred through the interface crack from the horizontal force ($S_{H,1}$) resisted by the slab at the loading section (see Fig. C.1 and Appendix C). This shear force was calculated for the three specimens with IF at the load immediately before the interface crack prolonged towards the support (V_{exp}). The uncracked interface length at V_{exp} ($l_{i,nc}$) was known, which was 1.08, 1.18 and 1.02 m for NWP2D2, NWP4D2 and HWP6D2, respectively. Following the procedure described in Appendix C, the mean values of shear stress resistances of the uncracked interface ($\tau_{i,exp}$) were obtained by dividing force $F_{i,nc}$ by the uncracked interface area. The results were respectively 1.97, 2.08 and 1.91 MPa for NWP2D2, NWP4D2 and HWP6D2.

As shown, the shear strength ($\tau_{i,exp}$) of the specimens whose failure mode was described as IF all had a similar value, of around 2.0 MPa and with a minimum value of 1.9 MPa. This value could vary for specimens with different characteristics, such as surface roughness, concrete quality and shear reinforcement.

4.1.3. Estimated shear strength for the specimens of this experimental programme

The component of the shear strength resisted by the precast beam (V_{pb}) could be estimated from the proposed strut-and-tie model by considering that all the vertical ties had reached their yielding strength. This assumption agrees with the measurements recorded at V_{exp} of the strain gauges located at the stirrups (Section 3.3). Stirrup w6 (see Fig. 5a) was the only that was generally less tensioned. However, its yielding was acceptable because this assumption did not significantly affect the result, as proved in a previous study by the authors [24]. The V_{pb} results for the specimens in this programme are shown in Table 4. The formulation of this model, described in detail in [24], is summarised in Appendix B.

The shear force resisted by the slab when the failure mode was slab bending failure ($V_{s,BF}$) was determined by the slab's ultimate bending moment at the cross-section above point EIC (see Appendix B), and by assuming that all the top longitudinal reinforcement bars reached their yielding strength. The $V_{s,BF}$ results are shown in Table 4.

The shear force resisted by the slab when the failure mode took place by slab shear ($V_{s,SF}$) was estimated by considering that the slab was subjected to a biaxial state of stresses and failure occurred when the concrete's principal stresses reached Kupfer's failure envelope [49]. The vertical shear stresses on the slab are not uniformly distributed along the flange width, but concentrate in the vicinity of the web [50]. In this paper, a shear-effective area of the slab which increased 45º from the cross-section width change was considered in line with previous research [3,38]. Thus to estimate $V_{s,SF}$, the vertical shear stress distribution in the slab was assumed to be uniform at an effective width (b_{eff}), which equalled the sum of web width and flange depth ($b+h_s$), and was parabolic on the slab cross-section, as in other studies found in the literature [33]. As explained later in Section 4.2.1, this assumption was consistent with the experimental results. The $V_{s,SF}$ results are shown in Table 4.

The shear force resisted by the slab when the failure mode was interface shear ($V_{s,IF}$) was estimated by: taking the upper limit of the shear stresses at the interface as being known (1.9 MPa for the specimens of this experimental programme because this was the minimum shear stress obtained); using the equations in Appendix C, where the uncracked interface length at V_{exp} ($l_{i,nc}$) was taken as the horizontal distance between EIC in Variant C (see Fig. 10), located at stirrup w4 (see Fig. 5a), and the end of the beam, which was 1.09 m. The $V_{s,IF}$ results are shown in Table 4.

The slab's shear strength was the minimum value between those obtained for the slab's three failure modes, V_s = min ($V_{s,BF}$, $V_{s,SF}$, $V_{s,IF}$). The value of the three slab resistances that matched this minimum value allowed the model to predict the failure mode.

The specimen's shear strength was obtained by adding the shear forces resisted by the prefabricated beam and the slab ($V_{pred} = V_{pb}+V_s$). The V_{pred} values obtained for the 19 specimens in this experimental programme are found in Table 4. Table 4 also shows the resultant failure mode according to the predicted shear strength values and the experimental to predicted shear strength ratio (V_{exp}/V_{pred}).

From comparing experimentally observed failure mode (third column in Table 4) to the governing failure mode according to the proposed model (tenth column in Table 4), it can be concluded that the model quite well captured the failure mode. Only in a few specimens (NWP4C2, HWP6C2, NWP2C2, NWP4D2) did the predicted failure mode not match that experimentally observed. However in all those specimens, the slab's minimum predicted shear strength value (V_s) came very close to the value predicted for the experimentally observed failure mode.

For all the specimens, the average value and the coefficient of variation of V_{exp}/V_{pred} were respectively 1.02 and 6.07%. These results indicate a good agreement of the shear strength predicted by this model with the experimental results.

4.2. Effect of test parameters on shear strength

4.2.1. Flange width

In this section, the existence of flanges and their width were analysed. To this end, the results of the rectangular cross-section specimens of a previous study by the authors [24], whose geometric and reinforcement characteristics were identical to those of the specimens herein presented, except for the absence of flanges, were employed to make a comparison. Five specimens with monolithic rectangular cross-sections (B1) and six specimens with composite rectangular cross-sections (B2) from series NW and HW were taken from this study.

Fig. 11 shows the results obtained for the monolithic specimens. By comparing beams B1 and C1, the strengths of the specimens with a flange width that equalled flange depth (C1) increased compared to those of rectangular sections (B1) by an average of 16% for all the fabrication batches. This result comes close to that of around 20-25% observed in the literature for beams with web reinforcement [25,32,33].

Of the D1 specimens, whose flange width was twice flange depth, only the specimens from series HWP5 and HWP6 could be compared. The shear strength of specimen HWP6D1 increased by 23% in relation to specimen HWP6B1 and by 6% in relation to specimen HWP6C1. However, the shear strength of specimen HWP5D1 was less than that of specimens HWP5B1 and HWP5C1. This could be an anomalous result due to a local effect of the applied load.

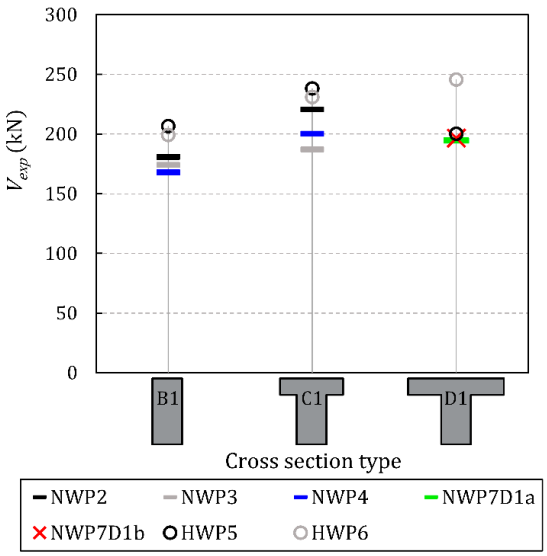

Fig. 11. Comparison of the shear strengths of beams B1, C1 and D1.

In Section 4.1.3, a shear-effective area that increased 45º from the cross-section width change [3,38], equal to the web width and flange depth sum, was considered for all the T-shaped specimens with slab shear failure (all the monolithic specimens failed in this way). This implied a 17% increase in the shear-effective area in relation to that of the rectangular specimens, which agrees the experimental results of specimens C1. As only one D1 specimen could be compared and its shear strength did not significantly increase *versus* specimen C1, the consideration of the same shear-effective area would seem appropriate.

Fig. 12 shows the comparison of the composite specimens. The shear strength of the T-shaped specimens C2, with flange width equalling flange depth, did not increase in most cases in relation to the rectangular specimens B2 of each fabrication batch. The shear strength of the specimens C2 from series NWP2, NWP3, NWP4 and HWP5 decreased 1% on average *versus* B2, while the shear strength of the C2 specimen from series HWP6 increased by 19%.

Regarding the T-shaped D2 specimens, whose flange width was twice flange depth, the shear strength increased 16% on average for series NWP2, NWP4 and HWP6 in relation to that of the rectangular specimens B2, but this increase was not significant (3% on average) for series NWP3 and HWP5.

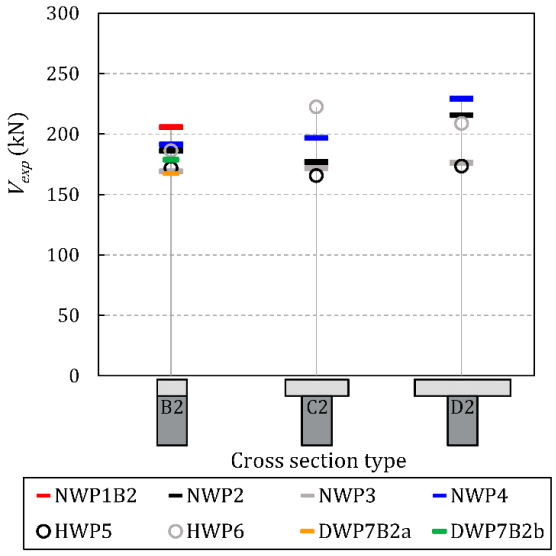

Fig. 12. Comparison among the shear strengths of beams B2, C2 and D2.

These observations of the flange width effect on the composite specimens are consistent with the variants of the mechanical model discussed in Section 4.1. In the specimens with an extended interface crack, in which the model's Variant A was adopted in most cases (see Table 4), the flange effect was not noticeable because the failure mode (slab bending failure) was explained by the slab's longitudinal reinforcement and not by the slab's shear effective area. Those specimens were those whose shear strength did not significantly differ from that of the rectangular specimens. On the contrary, in the specimens with a limited interface crack (Variant C), shear strength increased compared to specimens B2. Thus slab shear failure was considered to give a good approximation of the experimental shear strength (similar to the value obtained for interface failure) as the shear-effective area of flanges was taken into account (see $V_{s,SF}$ in Table 4).

4.2.2. Presence of an interface between concretes

In order to analyse how the presence of an interface influences shear strength, the beams with the same cross-section geometry and fabricated with one and two concretes were compared. Fig. 13 shows the results for the specimens with sections C1 and C2. When the shear strengths of the beams of the same fabrication batch were compared, the presence of an interface reduced the shear strength of the composite T-beams whose flange width equalled flange depth by 13% on average compared to the monolithic beams.

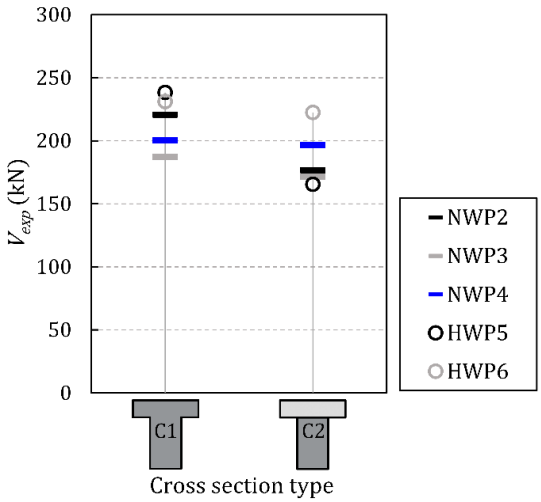

Fig. 13. Comparison between the shear strengths of beams C1 and C2.

Similarly, Fig. 14 shows the results for the specimens with sections D1 and D2. By comparing the beams of the same fabrication batch, the average reduction in shear strength due to the presence of the interface would be 14%.

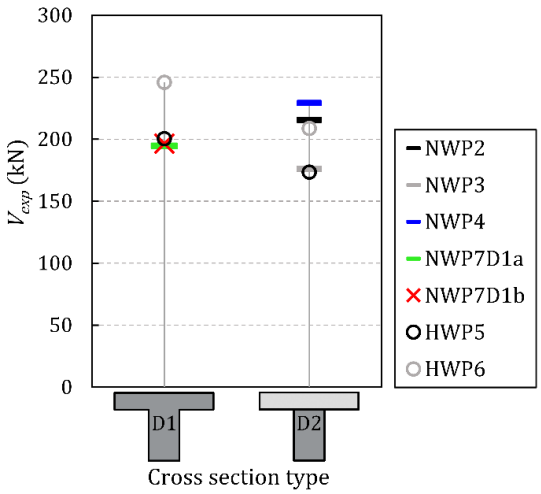

Fig. 14. Comparison between the shear strengths of beams D1 and D2.

The lower strength of the composite specimens *versus* the monolithic ones can be explained by the shear strength mechanisms described in Section 4.1.1. An interface existing between concretes causes a higher extension of the interface crack, which

can bring about weaker shear strength mechanisms, like that of Variant A (Fig. 10), with less resistant failure modes, like BF or IF (see Table 4). The monolithic specimens presented stronger shear strength mechanisms, like Variant C or B, which brought about the higher shear strengths provided by slab shear failure (SF in Table 4).

4.2.3. Strength of the concrete in beam and slab

When comparing the monolithic specimens of series NW fabricated with NSC, and HW fabricated with HCS, the better-quality concrete increased shear strength by 15% on average. This concrete strength effect was considered in the proposed model in Section 4.1 as the shear strength of the monolithic specimens was estimated from slab shear failure, in which the concrete strength of the beam's head is a variable of the formulation (see Appendix B).

Regarding the composite specimens, the shear transfer mechanism described in Section 4.1 also allowed the experimental results to be explained.

For the composite specimens failing by slab bending failure (BF) (specimens NWP2C2, NWP3C2, NWP4C2 and HWP5D2 in Table 4), the experimental shear strengths were similar (177, 172, 176 and 173 kN, respectively). This is consistent with the assumption that in this failure mode, the beam's shear reinforcement and the slab's longitudinal reinforcement reached their yielding strength.

When comparing composite specimens NWP4C2 and HWP5C2, whose failure was caused by slab shear failure, and both with similar interface crack length, shear strength significantly varied (197 and 166 kN, respectively, in Table 4). This demonstrates that shear strength depended directly on the compressive strength of the slab's concrete (33 and 22 MPa, respectively).

In the specimens with interface failure (IF in Table 4), no significant variations were observed in the shear strength with the compressive strength of both the beam and slab's concretes, but with the beam concrete's workability during casting. This was also observed by the authors in a previous study [24]. The specimens with drier concretes in the beam (see the slump measurements in Table 2), such as specimens NWP2D2 and NWP4D2, exhibited higher as-cast interface roughness and, therefore, higher interface shear strength. This resulted in slightly higher shear strength than in those specimens with more fluid concretes (HWP6D2). However, the compressive strength of the beam's concrete in the latter was higher.

4.3. Comparison of the test results with existing code provisions and the proposed model

The test specimens' shear strength was assessed with the shear formulations for elements with web reinforcement according to current design codes EC2 [21], MC-10 [22] at its three approximation levels, and the two equations of ACI 318-19 [23]

(named (a) and (b) in Section 22.5.5.1 of ACI 318-19). As no code accounts for the flanges effect on shear strength, only the web of specimens was considered. In the composite specimens, different shear area considerations were included: only the precast beam resisted shear, in which case the precast beam's effective depth (d_b) and the compressive strength of the beam's concrete ($f_{c,b}$) were used in the formulations; or the entire composite beam's web resisted shear, in which case the composite beam effective depth (d_c) and the compressive strength of the beam's concrete ($f_{c,b}$), the slab's concrete ($f_{c,s}$) or the weighted average of the compressive strengths of both concretes ($f_{c,wa}$) were used [1,4,24]. The mean value and the coefficient of variation (CV) of the experimental shear strength (V_{exp}) to the predicted value (V_{pred}) ratio are shown in Table 5. These statistical indicators were used to analyse the studied sample, although more elements in the sample would be necessary for the values of these indicators to be significant. Note that the specimens with similar concrete compressive beam and slab strengths (series NW) were assessed only with $f_{c,wa}$ when d_c was considered as the results were similar. The tested average values of the materials were used with all the formulations, and the partial safety factors for the concrete (γ_c) and steel material properties (γ_s) were 1.0. No formulation for any specimen offered unsafe results.

Table 5. Statistical indicators of the V_{exp}/V_{pred} ratio for the test specimens assessed with current codes formulations.

Specimens	No. of specimens	Method	EC2		MC-10 LI		MC-10 LII		MC-10 LIII		ACI 318-19 (a)		ACI 318-19 (b)	
			Mean	CV (%)	Mean	CV (%)	Mean	CV (%)	Mean	CV (%)	Mean	CV (%)	Mean	CV (%)
Monolithic	9	d_b, $f_{c,b}$	1.31	9.53	1.89	9.53	1.67	9.53	1.35	7.03	1.59	6.14	1.36	6.01
Composite (NW)	6	d_b, $f_{c,b}$	1.70	11.19	2.46	11.19	2.14	11.19	1.75	10.25	2.09	9.70	1.67	9.37
		d_c, $f_{c,wa}$	1.19	11.19	1.72	11.19	1.52	11.19	1.24	10.62	1.47	10.26	1.25	10.11
Composite (HW)	4	d_b, $f_{c,b}$	1.69	12.33	2.44	12.33	2.12	12.33	1.66	11.04	1.94	10.18	1.53	9.71
		d_c, $f_{c,b}$	1.18	12.33	1.71	12.33	1.51	12.33	1.18	11.06	1.36	10.18	1.15	9.84
		d_c, $f_{c,s}$	1.18	12.33	1.71	12.33	1.51	12.33	1.28	8.50	1.53	7.14	1.32	6.21
		d_c, $f_{c,wa}$	1.18	12.33	1.71	12.33	1.51	12.33	1.20	10.72	1.39	9.63	1.18	9.18

For the monolithic specimens, the code that better approached the experimental results was EC2, with a mean value of 1.31 and a low CV (see Table 5). Equation (b) of ACI 318-19 and Level III of MC-10 gave a similar result. When comparing these results to those for the rectangular specimens of [24], which were more accurate, all the formulations can be considered to be very much on the safety side as the flange effect was not taken into account.

For the composite specimens, the shear strengths predicted by considering that only the precast beam resisted shear were extremely safe with all the codes. When

considering the entire composite beam's effective depth in series NW, EC2 gave the most accurate result (mean value of 1.19). For series HW, EC2, MC-10 LI and MC-10 LII obtained the same results for all the perspectives as the calculation did not depend on the concrete compressive strength for these test specimens. The best result was provided by equation (b) of ACI 318-19 when using $f_{c,b}$ (mean value of 1.15) due to the higher compressive strength of the beam's concrete. Despite this good result, we should bear in mind that using $f_{c,b}$ is commonplace for calculating shear strength [16,19], but can lead to unsafe results if the beam's depth value is not much higher than that of the slab, as observed in [5]. In this case, using $f_{c,w/a}$ would be a safer practical solution for which EC2, MC-10 LIII and ACI 318-19 gave very good estimations.

The formulation described in Section 4.1 was also used to assess specimens' shear strengths. As the interface crack extension is unknown prior to testing, the weakest shear strength mechanisms observed in the experimental tests were considered. Thus the monolithic specimens were considered to resist shear by means of the Variant B of the strut-and-tie model (Fig. 10) and slab shear failure. The composite specimens were calculated with Variant A of the strut-and-tie model and slab bending failure. The results are shown in Table 6.

Table 6. Statistical indicators of the V_{exp}/V_{pred} ratio for the test specimens assessed with the proposed model.

	Monolithic	Composite (NW)	Composite (HW)
No. of specimens	9	6	4
Mean	1.03	1.15	1.15
CV (%)	7.55	11.19	12.11
Min. value	0.92	1.02	0.99
Max. value	1.15	1.36	1.33
No. of unsafe results	4	0	1

The proposed model gave a very good approximation to the monolithic specimens' actual strength (mean value of 1.03 and CV of 7.55%), albeit with some unsafe results. The composite specimens were well estimated by this methodology, whose good result was similar to the best one offered by the codes and with almost no unsafe results. The obtained dispersions were similar to those observed in Table 5. It should be noted that the model is based on a composite beam mechanical model supported by experimental results, and was developed for the shear strength assessment of the specimens included in this experimental programme. Further experimental research should be conducted to extend the application scope of this mechanical model.

5. Recommendations for practice

After performing the experimental tests, analysing the shear strength mechanisms and the influence of the considered variables, adapting the strut-and-tie model to these specimens and experimentally verifying the current codes' formulations and the proposed one, some preliminary practical rules for designing this type of composite elements were derived.

For increasing the shear strength of the composite structure, the most resistant observed mechanisms must be sought, which were the Variant C of the model with a slab shear failure. For the specimen to develop these mechanisms, the interface shear strength must be increased, by increasing the interface roughness or the reinforcement crossing the interface.

If the interface shear strength is improved, there are other measures that can increase the composite element's shear strength. First, the widening of the slab. The specimens tested in this paper proved the flanges can increase the specimen's shear strength when a slab shear failure takes place. The flange width that contributes to shear strength would be limited to once the flange depth, according to these experimental results. Second, the use of a better-quality concrete at the slab, since it increases the slab shear strength.

If the interface shear strength cannot be improved, the shear strength of the composite element can be safely estimated by the sum of the precast beam shear strength and the shear strength of the slab given by the yielding of the slab's longitudinal reinforcement (see the formulation presented in Appendix B).

It must be taken into account that the results and the discussion of this experimental analysis were derived from the tested specimens' dimensions, reinforcement and concrete quality. A generalization of the proposed lower-bound plasticity-based model to specimens of other characteristics will be needed in the future to better elaborate these practical rules.

6. Conclusions

The main findings of this study on the shear strength of concrete composite beams with T-shaped cross-section and web reinforcement are:

1. The plane in which the section width changes (interface) is a weakness plane in which interface cracks develop. These interface cracks divide the shear transmission into two load paths in both the monolithic and composite beams: one through the precast beam; one through the cast-in-place slab. The total shear strength of a specimen can be considered to be the sum of the shear

forces transmitted by each path. Ultimate shear is given by three possible failure modes in the slab: bending failure, shear failure and interface failure.

2. The mechanical model proposed in a previous study by the authors [24], which is adapted to the monolithic and composite T-shaped specimens of this paper, proved useful for understanding both the shear transfer mechanisms and failure modes of the experimental tests run in this work. The model accounts for the effect of flanges. Besides, the formulation of a failure mode detected in this paper (interface failure) is herein developed.
3. In the specimens with slab shear failure (all the monolithic specimens and some composite specimens), the presence of flanges increased shear strength. In this research work specimens, the shear strength increased in the same proportion as the shear-effective area increases when considering an effective slab width that equal the sum of the web width and flange depth (approx. 17%). Most of the specimens with extended interface cracking, which were composite specimens in this test programme, showed slab bending failure, and flanges did not increase shear strength.
4. The presence of an interface between concretes decreased the specimens' shear strength, since the greater interface cracking resulted in less resistant failure mechanisms, such as slab bending failure in the beams with extended interface cracking.
5. The shear strength of the tested specimens that presented an extended interface cracking did not depend on the compressive strength of either the beam or slab's concrete, since, according to the proposed model, their shear strength is given by the yielding of the slab's longitudinal reinforcement. The shear strength of the specimens in which interface cracking was short depended on the compressive strength of the slab's concrete, since the shear strength is given by the slab failing in shear.
6. When predicting the monolithic specimens' shear strength with the current codes formulations, EC2 [21] gives the best result, but still extremely safe as no code accounts for the flanges effect on shear strength. Regarding the composite specimens, EC2, the level III approximation of MC-10 [22] and equation (b) of ACI 318-19 [23], using the weighted average of the beam and slab's concrete compressive strengths, offer the best estimations, on the safety side. Predicting the monolithic specimens' shear strength with the proposed model gives very accurate results. The shear strength estimation performed with the proposed model for the composite specimens is also good, and slightly better than that of the current codes.
7. As a recommendation for practice, the improvement of the interface shear strength of composite beams is suggested for increasing their shear strength. This will derive in the specimen having a slab shear failure. In this case, the slab width and the slab's concrete strength could be increased with the same purpose. If the interface shear strength cannot be improved, the composite

specimen's shear strength can be safely predicted with the proposed model for beams with extended interface cracking.

This research work contributes to increase the number of experimental tests on concrete composite elements subjected to shear forces. Experimental data on the contribution of the cast-in-place slab to shear strength and a better understanding of shear strength mechanisms in concrete composite T-beams are provided. The mechanical model proposed to explain the experimental results could be used as a reference to develop a shear strength predictive model for concrete composite beams in the future. However, to delve into the slab's contribution to shear strength, further research should be conducted on more complex elements, such as T- or I-shaped beams with a cast-in-place slab on top and of different dimensions.

Acknowledgements

The authors would like to thank the Ministerio de Ciencia e Innovación (MCIN) and the Agencia Estatal de Investigación (AEI) for their support through grants BIA2015-64672-C4-4-R and RTI2018-099091-B-C21-AR, both funded by MCIN/AEI/ 10.13039/501100011033 and by "ERDF A way of making Europe". Author Lisbel Rueda-García was supported through grant BES-2016-078010 funded by MCIN/AEI/ 10.13039/501100011033 and by "ESF Investing in your future". The Regional Government of Valencia also supported this research through Project AICO/2018/250. This research work was undertaken at the Concrete Science and Technology University Institute (ICITECH) of the Universitat Politècnica de València (UPV; Spain) with concrete supplied by Caplansa.

References

[1] Kim C-G, Park H-G, Hong G-H, Kang S-M, Lee H. Shear Strength of Concrete Composite Beams with Shear Reinforcements. ACI Struct J 2017;114:827–37.

[2] Halicka A, Jabłoński Ł. Shear failure mechanism of composite concrete T-shaped beams. Proc Inst Civ Eng Struct Build 2016;169:67–75.

[3] Ribas González CR, Fernández Ruiz M. Influence of flanges on the shear-carrying capacity of reinforced concrete beams without web reinforcement. Struct Concr 2017. https://doi.org/10.1002/suco.201600172.

[4] Kim C-G, Park H-G, Hong G-H, Kang S-M. Shear strength of composite beams with dual concrete strengths. ACI Struct J 2016;113:263–74.

[5] Rueda-García L, Bonet JL, Miguel Sosa PF, Fernández Prada MÁ. Safety

assessment of shear strength current formulations for composite concrete beams without web reinforcement. In: Fédération Internationale du Béton (fib), editor. Proc. 2021 fib Symp. Concr. Struct. New Trends Eco-Efficiency Perform., Lisbon: 2021, p. 2305–14.

[6] Loov RE, Patnaik AK. Horizontal Shear Strength of Composite Concrete Beams With a Rough Interface. PCI J 1994;39:48–69.

[7] Saemann JC, Washa GW. Horizontal Shear Connections between Precast Beams and Cast-in-Place Slabs. ACI J Proc 1964;61:1383–409.

[8] Kahn LF, Slapkus A. Interface Shear in High Strength Composite T-Beams. PCI J 2004;49:102–10.

[9] Kovach J, Naito C. Horizontal Shear Capacity of Composite Concrete Beams without Interface Ties. ATLSS Report No. 05-09: 2008.

[10] Tan KH, Guan LW, Lu X, Lim TY. Horizontal shear strength of indirectly loaded composite concrete beams. ACI Struct J 1999;96:533–8.

[11] Fang Z, Jiang H, Liu A, Feng J, Chen Y. Horizontal Shear Behaviors of Normal Weight and Lightweight Concrete Composite T-Beams. Int J Concr Struct Mater 2018;12. https://doi.org/10.1186/s40069-018-0274-3.

[12] Hartmann DL, Breen JE, Kreger ME. Shear capacity of high strength prestressed concrete girders. Austin: 1988.

[13] Shahawy MA, Batchelor B deV. Shear Behavior of Full-Scale Prestressed Concrete Girders: Comparison Between AASHTO Specifications and LRFD Code. PCI J 1996;41:48–62. https://doi.org/10.15554/pcij.05011996.48.62.

[14] Ross BE, Ansley MH, Hamilton III HR. Load testing of 30-year-old AASHTO Type III highway bridge girders. PCI J 2011;56.

[15] Hamilton III HR, Llanos G, Ross BE. Shear performance of existing prestressed concrete bridge girders. 2009.

[16] Runzell B, Shield C, French C. Shear Capacity of Prestressed Concrete Beams. 2007.

[17] Cumming, A David., Shield, Carol K., French CE. Shear Capacity of High-Strength Concrete Pre-stressed Girders. 1998.

[18] Hawkins NM, Kuchma DA. Application of LRFD Bridge Design Specifications to High- Strength Structural Concrete: Shear Provisions. 2007.

[19] Avendaño AR, Bayrak O. Shear strength and behaviour of prestressed concrete beams. Technical Report: IAC-88-5DD1A003-3, Texas

Department of Transportation: 2008.

[20] Ruiz MF, Muttoni A. Shear strength of thin-webbed post tensioned beams. ACI Struct J 2009;106.

[21] CEN. EN 1992-1-1:2004. Eurocode 2: Design of concrete structures - Part 1-1: General rules and rules for buildings. 2004.

[22] Fédération International du Béton (fib). Model Code 2010. Ernst & Sohn; 2012.

[23] ACI Committee 318. Building code requirements for structural concrete (ACI 318-19); and commentary (ACI 318R-19). Farmington Hills: American Concrete Institute; 2019.

[24] Rueda-García L, Bonet Senach JL, Miguel Sosa PF, Fernández Prada MÁ. Analysis of the shear strength mechanism of slender precast concrete beams with cast-in-place slab and web reinforcement. Eng Struct 2021;246:113043. https://doi.org/10.1016/j.engstruct.2021.113043.

[25] Placas A. Shear failure of reinforced concrete beams. Faculty of Engineering of the University of London. Imperial College of Science and Technology, 1969.

[26] Giaccio C, Al-Mahaidi R, Taplin G. Experimental study on the effect of flange geometry on the shear strength of reinforced concrete T-beams subjected to concentrated loads. Can J Civ Eng 2002;29. https://doi.org/10.1139/l02-099.

[27] Zararis IP, Karaveziroglou MK, Zararis PD. Shear strength of reinforced concrete T-beams. ACI Struct J 2006;103:693–700.

[28] Kani MW, Mark W. Huggins, Rudi R. Wittkopp. Kani on shear in reinforced concrete. Toronto: University of Toronto, Dept. of Civil Engineering; 1979.

[29] Palaskas MN, Attiogbe EK, Darwin D. Shear strength of lightly reinforced T-beams. J Am Concr Inst 1981;78:447–55.

[30] Tureyen AK, Wolf TS, Frosch RJ. Shear strength of reinforced concrete T-beams without transverse reinforcement. ACI Struct J 2006;103.

[31] Ayensa A, Oller E, Beltrán B, Ibarz E, Marí A, Gracia L. Influence of the flanges width and thickness on the shear strength of reinforced concrete beams with T-shaped cross section. Eng Struct 2019;188:506–18. https://doi.org/10.1016/j.engstruct.2019.03.057.

[32] ACI/ASCE Task Committee 426. The shear strength of reinforced concrete members. ACI J 1973;99:1091–187.

[33] Cladera A, Marí A, Ribas C, Bairán J, Oller E. Predicting the shear-flexural strength of slender reinforced concrete T and I shaped beams. Eng Struct 2015;101. https://doi.org/10.1016/j.engstruct.2015.07.025.

[34] Swamy RN, Qureshi SA. An ultimate shear strength theory for reinforced concrete T-beams without web reinforcement. Matériaux Constr 1974;7:181–9. https://doi.org/10.1007/BF02473833.

[35] Leonhardt F, Walther R. Schubversuche an einfeldrigen Stahlbetonbalken mit und ohne Schubbewehrung zur Ermittlung der Schubtragfähigkeit und der oberen Schubspannungsgrenze. Heft 151. Berlin: Ernst & Sohn; 1962.

[36] Placas A, Regan PE, Baker ALL. Shear failure of reinforced concrete beams. J Amer Concr Inst 1971;68.

[37] Regan MM and PE. Shear Strength of Prestressed and Reinforced Concrete T-Beams. ACI Symp Publ 1974;42. https://doi.org/10.14359/17284.

[38] Ribas C, Cladera A, Mas B. Modelo cortante-flexión para el dimensionamiento a ELU de forjados de vigueta pretensada y bovedilla. VI Congr. Int. Estructuras ACHE, Madrid, Spain: 2014, p. 151–152.

[39] Fernández Ruiz M, Muttoni A, Sagaseta J. Shear strength of concrete members without transverse reinforcement: A mechanical approach to consistently account for size and strain effects. Eng Struct 2015;99:360–72. https://doi.org/10.1016/j.engstruct.2015.05.007.

[40] Rueda-García L, Bonet Senach JL, Miguel Sosa PF. Experimental study of concrete composite beams subjected to shear. Proc. fib Symp. 2019 Concr. - Innov. Mater. Des. Struct., 2019, p. 1779–86.

[41] UNE-EN 12350-2:2020. Testing fresh concrete - Part 2: Slump test. 2020.

[42] UNE-EN 12390-3:2020. Testing hardened concrete - Part 3: Compressive strength of test specimens. 2020.

[43] UNE-EN 12390-6:2010. Testing hardened concrete - Part 6: Tensile splitting strength of test specimens. 2010.

[44] UNE-EN 12390-13:2014. Testing hardened concrete - Part 13: Determination of secant modulus of elasticity in compression. 2014.

[45] Comisión Permanente del Hormigón. EHE-2008. Instrucción de Hormigón Estructural. Ministerio de Fomento. Madrid: 2008.

[46] UNE-EN ISO 6892-1:2017. Metallic materials - Tensile testing - Part 1: Method of test at room temperature. 2017.

[47] Rueda-García L, Bonet Senach JL, Miguel Sosa PF, Fernández Prada MÁ.

Experimental analysis of the shear strength of composite concrete beams without web reinforcement. Eng Struct 2021;229:111664. https://doi.org/10.1016/j.engstruct.2020.111664.

[48] Pansuk W, Sato Y. Shear mechanism of reinforced concrete T-Beams with stirrups. J Adv Concr Technol 2007;5. https://doi.org/10.3151/jact.5.395.

[49] Kupfer HB, Gerstle KH. Behavior of concrete under biaxial stresses. ASCE J Eng Mech Div 1973;99:853–66.

[50] Ribas C, Cladera A. Resistencia a cortante de los forjados de vigueta pretensada y bovedilla. Universitat Politècnica de Catalunya, 2013.

Appendices

These appendices contain further information that is not provided in the main body of the paper for sake of brevity.

Appendix A. Nomenclature

a	shear span
A_{sl}	area of the cross-section of the slab's longitudinal reinforcement
A_{sw}	area of the cross-section of the two legs of a stirrup
b	web width of the concrete section
b_{eff}	slab's effective shear width
d	effective depth
d'	slab's longitudinal reinforcement depth
d_b	precast beam's effective depth
d_c	the entire composite beam's effective depth
E_c	concrete's modulus of elasticity
E_s	modulus of elasticity of reinforcement
$f_{c,28}$	compressive strength of the concrete measured in cylinders at the age of 28 days
$f_{c,b}$	compressive strength of the beam's concrete measured in cylinders
$f_{c,s}$	compressive strength of the slab's concrete measured in cylinders
$f_{c,wa}$	weighted average of the beam and slab's concrete compressive strengths measured in cylinders estimated from the area ratio

f_{ct}	concrete's tensile strength
$F_{H,i}$	horizontal force transferred at the nodes located on the interface crack
$F_{i,nc}$	horizontal force at the interface of the principal span that was not cracked before V_{ic}
f_u	tensile strength of reinforcement
f_y	yield strength of reinforcement
h_s	cast-in-place slab height
$l_{i,nc}$	length of the interface of the principal span that was not cracked before V_{ic}
N_s	axial force in the slab
$Ø$	nominal diameter of a reinforcing bar
T_l	tension force of slab longitudinal reinforcement
T_w	tension force of web reinforcement
V	shear force
V_{exp}	experimental shear strength
V_{ic}	shear force at which the interface crack clearly extended along the interface
V_{pb}	the precast beam's shear strength
V_{pred}	the specimen's predicted shear strength value
V_s	slab shear strength
$V_{s,BF}$	slab shear strength provided by the slab bending failure
$V_{s,IF}$	slab shear strength provided by the interface failure
$V_{s,SF}$	slab shear strength provided by the slab shear failure
γ_c	partial safety factor for the concrete material properties
γ_s	partial safety factor for the steel material properties
ε_c	strain on the concrete surface
$\varepsilon_{s,i}$	average strain of stirrup i
$\varepsilon_{s,l}$	tension longitudinal reinforcement strain below the point load
ε_u	reinforcement strain at the maximum load

ε_y	reinforcement strain at yield strength
θ	angle between the strut and the axis of the member
ρ_l	reinforcement ratio of tension longitudinal reinforcement
ρ_w	reinforcement ratio of web reinforcement
σ_1, σ_2	principal stresses
σ_x	normal stress in the longitudinal direction
τ	tangential stress
$\tau_{i,exp}$	experimental shear stress at the interface between concretes

Appendix B. Summary of the mechanical model proposed by Rueda-García et al. [24]

Three variants of the proposed model are distinguished depending on the interface crack extension along the principal span. Fig. B.1 depicts the three variants in examples of the test specimens in this experimental programme.

Shear strength is estimated as the sum of the shear force transmitted along each load path (the precast beam and the cast-in-place slab):

$$V_{pred} = B_{V,7} + S_{V,7} = V_{pb} + V_s = V_{pb} + min\{V_{s,BF}, V_{s,SF}\} \quad \text{(B.1)}$$

The formulation to obtain these variables based on the strut-and-tie models of Fig. B.1 is summarized in Table B.1. The shear transmitted by the precast beam is limited by the yielding of stirrups' steel. Accordingly, the shear transmitted by precast beam V_{pb} is obtained, as are the horizontal forces that balance nodes i in Fig. B.1 ($F_{H,i}$), which represent the dowel action of the transverse reinforcement and the aggregate interlock at the cracked interface. The slab's strut-and-tie model receives these horizontal forces $F_{H,i}$, which have equal values and opposite directions (Fig. B.1). Two possible slab failure mechanisms are calculated. Firstly, slab bending failure due to the slab's longitudinal reinforcement ($V_{s,BF}$) yielding. In this case, horizontal ties 16-17, 15-16 or 14-15, in Variant A, B and C, respectively (Fig. B.1), are considered to yield. Secondly, slab shear failure ($V_{s,SF}$), in which case the slab is considered to be subjected to a biaxial state of stresses, and failure occurs when concrete principal stresses reach Kupfer's failure envelope [49]. The shear force transmitted through the slab (V_s) will be the lowest of the shear forces resisted by each mechanism. For a detailed explanation of the origin of each formula, see [24].

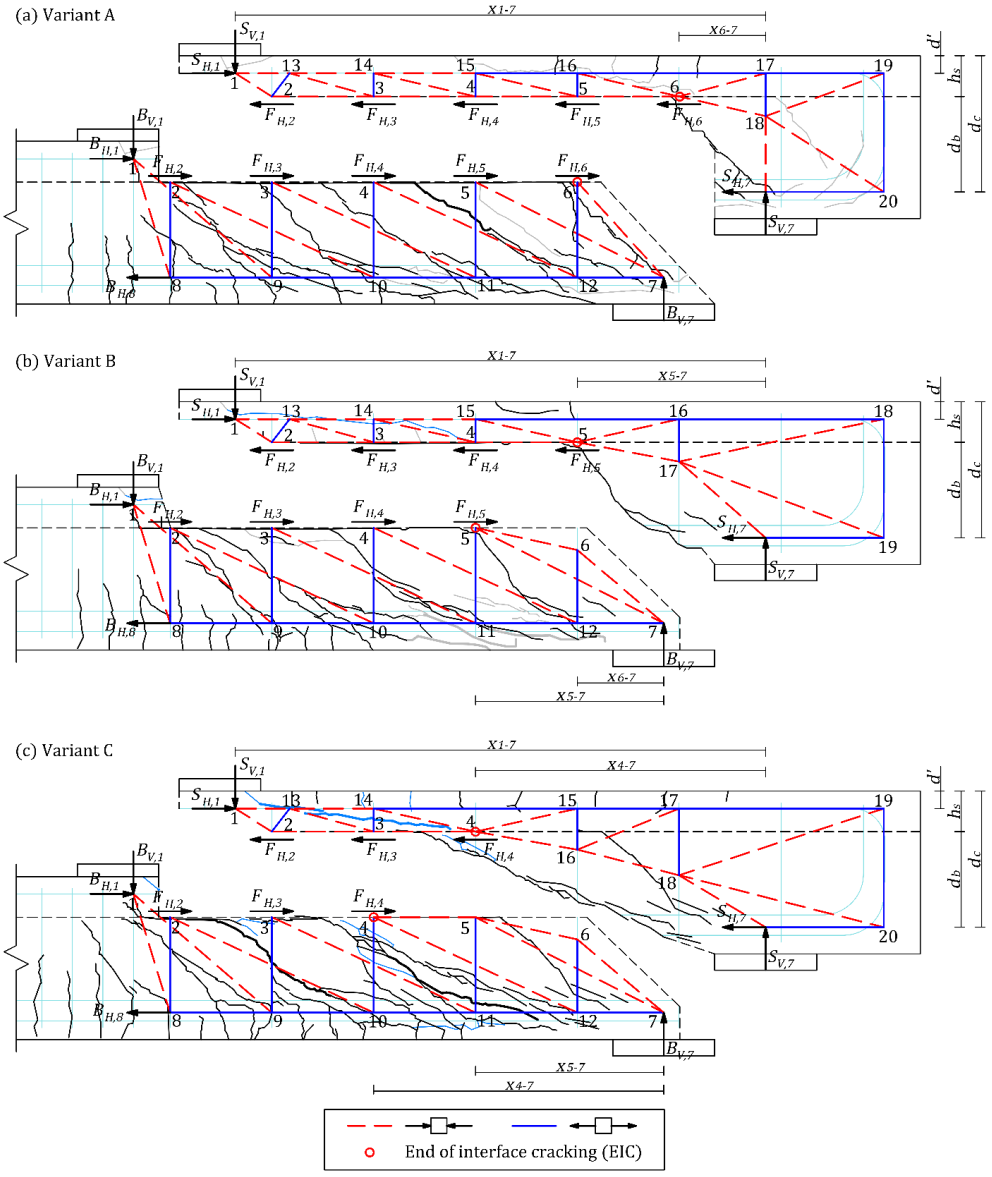

Fig. B.1. Proposed strut-and-tie models for the precast beam and the cast-in-place slab separately: (a) Variant A (specimen HWP5D2); (b) Variant B (specimen HWP5C2); (c) Variant C (specimen HWP6C1).

Table B.1. Formulation for obtaining the shear strength transmitted through the precast beam and the cast-in-place slab.

Variable	Variant of the model	Formulas
$F_{H,i}$	A	$T_w = A_{sw} \cdot f_y$ $F_{H,i} = T_w \cdot \cot\theta_i$, where i = 2, 3, 4, 5, 6
	B	$T_w = A_{sw} \cdot f_y$ $F_{H,i} = T_w \cdot \cot\theta_i$, where i = 2, 3, 4 $F_{H,5} = \frac{T_w(x_{5-7} + x_{6-7})}{d_b}$
	C	$T_w = A_{sw} \cdot f_y$ $F_{H,i} = T_w \cdot \cot\theta_i$, where i = 2, 3 $F_{H,4} = \frac{T_w(x_{4-7}+x_{5-7})}{d_b}$
V_{pb}	All	$V_{pb} = B_{V,7} = 2T_w$
$V_{s,BF}$	All	$T_l = A_{sl} \cdot f_y$ $V_{s,BF} = S_{V,7} = \frac{\left(\sum_{i=2}^{K} F_{H,i}\right) \cdot (h_s - d') \cdot d_b + T_l \cdot (h_s - d') \cdot (d_c - d')}{x_{1-7} \cdot d_b - x_{K-7} \cdot (d_c - d')}$
$V_{s,SF}$	All	$N_s = F_{H,K} + \frac{V_{s,SF} \cdot x_{1-7} - (h_s - d') \cdot \sum_{i=2}^{K} F_{H,i}}{d_c - d'}$ $\sigma_x = -\frac{N_s}{b_{eff} \cdot h_s}$ $\sigma_1 = \frac{\sigma_x}{2} + \sqrt{\left(\frac{\sigma_x}{2}\right)^2 + \tau^2} \leq f_{ct}$ (1) $\sigma_2 = \frac{\sigma_x}{2} - \sqrt{\left(\frac{\sigma_x}{2}\right)^2 + \tau^2} \geq -f_{c,s}$ (2) Substitute (1) and (2) in $\sigma_1 = \lvert f_{ct}\rvert + 0.8\frac{\lvert f_{ct}\rvert}{\lvert f_{c,s}\rvert}\sigma_2 \rightarrow Solve\ \tau$ $V_{s,SF} = 2/3 \cdot \tau \cdot b_{eff} \cdot h_s$

Forces $F_{H,i}$ are considered positive in the direction indicated in Fig. B.1.
x_{j-k} is the horizontal distance between nodes j and k in Fig. B.1.
θ_i is the angle between the strut that converges at node i and the axis of the member.
K is the identifier of the node located at the end of interface cracking (EIC in Fig. B.1).
The other variables are defined in Appendix A: Nomenclature.

Appendix C. Calculating the experimental interface shear strength

The experimental shear strength of the interface ($\tau_{i,exp}$) is estimated from the horizontal forces equilibrium in the slab strut-and-tie model of Variant C (Fig. C.1). The shear force resisted by the slab ($S_{V,1}$) is calculated as the difference between the experimental shear force at interface cracking (V_{ic}), which is the V_{exp} in the specimens with interface failure, and the shear strength of the precast beam (V_{pb}). With the $S_{V,1}$ value, the horizontal force at slab $S_{H,1}$ is calculated as:

$$S_{H,1} = \frac{\sum_{i=2}^{4} F_{H,i} \cdot d_b + S_{V,1} \cdot x_{1-7}}{d_c - d'} \tag{C.1}$$

where horizontal forces $F_{H,i}$ are calculated following the procedure described in Appendix B.

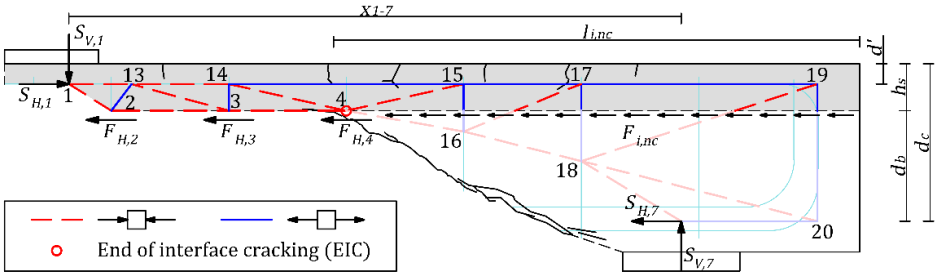

Fig. C.1. Isolated slab in the strut-and-tie model of the cast-in-place slab of Variant C.

The horizontal force at the uncracked interface (Fig. C.1) is calculated as:

$$F_{i,nc} = S_{H,1} - \sum_{i=2}^{4} F_{H,i} \tag{C.2}$$

Interface shear stress $\tau_{i,exp}$ is obtained as a distributed force in the uncracked interface area:

$$\tau_{i,exp} = \frac{F_{i,nc}}{b \cdot l_{i,nc}} \tag{C.3}$$

7th PAPER

Details:

Type of paper	Journal article
Title	*Experimental analysis of the shear resistance of precast concrete T-beams with a top cast-in-place slab*
Authors	Lisbel Rueda García José Luis Bonet Senach Pedro Francisco Miguel Sosa Miguel Ángel Fernández Prada
Status	Ready for submission to a scientific journal
Full reference	Rueda-García L, Bonet Senach JL, Miguel Sosa PF, Fernández Prada MÁ. Experimental analysis of the shear resistance of precast concrete T-beams with a top cast-in-place slab. 2022.

Experimental analysis of the shear resistance of precast concrete T-beams with a top cast-in-place slab

Lisbel Rueda García, lisruega@cam.upv.es

José Luis Bonet Senach, jlbonet@cst.upv.es

Pedro Fco. Miguel Sosa, pmiguel@cst.upv.es

Miguel Ángel Fernández Prada, mafernan@cst.upv.es

Universitat Politècnica de València, Camí de Vera s/n, 46022, Valencia, Spain

Abstract

Precast concrete T-beams with a cast-in-place slab on top are structural elements that are often employed in composite construction. Despite their widespread use, their structural behaviour upon shear forces has not yet been studied in-depth. Six composite specimens with different T-shaped cross-sections and concrete qualities, and with web reinforcement, were tested to analyse the shear transfer mechanisms and to assess the contribution of the cast-in-place slab to shear strength. The shear strength mechanisms deriving from experimental observations and measurements are provided. This study indicates that: placing a concrete cast-in-place slab on top of a prefabricated T-beam increases its shear strength; interface shear strength plays an essential role in concrete composite elements' vertical shear strength; widening the cast-in-place slab width does not increase shear strength in this test programme specimens; the compressive strength of the precast beam's concrete significantly influences composite beams' shear resistances. The formulations of EC2, MC-10 (Level III) and ACI 318-19 predict underestimated shear strengths compared to the experimental results, although the formulation of ACI 318-19 best captures the concrete strength influence on shear strength.

Keywords: precast construction, reinforced concrete, composite beam, T-beam, cast-in-place slab, shear strength, shear failure, interface shear, mechanical behaviour.

Highlights

Precast concrete T-beams with a cast-in-place slab on top are tested in shear

The contribution of the slab to shear strength is experimentally analysed

The shear strength mechanisms of monolithic and composite T-shaped beams are analysed

The tangential stresses at the interface and the interface shear strength are key

Current codes shear formulations underestimate composite elements' shear strength

Nomenclature

a	shear span
c	concrete cover
d	effective depth
E_c	concrete's modulus of elasticity
E_s	modulus of elasticity of reinforcement
$f_{c,28}$	compressive strength of the concrete measured in cylinders at the age of 28 days
$f_{c,b}$	compressive strength of the beam's concrete measured in cylinders
$f_{c,wa}$	weighted average of the beam and slab's concrete compressive strengths measured in cylinders estimated from the area ratio
f_{ct}	concrete tensile strength
f_u	tensile strength of reinforcement
f_y	yield strength of reinforcement
h	overall member height
$Ø$	nominal diameter of a reinforcing bar
V	shear force
V_{exp}	experimental shear strength
V_{pred}	specimen's predicted shear strength value
ε_c	strain on the concrete surface
ε_u	reinforcement strain at the maximum load
ε_y	reinforcement strain at yield strength
θ	angle between the strut and the axis of the member
ϱ_l	reinforcement ratio of tension longitudinal reinforcement
ϱ_w	reinforcement ratio of web reinforcement

1. Introduction

In order to save medium and large spans in the construction of bridges and buildings, using precast reinforced or prestressed concrete beams with T- or I-shaped cross-sections is a widespread practice, onto which a cast-in-place concrete layer is poured (see Fig. 1) to give concrete composite elements. In 2016 the Technical Committee 4.3 "Road bridges" of PIARC revealed that more than 70% of road bridges in European participating countries are made of reinforced or prestressed concrete [1]. Given the vast number of these structures, the study of their structural behaviour is especially important.

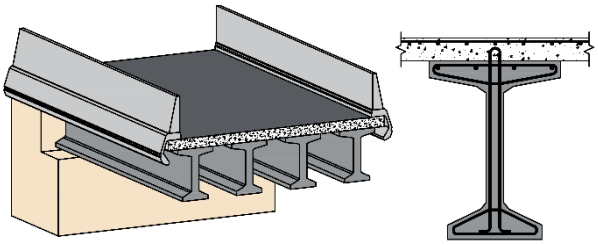

Fig. 1. Concrete composite beams bridge deck.

In the structural analysis of concrete composite beams, interface shear strength has been well-analysed since the 1960s [2–6] because the transfer of shear forces at the interface between two concretes is critical for composite members' integrity [7,8]. On vertical shear behaviour, there are fewer experimental studies into concrete composite beams, which mainly focus on the experimental verification of the shear strength of full-scale precast concrete beams with cast-in-place slabs on top according to design codes [9–18]. However, no studies have analysed the contribution of the cast-in-place slab to shear strength. Consequently, some aspects still need to be solved, such as which composite element depth, which concrete strength (precast beam concrete or slab concrete) or which slab width must be considered to assess the shear strength of concrete composite beams.

Such scarce knowledge is observed in current design codes, where indications about the shear treatment of these elements are limited. Section 10.9.3 of EC2 [19] allows concrete elements with a topping that is at least 40 mm thick to be designed as composite elements, provided that interface shear strength meets code requirements. However, no further indications about how these composite elements must be designed appear. Section 22.5.4 of ACI 318-19 [20] also indicates that the interface must be designed for the loads that will be transferred across it, and specifies that shear strength may be calculated with the properties of the element (precast beam or slab) that result in the most critical value or the properties of the individual elements. Nevertheless, further experimental evidence is required for

verifying the result of individual elements because the current ACI 318 design equation was developed based on test results obtained with monolithic beams [7]. Other current codes, such as MC-10 [21], do not mention this type of structural elements.

In previous publications [22–24], the authors compared the shear strengths of monolithic and composite rectangular and T-shaped beams both with and without shear reinforcement. The interface between concretes of composite T-shaped beams was at the height of the section width change. The main findings from these studies were: (i) both the interface between concretes and the plane on which section width changes in monolithic T-shaped specimens were a weakness plane that clearly modified the crack pattern of specimens by deviating the diagonal shear cracks along it (see Fig. 2); (ii) the horizontal crack along that weakness plane divided shear transmission into two load paths: one through the precast beam web and one through the beam head or cast-in-place slab; (iii) specimens' failure was given by the failure of the shear path through the beam head or the slab. All these findings were captured in a formulation based on a strut-and-tie model proposed by the authors for assessing specimens' shear strengths.

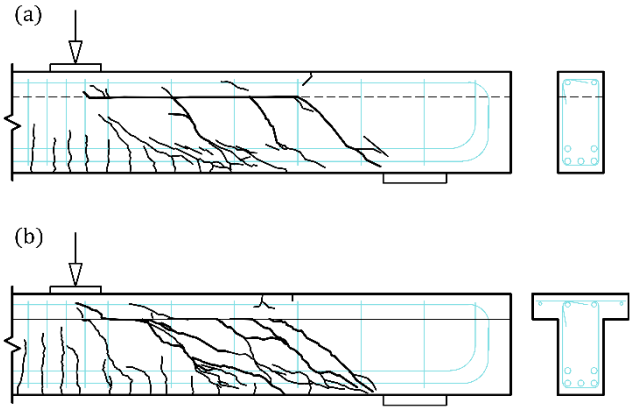

Fig. 2. Examples of crack patterns at the maximum load: (a) composite rectangular beam (NWP2B2 in [23]); (b) monolithic T-beam (NWP2C1 in [24]).

Given that both the interface and section width change can modify the crack pattern and, thus, the shear strength mechanisms of specimens, the aim of this paper is to study the contribution of the cast-in-place slab to shear strength in structures that have both weakness planes, such as T-beams with a cast-in-place slab on top, because they are frequently used in precast constructions, as explained above. For this purpose, six T-shaped specimens were experimentally tested. They were made of reinforced concrete with shear reinforcement and subjected to shear forces. The following items that influence shear strength were analysed by comparing different

cross-section types and concrete qualities: the presence of a cast-in-place slab on top; the presence of an interface between concretes; cast-in-place slab width; the compressive strength of the beam and slab concretes. The results of this analysis are herein presented. The experimental results are also compared to the shear strength predictions of current codes' shear formulations.

The research significance of this paper lies in it providing experimental results about the contribution of the cast-in-place slab to shear strength of concrete composite beams. This contribution is a problem that designers actually face in practice and one that still needs to be solved. The study herein performed of shear strength mechanisms sheds light on these structures' shear behaviour, and provides the basis for future development of a shear design and assessment formulation for composite concrete elements.

2. Test programme

2.1. Test parameters

The variable parameters considered in the specimens of this study to analyse the cast-in-place slab's contribution to shear strength were the following:

- Presence of a cast-in-place slab on top. Specimens E2 (see Fig. 3), formed by a monolithic T-beam (representing the precast beam) with a cast-in-place slab on top, were fabricated to be compared to specimens C1 from a previous experimental study by the authors [24] (see Fig. 2b). Specimens C1 had the same characteristics and dimensions as the monolithic T-beam of specimen E2, but without any cast-in-place slab on top.
- Presence of an interface between concretes. Specimens E1 (see Fig. 3) were monolithically fabricated. Specimens E2 were fabricated with two concretes cast at different times, so an interface between both concretes was created.
- Slab width. Two different slab widths were compared in this study: that of specimen E2, whose slab width equalled the flange width of the monolithic T-beam; that of specimen F2, whose slab was wider than the flange of the monolithic T-beam (see Fig. 3).
- Beam and slab concretes' compressive strengths. Two different compressive strengths for the precast beam concretes were used: normal-strength concrete (NSC), whose design compressive strength was 25 MPa; high-strength concrete (HSC), whose design compressive strength was 70 MPa. All the cast-in-place slabs were designed with NSC.

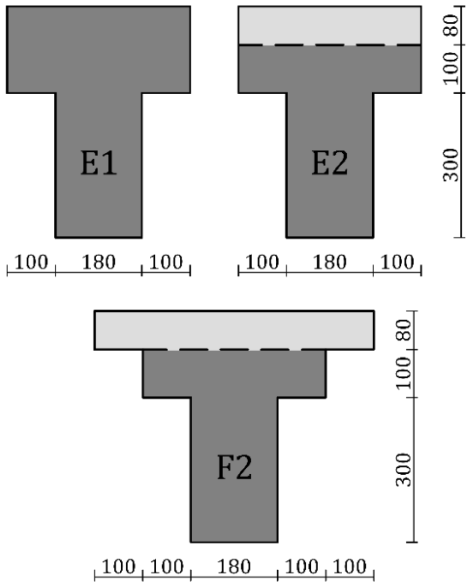

Fig. 3. Cross-section types (dimensions: mm).

2.2. Test specimens

Six specimens were tested in this experimental programme. Table 1 summarises their main characteristics. Two series of three reinforced concrete T-shaped specimens with web reinforcement were fabricated. In the first series (series NW), the three specimens (one for each cross-section type; E1, E2 and F2 in Fig. 3), were fabricated with normal-strength concrete (NSC) at both the precast beam and the cast-in-place slab. In the second series (series HW), the entire beam in specimen E1 and the precast beams of the composite specimens were fabricated with high-strength concrete (HSC); the slabs were produced with NSC.

Table 1. Main characteristics of the test specimens and their shear strength results.

Specimen	Type of precast beam concrete	Type of slab concrete	T-beam flange width (m)	T-beam flange depth (m)	Slab width (m)	Slab depth (m)	V_{exp} (kN)
NWE1	NSC	NSC	0.38	0.18	-	-	259
NWE2	NSC	NSC	0.38	0.10	0.38	0.08	241
NWF2	NSC	NSC	0.38	0.10	0.58	0.08	223
HWE1	HSC	NSC	0.38	0.18	-	-	327
HWE2	HSC	NSC	0.38	0.10	0.38	0.08	315
HWF2	HSC	NSC	0.38	0.10	0.58	0.08	315

The nomenclature of the six specimens was as follows: *xWzk*, where "*xW*" referred to the series name (NW or HW as explained above), "*z*" represented the cross-section shape (E or F in Fig. 3), and "*k*" denoted the number of concretes used to fabricate the specimen (1 for monolithic specimens, 2 for composite specimens).

Fig. 4 shows the dimensions and reinforcement of the specimens for each cross-section type. Specimens were 4.14 m long. The distance between supports was 3.00 m. Two non-centred point loads, separated by 0.40 m, applied the load to the top of beams and formed two different shear spans: a 1.60 metre-long principal span where failure was expected; a 1.00 metre-long reinforced span with additional web reinforcement to prevent shear failure. All the specimens were 0.48 m high (see Fig. 3). In the composite specimens (E2 and F2), the precast beam was 0.40 m high and the cast-in-place slab was 0.08 m high.

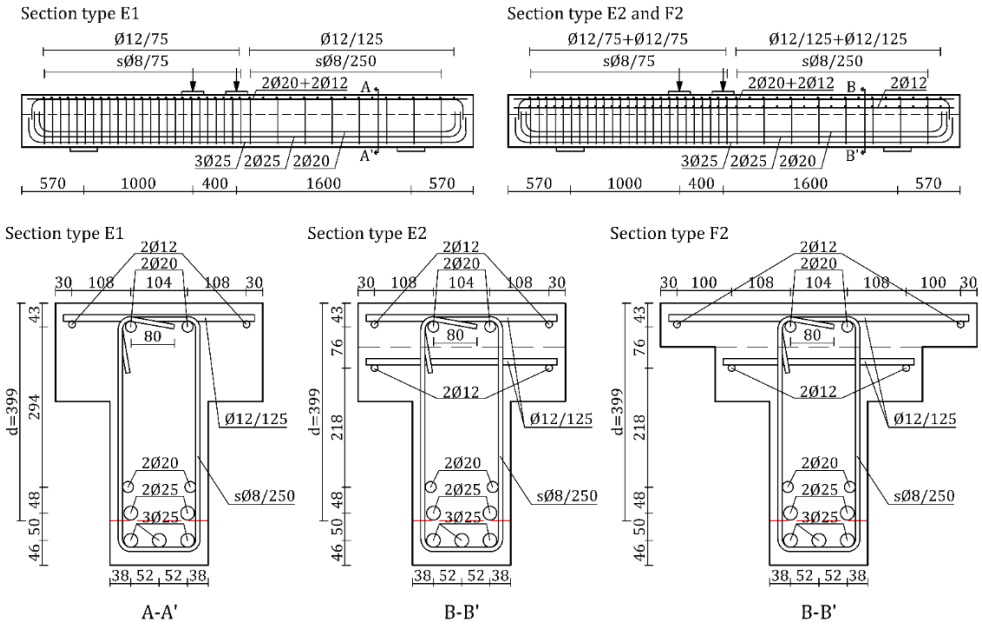

Fig. 4. Dimensions and reinforcement of specimens types E and F (dimensions: mm).

The following characteristics were fixed for all the specimens: the shear span-effective depth ratio ($a/d = 4$), which was selected to foster a shear failure governed by beam shear-transfer actions [25,26]; the longitudinal reinforcement ratio (ρ_l = 4.3%), to prevent bending failure; the shear reinforcement ratio (ρ_w = 0.22%), which met the maximum spacing requirements of the current codes considered in the design of these beams [19–21]. The interface roughness in the composite specimens

was "smooth" or "as-cast" according to current code definitions as concrete underwent no further treatment after vibration.

The interface reinforcement ratio, which equalled the shear reinforcement ratio (0.22%), and interface roughness were selected after a previous work by the authors [27] proved that they were appropriate for ensuring diagonal beam cracking before interface cracking. The transverse reinforcement at the flange of the T-beams and at the slab was designed to prevent the shear failure between web and flanges in both. Finally in the composite specimens, the time that elapsed between the precast beam concrete casting and the slab concrete casting was 24 h, which was set after a previous study by the authors [23] proved that marked differential shrinkage between the precast beam and slab concretes did not significantly influence the shear strength of the specimens of this experimental programme.

2.3. Fabrication of specimens

The fabrication process of the two specimen series (NW and HW) was conducted on two consecutive days. The precast beam concrete was poured on the first day. In the composite specimens, the concrete surface of the principal span, where failure was expected, was not further treated after vibration. Thus interface roughness was "smooth" or "as-cast". In the reinforced span, the surface was racked before concrete hardened to increase the interface shear strength in that span. "Very rough" interface roughness was obtained in that way. The slab concrete was poured in the composite specimens on the second day.

In this experimental programme, the precast beam concrete and the slab concrete were both cast while the entire length of beams was laid on the floor. Hence the beam and the slab of the composite specimens were simultaneously loaded.

2.4. Material properties

Table 2 shows the mechanical properties of the precast beam and slab concretes: the 28-day compressive strength ($f_{c,28}$), and the compressive strength (f_c), modulus of elasticity (E_c) and tensile strength (f_{ct}) at testing age. Specimens of series NW and HW were respectively tested 29 and 33 days after precast beam concrete pouring. The results were the average of two concrete cylinders (300 mm high, 150 mm diameter), and were obtained by following the provisions of UNE-EN 12390 [28–30]. Concrete tensile strength was calculated as 90% concrete tensile splitting strength, as indicated in [31]. Table 2 shows the average coefficients of variation (CV) of the measurements.

NSC had a water-cement ratio of 0.52, 325 kg/m^3 of Portland cement and a maximum aggregate size of 10 mm. HSC respectively had 0.44, 500 kg/m^3 and 10 mm.

Table 2. Concrete mechanical properties.

Series	$f_{c,28,b}$ (MPa)	$f_{c,28,s}$ (MPa)	$f_{c,b}$ (MPa)	$f_{c,s}$ (MPa)	$E_{c,b}$ (MPa)	$E_{c,s}$ (MPa)	$f_{ct,b}$ (MPa)	$f_{ct,s}$ (MPa)
NW	25	26	25	26	22386	23716	1.93	2.18
HW	63	29	67	30	33438	26288	4.06	2.69

Notation: suffix "b" refers to the beam's concrete; suffix "s" refers to the slab's concrete.
Average coefficients of variation of measurements: 2% for $f_{c,28}$ and f_c; 4% for E_c; 5% for f_{ct}.

The reinforcing steel mechanical properties are shown in Table 3. They were measured according to UNE-EN ISO 6892 [32] by averaging the results of two tests for each nominal diameter. Type C steel was used in these specimens according to EC2 [19].

Table 3. Average values of the transverse and longitudinal reinforcement properties.

Ø (mm)	f_y (MPa)	E_s (GPa)	ε_y (‰)	f_u (MPa)	ε_u (%)
8(1)	538	203	2.6	658	12.0
8(2)	515	218	2.4	647	36.4
12	529	196	2.7	651	30.3
20	541	194	2.8	654	26.7
25	548	235	2.3	658	21.6

(1) Stirrups of the principal span.
(2) Stirrups of the reinforced span.

2.5. Instrumentation

The strains on the surface of the reinforcing steel bars were measured by strain gauges (2 mm measuring length, 120 Ω resistance). Their locations are shown in Fig. 5a. Three pairs of strain gauges were located on the bottom bars of the tension longitudinal reinforcement on Sections A to C (see gauges G1 to G6 in Fig. 5a-b). A pair of strain gauges was located at the compression longitudinal reinforcement on Section C (G7 and G8). Five pairs of strain gauges were glued at the mid-length of the two legs of stirrups w4 to w8 (G9 to G18 in Fig. 5a).

The strains on the concrete surface were measured on top of specimens by strain gauges (60 mm measuring length, 120 Ω resistance). Three strain gauges were placed on Sections A and B (gauges C1 to C6 in Fig. 5a). Their locations for beam types E and F are shown in Fig. 5b.

Linear variable displacement transformers (LVDTs) were used at different locations: V1 to V5 (see Fig. 5c), to measure the vertical displacements on the concrete surface; O1 and O2, fixed at the top and bottom of the specimens to detect the beginning of cracking; horizontally placed LVDTs to measure the horizontal slip between the web and flanges (H1 to H4 in Fig. 5c) and between flanges and the slab (H5 to H8

in Fig. 5c). In specimens E1 (see Fig. 3), built monolithically without a slab, LVDTs H5 to H8 were not placed.

The forces at the hydraulic jack and the two bearing points were measured by three 1,000 kN load cells.

Two digital cameras took pictures during the tests at a rate of 0.5 Hz. They were synchronised with the measured load to assign each photogram to the corresponding load. A high-speed camera was used to detect the beginning of cracking and to record brittle failures.

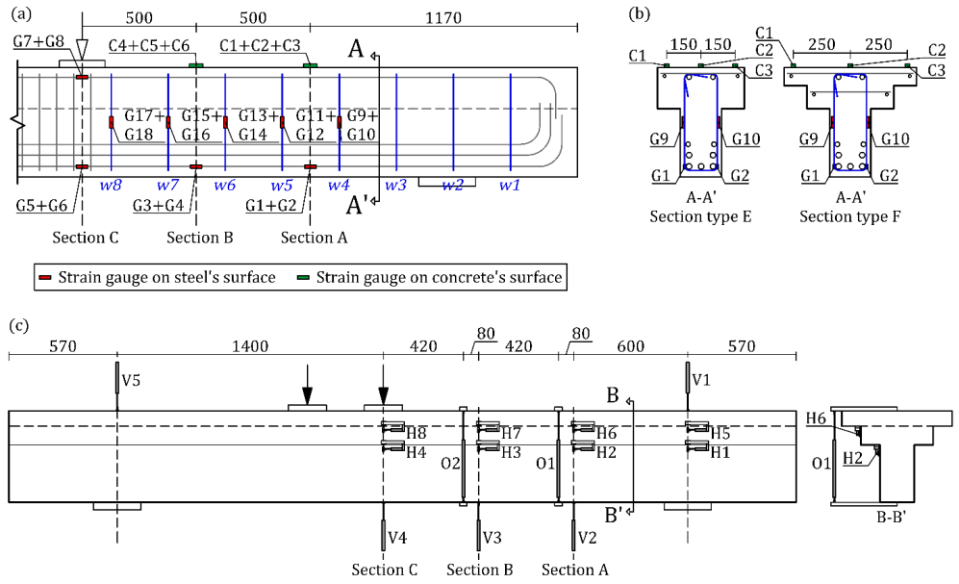

Fig. 5. Tests instrumentation: (a) strain gauges at the principal span; (b) strain gauges at section A-A' for beams types E and F; (c) LVDTs (dimensions: mm).

2.6. Test setup and procedure

A 1,200 kN hydraulic jack, fixed to a steel loading frame placed transversely to the beam's axis (see Fig. 6), applied the vertical load with displacement control (0.02 mm/s). A steel frame, equipped with a hinge to keep the load vertical despite the deformations of the beam's upper plane, divided the load into two equal point loads. These two loads were transmitted to the specimen by means of two square steel plates (200x200x30 mm), which were centred on the beam's upper plane width. Beams were laid on two bearing points that consisted of a steel plate (250 mm width), a ball bed to eliminate horizontal reactions and a hinge to allow for rotations.

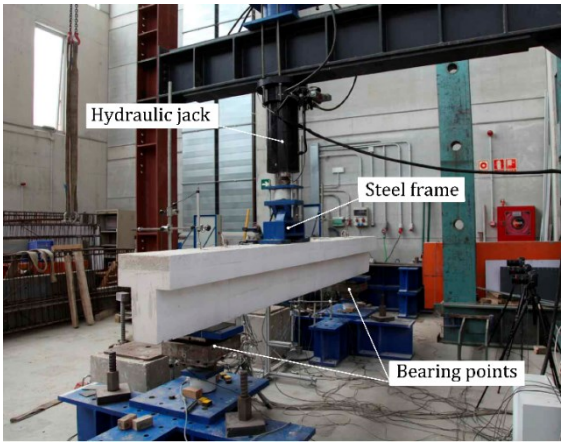

Fig. 6. Experimental setup.

3. Test results

3.1. Shear strength and shear-deflection relation

Specimens' vertical shear strengths are shown in Table 1 as V_{exp}. The relation throughout the test between shear force V at the principal span and the deflection below the point load (measured by LVDT V4, located on Section C in Fig. 5c) is shown in Fig. 7 for all the test specimens. The maximum shear force (V_{exp}) is marked with a circle on each curve.

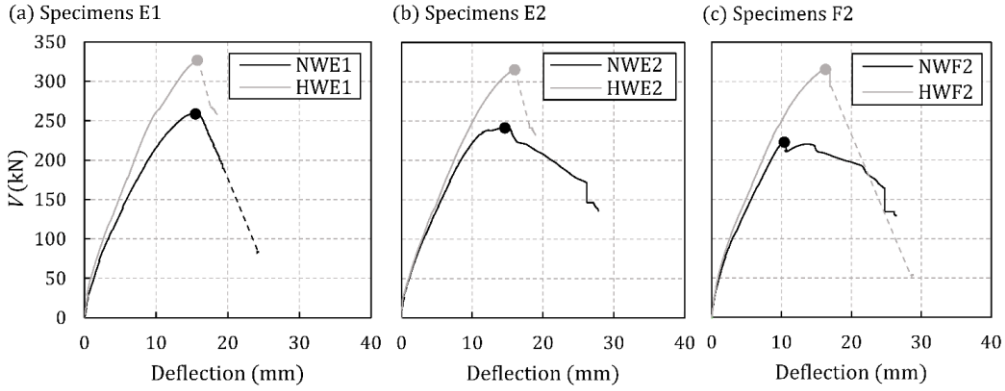

Fig. 7. Shear-deflection relation of the test specimens: (a) specimens with cross-section type E1; (b) specimens with cross-section type E2; (c) specimens with cross-section type F2.

3.2. Crack patterns

The crack patterns of the test specimens in different load stages are shown in Fig. 8: the cracks observed at the maximum shear force V_{exp}; the cracks that appeared immediately after V_{exp}, which were normally accompanied by a load drop (see the shear-deflection curves in Fig. 7); the cracks observed at the end of testing.

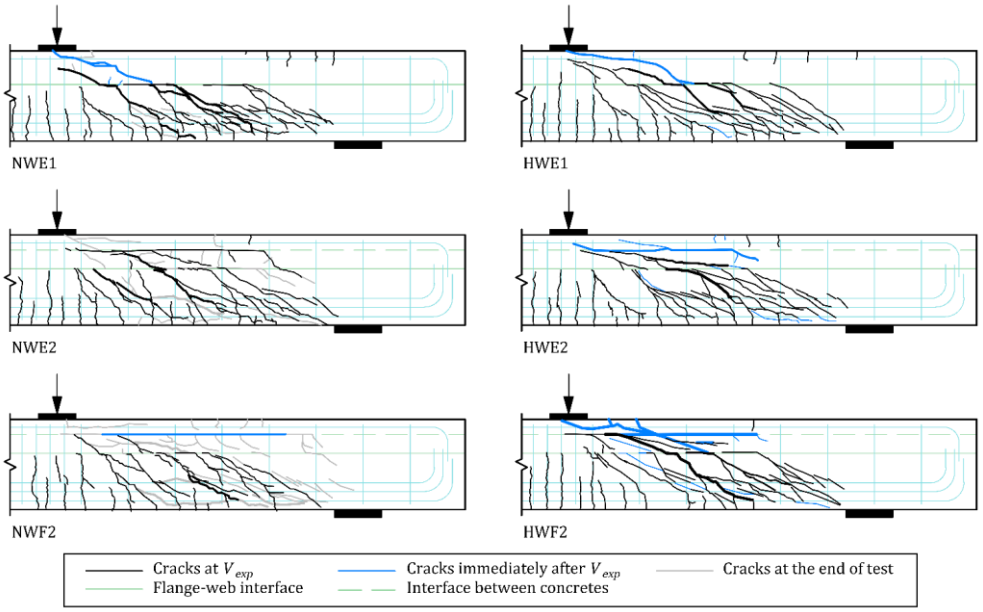

Fig. 8. Crack patterns of the test specimens in different test stages.

All the specimens showed similar crack patterns in the first load stages. Vertical bending cracks appeared for low load levels. With increasing load, the bending cracks located below the point loads vertically developed, while the bending cracks located at the shear span changed their trajectory in the direction of the point load, which is frequently observed in shear tests [33,34], and formed diagonal shear cracks. These diagonal cracks had a similar inclination for all the specimens, which was also similar to that observed in the monolithic T-shaped specimens with the cross-section type C1 of [24] (see Fig. 2b).

When the diagonal cracks of the principal span reached the plane in which section width changes (flange-web intersection), they deviated along that plane before penetrating the beam flange in the direction of the point load. This crack pattern has often been described in T-beams in the literature [34–39]. It was observed in all the specimens of this test programme because their lower part was a T-beam.

In the monolithic specimens (NWE1 and HWE1 in Fig. 8), the crack pattern upon the maximum shear load showed how these diagonal cracks penetrated the beam flange. In these specimens, sudden diagonal cracks crossed the flange immediately after V_{exp} with a pronounced load drop, as observed in the shear-deflection curves in Fig. 7a. These specimens' crack pattern was similar to that of the specimens C1 of [24] (Fig. 2b).

In the composite specimens (both E2 and F2), the diagonal cracks that penetrated the beam flange after surpassing the flange-web intersection stopped diagonally developing when they reached the interface plane between concretes. The cast-in-place slab remained intact until V_{exp} because the diagonal cracks did not continue over the interface. In all the composite specimens, an interface crack developed in this plane before reaching V_{exp} or immediately afterwards. This interface crack has been observed in many composite specimens tested by the authors in previous studies [23,24]. In specimen NWE2, a crack at the interface between concretes appeared shortly before the maximum shear load was reached (Fig. 8) at a load of around 235 kN (V_{exp} was 241 kN; see Table 1), with no noticeable load drop. In specimen NWF2, this interface crack suddenly developed after reaching V_{exp}, and was accompanied by a slight load drop (see Fig. 7c). In specimens HWE2 and HWF2, an extended interface crack appeared immediately after V_{exp} with a pronounced load drop (see Fig. 7b-c).

In all the specimens, vertical cracks appeared on top of the slab (see Fig. 8), mainly in the area located over the point at which the diagonal cracks closer to the support reached the flange-web intersection.

3.3. Instrumentation results

This section presents the most relevant instrumentation results.

First of all, the measurements of the strain gauges located at the mid-length of stirrups w4 to w8 (see Fig. 5a) at V_{exp} were analysed. The strain of stirrups w4 to w7 reached the steel yield strain in tension in all the specimens, which was 2.6‰ (see Table 3). The pair of gauges located at stirrup w8 gave lower strains in tension and were 1.7‰ on average for all the tested specimens.

The average strains measured at V_{exp} by the pair of strain gauges located on the tension longitudinal reinforcement at Section C (gauges G5 and G6 in Fig. 5a) below the point load were also analysed. In the series NW specimens, gauges measured a lower average strain than the steel yield strain in tension (2.3‰ according to Table 3), which was 2.1‰ on average for the three specimens. In the series HW specimens, the tension strains measured at V_{exp} were slightly higher than the yield strain, with 2.6‰ on average for all three specimens.

Finally, the strains measured throughout tests by the strain gauges located on top of specimens (C1 to C3 at Section A and C4 to C6 at Section B, as shown in Fig. 5a) are presented in Fig. 9.

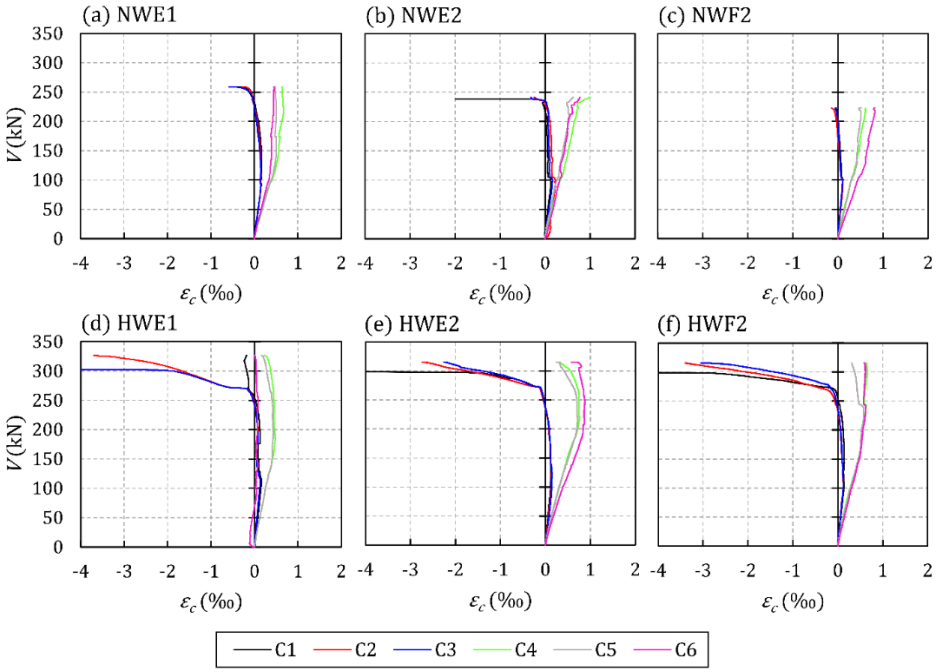

Fig. 9. Measurements of the strain gauges located on top of specimens: (a) specimen NWE1; (b) specimen NWE2; (c) specimen NWF2; (d) specimen HWE1; (e) specimen HWE2; (f) specimen HWF2 (positive ε_c for compression).

4. Failure modes

4.1. Monolithic specimens

Both monolithic specimens NWE1 and HWE1 showed similar crack patterns. Before V_{exp}, diagonal cracks reached the flange-web intersection and developed horizontally along this weakness plane before entering the flange. Immediately after V_{exp}, one diagonal crack suddenly crossed the flange towards the point load and caused specimen failure. This behaviour was similar to that observed in the monolithic T-shaped specimens with less slab depth previously tested by the authors (specimens C1 in [24]). Thus the shear strength mechanism proposed for specimens C1 according to the experimental observations was herein adapted to explain the failure mode of the specimens in this paper.

The flange-web intersection crack divided the transmission of shear into two load paths: one through the web below the flange-web intersection and one through the flange (both these load paths are represented in Fig. 10 by means of a strut-and-tie model). At the beam web, shear was transmitted by means of a multiple truss, in which vertical ties were the specimen's stirrups. At the flange a single truss was used, which represented the shear transmission at the beam head of a member without shear reinforcement. Both shear paths were connected at the flange-web intersection crack nodes, where the dowel forces of stirrups and the aggregate interlock action at the interface crack were considered to act.

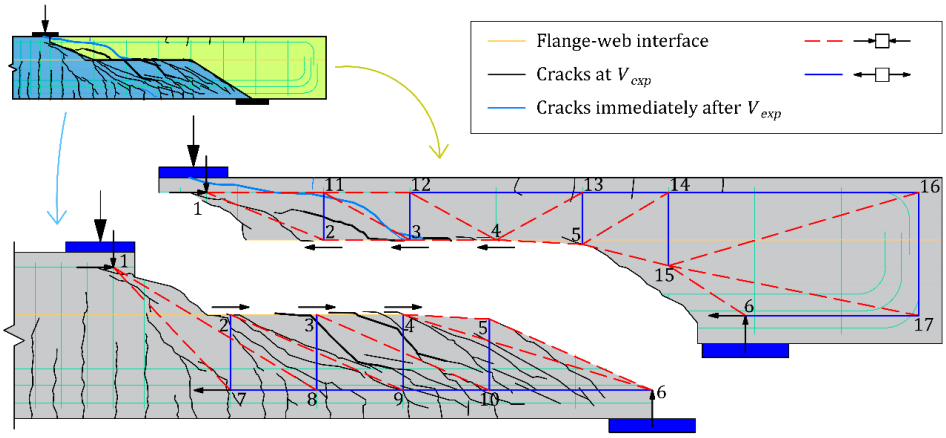

Fig. 10. Shear strength mechanism proposed for the monolithic specimens (example of specimen HWE1).

As observed in previous research works by the authors [23,24], the maximum shear load transmitted by the web shear path was considered to be limited by the yielding of stirrups and the inclination of the compression field struts at the web. Thus the shear transmitted through this path remained constant for higher loads, and the specimen's shear strength was reached upon the beam head's failure. As a diagonal crack suddenly crossed the flange immediately after V_{exp} (see Fig. 8), the beam head in the monolithic specimens was considered to fail in shear. So the failure mode of specimens E1 was identified as "flange shear failure" (SF).

The explained shear strength mechanism was supported by other experimental results in addition to the above-described crack pattern characteristics. As indicated in Section 3.3, the stirrups of the principal span (w4 to w7 in Fig. 5a) reached the steel yielding strain according to the strain gauge measurements. Furthermore, the strains measured at concrete surface in Section A (gauges C1-C3 in Fig. 9) showed a clear tendency towards tension, which is consistent with the tension tie of the flange strut-and-tie model in Fig. 10. The strain measured by the gauges located at Section B (C4-C6) slightly changed from compression towards tension about

halfway through the test. This is also consistent with the section being close to a transition area between compression and tension according to the strut-and-tie model in Fig. 10. Finally, vertical cracks on top of the flange appeared in the tension area, as observed in Fig. 8 and Fig. 10, which verified the existence of tension stresses.

4.2. Composite specimens

All the composite specimens displayed similar behaviour when analysing crack patterns. Before reaching V_{exp}, the diagonal cracks at the principal span became horizontal when they reached the flange-web intersection and entered the flange after shortly developing along the flange-web intersection. Immediately after V_{exp}, or shortly before V_{exp} with specimen NWE2, a crack developed along the interface between concretes.

Consequently, the shear strength mechanism observed in these specimens at V_{exp} was the same as that shown in Fig. 10 for the monolithic specimens. This was supported by similar instrumentation results to those observed in the monolithic specimens: principal span stirrups w4 to w7 were yielded (Fig. 5a), as indicated in Section 3.3; the same tendency of the strain gauges located on top of specimens (see Fig. 9) as observed in the monolithic specimens; similar specimens' crack patterns at V_{exp} as shown in Fig. 8, including the vertical cracks on top of the slab.

Nevertheless, failure was not given by the slab failing in shear, as observed in the monolithic specimens, but by the interface reaching its interface shear strength. Consequently, the failure mode in these four specimens was "interface failure" (IF).

As indicated with the monolithic specimens, the maximum shear transmitted through the web below the flange-web intersection was considered to be given by the yielding of stirrups' steel and compression struts' inclination. The vertical shear transmitted by the beam head was limited by the interface shear strength, which could be estimated from the strut-and-tie model of the flange in Fig. 10 by providing the horizontal component of struts 3-11 or 4-12 the interface shear strength value of the stretch between two stirrups.

Other shear strength mechanisms could develop after interface crack formation, such as the dowel action of the web reinforcement at the interface crack and the aggregate interlock at the interface crack. In specimens NWE2 and NWF2, these shear strength mechanisms could maintain a similar shear load to the load that caused IF, as seen on the smoothly descending branch of their shear-deflection curves in Fig. 7. On the contrary, a marked load drop took place for specimens HWE2 and HWF2 (Fig. 7) because these mechanisms were unable to maintain the load at which the interface crack appeared.

5. Effect of test parameters on shear strength

5.1. Presence of a cast-in-place slab on top

This section examines the contribution of the cast-in-place slab to shear strength in the T-shaped specimens. The results of three monolithic T-shaped specimens with section type C1 of [24], and with the same dimensions and characteristics as the precast T-beam of the composite specimens in this paper (see Fig. 3), were compared to specimen NWE2, which had a cast-in-place slab on top of the precast beam. As specimens C1 had less beam depth, their length and reinforcement were those that gave the same a/d, ϱ_l, ϱ_w and relative concrete cover (c/h ratio) as the specimens of this experimental programme. The specimens selected for comparison purposes (see Fig. 11) were those with similar concrete compressive strengths.

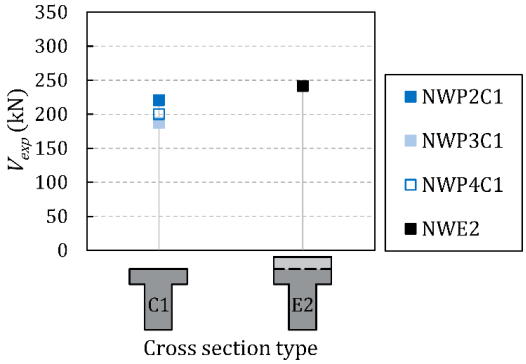

Fig. 11. Comparison between the shear strengths of the specimens with section types C1 [24] and E2 of the NW series.

The cast-in-place slab of specimen E2 increased shear strength by 19% on average *versus* specimens C1. Similarly, the effective depth of specimen E2 increased by 19% *versus* C1.

According to the shear strength mechanism explained in Section 4.2 for the composite specimens of this experimental programme (see Fig. 10), the composite specimen's shear strength depended on the shear strength of the interface between concretes. The composite specimen's cast-in-place slab contributed to shear transfer if the interface shear strength of specimen E2 sufficed to reach a higher vertical shear strength than that given by the monolithic precast beam (specimen C1) as the slab provided greater beam head depth. This contribution was limited by the interface shear failure (IF). This was the case of the specimens analysed in Fig. 11.

5.2. Presence of an interface between concretes

To study the influence of the interface between concretes on shear strength, the monolithic specimens with section type E1 (see Fig. 3) were compared to the specimens with the same characteristics, but with an interface between concretes (specimens E2). Fig. 12 shows this comparison for the specimens of series NW and HW of this test programme.

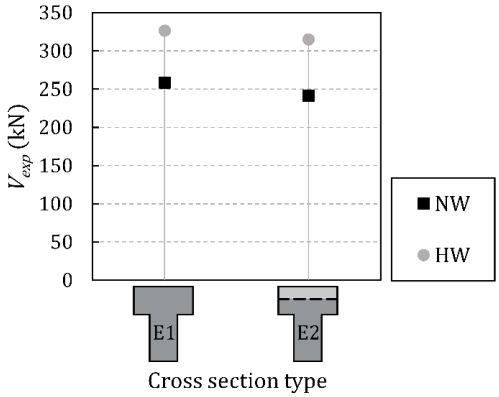

Fig. 12. Comparison between the shear strengths of the specimens with section types E1 and E2.

The interface between concretes of specimens E2 reduced shear strength by 7% and 4% for series NW and HW, respectively, compared to that of monolithic specimens E1.

The influence of the interface on composite specimens' shear strength can be explained by the shear strength mechanism introduced in Section 4. Accordingly, the interface can affect shear strength in three different ways: firstly, if the interface shear strength is very high, the composite beam (E2 in this test programme) behaves as a monolithic specimen and the specimen fails by SF; conversely, if the interface shear strength is too low, the slab cannot contribute to resist shear and the composite specimen's shear strength is that of the T-beam without the slab; finally, interface shear strength takes an intermediate value, for which the cast-in-place slab contributes to resist shear until IF.

The last situation occurred in the specimens of this experimental programme. By comparing the shear strengths of specimens C1, E1 and E2 from series NW (Fig. 11 and Fig. 12), the shear strength of specimen E2 was 7% lower than that of specimen E1, and was 19% higher than that of specimen C1.

5.3. Slab width

In Fig. 13 the shear strengths of the specimens with section types E2 and F2, which were compounded from a precast T-beam and a cast-in-place slab with two different widths (see Fig. 3), were compared to study the influence of slab width on composite specimens' shear strength.

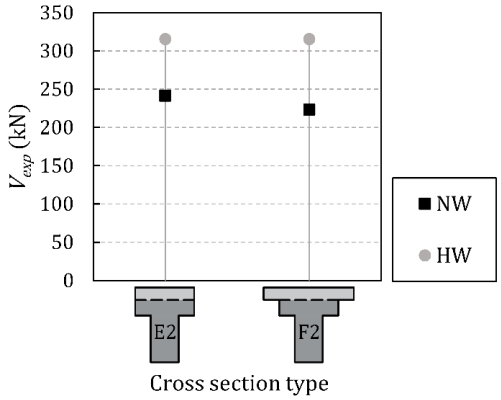

Fig. 13. Comparison between the shear strengths of the specimens with section types E2 and F2.

Fig. 13 shows that the wider slab of specimen F2 did not increase shear strength compared to specimen E2. In series NW, the shear strength of specimen F2 was 8% lower than that of specimen E2. In series HW, the wider slab made no difference because the shear strengths of both specimens were the same.

The slight difference in the shear strength of the specimens from series NW could be explained by the position of the neutral axis: in specimen NWF2 with a wider slab, the neutral axis was located higher than in specimen NWE2. Thus for the same shear force, the tangential stress at the interface between concretes was greater in specimen NWF2, so IF occurred with a lower load value. However, this difference in series HW went unnoticed.

Despite the observed results, no general conclusion about the contribution of slab width to shear strength in this specimen type can be drawn. More experimental research should be carried out on composite beams with different dimensions and characteristics to those herein studied.

5.4. Beam and slab concretes' compressive strengths

In this section, the specimens of series NW, with NSC at the precast beam and the slab, are compared to the specimens of series HW, with HSC at the precast beam, to analyse the influence on shear strength of using a better-quality concrete on the precast beam that is commoner in precast concrete plants.

As observed in Fig. 12 and Fig. 13, all the series HW specimens had higher shear strengths than their homologous series NW specimens. Shear strengths were 26%, 31% and 41% higher for specimens E1, E2 and F2, respectively.

In monolithic specimens E1, this increase in the shear strength of series HW could be given by: (i) the higher shear strength of the web below the flange-web intersection as better-quality concrete allowed a lower angle of the compression struts at the web (higher $cot\theta$); (ii) the existence of HSC at the flange, which increased the strength of the flange failing in shear (SF), as shown in [23] and [24].

In the composite specimens, in which the slab concrete had a lower compressive strength than the beam concrete, the shear strength increase of specimens HW could be due to: (i) the higher shear strength of the beam web given by the higher $cot\theta$; (ii) the presence of HSC in part of the composite beam head, which could make the location of the neutral axis higher and, therefore, lower the tangential stresses at the interface and postpone IF, i.e., the IF, which was the failure mode of the composite specimens of this experimental programme, occurred at a higher load than in the specimens made with NSC at both the precast beam and slab.

6. Comparing the test results to existing code provisions

The shear strengths of the test specimens predicted by current codes' shear formulations are analysed in this section. Three shear design procedures for beams with shear reinforcements were considered: formulation of EC2 [19]; the Level III Approximation of MC-10 [21]; the formula (b) of Table 22.5.5.1 of ACI 318-19 [20].

It should be noted that these three formulations neglect flanges' shear strength and, as explained in Section 1, they state that the shear strength of the entire composite specimen can only be considered if the interface is designed to resist the loads that will be transferred across it. Therefore, three shear strength values were calculated in this paper for composite specimens: that which produces IF ($V_{pred,if}$); the shear resistance of the precast beam alone ($V_{pred,pb}$); the shear resistance of the entire composite specimen as if it were a monolithic beam ($V_{pred,mb}$). The predicted shear strength V_{pred} was taken as $V_{pred,mb}$ if the shear force that produced IF $V_{pred,if}$ was higher. If not, V_{pred} was taken as $V_{pred,if}$ if it was higher than the shear strength of the precast beam alone $V_{pred,pb}$, or as $V_{pred,pb}$ if not. Thus $V_{pred} = \min\{V_{pred,mb}; \max\{V_{pred,pb}; V_{pred,if}\}\}$. To calculate $V_{pred,if}$, the interface shear strength was obtained from the formulation of the corresponding code for "smooth" or "as-cast" surfaces with interface reinforcement. $V_{pred,mb}$ was calculated by using the beam concrete compressive strength ($f_{c,b}$) in the EC2 formulation to obtain the maximum $cot\theta$, limited by the crushing of the compression struts at the beam web. In the MC-10 and ACI 318-19 formulations, the weighted average of the compressive strengths of the beam and slab concretes estimated from the area ratio ($f_{c,wa}$) was used. $f_{c,wa}$ has

been considered in previous research works [7,22–24,27,40]. It derived from the interpretation of Section 22.5.4 of ACI 318-19 for shear in composite concrete members, and proved to give accurate results and on the safety side when assessing composite elements. The results are presented in Table 4.

Table 4. The V_{exp}/V_{pred} ratios for the test specimens assessed with current codes' formulations.

Code formulation	NWE1	HWE1	NWE2	HWE2	NWF2	HWF2	Mean	CV (%)
EC2 [19]	1.33	1.68	1.55	2.03	1.44	2.03	1.68	16.17
MC-10 LIII [21]	1.41	1.52	1.63	1.82	1.50	1.82	1.62	9.73
ACI 318-19 (b) [20]	1.53	1.47	1.72	1.69	1.59	1.69	1.61	5.79

The tested average values of the material properties were used for all the formulations. The partial safety factors for concrete and steel material properties were taken as 1.0.

The results presented in Table 4 show that the current codes' formulations underestimated the shear strength of the monolithic and composite T-shaped specimens of this test programme, possible for two reasons: neglecting flanges' shear strength in the T-beams and underestimating the interface shear strength in the composite specimens as these specimens' predicted shear strength was always that of the precast T-beam alone ($V_{pred,pb}$).

According to Table 4, EC2 gave the best approximation for the specimens made of NSC (series NW) of the three considered codes. However for the specimens made of HSC, EC2 offered a much more conservative shear strength estimation than the other two codes because the EC2 shear formulation does not depend on concrete compressive strength for the specimens of this experimental programme. On the contrary, the MC-10 and ACI 318-19 formulations, which depend on concrete compressive strength, had similar V_{exp}/V_{pred} ratios of specimens HW to those of specimens NW with the same cross-sectional shape.

Table 4 shows the mean value and the CV of V_{exp}/V_{pred} for the six specimens of this test programme. The three considered formulations obtained a similar mean value. However, the CV of EC2 was very high (16.17%) compared to that of MC-10 (9.73%) and ACI 318-19 (5.79%). This indicates that ACI 318-19 better considered the influence of beam concrete compressive strength on the shear strength of the specimens of this test programme. Nevertheless, the high V_{exp}/V_{pred} mean values obtained with these three shear strength formulations revealed that they did not well capture the influence of the existence of both flanges and a cast-in-place slab. Thus to improve the current design shear formulations' accuracy, the effect of flanges should be considered and interface shear strength should be better estimated.

7. Summary and Conclusions

This paper presents the results of six reinforced concrete T-shaped specimens subjected to shear forces, which were experimentally tested to study the cast-in-place slab contribution to shear strength in concrete composite beams. By comparing different cross-section types and concrete qualities, the following points that influence shear strength were studied: the existence of a cast-in-place slab; the presence of an interface between concretes; cast-in-place slab width; the compressive strength of the beam and slab concretes. The observed shear strength mechanisms were analysed. Finally, the experimental shear strength was compared to that predicted by current design codes. The main findings of this study are:

1. In the monolithic T-beams, the cross-section width change is a weakness plane that deviates the diagonal shear cracks along it and divides the shear transmission into two load paths: one through the beam web below the cross-section width change and one through the beam head or flange. Failure occurs when the upper path, that at the flange, reaches its shear strength.
2. In the T-beams with a cast-in-place slab on top (composite beams), the interface between the T-beam and slab may crack at failure. Thus failure occurs when the interface shear stress exceeds the interface shear strength.
3. The composite specimen's shear strength takes an intermediate value between the shear strengths of the T-shaped specimen with no cast-in-place slab and the monolithic T-shaped specimen with the same depth as the composite specimen. The higher or lower strength is given by the interface shear strength.
4. For the specimens of this test programme, a wider cast-in-place slab does not increase specimens' shear strengths. The decrease observed in specimens NW can be explained by the rise in the neutral axis, which increases interface shear stresses and leads to premature interface failure.
5. The use of HSC on the precast beam in composite specimens increases shear strength by allowing a greater inclination of the compression struts at the beam web and postponing IF by reducing interface shear stresses because the neutral axis is higher.
6. The shear formulations for beams with web reinforcements of EC2, MC-10 Level III and ACI 318-19 formula (b) predict very conservative shear strengths for the specimens tested in this experimental programme because the shear strength of flanges is neglected and interface shear strength is underestimated. ACI 318-19 offers the most accurate results with a low CV, so this formulation best captures the effect of concrete compressive strength on shear strength.

The present paper provides experimental results about the contribution of the cast-in-place slab to shear strength in concrete composite beams, and analyses the shear strength mechanisms that these specimens develop. It sheds light on future shear formulation development for composite concrete elements. However, further research should be conducted in specimens with different dimensions and with prestressed reinforcement to better understand the shear behaviour of these structural elements, which are so common in current constructions.

Acknowledgements

Ministerio de Ciencia e Innovación (MCIN) and *Agencia Estatal de Investigación* (AEI) supported the present research work through grants BIA2015-64672-C4-4-R and RTI2018-099091-B-C21-AR, both funded by MCIN/AEI/ 10.13039/501100011033 and by "ERDF A way of making Europe". Author Lisbel Rueda-García was supported by grant BES-2016-078010 funded by MCIN/AEI/ 10.13039/501100011033 and by "ESF Investing in your future". The project was also carried out with the support of the Regional Government of Valencia through Project AICO/2018/250. This research work was undertaken at the Concrete Science and Technology University Institute (ICITECH) of the Universitat Politècnica de València (UPV; Spain) with concrete supplied by Caplansa.

References

[1] Comité technique 4.3 - Ponts routiers Technical Committee 4.3 - Road Bridges. Estimation of load carrying capacity of bridges based on damage and deficiency. PIARC World Road Association: 2016.

[2] Mast RF. Auxiliary Reinforcement in Concrete Connections. J Struct Div ASCE 1968;94:1485–504.

[3] Birkeland PW, Birkeland HW. Connections in Precast Concrete Construction. ACI J Proc 1966;63:345–68.

[4] Mattock AH, Hawkins NM. Shear Transfer in Reinforced Concrete—Recent Research. PCI J 1972;17:55–75. https://doi.org/10.15554/pcij.03011972.55.75.

[5] Loov RE, Patnaik AK. Horizontal Shear Strength of Composite Concrete Beams With a Rough Interface. PCI J 1994;39:48–69.

[6] Kahn LF, Slapkus A. Interface Shear in High Strength Composite T-Beams. PCI J 2004;49:102–10.

[7] Kim C-G, Park H-G, Hong G-H, Kang S-M. Shear strength of composite beams with dual concrete strengths. ACI Struct J 2016;113:263–74.

[8] Soltani M, Ross BE. Database evaluation of interface shear transfer in reinforced concrete members. ACI Mater J 2017;114:383–94. https://doi.org/10.14359/51689249.

[9] Avendaño AR, Bayrak O. Shear strength and behaviour of prestressed concrete beams. Technical Report: IAC-88-5DD1A003-3, Texas Department of Transportation: 2008.

[10] Nagle TJ, Kuchma DA. Nontraditional Limitations on the Shear Capacity of Prestressed Concrete Girders. University of Illinois at Urbana-Champaign: 2007.

[11] Hamilton III HR, Llanos G, Ross BE. Shear performance of existing prestressed concrete bridge girders. 2009.

[12] Runzell B, Shield C, French C. Shear Capacity of Prestressed Concrete Beams. 2007.

[13] Tawfiq K. Cracking and Shear Capacity of High Strength Concrete Girders. 1996.

[14] Ross BE, Hamilton HR, Consolazio GR. Experimental study of end region detailing and shear behavior of concrete i-girders. J Bridg Eng 2015;20. https://doi.org/10.1061/(ASCE)BE.1943-5592.0000676.

[15] Ross BE, Ansley MH, Hamilton III HR. Load testing of 30-year-old AASHTO Type III highway bridge girders. PCI J 2011;56.

[16] Ruiz MF, Muttoni A. Shear strength of thin-webbed post tensioned beams. ACI Struct J 2009;106.

[17] Raymond KK, Bruce RN, Roller JJ. Shear Behavior of HPC Bulb-Tee Girders. Seventh Int Symp Util High-Strength / High-Performance 2005;3:705–22.

[18] Shahawy MA, Batchelor B deV. Shear Behavior of Full-Scale Prestressed Concrete Girders: Comparison Between AASHTO Specifications and LRFD Code. PCI J 1996;41:48–62. https://doi.org/10.15554/pcij.05011996.48.62.

[19] CEN. EN 1992-1-1:2004. Eurocode 2: Design of concrete structures - Part 1-1: General rules and rules for buildings. 2004.

[20] ACI Committee 318. Building code requirements for structural concrete (ACI 318-19); and commentary (ACI 318R-19). Farmington Hills: American

Concrete Institute; 2019.

[21] Fédération International du Béton (fib). Model Code 2010. Ernst & Sohn; 2012.

[22] Rueda-García L, Bonet Senach JL, Miguel Sosa PF, Fernández Prada MÁ. Experimental analysis of the shear strength of composite concrete beams without web reinforcement. Eng Struct 2021;229:111664. https://doi.org/10.1016/j.engstruct.2020.111664.

[23] Rueda-García L, Bonet Senach JL, Miguel Sosa PF, Fernández Prada MÁ. Analysis of the shear strength mechanism of slender precast concrete beams with cast-in-place slab and web reinforcement. Eng Struct 2021;246:113043. https://doi.org/10.1016/j.engstruct.2021.113043.

[24] Rueda-García L, Bonet Senach JL, Miguel Sosa PF, Fernández Prada MÁ. Experimental study on the shear strength of reinforced concrete composite T-shaped beams with web reinforcement. Eng Struct 2022;255:113921. https://doi.org/10.1016/j.engstruct.2022.113921.

[25] Kani MW, Mark W. Huggins, Rudi R. Wittkopp. Kani on shear in reinforced concrete. Toronto: University of Toronto, Dept. of Civil Engineering; 1979.

[26] Fernández Ruiz M, Muttoni A, Sagaseta J. Shear strength of concrete members without transverse reinforcement: A mechanical approach to consistently account for size and strain effects. Eng Struct 2015;99:360–72. https://doi.org/10.1016/j.engstruct.2015.05.007.

[27] Rueda-García L, Bonet Senach JL, Miguel Sosa PF. Experimental study of concrete composite beams subjected to shear. Proc. fib Symp. 2019 Concr. - Innov. Mater. Des. Struct., 2019, p. 1779–86.

[28] UNE-EN 12390-3:2020. Testing hardened concrete - Part 3: Compressive strength of test specimens. 2020.

[29] UNE-EN 12390-6:2010. Testing hardened concrete - Part 6: Tensile splitting strength of test specimens. 2010.

[30] UNE-EN 12390-13:2014. Testing hardened concrete - Part 13: Determination of secant modulus of elasticity in compression. 2014.

[31] Comisión Permanente del Hormigón. EHE-2008. Instrucción de Hormigón Estructural. Ministerio de Fomento. Madrid: 2008.

[32] UNE-EN ISO 6892-1:2017. Metallic materials - Tensile testing - Part 1: Method of test at room temperature. 2017.

[33] Halicka A, Jabłoński Ł. Shear failure mechanism of composite concrete T-

shaped beams. Proc Inst Civ Eng Struct Build 2016;169:67–75.

[34] Palaskas MN, Attiogbe EK, Darwin D. Shear strength of lightly reinforced T-beams. J Am Concr Inst 1981;78:447–55.

[35] Placas A. Shear failure of reinforced concrete beams. Faculty of Engineering of the University of London. Imperial College of Science and Technology, 1969.

[36] Pansuk W, Sato Y. Shear mechanism of reinforced concrete T-Beams with stirrups. J Adv Concr Technol 2007;5. https://doi.org/10.3151/jact.5.395.

[37] Giaccio C, Al-Mahaidi R, Taplin G. Experimental study on the effect of flange geometry on the shear strength of reinforced concrete T-beams subjected to concentrated loads. Can J Civ Eng 2002;29. https://doi.org/10.1139/l02-099.

[38] Ayensa A, Oller E, Beltrán B, Ibarz E, Marí A, Gracia L. Influence of the flanges width and thickness on the shear strength of reinforced concrete beams with T-shaped cross section. Eng Struct 2019;188:506–18. https://doi.org/10.1016/j.engstruct.2019.03.057.

[39] Leonhardt F, Walther R. Schubversuche an einfeldrigen Stahlbetonbalken mit und ohne Schubbewehrung zur Ermittlung der Schubtragfähigkeit und der oberen Schubspannungsgrenze. Heft 151. Berlin: Ernst & Sohn; 1962.

[40] Kim C-G, Park H-G, Hong G-H, Kang S-M, Lee H. Shear Strength of Concrete Composite Beams with Shear Reinforcements. ACI Struct J 2017;114:827–37.

Chapter 5. Mechanical model for the shear strength prediction of composite beams with web reinforcement

During the analysis of the experimental tests, a strut-and-tie model for explaining the shear strength mechanism of the test specimens was developed. The model presents limitations for its general use, since the formulae are exclusive for the strut-and-tie models proposed for the thesis specimens. Consequently, the necessity of developing a generalized and simplified model based on the original model to design concrete composite elements was found.

In this chapter, a lower-bound plasticity-based model to predict the shear strength of concrete composite beams and monolithic T-shaped beams, based on the original model, is described by means of a journal article, in which a database of experimental tests is also created to verify the proposed model and compare it to the predictions of the current codes' formulations.

The scope of application of the proposed mechanical model covers concrete composite specimens with rectangular cross-section and composite T-shaped specimens consisting of a rectangular precast beam and top cast-in-place slab, as well as monolithic T-beams.

8th PAPER

Details:

Type of paper	Journal article
Title	*Shear strength prediction of slender reinforced concrete composite beams and monolithic T- and I-shaped beams with web reinforcement*
Authors	Lisbel Rueda García José Luis Bonet Senach Pedro Francisco Miguel Sosa Miguel Ángel Fernández Prada
Status	Ready for submission to a scientific journal
Full reference	Rueda-García L, Bonet Senach JL, Miguel Sosa PF, Fernández Prada MÁ. Shear strength prediction of slender reinforced concrete composite beams and monolithic T- and I-shaped beams with web reinforcement. 2022.

Shear strength prediction of slender reinforced concrete composite beams and monolithic T- and I-shaped beams with web reinforcement

Lisbel Rueda García, lisruega@cam.upv.es

José Luis Bonet Senach, jlbonet@cst.upv.es

Pedro Fco. Miguel Sosa, pmiguel@cst.upv.es

Miguel Ángel Fernández Prada, mafernan@cst.upv.es

Universitat Politècnica de València, Camí de Vera s/n, 46022, Valencia, Spain

Abstract

The use of precast concrete elements with a cast-in-place concrete slab on top or concrete composite elements for buildings is on the increase. Although they are used worldwide, certain aspects of their structural calculation still generate doubts in daily engineering practice, such as obtaining the composite elements' shear strength. The contribution of the slab to shear strength and the characteristics of which concrete (precast beam or slab concrete) should be considered are not clear.

Based on a mechanical model, proposed by the authors in a previous publication for the assessment of the shear behaviour of tested concrete composite specimens, afterwards extended to monolithic and composite T-shaped specimens, this paper proposes a simplified general model for predicting the shear strength of these elements which relates the shear strength of the element with the interface shear strength.

A database of 105 experimental results of composite rectangular and T-shaped beams and monolithic T- and I-shaped beams available in the literature was created to experimentally verify the proposed model. The model provides a mean value of the experimental/ predicted shear strength of 1.18, with a coefficient of variation of 16%, which are better results than the ones given by the shear strength formulations of the current codes EC2, MC-10 and ACI 318-19.

Keywords: precast construction, reinforced concrete, composite beam, T-shaped beam, shear strength, predictive model, shear database.

Highlights

A simplified model is proposed for predicting the shear strength of composite beams

The proposed model predicts the shear strength of monolithic T- and I-shaped beams

A database is created of composite rectangular and T-shaped beams failing in shear

The proposed model fits well with the experimental results in the database

The proposed model gives better results than the current shear codes formulations

Nomenclature

a	shear span
A_{sl}	area of the cross-section of the slab longitudinal reinforcement
A_{sw}	area of the cross-section of the two legs of a stirrup
b_{eff}	slab's effective shear width
b_w	web width of the concrete section
$cot\theta$	cotangent of θ
$cot\theta_{int}$	cotangent of θ given by the interface shear strength
$cot\theta_{str}$	cotangent of θ given by the crushing of the compression struts
d	effective depth
d'	slab longitudinal reinforcement depth
d_b	precast beam's effective depth
d_c	entire composite beam's effective depth
f_c	concrete's compressive strength
$f_{c,b}$	beam concrete compressive strength measured in cylinders
$f_{c,s}$	slab concrete compressive strength measured in cylinders
$f_{c,wa}$	weighted average of beam and slab concrete compressive strengths measured in cylinders estimated from the area ratio
f_{ct}	concrete tensile strength
$f_{ct,s}$	slab concrete tensile strength
$F_{H,i}$	horizontal force transferred at node i located on the interface crack
f_{yl}	yield strength of slab longitudinal reinforcement
f_{yw}	yield strength of transverse reinforcement
h	overall beam height

h_s	cast-in-place slab height
l	length of interface crack
l_{nc}	length of the uncracked interface of principal span at maximum shear load
N_s	axial force on slab
R_H	total horizontal force transferred along interface crack
R_{nc}	total horizontal force at the uncracked interface of the principal span at maximum shear load
s	stirrup spacing
T_l	tension force of slab longitudinal reinforcement at its yield strength
T_w	tension force of web reinforcement at its yield strength
V_{exp}	experimental shear strength
V_{pb}	precast beam shear strength
V_{pred}	specimen's predicted shear strength value
$V_{s,BF}$	slab shear strength provided by slab bending failure
$V_{s,IF}$	slab shear strength provided by interface failure
$V_{s,SF}$	slab shear strength provided by slab shear failure
α	multiplier factor of interface shear strength
θ	inclination of compression field struts with respect to the axis of the member
ρ_i	reinforcement ratio of the reinforcing steel crossing the interface
ρ_w	reinforcement ratio of web reinforcement
σ_1, σ_2	principal stresses
σ_x	normal longitudinal stress
τ	tangential stress
τ_R	interface shear strength

1. Introduction

Construction with precast concrete elements is now a booming market due to factors such as the speed of the construction process and significant cost savings [1].

Unlike in-situ construction, structural integrity plays an important role in precast construction. To ensure the joint operation of the elements, a layer of cast-in-place concrete is poured over them to create concrete composite elements. Given the intensive use of this construction method [1–3] it is especially important to study its structural behaviour to be able to create more economical designs and accurately assess the strength of the existing structures.

The interface shear strength of concrete composite elements consisting of a precast beam and a cast-in-place slab has been experimentally analysed in multiple publications [4–8]. However, their shear strength calculation has not been studied in depth [9,10] so that there is no indication of the shear strength calculation of composite elements with a clear criterion on whether or not the slab should be considered in the element's shear strength. Neither has the concrete strength been specified that should be used in the calculations (precast beam and/or slab concrete strength).

Some current design codes, like MC-10 [11], do not clarify how to account for the slab in calculating the strength of composite elements. EC2 Section 10.9.3 [12] mentions the possibility of designing elements with a cast-in-place slab of at least 40 mm as composite elements, as long as the shear at the interface is verified. Only ACI 318-19 [13] gives clear instructions on the shear strength calculation of composite beams, as long as the interface shear strength is met: using the properties of the element (precast beam or cast-in-place slab) that give the most critical shear strength value or the properties of the individual elements. However, relevant experimental and theoretical evidence is still needed to support the validity of the ACI 318-19 considerations since the design equation was developed on the basis of the experimental results from monolithic beams [1,9].

The authors recently carried out an experimental programme, which was presented in [14] and [15], on composite concrete beams with rectangular and T-shaped cross-sections. The specimens had web reinforcement and "smooth" or "as cast" interface roughness (as defined in the current codes [11–13]), and were subjected to vertical shear loads. The interface between concretes of the composite T-shaped specimens was at the height of the cross-section width change (see Fig. 1d). In these tests, the existence of an interface between the concretes was seen to modify the crack pattern, since the diagonal shear cracks deviated horizontally along the interface when they reached it (see Fig. 1b and d). Consequently, the shear strength mechanism developed in the specimens was different from the one usually studied in shear (see the monolithic specimen in Fig. 1a). This different behaviour was also observed in monolithic T-shaped beams [15] (Fig. 1c), since the cross-section width change is a weakness plane that also diverted the diagonal cracks along it, as seen in other publications [16–19].

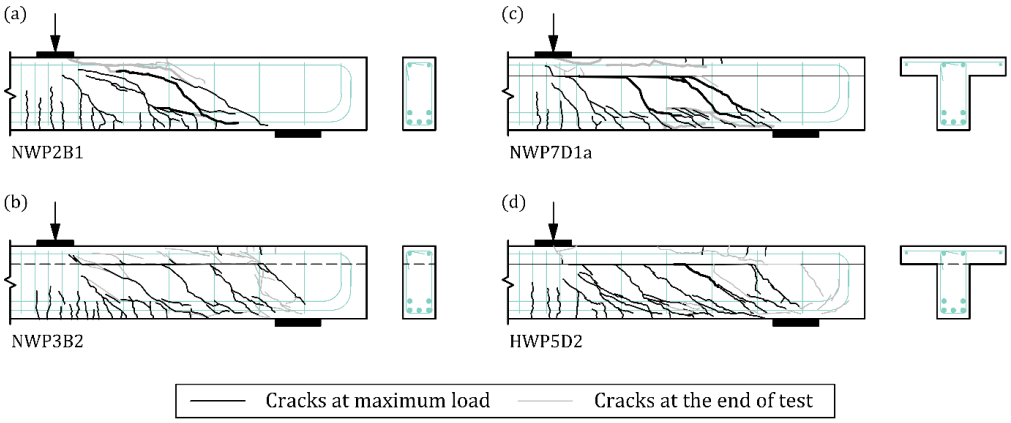

Fig. 1. Crack patterns in beams with different cross-sections: (a) monolithic rectangular beam; (b) composite rectangular beam; (c) monolithic T-shaped beam; (d) composite T-shaped beam. Adapted from [14,15].

Given that the shear strength mechanism can differ widely from that developed in a monolithic rectangular specimen with web reinforcement, the code's shear formulations may not be applicable to composite beams when this type of crack develops. Consequently, more experimental studies on beams of this type would be necessary either to check the validity of the existing shear formulations, to adapt them to composite elements if necessary, or to create new shear models for the design and assessment of composite elements.

Based on the experimental observations, the authors proposed a mechanical model for the shear assessment of the composite rectangular specimens tested in [14]. This evaluation model was extended to the composite and monolithic T-shaped specimens described in [15] to understand the results obtained regarding the different variables considered (flange width, compressive strength of precast beams and slabs concrete, and existence of an interface between the concretes).

The aim of this study is to create a generic formulation derived from the mechanical model proposed in [14] and [15], to predict the shear strength of composite elements with rectangular and T-shaped cross-sections and shear reinforcement, also applicable to monolithic elements with T-shaped cross-sections. For this, a simplified formulation is created based on the proposed mechanical model that is verified by the specimens in the authors' own experimental programme, as well as in other authors' studies with rectangular, T- and I-shaped cross-sections. A total of 28 of our own specimens and 77 specimens obtained from the literature are used to compile a database for the analysis. The results obtained are compared with those given by the current design codes' shear formulations.

This paper contributes to the formulation of a shear strength model for concrete composite elements by developing a simplified procedure based on a mechanical model derived from experimental observations and verifying this procedure by an experimental database. It also contributes to the calculation of the shear strength of monolithic T-shaped specimens by means of a formulation that accounts for the flanges' contribution to shear strength and to verifying the current codes' shear design provisions.

2. Brief description of the original model

The model proposed in [14], which was adapted for T-shaped beams in [15], is a shear mechanical model based on a strut-and-tie model, which explains the resistant behaviour found in the experimental tests carried out by the authors. The model is based on the cracking along the interface between concretes or along the plane in which the section width changes in T-shaped specimens. The model is thus applied to composite beams with rectangular and T-shaped cross-sections and to monolithic T-shaped beams, since they all underwent this horizontal cracking.

The model represents the division of the shear transmitted from the load to the support into two load paths: one through the beam web (or precast beam) and one through the beam head (or slab). As shown in Fig. 2, the shear transfer mechanism through the precast beam is represented by means of a multiple truss, while the shear transfer mechanism of the beam head is considered as that of a member without shear reinforcement and represented by means of a single truss. Both shear transfer mechanisms are connected through the nodes located at the interface crack. At the interface crack, the dowel action of transverse reinforcement and the aggregate interlock are considered to act. These are represented by the horizontal forces at the interface nodes (see forces $F_{H,i}$ in Fig. 2). Three variants of the strut and tie model were identified in the experimental tests according to the length of the interface crack at maximum load (Fig. 2). The crack pattern of the specimen must be known to calculate a specimen's shear strength with this model to be able to choose the model variant that best fits the crack pattern and the calculation is carried out with the formulae for that variant. Since the variant must be previously known, the application of the model as a predictive method is limited.

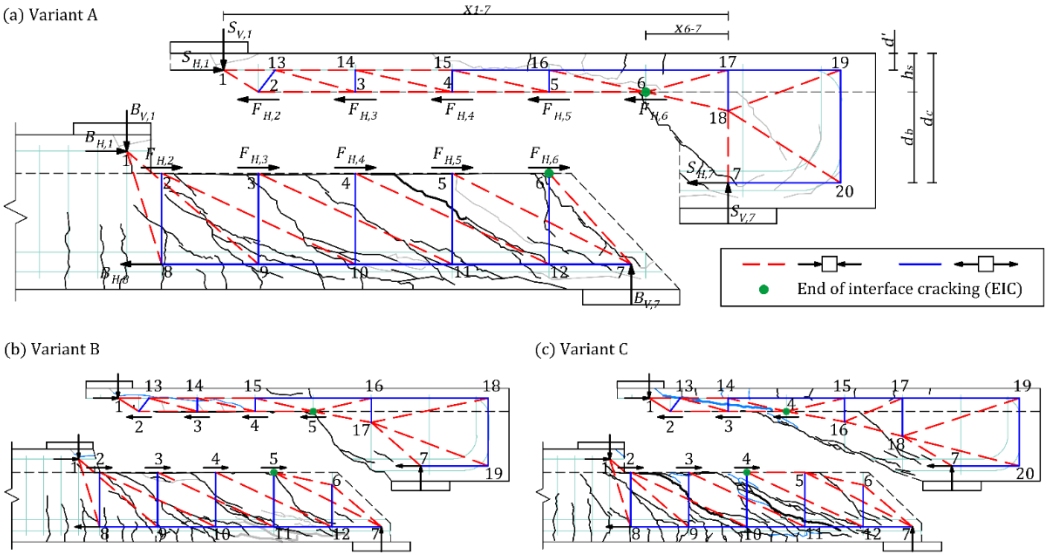

Fig. 2. Variants of the proposed strut-and-tie model in [14] for the different observed lengths of the interface crack: (a) Variant A; (b) Variant B; (c) Variant C.

The ultimate load is the sum of the shear resisted by the precast beam and the shear resisted by the slab. The precast beam reaches its maximum strength when the stirrup steel yields, i.e., when the tension force of the vertical ties that represent the stirrups in the precast beam (T_w) reaches the stirrups' yielding strength. The shear strength of the precast beam (V_{pb}) is thus calculated from the strut-and-tie model in Fig. 2 as shown in Eq. (1) in Table 1.

The horizontal forces at the nodes *i* of the interface crack ($F_{H,i}$ in Fig. 2) are obtained from the strut-and-tie model as indicated in Eq. (2) of Table 1, for each Variant of the strut-and-tie model.

The model assumes that the yielding strength of the stirrups is reached prior to slab failure and is considered to remain constant for increasing loads until the slab failure. The specimens' shear strength is thus reached when the slab fails. Three different failure modes were identified depending on the length of the interface crack: slab bending failure (BF), slab shear failure (SF) or interface failure (IF). As indicated in Table 1, the shear strengths given by the failure modes BF and SF are calculated for all the specimens, with the formulation of the model variant that they show (A, B or C). The failure mode IF is also calculated in Variant-C specimens. The slab shear strength is the minimum strength obtained from the three failure modes.

Table 1. Summary of the formulation of the original model.

Variable	Variant of the model	Formula	
Precast beam shear strength (V_{pb})	All	$V_{pb} = 2T_w$	(1)
Horizontal forces at the interface ($F_{H,i}$)	A	$F_{H,i} = T_w \cdot \cot\theta_i$, for i = 2, 3, 4, 5, 6	(2a)
	B	$F_{H,i} = T_w \cdot \cot\theta_i$, for i = 2, 3, 4 $F_{H,5} = \frac{T_w(x_{5-7}+x_{6-7})}{d_b}$	(2b)
	C	$F_{H,i} = T_w \cdot \cot\theta_i$, for i = 2, 3 $F_{H,4} = \frac{T_w(x_{4-7}+x_{5-7})}{d_b}$	(2c)
Slab bending failure ($V_{s,BF}$)	All	$V_{s,BF} = \frac{(\sum_{i=2}^{K} F_{H,i})\cdot(h_s-d')\cdot d_b + T_l\cdot(h_s-d')\cdot(d_c-d')}{x_{1-7}\cdot d_b - x_{K-7}\cdot(d_c-d')}$	(3)
Slab shear failure ($V_{s,SF}$)	All	$N_s = F_{H,K} + \frac{V_{s,SF}\cdot x_{1-7} - (h_s-d')\cdot\sum_{i=2}^{K} F_{H,i}}{d_c-d'}$	(4)
		$\sigma_x = -\frac{N_s}{b_{eff}\cdot h_s}$	(5)
		$\sigma_1 = \frac{\sigma_x}{2} + \sqrt{\left(\frac{\sigma_x}{2}\right)^2 + \tau^2} \le f_{ct,s}$	(6)
		$\sigma_2 = \frac{\sigma_x}{2} - \sqrt{\left(\frac{\sigma_x}{2}\right)^2 + \tau^2} \ge -f_{c,s}$	(7)
		$\sigma_1 = \lvert f_{ct,s}\rvert + 0.8\frac{\lvert f_{ct,s}\rvert}{\lvert f_{c,s}\rvert}\sigma_2$; where τ is solved by substituting (6) and (7) in (8)	(8)
		$V_{s,SF} = 2/3 \cdot \tau \cdot b_{eff} \cdot h_s$	(9)
Interface failure ($V_{s,IF}$)	C	$R_{nc} = \tau_R \cdot b_w \cdot l_{nc}$	(10)
		$V_{s,IF} = \frac{F_{i,nc}\cdot(d_c-d') + \sum_{i=2}^{4} F_{H,i}\cdot(h_s-d')}{x_{1-7}}$	(11)

Notation:
T_w is calculated as $T_w = A_{sw} \cdot f_{yw}$.
Forces $F_{H,i}$ are considered positive in the direction indicated in Fig. 2.
θ_i is the angle between the strut that converges at node i and the axis of the member.
x_{j-k} is the horizontal distance between nodes j and k in Fig. 2.
T_l is calculated as $T_l = A_{sl} \cdot f_{yl}$.
K is the identifier of the node located at the end of interface cracking (EIC in Fig. 2): 6 in Variant A, 5 in Variant B, 4 in Variant C.
The other variables are defined at the Nomenclature and in Fig. 2.

2.1. Slab bending failure (BF)

Slab bending failure occurs when the slab longitudinal reinforcement yields in tension. Vertical cracks were observed on the upper slab surface over the EIC (Fig. 2). The shear force resisted by the slab when it fails in bending ($V_{s,BF}$) is calculated

from the strut-and-tie model, considering that the tie at the end of the slab cantilever (tie 16-17, 15-16 or 14-15, in Variant A, B and C, respectively (Fig. 2)) has a tension force equal to the yield stress of the slab longitudinal reinforcement (T_l). The longitudinal reinforcement in the flanges in T-shaped beams is considered in this calculation, as long as it is inside the effective flange width defined in Section 5.3.2.1 of EC2 [12]. $V_{s,BF}$ is calculated from Eq. (3).

2.2. Slab shear failure (SF)

When the slab fails in shear, a sudden diagonal crack crosses the slab right after the maximum shear load. The model considers the slab to be subjected to a biaxial state of stresses and the failure occurs when the principal concrete stresses reach Kupfer's failure surface [20]. To obtain the slab shear strength ($V_{s,SF}$), first the axial force N_s existing in the slab cross-section on the left of the slab's right end (Fig. 2) must be calculated as a function of $V_{s,SF}$ (Eq. (4)). This axial force is transformed into an axial stress acting in the area of the slab defined by its depth h_s and the slab's effective shear width b_{eff} (Eq. (5)). The b_{eff} considered in this model for T-shaped specimens is equal to the sum of the web width and the flange depth [15], based on previous research [2,21] and experimental results. The principal tensile (σ_1) and compression (σ_2) stresses produced by the normal stress σ_x and a tangential stress τ are calculated from Eq. (6) and (7), which are replaced in the relationship between the principal stresses of the Kupfer failure surface (Eq. (8)). Once known τ, $V_{s,SF}$ can be calculated from Eq. (9).

2.3. Interface failure (IF)

In some composite T-shaped specimens in [15] the interface crack extended towards the support after reaching the maximum shear load. The previous crack pattern was that of Variant C in Fig. 2. In these specimens the failure mode was identified as interface failure. The shear strength resisted by the slab in case of interface failure ($V_{s,IF}$) is obtained from the Variant C strut-and-tie model, once the interface shear strength (τ_R) and the length of the uncracked interface (l_{nc}) are known. τ_R was experimentally obtained in [15] for the specimens in the test programme; l_{nc} is considered in Variant C as the distance between Node 4 in Fig. 2c and the end of the beam (see Eq. (10) and (11) in Table 1).

3. Simplified model proposed to predict the shear strength of concrete composite beams and monolithic T-shaped beams

The original model described in Section 2 has certain limitations. First, the model variant (A, B or C in Fig. 2) must be known, since the formulae to calculate the shear components resisted by the precast beam and the slab depend on it and the crack

pattern of the specimen at the maximum shear load must be known to determine the variant of the model. Second, the model is not generically applicable, since the formulae are exclusively for the strut-and-tie models proposed for the authors' specimens.

A generalized and simplified model based on the original model is therefore proposed here to predict the shear strength of concrete composite beams and monolithic T-shaped beams in which prior knowledge of the specimen's crack pattern is no longer needed.

3.1. Precast beam shear strength

To make the model independent of the strut-and-tie model geometry, a formulation is proposed that depends on an inclination angle θ of the compression field struts, fixed for the entire precast beam, as in design code formulations such as EC2 [12] and MC-10 [11]. The shear strength of the precast beam in composite specimens, or the web below the section width change in monolithic specimens (see Fig. 3) is calculated as:

$$V_{pb} = \frac{T_w \cdot d_b \cdot \cot\theta}{s} \tag{12}$$

where T_w is the tension force of web reinforcement when it reaches its yield strength, calculated as the area of the cross-section of the two legs of a stirrup (A_{sw}) multiplied by the yield strength of transverse reinforcement (f_{yw}); d_b is the precast beam's effective depth; s is the stirrup spacing.

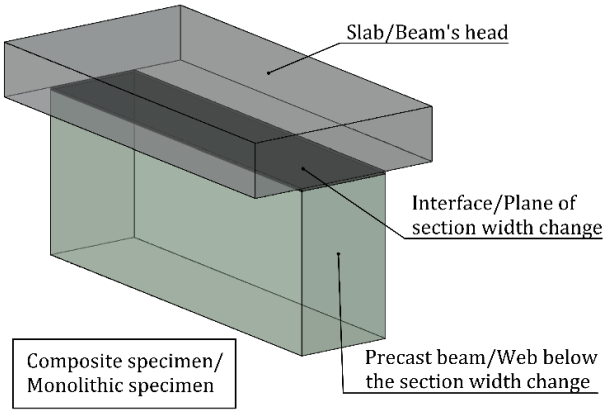

Fig. 3. Parts of a composite or monolithic T-shaped specimen.

The $\cot\theta$ may be limited by crushing of the compression struts, in which case it is calculated with the formulation of EC2 [12]:

$$1.0 \leq \cot\theta_{str} = \sqrt{\frac{\upsilon \cdot f_{c,b}}{\rho_w \cdot f_{yw}} - 1} \leq 2.5 \tag{13}$$

where $f_{c,b}$ is the beam's concrete compressive strength, ρ_w is the shear reinforcement ratio and ν is a strength reduction factor for concrete cracked in shear, defined as:

$$\rho_w = \frac{A_{sw}}{b_w \cdot s} \tag{14}$$

$$\upsilon = 0.6\left[1 - \frac{f_{c,b}}{250}\right] \tag{15}$$

where b_w is the beam web width.

In the experimental study carried out by the authors [14] the existence of an interface clearly modified the cracking pattern. As can be seen in Fig. 1a-b, the diagonal cracks in the monolithic specimen were more horizontal than in the composite specimen, so that the $cot\theta$ may also be limited by the interface shear strength (τ_R), in which case it is calculated as in Eq. (16) and limited to a value of 1, since the minimum V_{pb} is given by the minimum shear strength resisted by the precast beam itself.

$$\cot\theta_{int} = \frac{\tau_R \cdot b_w \cdot s}{T_w} \geq 1 \tag{16}$$

The interface shear strength may be calculated by means of the interface shear formulation given in EC2 [12] for stirrups inclined 90º with respect to the interface and considering the normal force across the interface acting simultaneously with the shear force as negligible, by staying on the safety side.

$$\tau_R = c \cdot f_{ct} + \rho_i \cdot f_{yw} \cdot \mu \leq 0.5 \cdot \nu \cdot f_c \tag{17}$$

where c and μ are factors which depend on the interface roughness and are defined in EC2 [12]. ρ_i is the interface reinforcement ratio calculated as the area of reinforcement crossing the interface divided by the interface area. The tensile strength of concrete f_{ct} is calculated from the experimental f_c using the formulae in EC2 [12]: $f_{ct} = 0.30 \cdot f_c^{2/3}$ if $f_c \leq 50$ MPa and $f_{ct} = 2.12 \cdot \ln(1+f_c/10)$ if $f_c > 50$ MPa. The considered concrete compressive strength f_c is the minimum of the beam and slab concrete compressive strengths.

The $cot\theta$ considered in Eq. (12) is the minimum value of the one given by the crushing of the compression struts ($cot\theta_{str}$) and the one given by the interface shear strength ($cot\theta_{int}$).

3.2. Slab shear strength

3.2.1. Slab bending failure

The shear force resisted by the slab on yielding of the slab longitudinal reinforcement is calculated as in Variant A of the original model (Eq. (3)), since it gives the lowest strength of the three variants. The distances $x_{1\text{-}7}$ and $x_{6\text{-}7}$ are approximated by the length of the shear span (a) and the stirrup spacing (s), respectively:

$$V_{s,BF} = \frac{R_H \cdot (h_s - d') \cdot d_b + T_l \cdot (h_s - d') \cdot (d_c - d')}{a \cdot d_b - s \cdot (d_c - d')} \tag{18}$$

where T_l is the tension force of the slab longitudinal reinforcement when it reaches its yield strength, calculated as the area of the cross-section of the slab longitudinal reinforcement (A_{sl}) located inside the effective flange width defined in Section 5.3.2.1 of EC2 [12] multiplied by the yield strength of slab longitudinal reinforcement (f_{yl}); h_s is the slab depth; d' is the slab longitudinal reinforcement depth; d_c is the entire composite beam's effective depth; and R_H is the total horizontal force transmitted along the interface crack, calculated as indicated in Eq. (19).

$$R_H = V_{pb} \cdot \frac{l}{d_b} \tag{19}$$

where l is the length of the interface crack, which may be approximated as the difference between a and s.

There also exists a possibility of a lack of slab longitudinal reinforcement in the specimens, in which case the slab shear strength calculated by bending failure is obtained from the concrete cracking moment at the slab end (Node 6 in Fig. 2a), i.e. considering that the slab's most highly tensioned fibre at that cross-section reaches the tensile strength of the slab concrete ($f_{ct,s}$), which is calculated from the experimental $f_{c,s}$ using the formula of EC2 [12]. The resulting equation is:

$$V_{s,BF} = \frac{R_H \cdot (h_s - d') \cdot \left(d_c - \frac{h_s}{3}\right) + \frac{f_{ct,s}}{6} \cdot b_{eff} \cdot h_s^2 \cdot (d_c - d')}{a \cdot \left(d_c - \frac{h_s}{3}\right) - s \cdot (d_c - d')} \tag{20}$$

where b_{eff} is the slab effective width, which is taken as the effective flange width defined in Section 5.3.2.1 of EC2 [12].

In the specimens with slab longitudinal reinforcement, $V_{s,BF}$ will be the highest of that obtained from the yielding of the slab longitudinal reinforcement through Eq. (18) and the one obtained from the concrete cracking in bending through Eq. (20).

3.2.2. Slab shear failure

Calculating the slab shear strength at its shear failure is similar to that in Section 2.2. Eq. (4) depends on the model variant considered, i.e. on the length of the interface crack, by means of force $F_{H,K}$. However, in the simplified model, N_s is always calculated at the end of the slab, which is considered to be at a distance l of the applied load. This provides the lowest axial force on the slab, which gives a lower $V_{s,SF}$ value, staying on the side of safety. N_s is obtained from:

$$N_s = \frac{V_{s,SF} \cdot a - R_H \cdot (h_s - d')}{d_c - d'} \tag{21}$$

where R_H is obtained from Eq. (19).

The rest of the formulation is the same as the one described in Section 2.2 (Eqs. (5-9) in Table 1). In Eq. (5), the slab effective width b_{eff} is taken as the effective shear width of the slab, not greater than the effective flange width defined in Section 5.3.2.1 of EC2 [12]. In rectangular specimens, the effective shear width is the entire width of the specimen ($b_{eff} = b_w$); while in T-shaped specimens, the effective shear width considered in this model is equal to the sum of the web width and the flange depth ($b_{eff} = b_w + h_s$), which corresponds to a shear-effective area of the slab that increases 45º from the cross-section width change (see Fig. 4), as considered in the experimental study of T-shaped specimens carried out by the authors [15], based on previous research [2,21] and the experimental results.

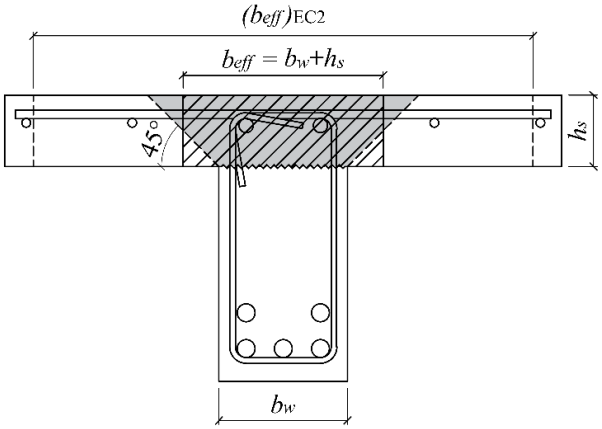

Fig. 4. Effective slab shear width considered in the slab shear failure of the proposed simplified model for T-shaped specimens.

3.3. Predicted shear strength

The model's predicted shear strength (V_{pred}) is obtained in different ways according to the specimen's cross-sectional shape.

In composite rectangular specimens, if the inclination of the compression stress field ($cot\theta$) is limited by the interface shear strength ($cot\theta_{int}$ in Eq. (16)), which means interface cracking is likely, V_{pred} will be the sum of the shear resisted by the precast beam (V_{pb}) and the minimum of the shear forces resisted by the slab failing in bending ($V_{s,BF}$) and the slab failing in shear ($V_{s,SF}$). On the other hand, if $cot\theta$ is not limited by the interface shear strength but by the crushing of the compression struts ($cot\theta_{str}$ in Eq. (13)), the interface is considered to not modify the specimen's shear behaviour, thus the specimen behaves as a monolithic beam. In this case, the proposed model, which is based on the deviation of diagonal cracks along the interface, is not applicable. V_{pred} is thus calculated with the shear formulation in EC2 [12] for beams with web reinforcement, using the beam's concrete compressive strength ($f_{c,b}$) in calculating $cot\theta$ (see Eq. (13)), since that equation accounts for the beam web stresses.

In monolithic and composite T-shaped specimens, if the interface shear strength limits $cot\theta$, the shear strength of the specimen is calculated as that of a specimen with extended interface cracking, in which case V_{pred} is obtained as $V_{pb}+\min(V_{s,BF}, V_{s,SF})$. If the inclination of the compression stress field is not limited by the interface shear strength, the shear strength of the slab is considered to be given by its shear failure, thus V_{pred} is calculated as $V_{pb}+V_{s,SF}$.

4. Summary of the proposed simplified model

The shear strength of composite rectangular and T- and I-shaped specimens, and monolithic T- and I-shaped specimens, is calculated with the proposed model as indicated in Table 2.

Table 2. Guidelines for the application of the proposed simplified model.

Requirement	Composite rectangular specimens	Monolithic and composite T- and I-shaped specimens
$cot\theta_{str}$ (Eq. (13)) < $cot\theta_{int}$ (Eq. (16))	$V_{pred} = V_{pred}$ (EC2 [12]) using $f_{c,b}$	$V_{pred} = V_{pb}$ (Eq. (12)) + $V_{s,SF}$ (Eqs. (21), (5-9))
$cot\theta_{str}$ (Eq. (13)) ≥ $cot\theta_{int}$ (Eq. (16))	▪ If $A_{sl} > 0$, $V_{pred} = V_{pb}$ (Eq. (12)) + min{$V_{s,SF}$ (Eqs. (21), (5-9)), max{$V_{s,BF}$ (Eq. (18); $V_{s,BF}$ (Eq. (20))}} ▪ If $A_{sl} = 0$, $V_{pred} = V_{pb}$ (Eq. (12)) + min{$V_{s,SF}$ (Eqs. (21), (5-9)), $V_{s,BF}$ (Eq. (20))}	

5. Strengths of the proposed simplified model

Some strengths of the simplified proposed model should be highlighted:

- The proposed model is generalized to specimens of different dimensions from those of the specimens tested by the authors in [14] and [15], thanks to the introduction of $cot\theta$ and the generalization of the formulae of the original model (presented in [14,15] and summarised in Section 2) so that they do not depend on the geometry of the strut-and-tie model but on the geometry and reinforcement of the specimen.
- The proposed model related the shear strength of the specimen to the interface shear strength, which was a pending aspect of the original model. This is especially important since many studies point out the influence of the interface between concretes in the vertical shear strength of composite elements if it is not strong enough to avoid deviating diagonal cracks along it [10,14,15,22,23].
- The original model (Section 2) requires identifying the variant of the strut-and-tie model adopted by each specimen (Fig. 2), which helps to understand the mechanical behaviour of the element, but fails to predict the shear strength. The simplified model can predict the ultimate shear load and the failure mode by relating vertical shear strength to interface shear, distinguishing between slab bending failure, slab shear failure or common monolithic beam shear failure (this last case when rectangular composite beam shear strength is not limited by interface shear strength).
- The three possible slab failure modes in the original model (BF, SF and IF) are reduced to two in the simplified model (BF and SF), due to the introduction of the interface shear strength. In the experimental programme on T-shaped beams carried out by the authors [15], in which interface failure (IF) was detected in beams with high interface shear strength, the shear strength $V_{s,IF}$ gave very similar results to the shear strength $V_{s,SF}$ obtained from Variant C of the strut-and-tie model (Fig. 2c). In the simplified model the slab shear strength of the specimens with a high interface shear strength is obtained from the formulation of $V_{s,SF}$, which gives a similar value to that obtained by IF. Also, the non-cracked interface length, required to obtain $V_{s,IF}$, is no longer needed.
- In T-shaped monolithic specimens, the model considers a possible cracking of the plane in which section width changes due to the transmission of a high horizontal force along a narrow interface plane.

Interface shear strength is an important aspect of the proposed model. There are multiple proposals in the literature for modifying the current codes interface shear formulations [24]. However, the current codes remain conservative since interface

shear depends on many different variables [25] and give interface shear strengths that err too much on the side of safety. The accuracy of the proposed model may be improved in the future with a more precise interface shear formulation.

6. Experimental verification

6.1. Description of database

Experimental data is gathered in this paper to verify the proposed simplified model. The following references of experimental campaigns on beams subjected to shear forces are considered: 24 composite rectangular specimens from Rueda-García *et al.* [14], Halicka [22] and Kim *et al.* [1]; 28 composite T-shaped specimens compound of a rectangular precast beam with a cast-in-place slab on top from Rueda-García *et al.* [15], Halicka and Jabłoński [3] and Jabłoński and Halicka [23]; 37 T-shaped and 16 I-shaped monolithic specimens from Rueda-García *et al.* [15], Kani *et al.* [26] and the ACI-DAfStb Evaluation Database for shear tests on slender reinforced concrete beams with stirrups [27]. The following selection criteria are used: the beams are made of reinforced concrete, have web reinforcement, are subjected to point loads, have enough tension longitudinal reinforcement to avoid bending failure and fail in shear. The number of specimens from each author, and the variation ranges of the a/d ratio, the tension longitudinal reinforcement ratio (ρ_l) and the transverse reinforcement ratio (ρ_w) are shown in Table 3.

In general, the selected shear slenderness ratios (a/d) are over 2.50 to avoid direct load transfer from the point load to the support and ensure a shear failure mainly governed by beam shear-transfer actions [28], since these mechanisms can be explained by the truss model. Nonetheless, a lower a/d ratio is accepted in the composite specimens in [3] and [23], considering that, an interface crack appears if the interface shear limits the precast beam shear strength, so that the a/d ratio increases, since the precast beam d decreases. If interface shear does not limit precast beam shear strength the model result is on the side of safety since the added strength given by the arch effect is not considered in the model. In the specimens described in [3] and [23] interface shear strength limits precast beam shear strength in all cases, so that the a/d ratio increases from 1.89 to 2.59.

The composite specimens considered in this study are those that failed in vertical shear and not in interface shear, the latter being more common in the literature, as mentioned in Section 1.

Table 3. Summary of the evaluation database and main results of the proposed model.

Specimen type	Author	No. of specimens	a/d	ϱ_l (%)	ϱ_w (%)	Mean	CV (%)
Composite rectangular specimens	Rueda-García *et al.* [14]	9	4.01	4.08	0.22	1.18	7.33
	Halicka [22]	9	2.84	2.26	0.42	1.17	9.29
	Kim *et al.* [1]	6	2.50-4.00	1.75-2.87	0.12-0.32	1.43	6.83
Composite T-shaped specimens	Rueda-García *et al.* [15]	10	4.01	4.08	0.22	1.17	9.43
	Halicka & Jabłoński [3]	3	1.89	2.08	0.42	1.63	3.35
	Jabłoński & Halicka [23]	15	1.89	2.08	0.42	1.37	14.75
Monolithic T- and I-shaped specimens	Rueda-García *et al.* [15]	9	4.01	4.08	0.22	0.99	7.62
	Kani *et al.* [26]	3	5.00	1.80	0.17-0.23	1.02	3.70
	Kautsch [27]	2	2.68	2.87	0.32-0.43	1.04	2.08
	Hamadi & Regan [27]	2	3.46	2.99	0.38-0.52	1.00	0.47
	Leonhardt *et al.* 1962a [27]	3	3.50	2.79-8.38	0.34-1.03	1.05	6.61
	Leonhardt *et al.* 1962b [27]	1	3.03	10.30	2.83	0.91	-
	Leonhardt *et al.* 1963 [27]	6	3.33	4.52	0.31-1.25	1.16	4.42
	Levi & Marro [27]	7	4.04	8.02-12.53	0.84-1.26	1.08	9.38
	Lyngberg [27]	2	2.78	3.88	0.52	1.16	0.47
	Moayer & Regan [27]	1	3.50	1.90	0.22	0.93	-
	Özden [27]	3	3.52	3.83	0.61	0.97	5.88
	Petersson [27]	1	3.24	3.02	0.84	0.87	-
	Regan [27]	8	3.50-7.10	4.16	0.40-0.82	1.15	11.78
	Reineck [27]	2	4.27	5.42-6.79	1.21-1.62	1.16	0.44
	Soerensen [27]	1	3.52	3.83	0.34	1.11	-
	Strobandn [27]	2	2.56	5.06-8.30	0.68-1.52	1.14	1.28

The monolithic specimens from Kani *et al.* [26] are those with a regular stirrup distribution that failed in shear. The specimens selected from the ACI-DAfStb Evaluation Database [27] are the T- and I-shaped specimens from the small dataset (A2+A3) in [27], in which the stirrups stresses are known and are equal or close to the steel yield strength.

The concrete compressive strengths used in the database specimens are between 20 and 60 MPa in 95% of the specimens. The compressive strength of the others is either close to 60 MPa or well above it in case of the two specimens from Strobandn [27] (88 MPa).

95% of the T-shaped specimens have an h_s/h ratio between 0.12 and 0.25. Only the three specimens in Kani *et al.* [26] (0.34) and one in Regan [27] (0.47) have a higher ratio.

6.2. Assumptions for the application of the proposed model

Many studies on the shear strength of concrete interfaces have pointed out that the interface shear formulations in the current design codes provide very safe strength values [1,5,6,8,9,29,30]. From the application of the proposed model to the specimens in the database, it is found necessary to increase the interface shear strength given by the EC2 formulation (Eq. (17)), so a parameter α is defined that multiplies the interface shear strength obtained from Eq. (17).

To estimate this multiplier α, the 286 results of interface shear-transfer experiments obtained from a database by Soltani and Ross [30], in which no additional permanent net compressive force normal to the shear plane was applied, are assessed with the EC2 formulation for interface shear (Eq. (17)). A total of 38 specimens with a "smooth" interface, 184 with a "rough" interface and 64 specimens casted monolithically are used.

The factors c and μ used in Eq. (17), which depend on interface roughness, are shown in Table 4. Those used for "smooth" and "rough" interfaces are defined in EC2 [12]. For monolithically placed concrete, the considered values of c and μ come from the keyed interface in the formula proposed in [31], derived from Randl's studies [25]. These are used to assess the interface shear strength of the section width change plane of monolithic T- and I-shaped specimens, (see Fig. 3), since the failure of this plane is also considered by means of Eq. (16) in the proposed model.

Table 4. Values of the factors c and μ in Eq. (17) and multiplier α considered in the application of the proposed model.

Interface roughness	c	μ	α
"Smooth" or "as cast"	0.2	0.6	1.9
"Rough" and "very rough"	0.4	0.7	1.3
Concrete placed monolithically	1.0	0.9	1.1

The ratio between the experimental and predicted interface shear strength is calculated for the 286 specimens. The multiplier α for each roughness is obtained from the average of this ratio for all the specimens with the same interface roughness. The results are shown in Table 4. The values of these α factors for "smooth" and "rough" interfaces match those obtained in a previous study by the authors [29] in which the interface shear strengths of 4 composite specimens of the same characteristics as those tested in [14] and [15] with "smooth" and "very rough" interfaces were experimentally measured by means of sets of 3 strain gauges at different beam heights in multiple cross-sections along the shear span and compared to the values predicted in the current codes. Smooth interface experimental value was on average 2.0 times higher than the predicted strength and was 1.3 times higher in very rough specimens.

The consideration of α generally agrees with the cracking patterns observed in the specimens in the dataset, although this multiplier α must be understood as a solution given in this paper not universally used since further research should be conducted to adjust the interface shear formulations, as explained in Section 5.

6.3. Results

The model gives a mean value of the V_{exp}/V_{pred} ratio of 1.18 and coefficient of variation (CV) of 16.18% for the 105 specimens in the database. The mean value of the subset of composite rectangular beams is 1.24 and the CV is 12.00%. For composite T-shaped specimens, the mean value is 1.32 and the CV is 16.17%. For the monolithic T- and I-shaped specimens the model gives a mean value of 1.07 with a CV of 10.46%. The mean value and CV of each author's set of specimens are shown in Table 3.

The mean values of the V_{exp}/V_{pred} ratio of each author's set of specimens are in general close to 1.00. The coefficients of variation obtained are frequently given in the literature on shear models [27,32–35], since the model is applied to experimental beam shear failure programmes in which the results are usually highly scattered. The highest mean values (for the specimens of Kim *et al.* [1] and Halicka and Jabłoński [3]) show a low coefficient of variation, which shows that the model adequately captures the specimens' resistance mechanism. For the 15 specimens in Jabłoński and Halicka [23], the authors tested 5 subsets of 3 specimens each with different interface characteristics in which the model gives similar results within each subset but different between the different subsets, so that the model shows a high CV in Table 3.

In general, the model predicts the failure mode of the composite specimens in the database well, except for some composite specimens in Rueda-García *et al.* [14,15] and Kim *et al.* [1], in which interface shear strength is underestimated. In these specimens the model predicts BF failure (slab bending failure) when the failure mode in the specimens was SF (slab shear failure) or common monolithic beam shear failure. This is due to the experimental scattering of the interface shear strength between the interfaces of the same roughness, for which the model offers a safe result.

The model predicts SF failure in most cases of monolithic T- and I-shaped specimens, commonly found in these specimens. However, it predicts possible interface cracking in a few specimens in the database, for which the minimum value of shear strength given by SF and BF is taken to stay on the safe side.

Given the accurate results and the characteristics of the database explained in Section 6.1, it can be stated that the proposed formulation has been verified for composite rectangular and T-shaped specimens and monolithic T- and I-shaped specimens

made of reinforced concrete with web reinforcement, with concrete compressive strengths up to 60 MPa, h_s/h ratios below 0.30, in which the stirrups steel yields or is close to yielding. Its application to specimens with higher values is questionable and further research should be conducted for its use.

7. Comparison with existing code formulations

The proposed simplified formulation is compared with the predictions of three shear design procedures for members with web reinforcement in the current codes, applied to the 105 specimens in the database: EC2 [12], the Level III Approximation of MC-10 [11] and the formulation (b) in Section 22.5.5.1 of ACI 318-19 [13].

As explained in the Introduction, both EC2 and ACI 318-19 allow considering the slab strength in composite specimens, as long as the interface is designed for the loads transferred across the interface. In this paper, the vertical shear force provided by the interface shear strength of the specimens is thus first calculated from the interface shear formulation of the corresponding code and then compared to the shear strength of only the precast beam and that of the entire composite beam. The shear strength of the specimen is the one given by the entire composite depth when not limited by interface shear. On the other hand, if the shear strength given by the interface shear is higher than that of only the precast beam the specimen shear strength is the one given by the interface shear, otherwise it is the one that considers only the precast beam. These considerations are used with the three codes considered [11–13].

The precast beam shear strength is calculated with all the codes by using precast beam depth (d_b) and compressive strength of the beam concrete ($f_{c,b}$). The shear strength of the entire composite specimen is obtained from the entire composite beam depth (d_c) and $f_{c,b}$ when using the EC2 formulation, since Eq. (13), in which the compressive strength of concrete is needed, accounts for the beam web stresses. When using ACI 318-19 equation, the shear strength of the entire composite specimen is obtained with d_c and the weighted average of the concrete strengths of both the beam and slab estimated from the area ratio ($f_{c,wa}$). The use of $f_{c,wa}$ comes from the interpretation of ACI 318-19, which allows calculating the shear strength by using the properties of the individual elements (precast beam and slab), i.e. the sum of their respective shear strengths, as in previous studies [1,9,36] with good results. Finally, d_c and $f_{c,wa}$ are also used for the MC-10 formulation, since the code does not mention how shear strength of composite specimens should be assessed, but previous studies by Kim *et al.* [9] and the authors [14,36] proved that $f_{c,wa}$ gave accurate and safe results when assessing composite elements.

Table 5 gives the mean value and coefficient of variation of the relation between the experimental and predicted shear strengths (V_{exp}/V_{pred}) for each code considered and

the proposed model. The results are given for each type of specimens and for all specimens. In all the formulations the tested average values of the materials are used and the partial safety factors for concrete and steel material properties are taken as 1.0.

Table 5. Statistical indicators of the V_{exp}/V_{pred} ratio for the specimens of the database with different shear formulations.

Specimen type	No. of specimens	Proposed model		EC2		MC-10 LIII		ACI 318-19 (b)	
		Mean	CV (%)	Mean	CV (%)	Mean	CV (%)	Mean	CV (%)
Composite rectangular	24	1.24	12.00	1.35	28.62	1.65	25.82	1.34	15.61
Composite T-shaped	28	1.32	16.17	1.75	17.68	1.85	18.97	1.86	20.47
Monolithic T- and I-shaped	53	1.07	10.46	1.27	19.68	1.43	17.09	1.46	15.85
All	105	1.18	16.18	1.42	25.74	1.59	23.19	1.54	22.08

As can be seen in Table 5, the proposed model gives the best mean values for all the specimen types, with a lower coefficient of variation than the three codes' formulations.

The scatter plots of the model and the three considered formulations of the current codes for the 105 specimens of the database are shown in Fig. 5.

For the monolithic T- and I-shaped specimens in the database the proposed model gives the most accurate result of all the formulations considered (see Table 5 and Fig. 5). This increased safety of the codes' formulations may be due to the fact that the codes do not account for the contribution of the flanges to shear strength, specifically stated in MC-10 [11].

For the composite rectangular specimens, the codes give a much safer result than the one given by the proposed model. In most of the specimens in the present database, the shear strength values predicted by the codes are those of the shear strengths obtained when considered as precast beams, since the interface shear is considerably underestimated.

The mean values of V_{exp}/V_{pred} of composite T-shaped specimens for the current codes in Table 5 clearly increase, since the interface strength is underestimated and flanges shear strength is not considered. The proposed model's prediction is similar to that of composite rectangular specimens.

Finally, by comparing the shear strength predictions of the proposed model for composite rectangular and T-shaped beams and monolithic specimens (Table 5), it can be seen that an interface between concretes increases the uncertainty, although

its existence is considered in the model, since the mean value and CV of composite specimens are higher than the good results for monolithic T-shaped specimens. A more in-depth study of interface shear would thus improve the proposed model's accuracy.

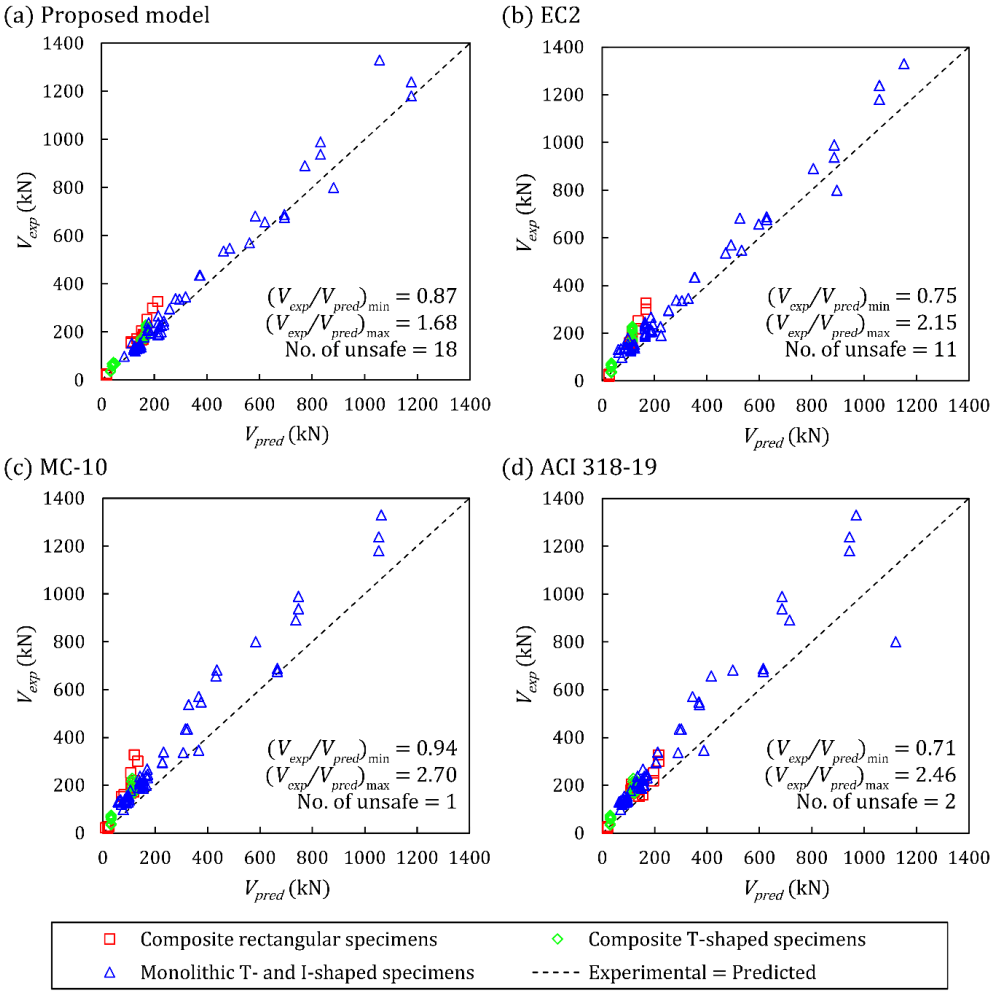

Fig. 5. Correlation between the predicted and the experimental value for the specimens of the database with different formulations: (a) Proposed model; (b) EC2; (c) MC-10 LIII; (d) ACI 318-19 (b).

8. Summary and Conclusions

The aim of this study is to provide a simplified formulation for predicting the shear strength of composite concrete beams with rectangular and T-shaped cross-sections and web reinforcement, also applicable to monolithic T-shaped beams. For this, the model proposed by the authors in previous publications [14,15] to analyse the shear strength mechanisms of experimental tests is simplified and generalized for application as a predictive model. The proposed simplified model is experimentally verified on a database of experimental studies in the literature and the results are compared to those obtained with the shear design provisions in the current codes. The study's relevant points and conclusions are as follows:

1. The interface in composite beams and the plane in which section width changes in T-shaped beams is a weakness plane that limits the shear strength of the element. The proposed simplified model for predicting the shear strength of these elements includes the interface shear strength of the weakness plane in its formulation, which is a novel element with respect to the original model.
2. The model's concept is based on the cracking of the weakness plane, so that the shear strength of the beam is given by the sum of the shear strengths of the two transmission paths in which the interface crack divides the shear load: the shear strength of the precast beam or the web below the section width change, and the shear strength of the slab or the beam head.
3. The model takes into account the interface shear strength or the maximum concrete stress in the compression field to determine the shear strength of the precast beam. The maximum shear load is given by the slab failure. The model can distinguish different types of slab failure. When interface shear limits the shear strength of the precast beam, interface cracking is likely, so that the slab strength is given by the minimum of the shear forces resisted by the slab failing in bending and the slab failing in shear. Otherwise, the slab is considered to fail in shear in T-shaped beams or the specimen is treated as a monolithic specimen in composite rectangular beams.
4. 105 slender reinforced concrete specimens subjected to point loads and failing in shear with web reinforcement are included in the experimental database in this paper: 24 composite rectangular specimens, 28 composite T-shaped specimens consisting of a rectangular precast beam with a cast-in-place slab on top and 53 monolithic T- and I-shaped specimens.
5. The proposed model gives good results for the mean value and coefficient of variation (CV) of the relationship between the experimental and the predicted shear strengths for the 3 specimen types analysed: a mean value of 1.24 and a CV of 12.00% for composite rectangular beams, 1.32 and 16.17% for

composite T-shaped beams, and 1.07 and 10.46% for monolithic T- and I-shaped beams.

6. Three shear formulations from the current design codes (EC2, MC-10 and ACI 318-19) are compared with the model results. The proposed model gives better results in all cases. The codes underestimate the interface shear strength and do not account for the flanges' contribution to shear strength, both important factors.

The proposed model lays the foundations for a simplified, easy-to-use formulation for shear design and assessment of composite concrete elements. However, it has certain limitations, basically given by the definition of the characteristics of the interface between concretes and the calculation of its shear strength, for which further studies are needed.

Acknowledgements

This research work was possible thanks to the support of the *Ministerio de Ciencia e Innovación* (MCIN) and the *Agencia Estatal de Investigación* (AEI) through Grants BIA2015-64672-C4-4-R and RTI2018-099091-B-C21-AR, both funded by MCIN/AEI/ 10.13039/501100011033 and by the "ERDF A way of making Europe". Author Lisbel Rueda-García was supported through Grant BES-2016-078010 funded by MCIN/AEI/ 10.13039/501100011033 and by the "ESF Investing in your future". The project was also supported by the Regional Government of Valencia through Project AICO/2018/250 and was undertaken at the Concrete Science and Technology University Institute (ICITECH) of the Universitat Politècnica de València (UPV; Spain).

References

[1] Kim C-G, Park H-G, Hong G-H, Kang S-M, Lee H. Shear Strength of Concrete Composite Beams with Shear Reinforcements. ACI Struct J 2017;114:827–37.

[2] Ribas González CR, Fernández Ruiz M. Influence of flanges on the shear-carrying capacity of reinforced concrete beams without web reinforcement. Struct Concr 2017. https://doi.org/10.1002/suco.201600172.

[3] Halicka A, Jabłoński Ł. Shear failure mechanism of composite concrete T-shaped beams. Proc Inst Civ Eng Struct Build 2016;169:67–75.

[4] Loov RE, Patnaik AK. Horizontal Shear Strength of Composite Concrete Beams With a Rough Interface. PCI J 1994;39:48–69.

[5] Kovach J, Naito C. Horizontal Shear Capacity of Composite Concrete Beams without Interface Ties. ATLSS Report No. 05-09: 2008.

[6] Fang Z, Jiang H, Liu A, Feng J, Chen Y. Horizontal Shear Behaviors of Normal Weight and Lightweight Concrete Composite T-Beams. Int J Concr Struct Mater 2018;12. https://doi.org/10.1186/s40069-018-0274-3.

[7] Jiang H, Fang Z, Liu A, Li Y, Feng J. Interface shear behavior between high-strength precast girders and lightweight cast-in-place slabs. Constr Build Mater 2016;128. https://doi.org/10.1016/j.conbuildmat.2016.10.088.

[8] Kahn LF, Slapkus A. Interface Shear in High Strength Composite T-Beams. PCI J 2004;49:102–10.

[9] Kim C-G, Park H-G, Hong G-H, Kang S-M. Shear strength of composite beams with dual concrete strengths. ACI Struct J 2016;113:263–74.

[10] Rueda-García L, Bonet Senach JL, Miguel Sosa PF, Fernández Prada MÁ. Experimental analysis of the shear strength of composite concrete beams without web reinforcement. Eng Struct 2021;229:111664. https://doi.org/10.1016/j.engstruct.2020.111664.

[11] Fédération International du Béton (fib). Model Code 2010. Ernst & Sohn; 2012.

[12] CEN. EN 1992-1-1:2004. Eurocode 2: Design of concrete structures - Part 1-1: General rules and rules for buildings. 2004.

[13] ACI Committee 318. Building code requirements for structural concrete (ACI 318-19); and commentary (ACI 318R-19). Farmington Hills: American Concrete Institute; 2019.

[14] Rueda-García L, Bonet Senach JL, Miguel Sosa PF, Fernández Prada MÁ. Analysis of the shear strength mechanism of slender precast concrete beams with cast-in-place slab and web reinforcement. Eng Struct 2021;246:113043. https://doi.org/10.1016/j.engstruct.2021.113043.

[15] Rueda-García L, Bonet Senach JL, Miguel Sosa PF, Fernández Prada MÁ. Experimental study on the shear strength of reinforced concrete composite T-shaped beams with web reinforcement. Eng Struct 2022;255:113921. https://doi.org/10.1016/j.engstruct.2022.113921.

[16] Placas A. Shear failure of reinforced concrete beams. Faculty of Engineering of the University of London. Imperial College of Science and Technology, 1969.

[17] Giaccio C, Al-Mahaidi R, Taplin G. Experimental study on the effect of flange geometry on the shear strength of reinforced concrete T-beams

subjected to concentrated loads. Can J Civ Eng 2002;29. https://doi.org/10.1139/l02-099.

[18] Leonhardt F, Walther R. Schubversuche an einfeldrigen Stahlbetonbalken mit und ohne Schubbewehrung zur Ermittlung der Schubtragfähigkeit und der oberen Schubspannungsgrenze. Heft 151. Berlin: Ernst & Sohn; 1962.

[19] Palaskas MN, Attiogbe EK, Darwin D. Shear strength of lightly reinforced T-beams. J Am Concr Inst 1981;78:447–55.

[20] Kupfer HB, Gerstle KH. Behavior of concrete under biaxial stresses. ASCE J Eng Mech Div 1973;99:853–66.

[21] Ribas C, Cladera A, Mas B. Modelo cortante-flexión para el dimensionamiento a ELU de forjados de vigueta pretensada y bovedilla. VI Congr. Int. Estructuras ACHE, Madrid, Spain: 2014, p. 151–152.

[22] Halicka A. Influence new-to-old concrete interface qualities on the behaviour of support zones of composite concrete beams. Constr Build Mater 2011:4072–8.

[23] Jabłoński Ł, Halicka A. Influence of the interface reinforcement on static performance of concrete composite T-shaped beams. Bud i Archit 2020;19:063–76. https://doi.org/10.35784/bud-arch.2170.

[24] Duarte dos Santos PM. Assessment of the Shear Strength between Concrete Layers. 2009.

[25] Randl N. Design recommendations for interface shear transfer in fib Model Code 2010. Struct Concr 2013;14:230–41. https://doi.org/10.1002/suco.201300003.

[26] Kani MW, Mark W. Huggins, Rudi R. Wittkopp. Kani on shear in reinforced concrete. Toronto: University of Toronto, Dept. of Civil Engineering; 1979.

[27] Reineck K-H, Bentz E, Fitik B, Kuchma DA, Bayrak O. ACI-DAfStb databases for shear tests on slender reinforced concrete beams with stirrups. ACI Struct J 2014;111. https://doi.org/10.14359/51686819.

[28] Fernández Ruiz M, Muttoni A, Sagaseta J. Shear strength of concrete members without transverse reinforcement: A mechanical approach to consistently account for size and strain effects. Eng Struct 2015;99:360–72. https://doi.org/10.1016/j.engstruct.2015.05.007.

[29] Rueda-García L, Bonet Senach JL, Miguel Sosa PF. Experimental study of concrete composite beams subjected to shear. Proc. fib Symp. 2019 Concr. - Innov. Mater. Des. Struct., 2019, p. 1779–86.

[30] Soltani M, Ross BE. Database evaluation of interface shear transfer in reinforced concrete members. ACI Mater J 2017;114:383–94. https://doi.org/10.14359/51689249.

[31] CEN. PT1 prEN 1992-1-1/D2 Eurocode 2: Design of concrete structures - Part 1-1: General rules, rules for buildings, bridges and civil engineering structures. 2020.

[32] Muttoni A, Fernández Ruiz M. Shear strength of members without transverse reinforcement as function of critical shear crack width. ACI Struct J 2008;105.

[33] Marí A, Cladera A, Bairán J, Oller E, Ribas C. Shear-flexural strength mechanical model for the design and assessment of reinforced concrete beams subjected to point or distributed loads. Front Struct Civ Eng 2014;8. https://doi.org/10.1007/s11709-014-0081-0.

[34] Cladera A, Marí A, Ribas C, Bairán J, Oller E. Predicting the shear-flexural strength of slender reinforced concrete T and I shaped beams. Eng Struct 2015;101. https://doi.org/10.1016/j.engstruct.2015.07.025.

[35] Reineck K-H, Bentz EC, Fitik B, Kuchma DA, Bayrak O. ACI-DAfStb database of shear tests on slender reinforced concrete beams without stirrups. ACI Struct J 2013;110.

[36] Rueda-García L, Bonet JL, Miguel Sosa PF, Fernández Prada MÁ. Safety assessment of shear strength current formulations for composite concrete beams without web reinforcement. In: Fédération Internationale du Béton (fib), editor. Proc. 2021 fib Symp. Concr. Struct. New Trends Eco-Efficiency Perform., Lisbon: 2021, p. 2305–14.

Chapter 6. Numerical modelling of the experimental programme specimens with web reinforcement

During a stay abroad at ETH Zurich (Switzerland) of the doctoral student, some of the specimens with web reinforcement of the experimental programme were numerically modelled with the software IDEA StatiCa Detail, in which the Compatible Stress Field Method (CSFM) is implemented.

In this chapter, the theoretical basis of the software, the problems faced during the modelling and the solutions proposed are described. The numerical model contributes to the verification of the experimental shear strengths, the failure modes and the proposed mechanical model.

1. Introduction

The behaviour of the specimens tested in this thesis has been mainly explained by strut-and-tie models [1], which are mechanically consistent and powerful models that give direct information about the load-carrying behaviour of the structure.

Despite the advance of computational tools, strut-and-tie models are still used in the engineering practice due to their many advantages. However, their application is typically manual and requires several iterations, so it can be tedious and time-consuming. To overcome this drawback, many authors have tried to develop software for the structures modelling using strut-and-tie models (such as CAST [2], AStrutTie [3] or MEFBT [4]), that have not spread much in practice since they still require a close interaction of the user with the software.

With the aim of facilitating the use of strut-and-tie models and stress fields in the engineering practice, a user-friendly stress fields commercial software was developed by ETH Zurich and the software company IDEA StatiCa [5]. The software is called IDEA StatiCa Detail and implements the mechanical principles of the Compatible Stress Field Method (CSFM) [6]. The CSFM is a simplified non-linear finite element-based continuous stress field analysis procedure. For its application, simple constitutive laws for concrete and steel materials are used, in contrast to the additional materials properties that usually nonlinear finite element analyses require. CSFM implements the tension stiffening effect to capture serviceability and deformation capacity aspects, on the basis of the effective amount of reinforcement, which is automatically computed by the software.

In the present research work, the software IDEA StatiCa Detail was used to predict the ultimate loads and failure modes of the monolithic and composite specimens of the experimental programme with web reinforcement, which were compared to the experimental outcomes.

In this chapter, the main characteristics of the software are first listed. Secondly, the modelling particularities of the monolithic rectangular beams of the test programme are explained, and the numerical predictions are discussed. Afterwards, the monolithic T-shaped beams are modelled and analysed. Finally, some preliminary observations about the modelling of composite specimens are given.

2. IDEA StatiCa® Detail

This section explains the capabilities of the software IDEA StatiCa Detail (ISD). First, the assumptions of the CSFM, which are implemented in this software, are listed. Then, the constitutive models considered in the software are explained, as

well as the generation of the finite element mesh. Finally, data input steps to model these specimens is described in detail.

The present work was carried out with a research version of the software IDEA StatiCa Detail 21.0. This research version has advanced features compared to the commercial version, such as modifying the default mesh size or some material parameters. The features described in the following are available in the commercial version unless stated otherwise.

2.1. Software assumptions

According to Kaufmann *et al.* [6,7], the CSFM assumes fictitious, rotating, stress-free cracks that open without slip. It considers the equilibrium at the cracks together with the average strains of the reinforcement. As shown in Fig. 1, the concrete and reinforcement stresses are maximum at the cracks, while the concrete tensile strength is neglected, except for its stiffening effect on the reinforcement.

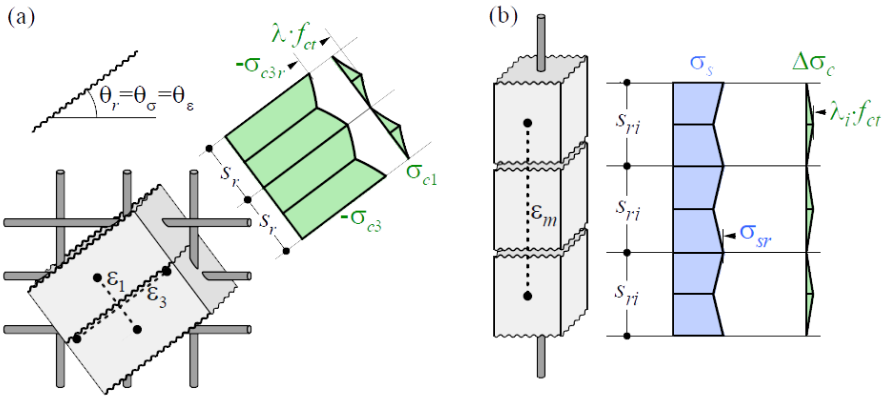

Fig. 1. Assumptions of the CSFM: (a) principal stresses in concrete; (b) stresses in the reinforcement direction (from Kaufmann et al. [7]).

The principal directions of stresses and strains coincide (see Fig. 1a). In the crack state, the behaviour of the main directions is decoupled (except for the compression softening effect). Thus, simple uniaxial constitutive laws can be used.

2.2. Constitutive models

2.2.1. Concrete

The concrete constitutive laws of the CSFM are based on the uniaxial compression constitutive laws described by the design codes, which only depend on the concrete compressive strength. In the software, the parabola-rectangle diagram is used by default, but a simpler bilinear diagram (elastic-perfectly plastic) can also be selected.

The compressive strength of cracked concrete is reduced based on the principal tensile strain (ε_1) by multiplying the compressive strength of concrete f_c by a reduction factor k_{c2} [7]. This gives the effective compressive strength shown in Fig. 2. This reduced compressive strength due to transverse tension stresses is known as compression softening.

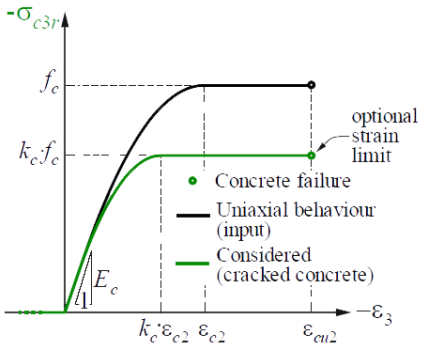

Fig. 2. Input and considered stress-strain relations for concrete (from Kaufmann et al. [7]).

The reduction relationship k_{c2} - ε_1 implemented in ISD [7] is a generalization of the *fib* Model Code 2010 [8] (MC-10) proposal for shear verifications that limits the effective concrete strength to 0.65 times the concrete compressive strength, not applicable to other loading cases.

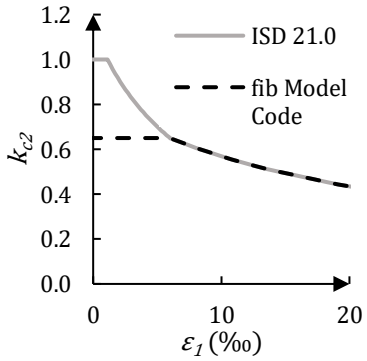

Fig. 3. Compression softening laws of IDEA StatiCa Detail [7] and MC-10 [8].

The software implementation does not consider an explicit failure for concrete in compression in terms of strains: to avoid numerical instability a quasi-infinitely plastic branch after the peak stress is considered. Nonetheless, the ultimate capacity is properly predicted by considering a η_{fc} reduction factor to increase the brittleness of concrete as its strength rises. This η_{fc} factor is defined in MC-10 [8] as follows:

$$f_{cd} = \frac{\eta_{fc} \cdot k_{c2} \cdot f_{ck}}{\gamma_c} \tag{1}$$

$$\eta_{fc} = \left(\frac{30}{f_{ck}}\right)^{1/3} \leq 1 \tag{2}$$

2.2.2. Reinforcing steel

An idealized bilinear stress-strain diagram is used for bare reinforcing bars, as defined in the design codes. The stress-strain relation is modified to account for the tension stiffening (see Fig. 4), so that the average stiffness of the bars embedded in the concrete (ε_m) is captured. Tension stiffening will be described in Section 2.2.4.

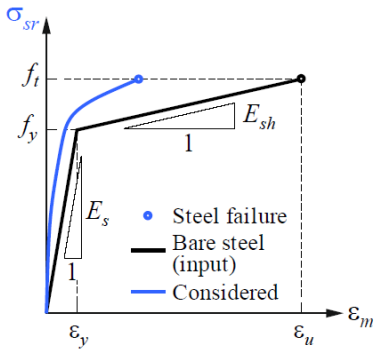

Fig. 4. Stress-strain diagram of reinforcement (from Kaufmann et al. [7]).

2.2.3. Bond model (anchorage)

The bond-slip between reinforcement and concrete is introduced by considering the rigid-perfectly plastic constitutive relationship of Fig. 5. f_{bd} is the design value of the ultimate bond stress specified in the design codes for the specific bond conditions [7]. The purpose of this consideration is to verify the bond prescriptions (the anchorage of reinforcement) according to design codes.

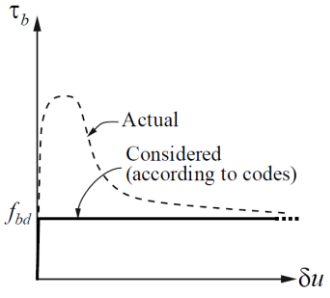

Fig. 5. Bond-slip relationship for anchorage length verifications (from Kaufmann et al. [7]).

2.2.4. Tension stiffening

The consideration of tension stiffening increases the steel stiffness and reduces its ductility. Two cases are implemented regarding the tension stiffening: stabilized cracking and non-stabilized cracking. In both cases, the concrete is considered fully cracked before loading.

When the crack pattern is fully developed (stabilized cracking), the tension stiffening is introduced by means of the Tension Chord Model (TCM) [9,10]. In this model, the distribution of bond shear between cracks (τ_b), the steel and concrete stresses (σ_s, σ_c) and the steel strains between cracks (ε_s), considering average crack spacing (λ = 0.67), are the ones shown in Fig. 6a.

The application of the TCM depends on the effective reinforcement ratio (ρ_{eff}), which is defined as the reinforcement area (A_s) divided by the effective area of concrete in tension ($A_{c,tension}$). Thus, assigning to each rebar the proper concrete area acting in tension is crucial. The ISD has implemented an automatic procedure to define the corresponding effective reinforcement ratio (ρ_{eff}) for any configuration of reinforcement, consisting on the determination of the maximum concrete area that each rebar can activate (the procedure is described in [7]).

The above-mentioned procedure for calculating the effective reinforcement ratio for the application of the TCM is used by default in ISD. However, the software allows the introduction of a different ρ_{eff}. For example, the effective reinforcement ratio for applying the TCM may be calculated with the procedure proposed by Burns in [11] in order to investigate serviceability criteria. In this procedure, the steel stresses at the crack for a bending moment equal to the cracking bending moment (M_{cr}) are set equal to the steel stresses at the crack of an equivalent tension chord [12]. The ρ_{eff} of this equivalent tension chord is obtained as:

$$\rho_{eff} = \left[\frac{M_{cr}(d-x)E_s}{f_{ctm} \cdot E_c \cdot I_e} + 1 - n\right]^{-1} \quad (3)$$

where d is the effective beam depth; x is the neutral axis depth; E_s is the modulus of elasticity of the steel; f_{ctm} is the mean value of axial tensile strength of concrete; E_c is the modulus of elasticity of the concrete; I_e is the inertia of the cracked concrete cross-section; n is the relationship between E_s and E_c.

The procedure of Burns [11] considers a lower area of concrete in tension than the procedure implemented in ISD, so it provides a higher ρ_{eff}. This implies that a lower quantity of concrete is subjected to tension stiffening, and, thus, the shear-deflection curve of the specimens is less stiff.

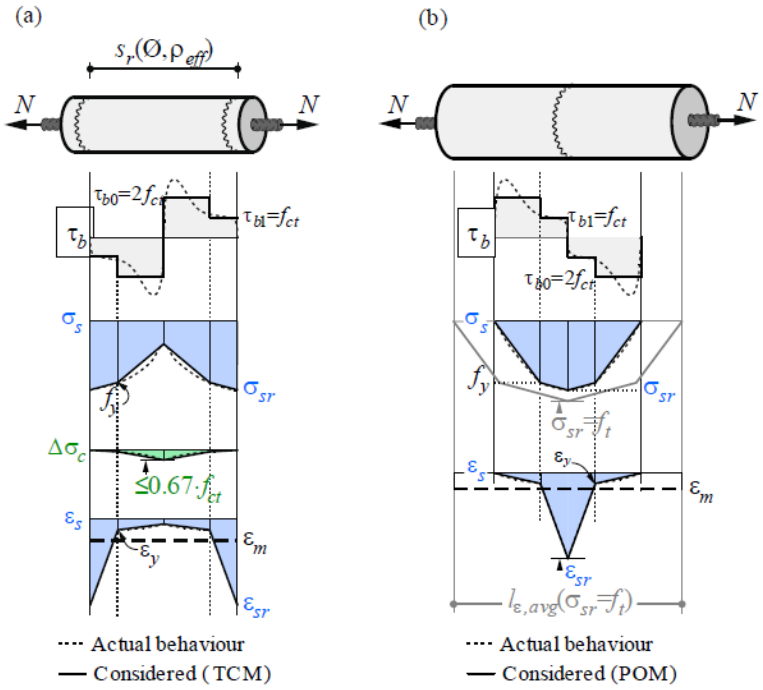

Fig. 6. Tension-stiffening models' assumptions: (a) Tension Chord Model (TCM); (b) Pull-Out Model (POM) (from Kaufmann et al. [7]).

On the other hand, the crack pattern is considered non-stabilized in local cracks triggered by geometric discontinuities and areas with low amount of reinforcement (below ϱ_{cr}), i.e., regions with a reinforcement below the minimum reinforcement amount for carrying loads without yielding. ϱ_{cr} is approximately 0.6% for conventional concrete and reinforcing steel.

For stirrups, the reinforcement ratio is usually below 0.6%. Then, the cracking is considered non-stabilized, and the tension stiffening is implemented with the Pull-Out Model (POM), which analyses the behaviour of a single crack and whose assumptions are shown in Fig. 6b.

2.3. Finite element mesh

The software ISD automatically generates the finite element mesh, so no specialized knowledge is required. The programme, based on the shape and size of the structure and taking into account the larger diameter of the reinforcing bars, automatically determines the size of the elements. However, the research version allows the user to define the finite element mesh size.

The CSFM considers continuous stress fields in the concrete, complemented by discrete tension ties representing the reinforcement bars [7]. Thus, ISD uses 2D finite elements for concrete modelling and 1D finite elements for the reinforcement. The calculation model considers a plane stress state. The concrete is modelled using quadrilateral and trilateral shell elements (CQUAD4 and CTRIA3) that do not admit stresses or strains in the normal direction to the plane. The reinforcement elements are modelled by two-node elements (CROD), which only admit compression and tension stresses and strains.

In ISD the reinforcing bars are divided into finite elements with a similar length to that of the concrete finite elements. The concrete and reinforcement finite elements are connected using multi-point constraints (MPC) elements. The reinforcement can then occupy an arbitrary position in relation to that of the concrete elements. In case the anchorage length verification needs to be calculated, bond and anchorage end spring elements are inserted between the reinforcement and the MPC elements [7].

2.4. Modelling description

2.4.1. Geometry definition

This section of the software includes the cross-section geometry definition, the supports description and the definition of the bearing plates for introducing loads.

In this study, the supports were introduced as "distributed", which means that the point support is distributed over a specified length considering a constant reaction stress.

2.4.2. Loads definition

An analysis of the structural behaviour at failure was carried out in this study. Thus, two point loads of a greater value than those registered during tests were introduced. The software will then automatically give the maximum load resisted by the defined structural element.

2.4.3. Reinforcement definition

The longitudinal and transverse reinforcement are defined in this section. Their diameters and anchorage types at the end of the reinforcing bars are defined.

In this project, the longitudinal reinforcing bars were anchored with perfect bonded conditions at both ends, since no anchorage problems were registered during tests.

2.4.4. Materials definition

In this section, the user can define the experimental material properties. Thus, for the specimens of this test programme, the experimental properties of the materials were introduced, considering the partial safety factors for concrete (γ_c) and steel material properties (γ_s) as 1.0.

Regarding the reinforcing steel bars, the diagram used was "bilinear with an inclined top branch". All the parameters needed for defining this diagram were the ones experimentally obtained: modulus of elasticity of the steel (E_s), yield strength of reinforcement (f_{yk}), relationship between the yield strength of reinforcement and the tensile strength of reinforcement (f_{uk}) and the strain at f_{uk}. The user can decide in this step between considering or not the tension stiffening.

For the concrete, the parabola-rectangle diagram in ISD was defined with the characteristic compressive cylinder strength of concrete (f_{ck}) and the compressive strain in the concrete at the design value of concrete compressive strength (f_{cd}), which is ε_{c2}. Since E_c was the experimental property available and not ε_{c2}, a conversion was needed by means of Eq. (4), which derives from the parabola-rectangle formulation of EC2 [13].

$$\varepsilon_{c2} = \frac{\sigma_c}{E_c \cdot \left[1 - \left(1 - \frac{\sigma_c}{f_{c,exp}}\right)^{1/n}\right]} \tag{4}$$

where σ_c is the compressive stress reached during the concrete modulus of elasticity test, $f_{c,exp}$ is the compressive strength of concrete reached during the concrete compressive strength test and n is an exponent defined in Table 3.1 of EC2 [13], which is equal to 2 if $f_{ck} < 50$ MPa and equal to $1.4+23.4[(90- f_{ck})/100]^4$ if $f_{ck} \geq 50$ MPa.

The compression softening of concrete can be defined by user in the research version if the default diagram is not used. The diagram can be defined by points or by the definition of parameters L1, L2 and L3. The relationship between these parameters is:

$$k_{c2} = \frac{L3}{L1 + L2 \cdot \varepsilon_1} \tag{5}$$

2.4.5. Calculation setup

From the calculation setup, the main settings that were controlled in this research work are:

- "Number of increments (permanent part)". This defines the number of portions in which the introduced load must be divided.
- "Minimal number of elements per smaller dimension". When the elements are 2D beams, like in this research work, the smaller dimension is the beam height. The software divides the beam height in as many finite elements as indicated in this setting.

- "Multiplier of flange depth". Since the ISD works in 2D, there exists this setting for T-shaped specimens with which the effective flange width (b_{eff}) is defined. This number is the inverse of the slope considered for the expansion of the compression field into the flange.
- "Material factors". The partial safety factors of the materials are defined herein.

2.4.6. Results display

ISD offers multiple ways of displaying different results. The most used ones in this research work were: the stress flow; the stress check value of concrete and steel, which draws the ratio of stress and strength for the selected material and the applied portion of the load; the compressive concrete and steel stresses; the direction of principal stresses; the compressive strength reduction factor, which draws the distribution of $k_{\varepsilon 2}$; the deformations; the calculated reinforcement ratio.

The software shows all the data and results in an Excel sheet for each load portion: information about nodes location, names and nodes of the finite elements, considered characteristics of the materials, deformation in nodes, stress and strains in concrete and steel and maximum load and reactions.

2.4.7. Obtention of the load-deflection curve

At the time of carrying out this research work, ISD 21.0 was not able to easily display the load-deflection curve for a given node. Consequently, the deformation of the node for each load step had to be extracted from the output Excel sheets. This extraction was conducted via a MATLAB script.

2.4.8. Batch calculations

The research version of ISD has this useful tool for research, which allows running multiple batch calculations of the same model using different parameters.

This option requires programming a JSON file for every variant of the model with the different instructions regarding the variable parameters considered. In this work, the batch calculations were used for varying the number of increments, the number of finite elements and the different considerations regarding tension stiffening.

3. Modelling of monolithic rectangular specimens

Five monolithic rectangular specimens with web reinforcement were modelled in this stage: NWP2B1, NWP3B1, NWP4B1, HWP5B1 and HWP6B1. The objective was to study the accuracy of the software in estimating the ultimate load and failure mode of the specimens. The influence of different variables considered relevant for these tests was analysed: the finite element mesh size, the compression softening

model and the tension stiffening model. The conclusions reached in this first stage were applied in the modelling of the following specimens: monolithic T-shaped specimens and composite specimens.

3.1. IDEA StatiCa Detail model definition

First, the longitudinal and cross-sectional geometry of the specimens were defined as a beam. The supports of the specimens were modelled as a point support distributed over a specified length so that no abrupt changes of distributed stress appear. Two steel bearing plates were defined for distributing the concentrated loads.

Secondly, a load case consisting in two vertical point loads of 500 kN each, located on the two bearing plates, was defined. This load case was included into a ULS combination in which the load was multiplied by 1.0.

Regarding the reinforcement, three layers of longitudinal reinforcement were defined: two layers for the bottom longitudinal reinforcement and one layer for the top longitudinal reinforcement. Perfect bond conditions at the end of the bars were defined, as observed in Fig. 5, since no anchorage problems were expected at the end of these specimens.

The transverse reinforcement was modelled separately for the principal and the reinforced spans, so different stirrups spacings could be defined. In the specimens of the experimental programme the stirrups had different concrete covers to the lateral edge of the cross-section (15 mm) and the upper and lower edges (25 mm). Since the IDEA StatiCa Detail makes a 2D calculation, the concrete cover of 25 mm was the one defined in this case.

The concrete constitutive law defined for these specimens was the parabola-rectangle type, as explained in Section 2.4.4, in which f_{ck} was taken as the f_c experimentally measured for each concrete from the concrete cylinders' tests. Regarding the steel constitutive laws, the modulus of elasticity E_s, the yield strength f_{yk}, the ratio between the tensile strength and the yield strength (f_{uk}/f_{yk}) and the strain at maximum load ε_{uk} were introduced manually from the average results of the steel experimental tests. Each steel type was assigned to its respective reinforcement of the defined above.

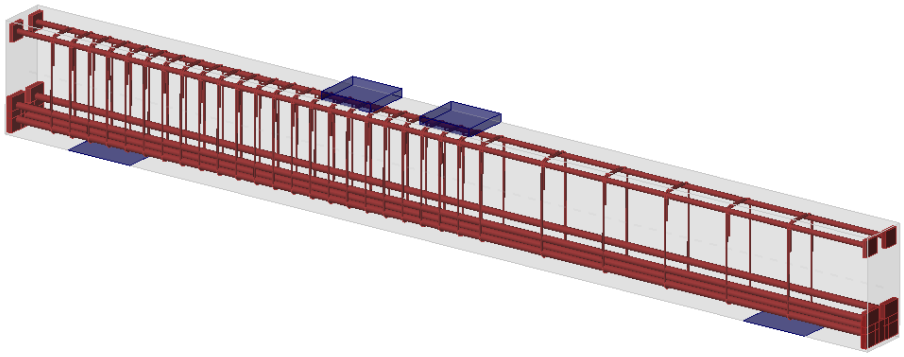

Fig. 7. Example of the geometry and reinforcement definition in ISD for monolithic rectangular specimens.

3.2. Analysed variables

3.2.1. Finite element mesh size

Different finite element (FE) mesh sizes were studied to determine the best size for modelling these specimens, i.e., the size that offers accurate results with a low computational cost. These considered sizes are described in Table 1.

Table 1. Finite element mesh sizes considered in the analysis.

Model ID	No. of FE per smaller dimension	Size of the FE (mm)
05FE	5	80.0
10FE	10	40.0
15FE	15	26.7
20FE	20	20.0
25FE	25	16.0
30FE	30	13.3
35FE	35	11.4

3.2.2. Compression softening model

Two compression softening models were considered to analyse their accuracy to the experimental results. First, the default compression softening model described in Section 2.2.1 (ISD 21.0). Secondly, the compression softening model of the Modified Compression Field Theory (MCFT) from Vecchio and Collins [14], whose parameters L1, L2 and L3 are 0.80, 1.70 and 1.00, respectively. The two considered laws are represented in Fig. 8.

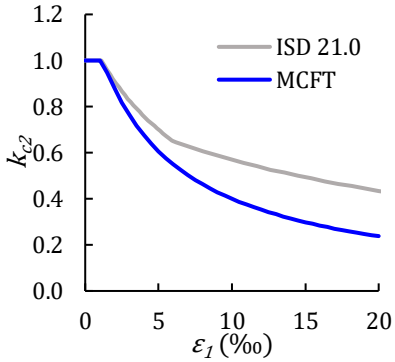

Fig. 8. Compression softening laws of IDEA StatiCa Detail and MCFT [14].

3.2.3. Tension stiffening model

Different tension stiffening modelling approaches were considered to analyse their influence in the ultimate load and the stiffness. Table 2 defines the six considered approaches, differentiating the tension stiffening model used in the stirrups and in the longitudinal reinforcement. The procedure used to calculate ϱ_{eff} from the two described in Section 2.2.1 (i.e. the one implemented in ISD or the procedure of Burns [11]) is indicated in brackets in Table 2.

Table 2. Considered perspectives regarding tension stiffening.

Model ID	Tension stiffening model for the stirrups	Tension stiffening model for the longitudinal reinforcement
TSA	Pull-out model	Tension chord model (ISD)
TSB	Tension chord model	Tension chord model (ISD)
TSC	No tension stiffening	Tension chord model (ISD)
TSD	Pull-out model	No tension stiffening
TSE	Pull-out model	Tension chord model (Burns)
TSF	No tension stiffening	No tension stiffening

3.3. Results and discussion

3.3.1. Overall structural behaviour

The first results observed in the first tests modelled with ISD to verify the performance of the software, before analysing the variables considered, were the compression fields. The stress flow representation is one of the main outputs of the programme, as it gives a fairly good idea of the structural behaviour and failure mode.

The stress flows were compared with the crack patterns of the specimens and the observed failure modes. An example of this comparison is shown in Fig. 9 by overlapping the stress flow of beam NWP2B1 (in this case the model 10FE of Table 1 was used with the rest of variables set by default) and the crack pattern of this beam at maximum load.

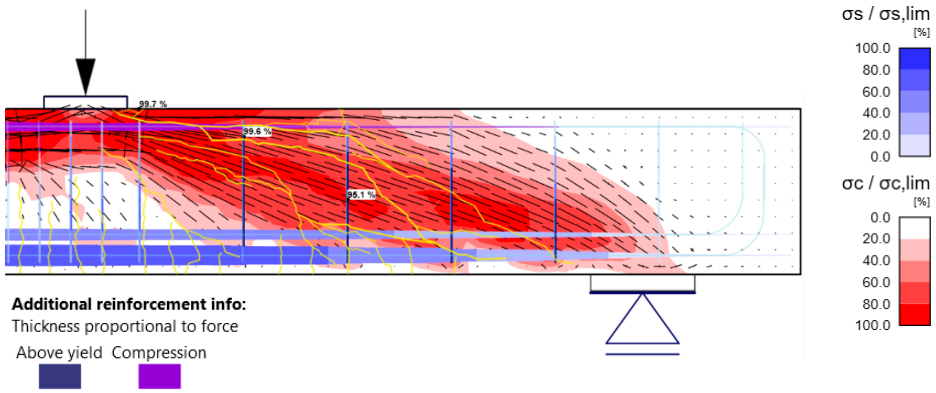

Fig. 9. Representation of the stress flow and crack pattern of the specimen NWP2B1.

The direction of the compressive stress fields, shown in red in Fig. 9, is analogous to the common truss model for beams with stirrups. The resultant of shear components, such as the aggregate interlock across the crack or the shear transmitted by the stirrups, will have a similar direction to that observed in the stress flow, although the direction of the diagonal cracks does not match that of the compressive stresses at the beam's web, what is common in shear. Thus, the model gives *a priori* a very consistent result of the compressive stress field. In addition, there is a high compressive stress concentration in the compression chord, so failure is possibly occurring in the compression chord according to the numerical model. Finally, the tension in the stirrups is above the steel yield strength, so the model shows that the stirrups of the main shear span yield.

3.3.2. Finite element mesh size comparison

In Fig. 10 the results of the relationship between the experimental shear strength V_{exp} and the predicted shear strength V_{pred} are plotted for the seven finite element mesh sizes and for the five specimens. The plot shows that the models with the largest FE mesh sizes (05FE, 10FE and 15FE) gave a very unsafe prediction of the ultimate shear load. Table 3 shows the results for each specimen, as well as the mean value for all of them and the coefficient of variation (CV) for each model. The size of the FE is also included in this table. Finally, the shear-deflection curves given by the software for all the models are compared to the experimental curves in Fig. 11. The deflection was measured below the point load. In these plots, the theoretical

shear-deflection relationships corresponding to the beam before cracking (calculation of the deflection with the homogenized inertia of the cross-section) and after cracking (calculation of the deflection with the inertia of the cracked cross-section) are represented with a continuous and a dashed red line, respectively.

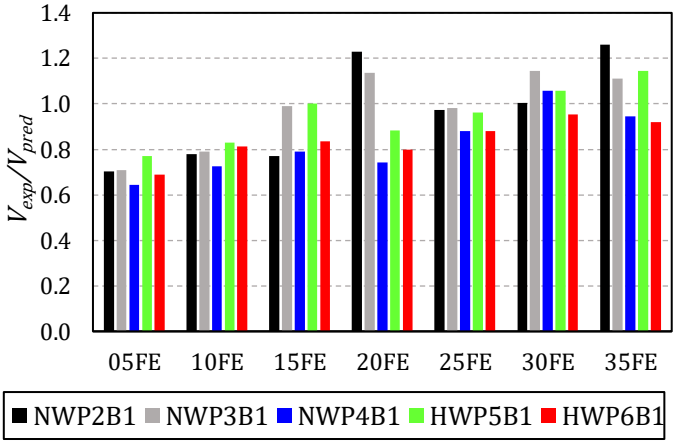

Fig. 10. Comparison of the different FE mesh size models for the five B1 specimens.

Table 3. Values of V_{exp}/V_{pred} of the different FE mesh size models for the five B1 specimens.

Model ID	Size of the FE (mm)	NWP2B1	NWP3B1	NWP4B1	HWP5B1	HWP6B1	Mean	CV (%)
05FE	80	0.70	0.71	0.64	0.77	0.69	0.70	6
10FE	40	0.78	0.79	0.73	0.83	0.81	0.79	5
15FE	26.7	0.77	0.99	0.79	1.00	0.83	0.88	11
20FE	20	1.23	1.14	0.74	0.88	0.80	0.96	20
25FE	16	0.97	0.98	0.88	0.96	0.88	0.94	5
30FE	13.3	1.01	1.14	1.06	1.06	0.95	1.04	6
35FE	11.4	1.26	1.11	0.94	1.14	0.92	1.08	12

The great difference between the prediction of the three models with the largest mesh sizes (05FE, 10FE and 15FE) and the rest of the models, shown in Fig. 10, Table 3 and Fig. 11, was attributed to the fact that in these three models the finite element size was greater than the concrete cover of 25 mm (see the FE mesh sizes in Table 3). It was concluded that the software assigns the mechanical capacities of the transverse reinforcement to the concrete FE located at the concrete cover if the size of that FE is greater than the concrete cover thickness. Since the tested specimens had a local failure at the compression chord, the software overestimated

the beam head resistance capacity by giving the concrete cover the characteristics of a reinforced concrete.

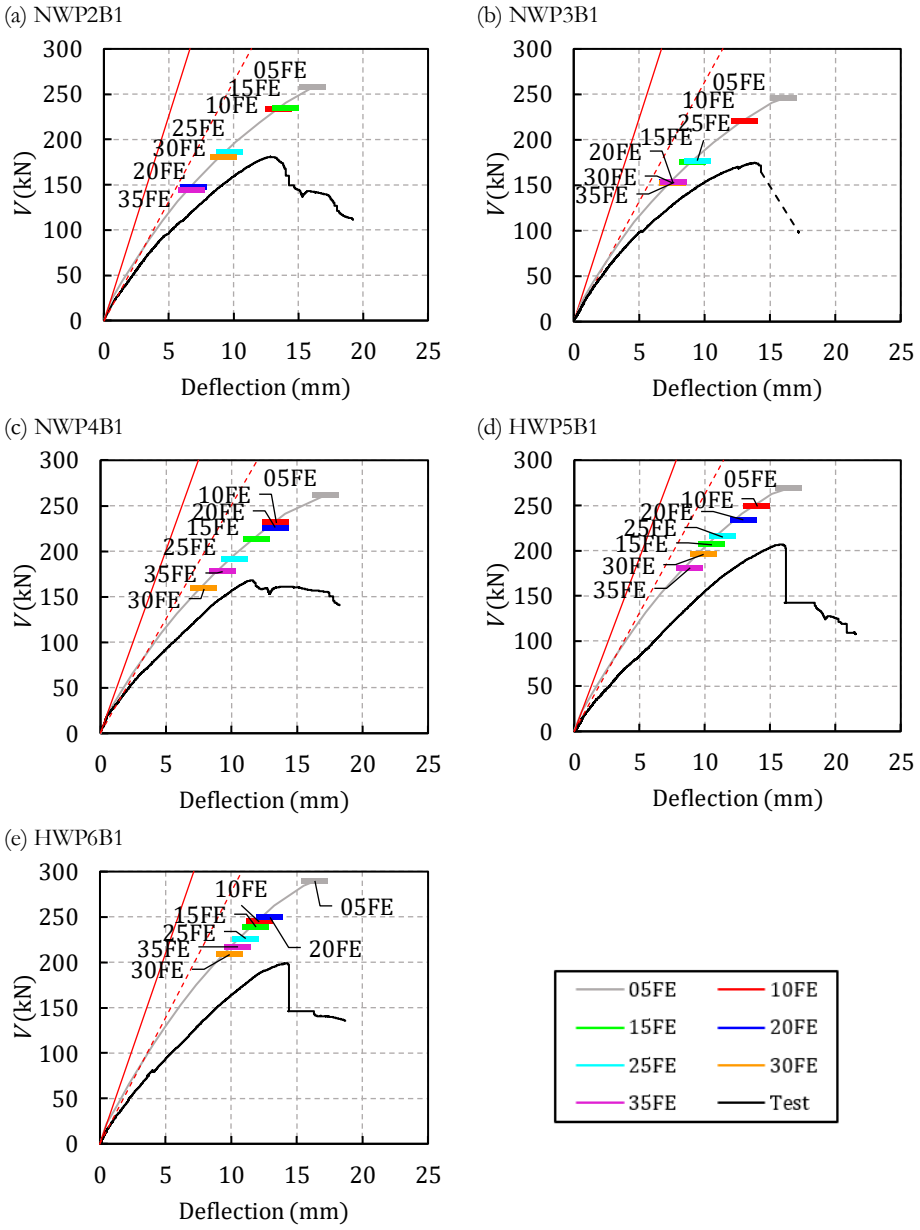

Fig. 11. Experimental shear-deflection curves of the B1 specimens and predicted curves for each FE mesh size: (a) NWP2B1; (b) NWP3B1; (c) NWP4B1; (d) HWP5B1; (e) HWP6B1.

By comparing the examples of Fig. 12 and Fig. 13, which represent the k_{c2} for the same specimen calculated with two different models (05FE and 25FE, respectively), this greater strength of the concrete cover can be observed. While the model with the biggest FE size (05FE) is not able to capture any local decrease of k_{c2} at the compression chord, the model of 25FE shows transverse tension stresses at the concrete cover near the point load, what indicates the possible failure of that area.

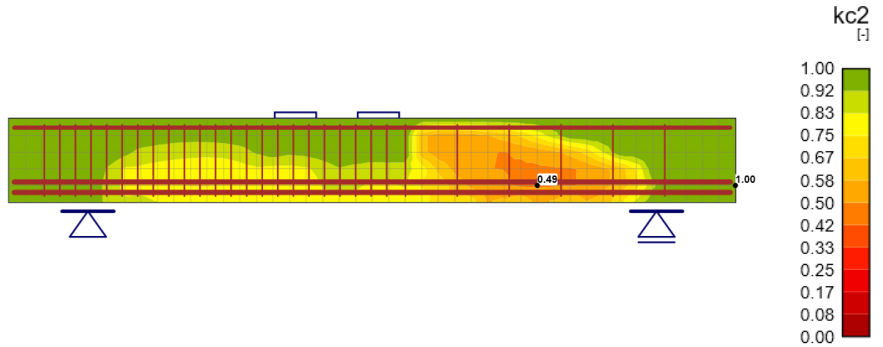

Fig. 12. Representation of k_{c2} at maximum load in the specimen NWP2B1 with the model 05FE.

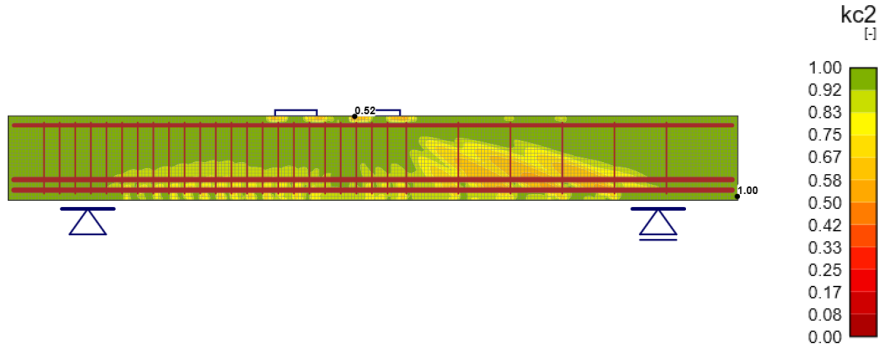

Fig. 13. Representation of k_{c2} at maximum load in the specimen NWP2B1 with the model 25FE.

Regarding the shear-deflection curves, as observed in Fig. 11 the relation was the same for all the models, so the only difference between them was the ultimate shear predicted.

Given the obtained results, it can be stated that the models with a smaller FE mesh size well capture the failure mode, since the failure occurs at the beam head or compression chord. Consequently, it would be acceptable to adopt any of the models that have a smaller FE mesh size than the concrete cover (20FE, 25FE, 30FE and 35FE), but the most suitable would be 30FE, which gives less scattering

and better mean value of V_{exp}/V_{pred}, with a not as high computational cost as that of using more FE.

3.3.3. Compression softening model comparison

In Fig. 14 the results of the two different compression softening models considered in ISD are represented for the five B1 specimens. The numerical results of the relation V_{exp}/V_{pred} are given in Table 4, as well as the mean value and the coefficient of variation. Finally, the shear-deflection curves for the five specimens with the two models are compared in Fig. 15. For this comparison all the specimens were calculated with a finite element mesh size of 30 FE per smaller dimension (model 30FE).

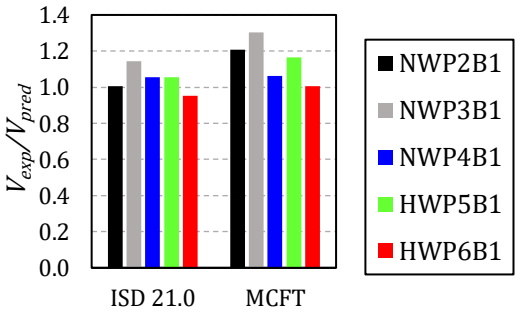

Fig. 14. Comparison of the compression softening models for the five B1 specimens.

Table 4. Values of V_{exp}/V_{pred} of the different compression softening models for the five B1 specimens.

Model ID	NWP2B1	NWP3B1	NWP4B1	HWP5B1	HWP6B1	Mean	CV (%)
ISD 21.0	1.01	1.14	1.06	1.06	0.95	1.04	6
MCFT	1.21	1.30	1.06	1.17	1.01	1.15	9

The results given in Fig. 14 and Table 4 show that the compression softening model used in ISD by default predicted better the experimental results than the compression softening model formulated in the Modified Compression Field Theory (MCFT) of Vecchio and Collins [14], which gave a very safe result of the ultimate shear load. Besides, as shown in Fig. 15, the shear-deflection relation did not vary with the compression softening model, but the ultimate load did.

The compression softening formulation of MCFT gives a safe prediction of the specimens' shear strengths because the reduction of the concrete compressive strength derived in terms of average stresses, i.e., accounting for the contribution of concrete tensile stresses to the strength, as considered in the MCFT, may be excessive when it is applied to models such as the CSFM that consider maximum

stresses at cracks, i.e., without any contribution from concrete in tension, as explained in [7].

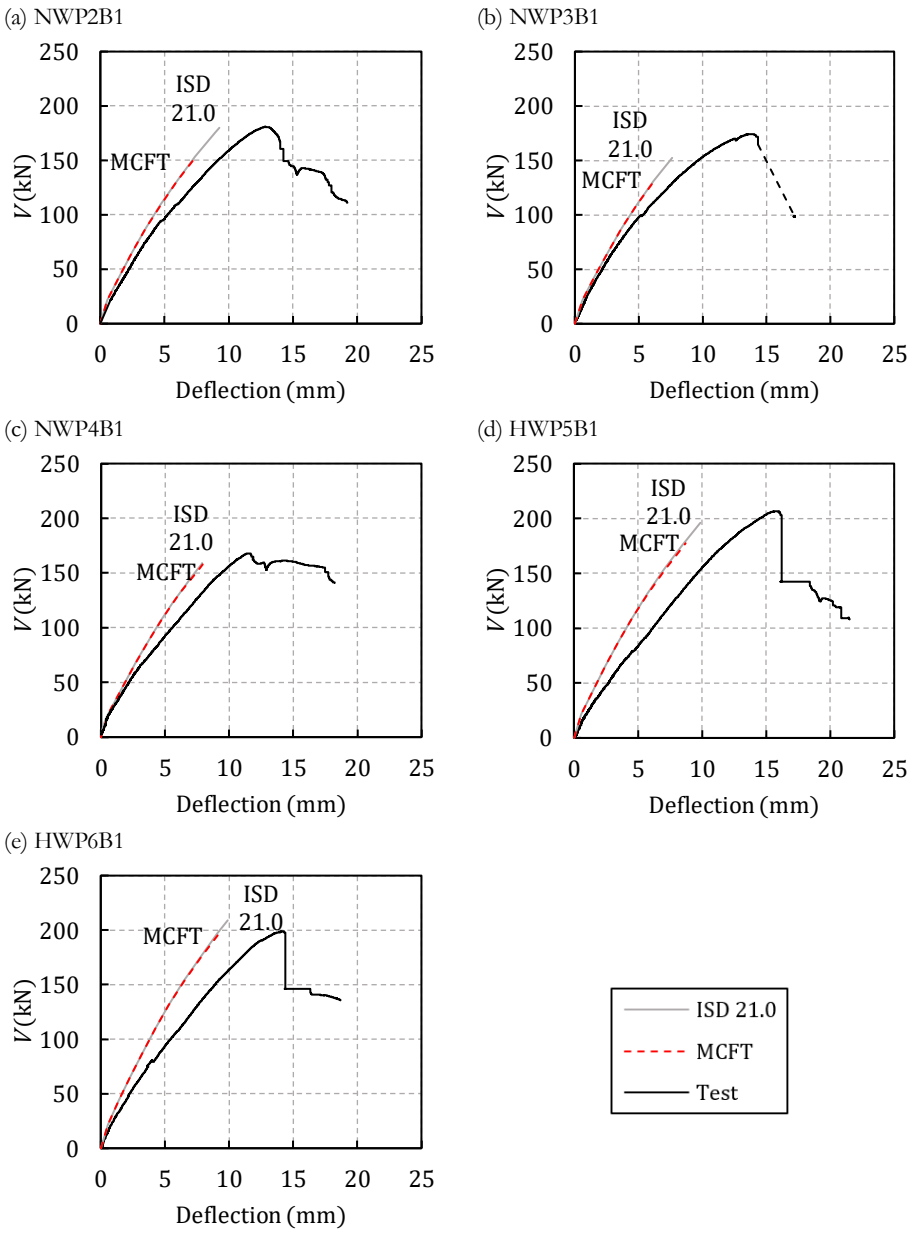

Fig. 15. Experimental shear-deflection curves of the B1 specimens and predicted curves for each compression softening model: (a) NWP2B1; (b) NWP3B1; (c) NWP4B1; (d) HWP5B1; (e) HWP6B1.

3.3.4. Tension stiffening model comparison

As observed in the shear-deflection relationships of Fig. 11 and Fig. 15, the shear-deflection curves of the numerical models present greater stiffness than the experimental curve in all cases. For analysing this stiffness, a comparative study was carried out between different models of tension stiffening in the transverse and longitudinal reinforcement, to observe its influence in the modelling and determine the model that best fits the experimental results.

First, the consideration or not of tension stiffening in the reinforcements is analysed in Section 3.3.4.1. Secondly, the tension stiffening model that should be considered in the stirrups in studied in Section 3.3.4.2. Thirdly, the tension stiffening model in the longitudinal reinforcement is analysed in Section 3.3.4.3.

In all the models of this section 30 FE per smaller dimension (model 30FE) and the compression softening model by default in ISD (the one of the CSFM) were used.

3.3.4.1. Consideration of tension stiffening

In this section the models TSA and TSF described in Table 2 are compared. The first one considers tension stiffening in the way the software does it by default: POM in the stirrups and TCM, obtained with the method proposed in the CSFM [7], in the longitudinal reinforcement. The second one, TSF, does not consider tension stiffening in any reinforcement. The results of V_{exp}/V_{pred} for each specimen, the mean values of the models and the coefficients of variation are presented in Table 5. The experimental and predicted shear-deflection curves for the five specimens are shown in Fig. 16, as well as the theoretical shear-deflection curves before and after the beam cracking.

Table 5. Values of V_{exp}/V_{pred} of models TSA and TSF for the five B1 specimens.

Model ID	NWP2B1	NWP3B1	NWP4B1	HWP5B1	HWP6B1	Mean	CV (%)
TSA	1.01	1.14	0.91	1.06	1.01	1.02	8
TSF	1.19	1.25	1.11	1.20	1.08	1.17	5

It is observed in Fig. 16 how the TSA model correctly reproduces the rigidity corresponding to the uncracked beam in the first load steps, since it generally coincides with the one measured experimentally with the load cells and the displacement transformers. After cracking, both the experimental curve and that of the TSA model show the loss of stiffness of the element. However, the model curve shows less flexibility than the experimental curve.

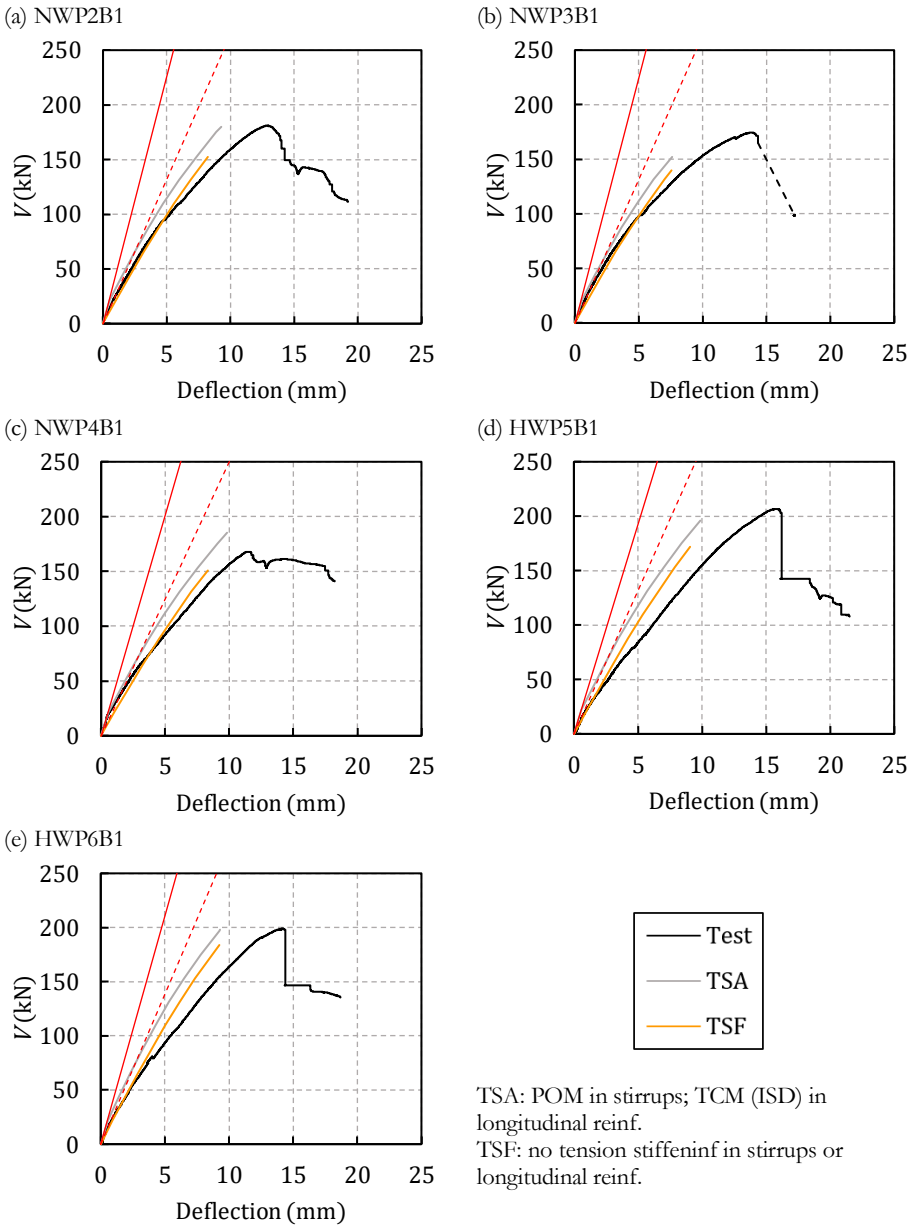

Fig. 16. Experimental shear-deflection curves of the B1 specimens and predicted curves for models TSA and TSF: (a) NWP2B1; (b) NWP3B1; (c) NWP4B1; (d) HWP5B1; (e) HWP6B1.

The curve of the TSF model reproduces a greater flexibility with respect to the TSA curve, however, it does not adapt properly to the experimental curve in the first load

steps. This is because, by not considering the tension stiffening, we are assuming that the concrete between cracks does not suffer tension stresses due to the bond between reinforcement and concrete that reduce the stresses in the reinforcement. On the contrary, we are considering the stress-strain relationship of the reinforcement inside the concrete is that of a bare steel reinforcing bar. Thus, the response of the element is more flexible. This consideration, therefore, is not appropriate to reproduce the initial behaviour of the specimens.

Regarding the ultimate load, the TSA model reaches a higher shear load than the TSF model. This may be due to the fact that, in the TSF model, in which a more deformable behaviour is obtained, the concrete of the compression chord, where the failure of these specimens was located, reaches the ultimate stress (f_c) earlier.

3.3.4.2. Tension stiffening in the stirrups

To analyse how the tension stiffening in the stirrups influences the models' results, the models TSA, TSB and TSC, corresponding to POM, TCM and no tension stiffening in the stirrups, respectively, are compared. In all of them, the TCM (CSFM) is considered in the longitudinal reinforcement. The results of V_{exp}/V_{pred} are shown in Table 6. The experimental and predicted shear-deflection curves for the five specimens are shown in Fig. 17.

Table 6. Values of V_{exp}/V_{pred} of models TSA, TSB and TSC for the five B1 specimens.

Model ID	NWP2B1	NWP3B1	NWP4B1	HWP5B1	HWP6B1	Mean	CV (%)
TSA	1.01	1.14	0.91	1.06	1.01	1.02	8
TSB	1.20	1.22	1.08	1.10	1.04	1.13	6
TSC	1.06	1.28	0.95	1.12	1.07	1.10	10

To observe the effect of tension stiffening on the material constitutive laws, the stress-strain relationship of the steel of one of the stirrups (in particular, the fourth stirrup starting from the right end in Fig. 12 in the specimen NWP2B1), obtained in ISD, is represented for the three models in Fig. 18. The POM is the one that stiffens the reinforcement the most. Consequently, the shear-deflection curve of the TSA model (represented in Fig. 17) is the one with the highest stiffness of the three models, followed by the TSB curve. The stress-strain curve of the steel for the TSC model, without tension stiffening, is that corresponding to bare reinforcement, so the TSC model provides the most flexible shear-deflection curve.

As expected, not considering tension stiffening in the stirrups does not modify the slope of the initial branch of the shear-deflection relationship (see Fig. 17), unlike model TSF did (see Section 3.3.4.1), in which none of the reinforcements were modelled with tension stiffening, since the bending behaviour in the first load stages is determined by the longitudinal reinforcement.

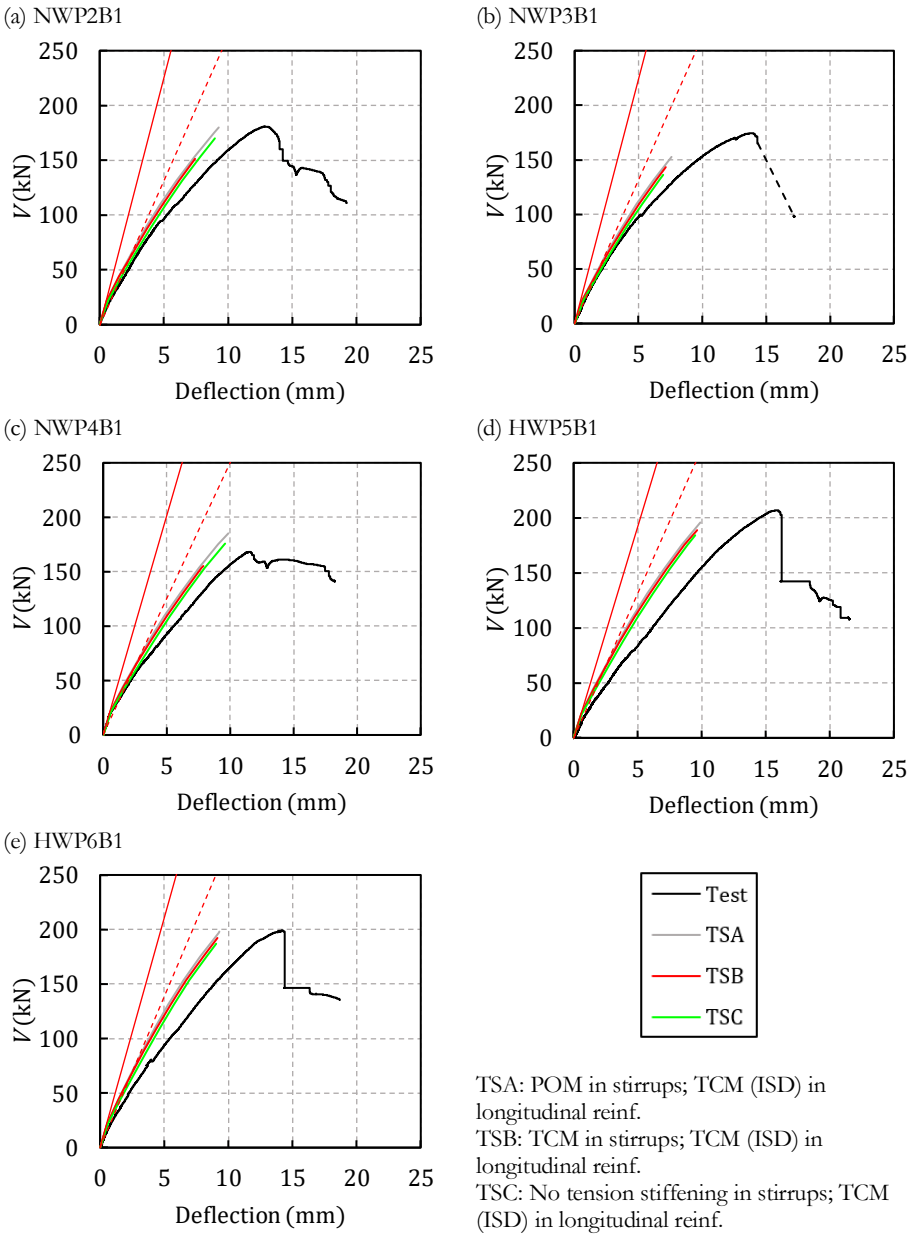

Fig. 17. Experimental shear-deflection curves of the B1 specimens and predicted curves for models TSA, TSB and TSC: (a) NWP2B1; (b) NWP3B1; (c) NWP4B1; (d) HWP5B1; (e) HWP6B1.

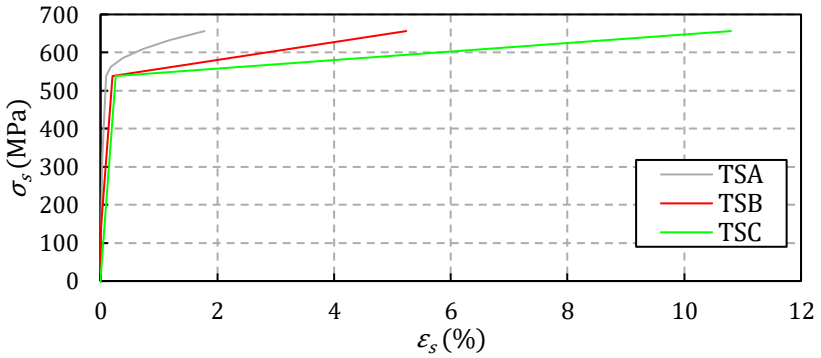

Fig. 18. Stress-strain relationship considered by ISD for one of the stirrups of the principal span of beam NWP2B1 with the models TSA, TSB and TSC.

In general, the TSA model gives a higher ultimate load than the TSB, and the TSB gives a higher load than the TSC (see Table 6), which may be because the greater flexibility of the beam makes the compression chord reaches the ultimate stress at a lower load. In some cases, the TSB model gives a lower ultimate load than the TSA and TSC models, which could only be attributed to numerical convergence problems.

Given the mean values and coefficients of variation shown in Table 6, model TSA is the one that best predicts the ultimate shear of the three models.

3.3.4.3. Tension stiffening in the longitudinal reinforcement

To analyse the effect of tension stiffening in the longitudinal reinforcement, models TSA, TSD and TSE, described in Section 3.2.3, are compared. Model TSA uses the TCM by calculating the ϱ_{eff} with the technic implemented in ISD. Model TSD does not consider tension stiffening in the longitudinal reinforcement. Model TSE uses the TCM by obtaining the ϱ_{eff} with Burns' formula [11]. In all the models, the POM in the stirrups was considered.

The results of V_{exp}/V_{pred} are shown in Table 7. The experimental and predicted shear-deflection curves for the five specimens are shown in Fig. 19. Besides, the obtained ϱ_{eff} with both calculation procedures (ISD and Burns) for each beam are shown in Table 8, and an example of the stress-strain relationship of the tension longitudinal reinforcement considered by the software in the specimen NWP2B1 is shown in Fig. 20 for the three models compared.

As observed in Table 8, the ρ_{eff} obtained with Burns' formula is very high for these specimens, so it is equivalent to not considering tension stiffening, which is observed in the overlap of the steel curves used in the TSD and TSE models shown in Fig. 20. Consequently, the shear-deflection curves of models TSD and TSE also overlap (see Fig. 19). Regarding the model TSA, although it considers a much lower ρ_{eff} than that calculated with Burns' formula (see Table 8), which means that the considered area of concrete in tension is greater than that of Burns, the steel stress-strain curve does not significantly differ from those of models TSD and TSE (see Fig. 20). For this reason, the shear-deflection curves of the three models are very similar (see Fig. 19), although those of models TSD and TSE are slightly more flexible than those of model TSA. The comparison of the experimental and predicted shear-deflection curves in Fig. 19 shows that, in general for all the specimens, the TSA model better captures the initial stiffness of the curves, while models TSD and TSE show a slightly lower stiffness than the experimental one in the first load steps. Besides, the model that better approximates the ultimate shear load is the model TSA according to the results shown in Table 7 (mean V_{exp}/V_{pred} value of 1.02 with a coefficient of variation of 8%).

Table 7. Values of V_{exp}/V_{pred} of models TSA, TSD and TSE for the five B1 specimens.

Model ID	NWP2B1	NWP3B1	NWP4B1	HWP5B1	HWP6B1	Mean	CV (%)
TSA	1.01	1.14	0.91	1.06	1.01	1.02	8
TSD	1.20	1.05	1.09	1.08	1.02	1.09	6
TSE	1.02	1.22	1.08	1.01	1.02	1.07	8

Table 8. Calculated ρ_{eff} with the procedure implemented in ISD and the formula of Burns [11].

ρ_{eff} calculation	NWP2B1	NWP3B1	NWP4B1	HWP5B1	HWP6B1
ISD	0.053	0.058	0.054	0.055	0.067
Burns	0.247	0.249	0.285	0.476	0.367

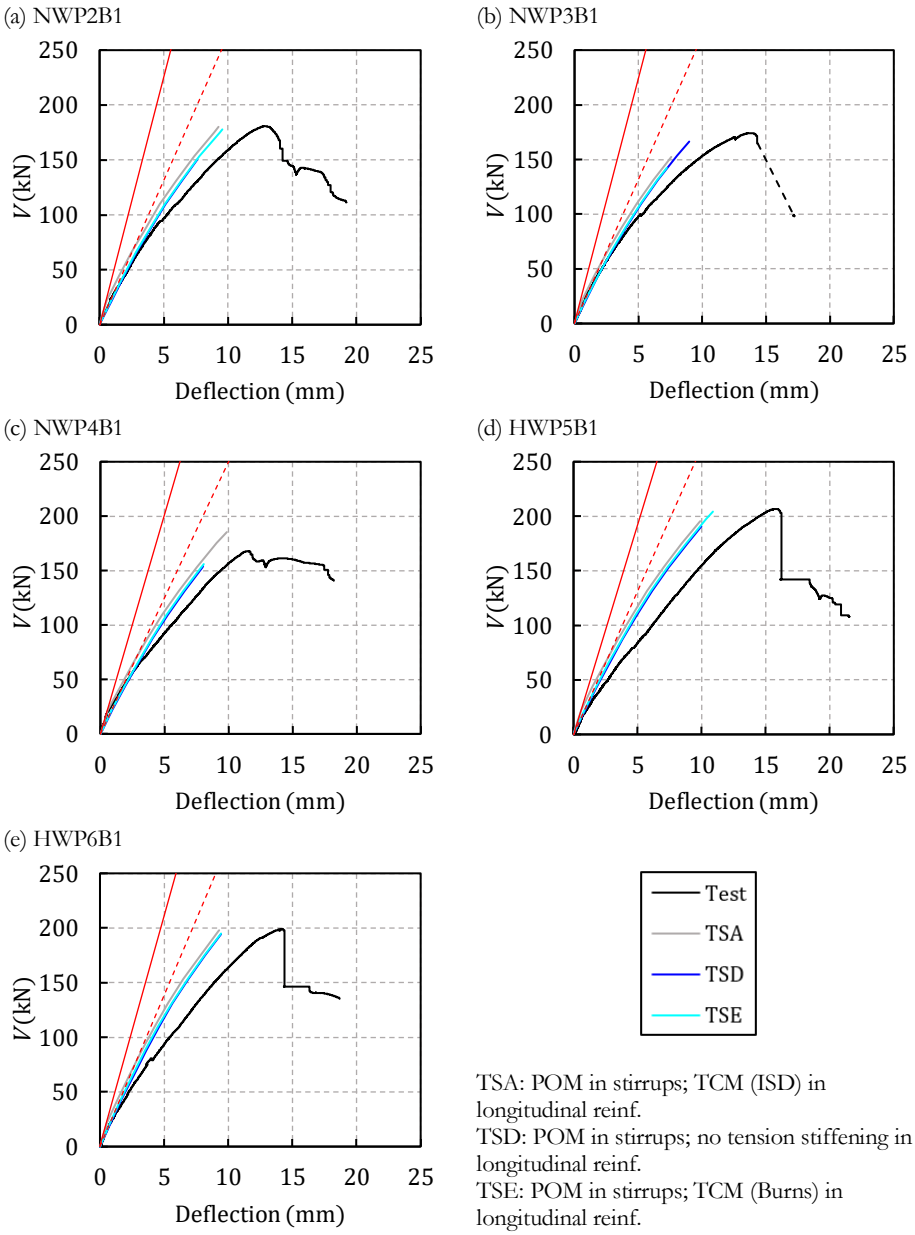

Fig. 19. Experimental shear-deflection curves of the B1 specimens and predicted curves for models TSA, TSD and TSE: (a) NWP2B1; (b) NWP3B1; (c) NWP4B1; (d) HWP5B1; (e) HWP6B1.

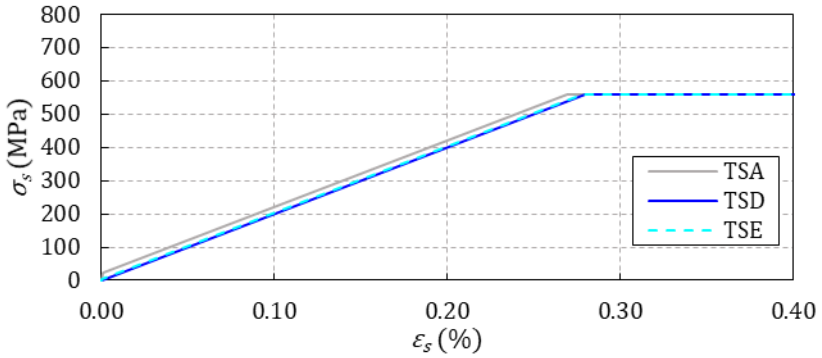

Fig. 20. Stress-strain relationship considered by ISD for the tension longitudinal reinforcement of beam NWP2B1 with the models TSA, TSD and TSE.

3.4. Conclusions

From the previous analysis on the monolithic rectangular specimens, the following conclusions can be stated:

- The finite element mesh size must be smaller than the concrete cover. The number of finite elements per smaller dimension that better fits the experimental results with a reasonable computational cost is 30.
- The compression softening model that better adjusts the experimental results is the one implemented in ISD 21.0.
- The tension stiffening models considered in the reinforcements that offer better results are the Pull-Out Model (POM) in the stirrups and the Tension Chord Model (TCM) in the longitudinal reinforcement. In the TCM, the calculation of ρ_{eff} with the procedure implemented in ISD 21.0 gives the best result. This was the model TSA in Table 2.

4. Modelling of monolithic T-shaped specimens

In this section, nine monolithic T-shaped specimens with web reinforcement were modelled: five specimens with cross-section type C1 (NWP2C1, NWP3C1, NWP4C1, HWP5C1 and HWP6C1) and four specimens with cross-section type D1 (NWP7D1a, NWP7D1b, HWP5D1 and HWP6D1). The specimens were modelled taking into account the conclusions derived from the modelling of the rectangular specimens. The main parameter studied when modelling the T-shaped specimens was the effective slab width.

4.1. IDEA StatiCa Detail model definition

To define the models of the monolithic T-shaped specimens, only two characteristics were varied with respect to the modelling of monolithic rectangular specimens described in Section 3.1.

First, the cross-section geometry of the specimens, which had flanges of different dimensions for cross-sections C1 and D1.

Second, the compression longitudinal reinforcement, which had more bars than in the monolithic rectangular beams.

As a conclusion of the previous work on rectangular specimens, the longitudinal reinforcement was modelled with the Tension Chord Model (TCM) by default, the transverse reinforcement was modelled with the Pull-Out Model (POM), the compression softening model considered was the one defined in ISD 21.0 by default and the number of finite elements per smaller dimension was 30.

4.2. Analysed variables

The only variable studied in the modelling of the monolithic T-shaped specimens was the effective flange width (b_{eff}). This variable is defined in ISD by means of the "Multiplier of flange depth" (MFD) in the calculation setup (see Section 2.4.5). This number is the inverse of the slope considered for the expansion of the compression field into the flange [7], i.e., the considered width of a flange divided by the flange depth.

In the specimens with cross-section type C1, three MFDs were defined (1.00, 0.67 and 0.50), which gave the effective flange widths shown in Fig. 21. In the specimens D1, four MFDs were considered (2.00, 1.33, 0.67 and 0.50) as shown in Fig. 22.

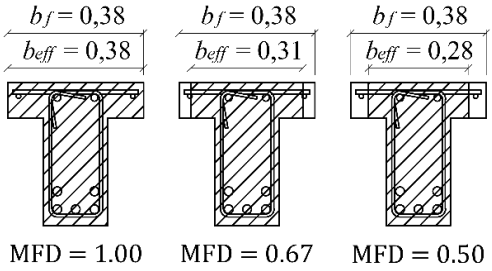

Fig. 21. Effective flange widths considered in specimens C1.

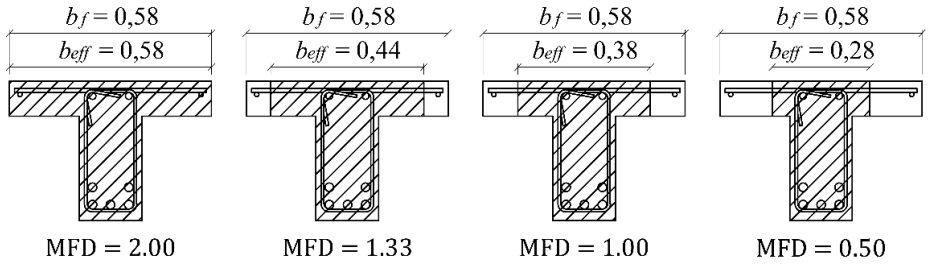

Fig. 22. Effective flange widths considered in specimens D1.

The MFD used in ISD by default is 1.00, so its effect was analysed in both cross-section types (C1 and D1). In the specimens C1, it is equivalent to considering the entire flanges width. The MFD of 2.00 was considered also in the specimens D1 to account for the entire flanges width. The MFD 0.50 was also analysed in both cross-section types. Additionally, in the specimens C1 a MFD of 0.67 was considered, and a MFD of 1.33 in specimens D1.

The MFD values of 0.67 and 1.33 were estimated based on a preliminary analysis run with ISD. This analysis showed two stirrups (named S1 and S2 in Fig. 23) carried the load through the web to the beam head, where the load was able to spread in the flanges given the existing distance until the point load. Conversely, two stirrups (S3 and S4 in Fig. 23) carried the load directly to the point load, without its spread in the flanges.

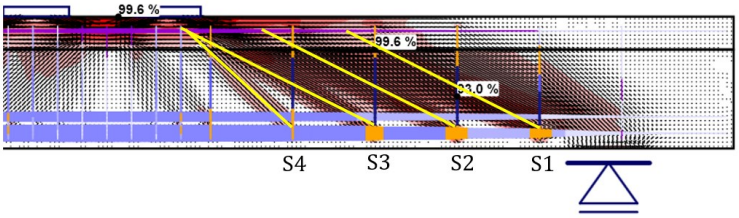

Fig. 23. ISD representation of stress field in a T-shaped specimen.

By means of a simplified strut-and-tie model (see Fig. 24), consisting on two superimposed trusses, in which the yielding of the stirrups was considered, the formulae for calculating the horizontal forces at the node located under the point load (node 1) were obtained. First, the horizontal compressive force transmitted through the flanges (struts 1-3 and 1-8). Second, the horizontal component of the compressive force transmitted diagonally through the web directly to trusses S3 and S4 (struts 1-2 and 1-7). The effective width b_{eff} was obtained as the weighted average of those horizontal forces with respect to flanges and web widths, and resulted in a

b_{eff} of 0.31 m for specimens C1 (equivalent to a MFD of 0.67) and 0.44 m for specimens D1 (equivalent to a MFD of 1.33).

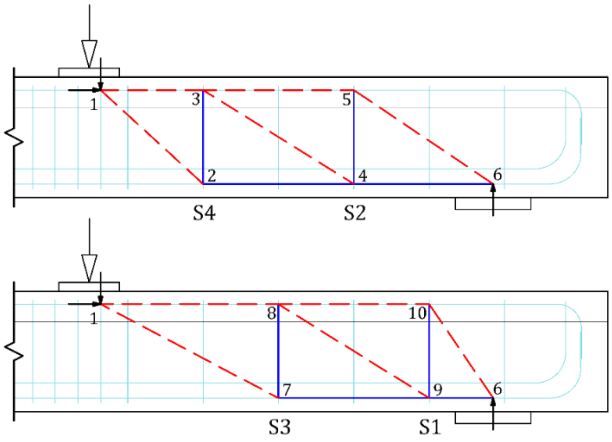

Fig. 24. Simplified strut-and-tie model for estimating the b_{eff}.

Regarding the compression longitudinal reinforcement, the models that considered the entire flanges width (MFD = 1.00 in specimens C1 and MFD = 2.00 in specimens D1) were modelled with 2Ø20+2Ø12, since they were inside the effective width (see Fig. 21 and Fig. 22). In the rest of the models, only 2Ø20 were considered.

4.3. Results and discussion

4.3.1. Effective flange width

The relationships between the experimental result and the predicted result with the different effective flange width models are compared for all the specimens in Fig. 25. For the analysis of the ISD results, the specimen HWP5D1 was removed from the dataset. Specimen HWP5D1 reached similar shear strength to that of the specimens NWP7D1a and NWP7D1b (200, 195 and 197 kN, respectively), although its concrete compressive strength f_c was much higher (f_c = 42 MPa in specimen HWP5D1 and f_c = 24 MPa in specimens NWP7D1a and NWP7D1b). Thus, HWP5D1 shear strength was considered anomalous in Chapter 4 (6th paper). The numerical results of the ratio V_{exp}/V_{pred} for the five C1 specimens and the three D1 specimens are presented in Table 9 and Table 10, respectively, as well as the mean value and coefficient of variation (CV) for all the specimens. Finally, the experimental shear-deflection curves of the specimens are compared with the predicted by the different models in Fig. 26 (C1 specimens) and Fig. 27 (D1 specimens). In these plots, the theoretical shear-deflection relationships corresponding to the beam before cracking and after cracking are represented with a continuous and a dashed red line, respectively.

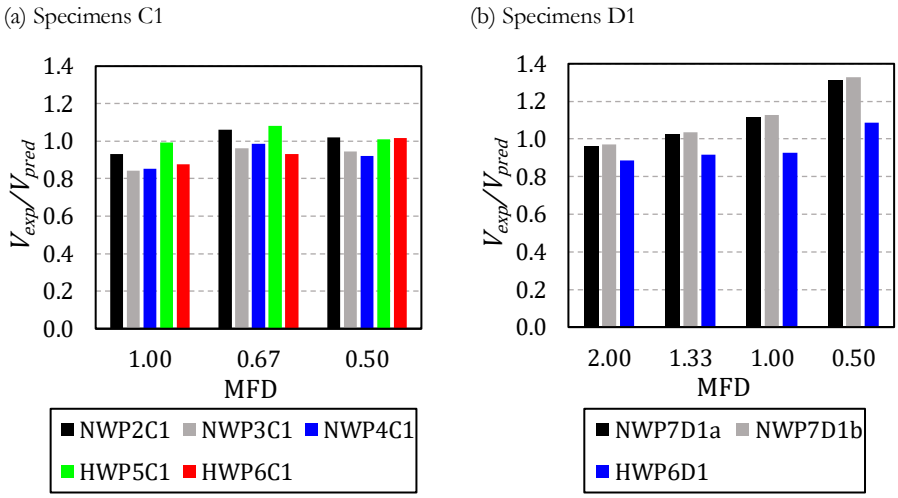

Fig. 25. Comparison of the different effective flange width models: (a) Specimens C1; (b) Specimens D1.

Table 9. Values of V_{exp}/V_{pred} of the different effective flange width models for the five C1 specimens.

MFD	NWP2C1	NWP3C1	NWP4C1	HWP5C1	HWP6C1	Mean	CV (%)
1.00	0.93	0.84	0.85	0.99	0.88	0.90	6
0.67	1.06	0.96	0.99	1.08	0.93	1.00	6
0.50	1.02	0.95	0.92	1.01	1.02	0.98	4

Table 10. Values of V_{exp}/V_{pred} of the different effective flange width models for the three D1 specimens.

MFD	NWP7D1a	NWP7D1b	HWP6D1	Mean	CV (%)
2.00	0.96	0.97	0.89	0.94	4
1.33	1.03	1.04	0.92	0.99	6
1.00	1.11	1.13	0.93	1.06	9
0.50	1.31	1.33	1.09	1.24	9

The presented results in Fig. 25a and Table 9 show that considering the entire flanges width in the specimens C1 offered an unsafe estimation of the shear strength. However, considering a flange width of 2/3 the flange depth (MFD = 0.67) or 1/2 the flange depth (MFD = 0.50) provided very similar results and very precise. In particular, the model with MFD = 0.67 gave a mean value of 1.00 with a low coefficient of variation (6%). The shear-deflection curves of the three models (Fig. 26) were similar, although the curve for MFD = 1.00 presented a slightly higher stiffness. The main differences between them were related to the ultimate shear strength.

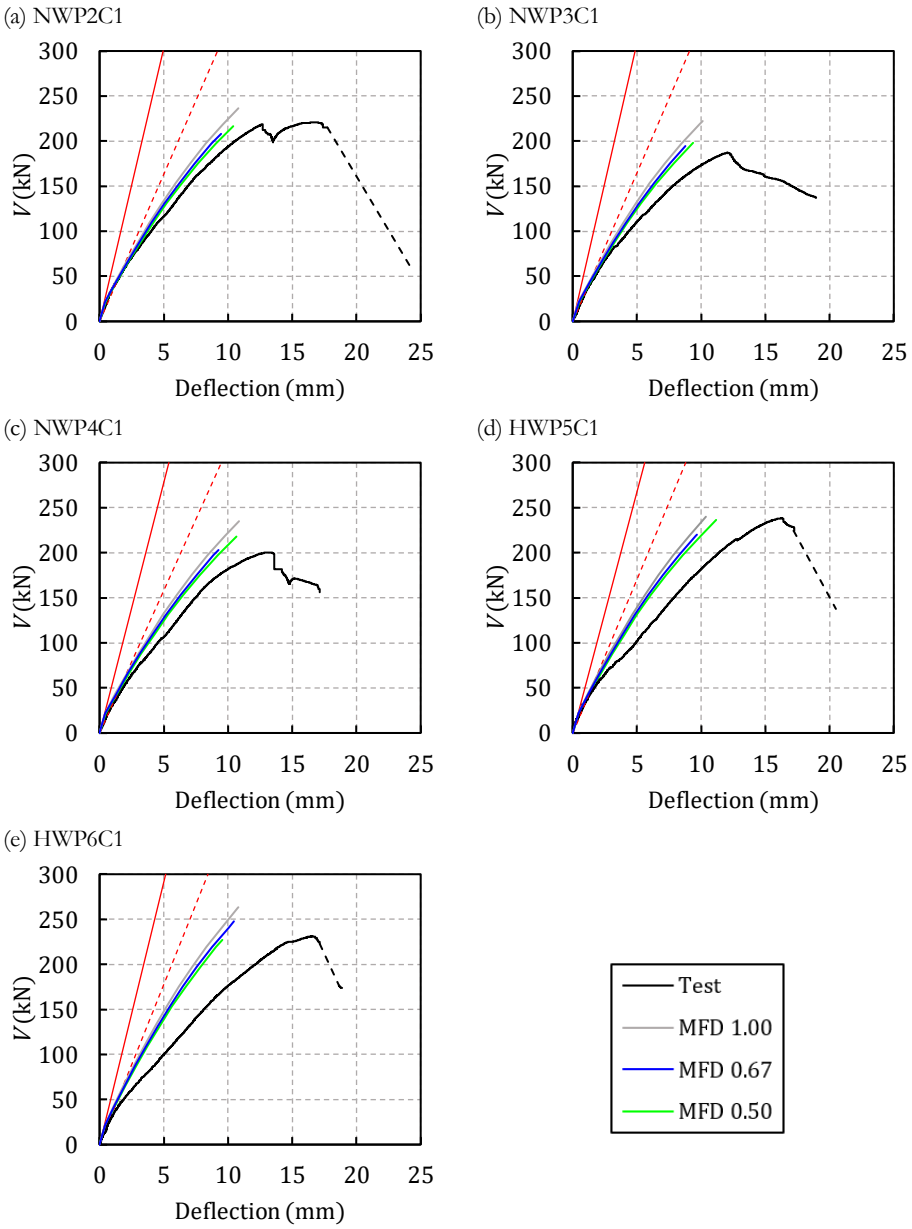

Fig. 26. Experimental shear-deflection curves of the C1 specimens and predicted curves for each effective flange width model: (a) NWP2C1; (b) NWP3C1; (c) NWP4C1; (d) HWP5C1; (e) HWP6C1.

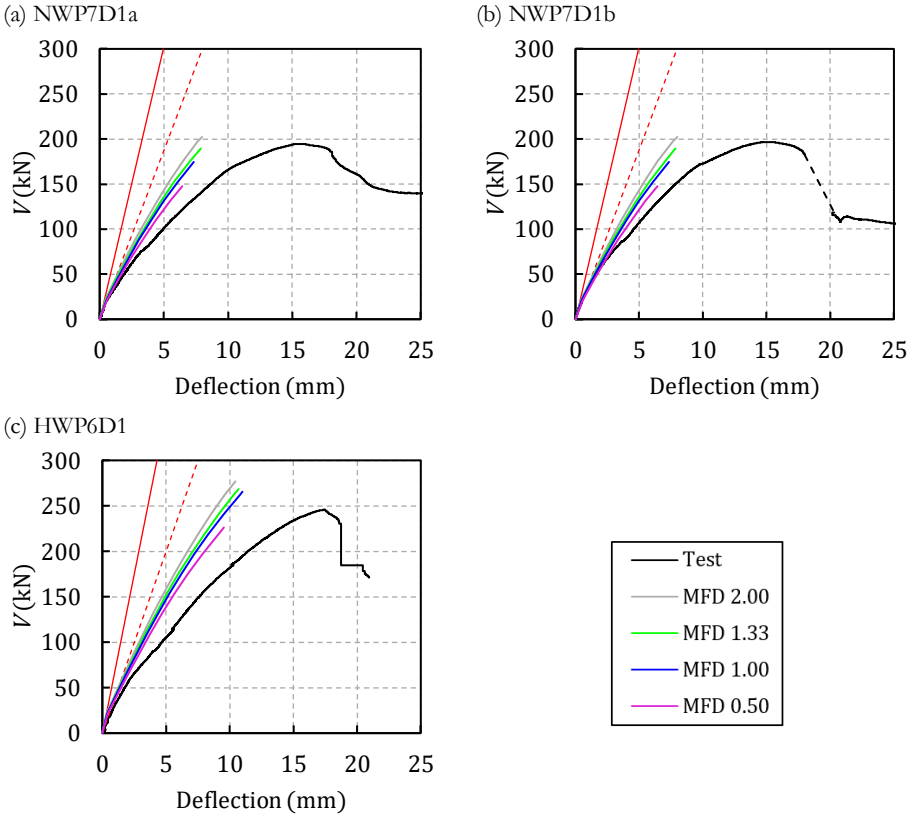

Fig. 27. Experimental shear-deflection curves of the D1 specimens and predicted curves for each effective flange width model: (a) NWP7D1a; (b) NWP7D1b; (c) HWP6D1.

Regarding the specimens with cross-section type D1, the results shown in Fig. 25b and Table 10 indicate the model that better predicted the ultimate shear force was that of MFD = 1.33, with a mean value of 0.99 and a low coefficient of variation (6%). On the other hand, considering the entire flanges width (MFD = 2.00) led to unsafe estimations, considering the default value (MFD = 1.00) gave an adequate prediction (mean value of 1.06) and considering 1/4 of each flange width underestimated the shear strength of the specimens (mean value of 1.24). As observed in specimens C1, the shear-deflection curves presented in Fig. 27 show the stiffness of the curves is reduced when the considered effective flange width decreases. In the first load stages, the stiffness is similar with all the models.

4.3.2. Shear strength increase due to the flanges

In this section, the predicted values of the models developed in ISD are compared to the experimental values to analyse the accuracy of the numerical model in

capturing the effect of flanges on shear strength. To that aim, the predictions for the specimens B1, C1 and D1 are compared. The models were defined taking into account the conclusions derived from the analysis of B1 specimens (Section 3.4). Regarding the effective flange width, the T-shaped specimens were modelled with the MFD that better results gave: 0.67 for specimens C1 and 1.33 for specimens D1.

Table 11 shows the shear strength increase (ΔV) given by the flanges, calculated as $\Delta V = (V_{C1}-V_{B1})/V_{B1}$, where V_{C1} is the shear strength of the T-shaped specimen C1 and V_{B1} is the shear strength of the rectangular specimen B1. This increase is obtained for the numerical models and the experimental tests.

Table 11. Shear strength increase given by the flanges in the specimens C1.

Series	Specimens compared	ΔV model (%)	ΔV test (%)
NWP2	NWP2B1 vs NWP2C1	15.6	22.0
NWP3	NWP3B1 vs NWP3C1	27.6	7.4
NWP4	NWP4B1 vs NWP4C1	27.8	19.2
HWP5	HWP5B1 vs HWP5C1	12.5	15.2
HWP6	HWP6B1 vs HWP6C1	18.7	16.0
Mean		20.4	16.0

Regarding the specimens with cross-section D1, only the beams from series HWP6 could be compared, since HWP5D1 gave an anomalous result and series NWP7 did not have rectangular specimens. The results of comparing the specimens B1 and D1 are shown in Table 12. The increase in shear strength given by the flanges of beam D1 compared to specimen C1 was also calculated, as $\Delta V = (V_{D1}-V_{C1})/V_{C1}$.

Table 12. Shear strength increase given by the flanges in the specimens D1.

Series	Specimens compared	ΔV model (%)	ΔV test (%)
HWP6	HWP6B1 vs HWP6D1	28.5	23.4
HWP6	HWP6C1 vs HWP6D1	8.3	6.4

This analysis proves there is little difference between the increase in shear strength given by the flanges predicted by the model and that experimentally observed in both specimens C1 (Table 11) and D1 (Table 12).

4.4. Conclusions

As a result of the previous analysis on the monolithic T-shaped specimens, the following conclusions can be drawn:

- ISD 21.0 better predicts the shear strength of specimens C1 when a multiplier of flange depth (MFD) of 0.67 is used in the calculation, i.e., when the

compression field is considered to expand into the flanges 2/3 of the flange depth.

- The numerical model of specimens D1 predicts the most accurate result when a MFD of 1.33 is used in the calculation, which is the equivalent to considering the compression field expands into the flanges 8/6 of the flange depth.
- The increase in shear strength given by the flanges in the model is similar to that experimentally obtained: in the specimens C1 the flanges increased shear strength 20.4% in the model *versus* 16.0% in the experimental tests; in the analysed specimen D1 the numerical shear strength was 28.5% higher, while the experimental shear strength was 23.4% higher.

5. Modelling of composite specimens

Due to the limited duration of the doctoral student's stay abroad, only a preliminary analysis of the following composite specimens could be carried out: NWP1B2, NWP2B2, NWP3B2, NWP4B2, HWP5B2, HWP6B2, DWP7B2a and DWP7B2b. Based on these analyses, recommendations for future analysis of composite specimens in ISD are given.

5.1. IDEA StatiCa Detail model definition

To define the models of the composite rectangular specimens, few characteristics were varied with respect to the modelling of monolithic rectangular specimens described in Section 3.1.

First, three concrete layers were defined: beam, slab and interface (see Fig. 28). The beams were modelled with 30 finite elements per smaller dimension. The interface concrete layer depth was equal to the depth of a concrete finite element.

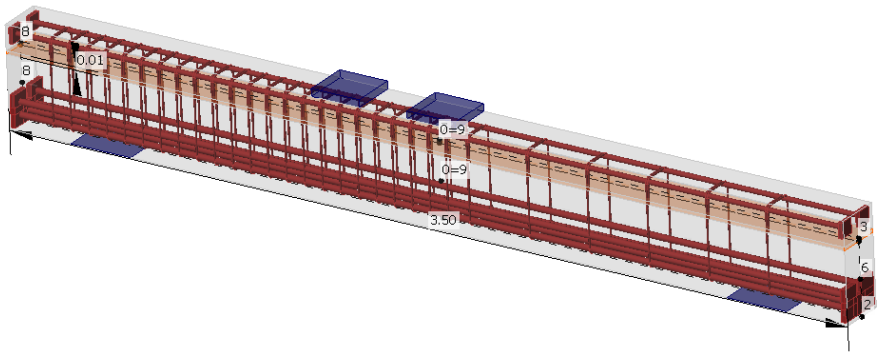

Fig. 28. Example of the geometry and reinforcement definition in ISD for composite rectangular specimens.

Second, the compression softening model of the interface concrete was modified. This was the variable analysed in the composite specimens, so its definition and results are explained in the following.

5.2. Analysed variables

The experimental results of the composite specimens showed that the interface between concretes can be a weakness plane that modifies the trajectory of the diagonal shear cracks by forcing the cracks to develop along it. The weakness of the interface depends on the interface shear strength, so the specimens with a higher interface shear strength can show a monolithic behaviour.

Given the influence of the interface on the crack patterns, the ideas that came up to numerically modelling these specimens were related to weaken the interface strength. In order to weaken the strength of the interface with ISD, a concrete layer was created to represent the interface.

To model the interface between concretes, different techniques were proposed that weaken this layer to generate the formation of a crack in it. The simplest solution was to reduce the compressive strength of the interface concrete. However, this solution was discarded because of the lack of a solid theoretical basis and the difficulty in deciding how much the strength must be reduced for each concrete. Therefore, a solution more consistent with the formulation implemented in ISD was proposed, which was modifying the compression softening law of the interface concrete (the relationship k_{c2} - ε_1 of the concrete).

A model that physically represented the behaviour of the interface was sought: it does not crack if compressed, but weakens or cracks with the appearance of small tension stresses. The difficulty of this technique lies in the definition of the relationship k_{c2} - ε_1. Defining this law would require a detailed study of the interface crack openings in the specimens, since if the interface crack reaches a large crack opening in a short time the k_{c2} would drop suddenly. On the other hand, it would be necessary to study the aggregate interlock normal stresses resisted by the cracked interface, by means of DIC or other techniques. These stresses could be those representing the remaining strength of the concrete for high values of ε_1 (the value of the asymptote in k_{c2} for high values of ε_1). The compression softening law should also depend on the interface roughness, so a more detailed study of the roughness in these specimens should be carried out.

In this preliminary study carried out in this thesis, in the absence of an adequate characterisation of the interface between concretes for each specimen, a general k_{c2} - ε_1 law is proposed for all of them. A compression softening law was proposed which shows a sudden drop in k_{c2} for small tensile strains, since significant crack openings were observed in these specimens. In addition, an average aggregate

interlock normal stress of 1.5 MPa was taken which, for a standard concrete of 30 MPa, gives a k_{c2} of 0.05. With all this, the curve shown in Fig. 29 was defined, which is compared with other curves mentioned above. This curve is given by the parameters L1 = 1, L2 = 1000 and L3 = 1 in Eq. 5 of Section 2.4.4.

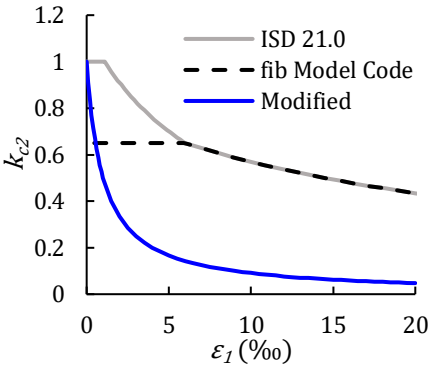

Fig. 29. Modified compression softening law proposed for the interface concrete layer.

In this analysis, two compression softening laws were compared: the compression softening law identified as "Modified" in Fig. 29 (KCMod) and the default compression softening law in ISD (KCDef).

5.3. Results and discussion

Table 13 shows the relationship between the experimental and the predicted value for the eight B2 specimens with the modified compression softening law and the default one. The mean value and coefficient of variation are also indicated. In Fig. 30 and Fig. 31, the shear-deflection curves given by the software for the two models are compared to the experimental curves.

Table 13. Values of V_{exp}/V_{pred} of the different compression softening laws for the eight B2 specimens.

Specimen	KCMod	KCDef
NWP1B2	1.36	1.31
NWP2B2	1.20	1.20
NWP3B2	1.11	0.99
NWP4B2	1.27	1.27
HWP5B2	1.40	1.40
HWP6B2	1.12	1.12
DWP7B2a	1.19	1.06
DWP7B2b	1.27	1.14
Mean	1.24	1.19
CV (%)	8	11

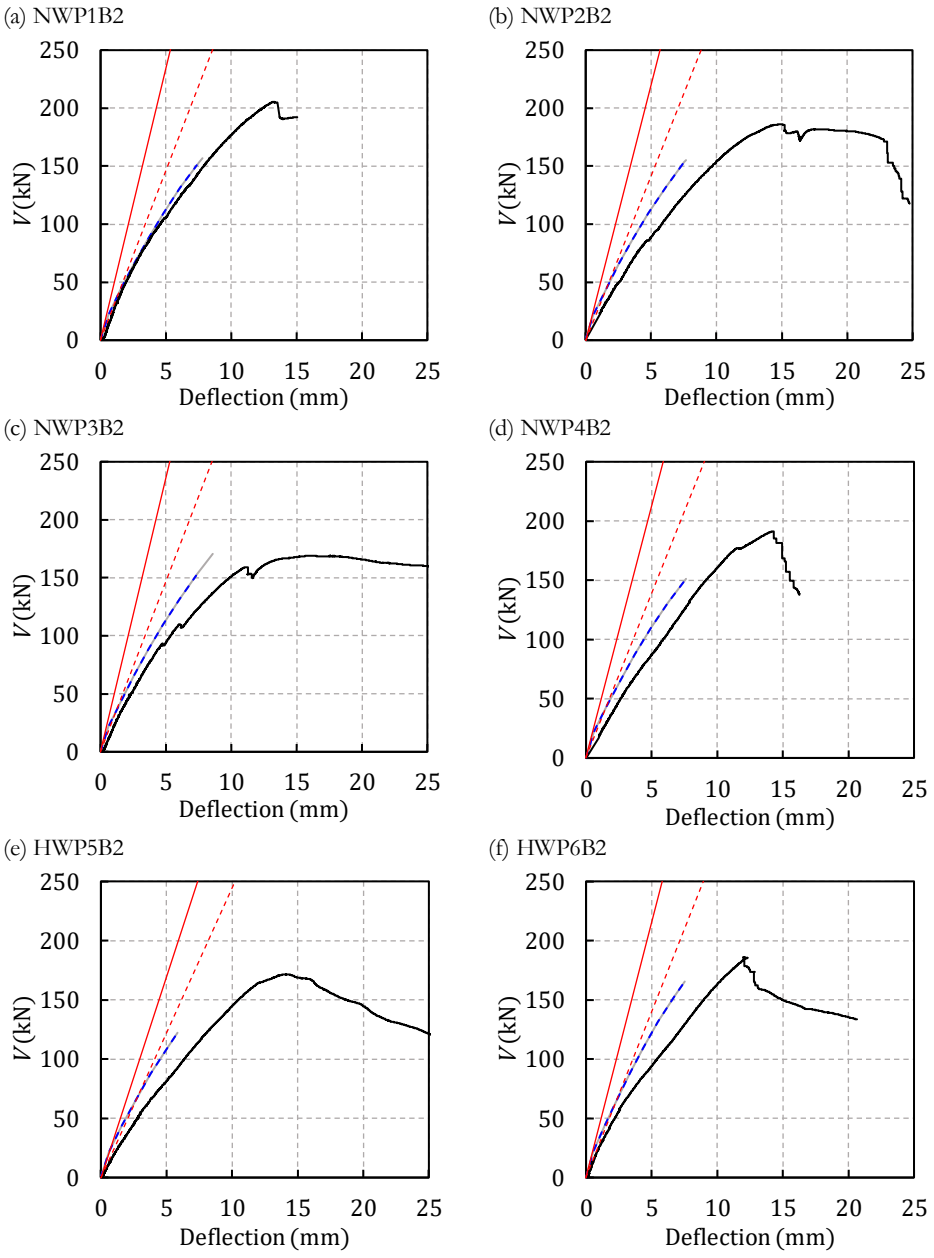

Fig. 30. Experimental shear-deflection curves of B2 specimens and predicted curves for each compression softening law: (a) NWP1B2; (b) NWP2B2; (c) NWP3B2; (d) NWP4B2; (e) HWP5B2; (f) HWP6B2.

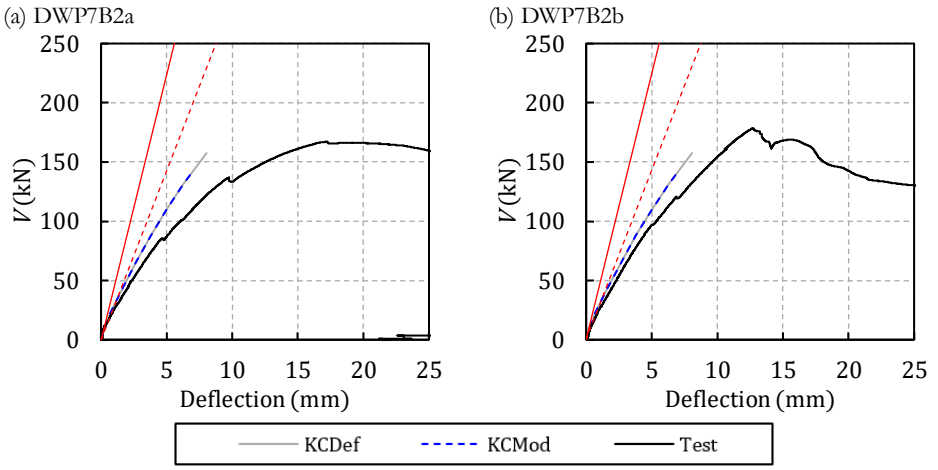

Fig. 31. Experimental shear-deflection curves of B2 specimens and predicted curves for each compression softening law: (a) DWP7B2a; (b) DWP7B2b.

These results show that only in the beams where the slab concrete had a higher compressive strength than the beam concrete (NWP3B2, DWP7B2a and DWP7B2b) and those beams with very similar compressive strengths (NWP1B2), a different shear strength prediction was obtained by weakening the interface concrete. Fig. 32a shows tensile strains appear at the interface between concretes in specimen NWP3B2 and, therefore, k_{c2} decreases at this interface (Fig. 32b). This may be due to the fact that when the slab has a better concrete than the beam, the interface reaches tensile strains at some points, so that decreasing k_{c2} influences the ultimate strength.

In the proposed compression softening law, when there is no tensile strain ($\varepsilon_1 = 0$) k_{c2} is not reduced, which means that if the interface is compressed no cracking occurs. If the model at the interface height shows compressive strains, as in the specimens where the strength of the beam concrete is greater than the strength of the slab concrete, the modified compression softening law will not cause any change in the strength of the element. However, it was experimentally observed in some cases that the interface cracked.

Regarding the low strength predicted by the model in specimen HWP5B2, the model gives an early failure because the slab, where the failure occurs, had a very low compressive strength concrete.

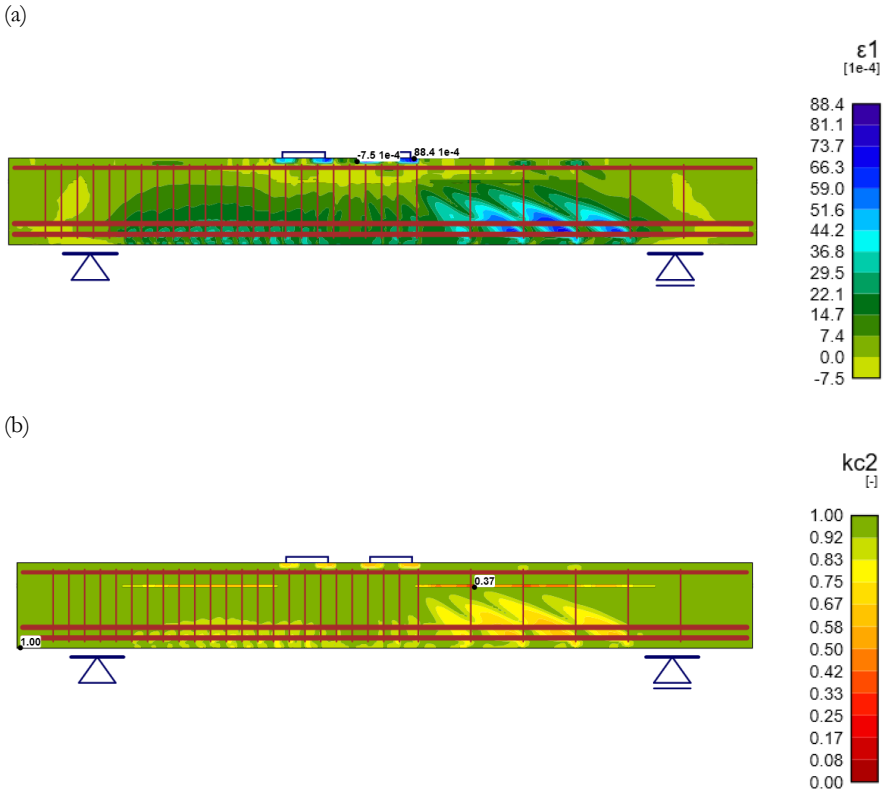

Fig. 32. Results at maximum load of the modified compression softening law for the specimen NWP3B2: (a) ε_1; (b) k_{c2}.

Table 13, Fig. 30 and Fig. 31 show that the predictions of KCMod are very safe. This means that, although the described approach of modifying the compression softening law is considered appropriate for modelling these specimens, the proposed law does not capture well the effect of the interface in the shear strength. The development of a numerical model that adequately represents the interface between concretes would require further work, which is proposed as a future research line.

Besides, the shear strength given by the KCDef model, in which the compression softening law is not modified, is very much on the safety side, and the difference between the predictions of KCMod and KCDef models is small. Thus, further research should be conducted to find out the reasons why the model predictions are very safe in comparison to those for monolithic specimens, preferably by modelling a greater number of composite specimens.

5.4. Conclusions

The preliminary results show that a potential approach to model the construction joint between two concretes in ISD is to weaken the concrete compression softening law in the interface. In this section, some guidelines have been proposed to do so, and one option has been evaluated. The results show that a detailed characterisation of the interface between concretes (e.g., by analysing crack openings and normal stresses at the interface crack) would be needed to derive a compression softening law for the interface concrete on a mechanical basis.

6. Summary and Conclusions

A detailed study on the numerical modelling of the monolithic specimens with web reinforcement of this thesis with the IDEA StatiCa Detail (ISD) software is presented in this chapter. Emphasis is placed on defining the appropriate finite element mesh size, the compression softening law for the concrete and the tension stiffening model for the reinforcement, as well as the effective flange width of the T-shaped specimens. This analysis is a preliminary step to the numerical modelling of the composite specimens, for which a first approach is made on how to model such specimens. The main findings of this analysis, as well as the limitations of the numerical model, are:

- The stress flow shown by the software (mainly the compressive stress fields in concrete and tension stresses in reinforcing bars) gives a good idea of the structural behaviour of the specimens. This can be used to support the definition of strut-and-tie models showing the mechanical behaviour of the specimens.
- The finite element mesh size must be smaller than the concrete cover thickness so that the numerical model does not assign the mechanical properties of the reinforcing steel to the non-reinforced concrete in the concrete cover.
- In the monolithic rectangular beams, the default compression softening law for the concrete implemented in ISD and the default tension stiffening defined in the programme, for both the longitudinal reinforcement and the stirrups, gave very good estimations of the ultimate shear. Regarding the definition of the shear-deflection curve, although these default values were the ones that best modelled the actual behaviour of the specimens, the stiffness of the model curves was much higher than the experimental one, despite the many attempts that were made to improve them in different ways.
- Although the software performs a 2D analysis, the use of a multiplier factor for the expansion of the compression field into the flange in the monolithic T-beams gave a very good estimation of the specimens' shear strengths.

However, again the deformations were not well captured by the programme, as the shear-deflection curves showed the same problem as in the rectangular beams.

- The preliminary analysis of the composite rectangular specimens showed that the best solution for modelling these specimens consists of creating a thin concrete layer that represents the interface and defining a weaker compression softening law for the concrete in this layer. A compression softening law that physically represented the behaviour of the interface was sought: the interface did not crack if compressed but weakened or cracked with the appearance of small tension stresses. A modified compression softening law was compared to the one used in ISD by default. Both models gave very safe estimations of the ultimate shear strength.

The main line of future research proposed for the correct numerical modelling of composite specimens with ISD is:

- Further research should be conducted for the development of a compression softening law that adequately represents the interface between concretes. Defining this law would require a detailed study of the interface crack openings in the specimens and the aggregate interlock normal stresses resisted by the cracked interface. Besides, the compression softening law should also depend on the interface roughness, so a more detailed study of the roughness in experimental tests should be carried out.

7. References

[1] Schlaich J, Schaefer K, Jennewein M. Toward a consistent design of structural concrete. PCI J 1987;32:74–150. https://doi.org/10.15554/pcij.05011987.74.150.

[2] Tjhin TN, Kuchma DA. Computer-based tools for design by strut-and-tie method: Advances and challenges. ACI Struct J 2002;99:586–94.

[3] HanGil IT. n.d. AStrutTie 2020 2020.

[4] Miguel PF, Fernández Prada MÁ, Bonet JL, Pastor JM. Modelo automático para determinar el esquema de bielas y tirantes de una región D de forma cualquiera. II Congr. ACHE, 2002.

[5] IDEA StatiCa. IDEA StatiCa Detail 2018.

[6] Mata-Falcón J, Tran DT, Kaufmann W, Navrátil J. Computer-aided stress field analysis of discontinuity concrete regions. Comput. Model. Concr. Struct., CRC Press; 2018, p. 641–50. https://doi.org/10.1201/9781315182964-77.

[7] Kaufmann W, Mata-Falcón J, Weber M, Galkovski T, Tran DT, Kabelac J,

et al. Compatible stress field design of structural concrete. Principles and validation. 2020.

[8] Fédération International du Béton (fib). Model Code 2010. Ernst & Sohn; 2012.

[9] Marti P, Alvarez M, Kaufmann W, Sigrist V. Tension Chord Model for Structural Concrete. Struct Eng Int J Int Assoc Bridg Struct Eng 1998;8:287–98. https://doi.org/10.2749/101686698780488875.

[10] Alvarez M. Einfluss des Verbundverhaltens auf das Verformungsvermögen von Stahlbeton. Doctoral thesis. Institute of Structural Engineering. ETH Zurich, 1998.

[11] Burns C. Serviceability Analysis of Reinforced Concrete Based in the Tension Chord Model. Doctoral Thesis. ETH Zurich, 2011. https://doi.org/https://doi.org/10.3929/ethz-a-007179384.

[12] Galkovski T, Mata-Falcón J, Kaufmann W. Determination of the effective concrete area in tension relevant for modelling tension stiffening in SLS and ULS design. In: (fib) FI du B, editor. Proc. 2021 fib Symp. Concr. Struct. New Trends Eco-Efficiency Perform., Lisbon: 2021, p. 1598–607.

[13] CEN. EN 1992-1-1:2004. Eurocode 2: Design of concrete structures - Part 1-1: General rules and rules for buildings. 2004.

[14] Vecchio FJ, Collins MP. Modified Compression Field Theory for Reinforced Concrete Elements Subjected to Shear. J Am Concr Inst 1986;83:219–31.

Chapter 7. General discussion of the results

This chapter gives an overview of the previous chapters of the thesis. The work carried out is briefly presented and the main results and future lines of improvement are discussed from a critical point of view. In this way, the reader can read this chapter together with Chapter 1. "Introduction" and get an overview of the work done in this thesis.

Some examples of the most important results are given in this chapter. However, further details can be found in the respective papers of the thesis.

The discussion is divided into three parts: experimental study, mechanical model and numerical model.

1. Experimental study

1.1. Characterisation of the interface between concretes

The first phase of the experimental programme was the characterisation of the interface between concretes in composite specimens with and without shear reinforcement (Chapter 2 in this thesis). The aim was to define the interface roughness and the ratio of reinforcement crossing the interface that led to a shear failure of the specimens influenced by the presence of the interface, i.e., the trajectory of the diagonal shear crack was affected by the interface between concretes. Hence, a pure horizontal shear failure of the specimens or a vertical shear failure like that of monolithic specimens were avoided.

The methodology, experimental results and analysis of the test results were described by means of two conference papers:

- 1st paper: Rueda-García L, Bonet Senach JL, Miguel Sosa PF. Experimental study of concrete composite beams subjected to shear. Proceedings of the fib Symposium 2019: Concrete - Innovations in Materials, Design and Structures, 2019, p. 1779–86.
- 2nd paper: Rueda-García L, Bonet Senach JL, Miguel Sosa PF. Influence of interface roughness and shear reinforcement ratio in vertical shear strength of composite reinforced concrete beams. Hormigón y Acero 2022; 72.

Three composite rectangular specimens without shear reinforcement and four composite rectangular specimens with shear reinforcement were tested. The specimens were simply supported and with two point loads. The characteristics of these specimens are summed up in Table 1 and Fig. 1.

Table 1. Main characteristics of the test specimens for the characterisation of the interface between concretes.

Specimen	Interface roughness	Stirrups	Connectors	Reinforcement layout
SCR0	Very rough	-	-	A
SCR250	Very rough	-	hØ8@250	B
SCR125	Very rough	-	hØ8@125	C
CCL250	Smooth or as cast	Ø8@250	-	D
CCR250	Very rough	Ø8@250	-	D
CCL125	Smooth or as cast	Ø8@250	hØ8@250	E
CCR125	Very rough	Ø8@250	hØ8@250	E

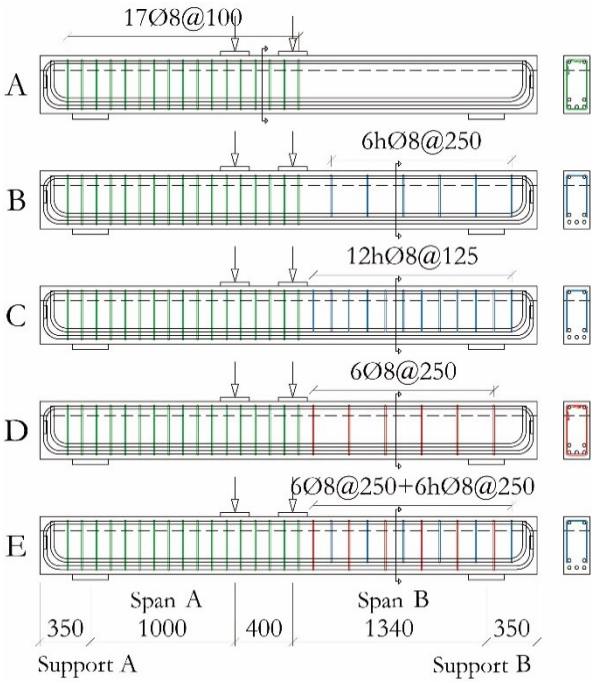

Fig. 1. Reinforcement layouts of the test specimens for the characterisation of the interface between concretes (dimensions: mm).

During the design of these specimens, the predicted failure mode for these beams was determined by comparing the horizontal shear strength and the vertical shear strength given by the current design codes' formulations. Of the three specimens without shear reinforcement, SCR0 and possibly SCR250 were expected to reach their horizontal shear failure before their vertical shear failure. In the specimens with shear reinforcement, the horizontal shear failure was expected only in the specimens with smooth interface (CCL250 and CCL125).

However, the failure observed in the specimens was very different from that expected. Pure horizontal shear failure did not occur in any specimen. Among the specimens without shear reinforcement, specimen SCR0, without any transverse reinforcement, was the only one showing diagonal cracking influenced by the presence of an interface between concretes. On the contrary, the other two specimens showed a crack pattern similar to that of monolithic specimens (see Fig. 2). In the specimens with shear reinforcement, only the crack patterns of those specimens with a smooth interface were influenced by the presence of the interface.

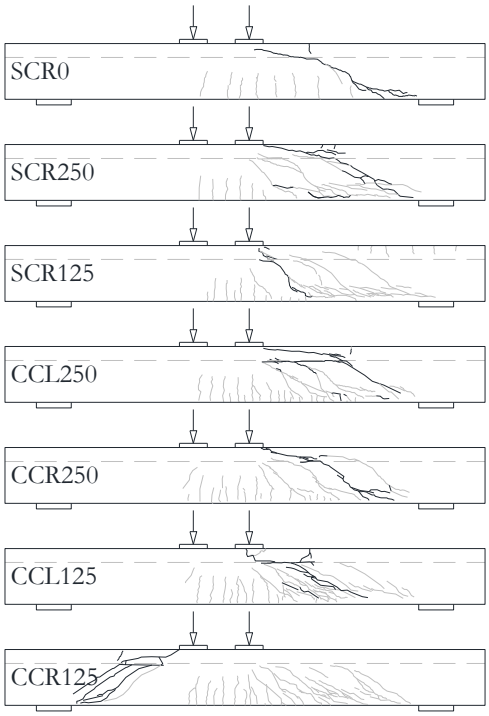

Fig. 2. Crack patterns of the test specimens for the characterisation of the interface between concretes.

The first conclusion drawn from these specimens was that the codes greatly underestimate the horizontal shear strength of concrete interfaces. Through this test programme, the shear strength of the interface could not be defined, as none of the specimens showed horizontal shear failure. However, it was possible to define the ideal interface reinforcement and roughness for the remaining tests of the experimental programme, which were those of specimens SCR0 and CCL250 for the specimens without and with shear reinforcement, respectively. These interface characteristics were chosen because these specimens showed the desired behaviour: in both, diagonal cracking was affected by the presence of an interface between concretes, but no horizontal shear failure occurred, and the specimens did not behave as monolithic beams. The latter two failure modes were not the subject of study in this research.

To experimentally obtain the horizontal shear strength of these specimens, a methodology that used strain gauges placed on the concrete surface and the longitudinal reinforcement was devised. The measurements of these gauges were used to obtain the strains plane at different beam cross-sections and, using the method of global force equilibrium, the horizontal shear stress was obtained at the

stretches between cross-sections. The method gave good results. However, the strength value obtained was a lower bound of the actual horizontal shear strength of the specimens because, as mentioned above, there was no horizontal shear failure in any of the specimens. This method is suitable for specimens with low interface cracking. It could not be used for the specimens with web reinforcement in the experimental programme because they presented, in general, extended interface cracking. To use this methodology, more gauges should be placed above and below the interface at the beam cross-section to obtain the strains plane once the interface is cracked.

Through these tests, it was also found out that the interface connectors placed during the design for increasing the horizontal shear strength of the specimens without increasing their vertical shear strength did not get the desired effect. The shear strengths reached by the specimens showed that these connectors did increase the vertical shear strength despite not being close stirrups. This was because the anchor length of the horizontal shear connectors almost covered the entire beam depth in these specimens. If the beam had had a greater depth, connectors would not have covered the entire web, and thus would not have behaved as vertical shear reinforcement. Should these connectors have been necessary in the subsequent tests to increase the shear strength of the specimens, further research should have been conducted to find adequate connectors that do not increase vertical shear strength in the specimens of the experimental programme.

1.2. Concrete composite beams without web reinforcement

As explained in Chapter 1. "Introduction", the objective of this research was to understand the shear behaviour of precast concrete beams common in civil engineering, such as those used in the construction of road bridges, covered by a cast-in-place slab. To achieve this objective, starting from a simpler approach was necessary before analysing more complex cases. Therefore, in the second phase of the experimental programme the shear behaviour of composite beams without web reinforcement was studied.

The experimental tests carried out in this phase were described and analysed in the following journal article:

- 3rd paper: Rueda-García L, Bonet Senach JL, Miguel Sosa PF, Fernández Prada MÁ. Experimental analysis of the shear strength of composite concrete beams without web reinforcement. Engineering Structures 2021;229:111664. https://doi.org/10.1016/j.engstruct.2020.111664.

In this experimental phase, 21 monolithic and composite specimens with different cross-sectional shapes were tested in shear. The analysed variables were: the cross-sectional shape (see the different shapes in Fig. 3); the presence of an interface

between two concretes (monolithic or composite specimens); the strengths of the two concretes in the composite beams (normal-strength or high-strength concrete); the differential shrinkage between concretes (different times elapsed between the beam and the slab concrete casting). The main characteristics of these beams are summed up in Table 2.

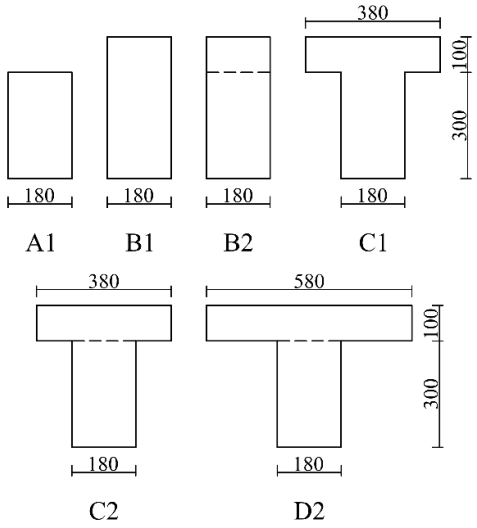

Fig. 3. Cross-section types of the specimens without web reinforcement (dimensions: mm).

Table 2. Characteristics of the specimens without web reinforcement.

Series	Type of beam's concrete	Type of slab's concrete	Days between beam and slab's concrete pouring	Number of specimens for each cross-sectional type					
				A1	B1	B2	C1	C2	D2
NO	NSC	NSC	1	2	2	3	2	2	2
HO	HSC	NSC	1	1	1	1	1	1	1
DO	NSC	NSC	134	0	0	2	0	0	0

To study these specimens, the shear-deflection relationships and the crack-patterns were carefully analysed. The failure modes were described through strut-and-tie models that represented the shear transfer mechanisms observed. Furthermore, the ultimate shear loads of the specimens were compared to analyse the influence of the four test parameters on shear strength. Finally, the vertical and horizontal shear strength predictions of the current design codes were compared to the experimental results.

The shear-deflection relationships revealed the existence of two local maximums in shear load (see the example of Fig. 4). The first maximum corresponded to the

critical shear crack formation. The second local maximum, sometimes higher than the first, was due to the deviation of the compression strut over the critical crack by the arching action mechanism.

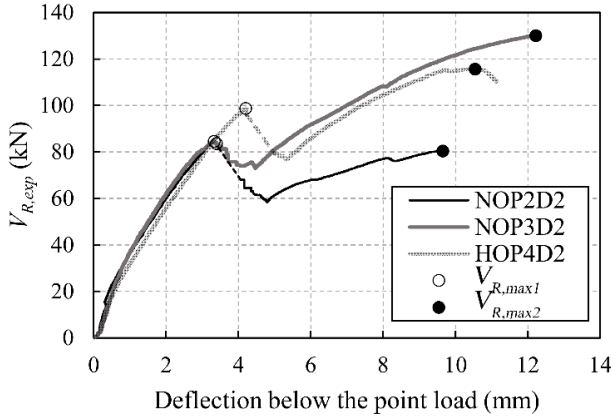

Fig. 4. Shear-deflection relationship of the specimens D2 without web reinforcement.

In the composite rectangular specimens (B2) and the monolithic and composite T-shaped specimens (C1, C2 and D2), the interface between concretes or the cross-section width change in the T-shaped specimens deviated the critical shear crack horizontally along it, as shown in the examples of Fig. 5. The specimens in which the critical shear crack left intact a wide enough depth of the compression chord developed major arching action and thus reached higher second local maximums in shear.

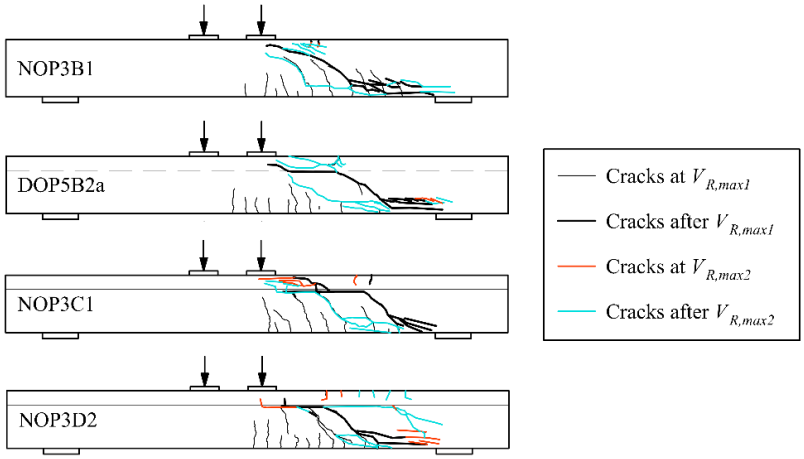

Fig. 5. Examples of crack patterns of beams without web reinforcement.

However, no behaviour pattern was observed on the degradation level of the compression chord after the critical shear crack formation. The high tension longitudinal reinforcement ratio in the beams of this experimental programme (4.0%) could be one of the reasons why the high arch effect could develop in some of the specimens. The great deflection of the longitudinal tie allowed a membrane effect to resist a portion of shear force, as shown in Fig. 6. Consequently, to understand the origin of this behaviour and determine when it will take place, further experimental research should be conducted in the future with different beam dimensions and reinforcement ratios. In the specimens of this experimental programme, it was considered unsafe to take the shear's absolute maximum as the element's shear strength, since the reasons that caused that behaviour were not clear. Thus, the first local maximum in shear was taken as the shear strength of the element.

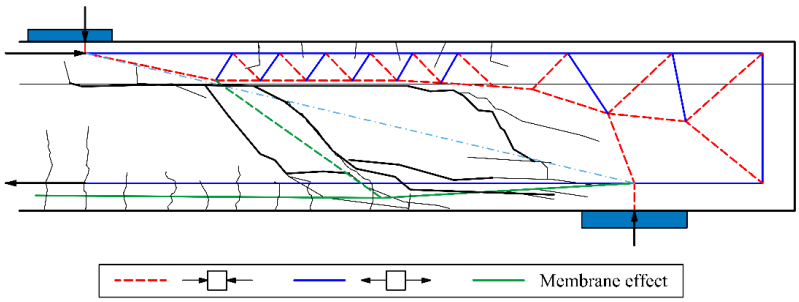

Fig. 6. Arch effect at collapse of the specimens without web reinforcement.

Regarding the test parameters, the following conclusions were drawn:

- The cast-in-place concrete slab increased the element's shear strength compared to the shear strength of only the beam as the slab was seen to add depth to the shear area. This was found out by comparing the specimens A1 and B2 of this experimental programme. However, this conclusion cannot be extended to other specimens, since the interface conditions are key. Consequently, it was specified that this behaviour is possible as long as the horizontal shear at the interface in the composite beams is verified.
- The interface between concretes deviated the direction of the critical shear crack. Regarding the shear strength, little differences were found in the shear's first local maximum. It was even observed that, if a portion of the critical shear crack developed along the interface, the composite beam had a higher shear strength than the monolithic beam, which could be due to the greater compression chord depth. However, this observation was questioned, and the authors concluded that the number of experimental tests for drawing conclusions in this subject was not enough.

- The rectangular and T-shaped specimens had similar shear's first local maximums, because shear strength was governed by the shear transfer actions that occurred at the beam's web. Afterwards, the specimens type D, with wider flanges, reached higher shear's second local maximums than the specimens type C.
- The specimens with HSC in the beam showed slightly greater shear strength than those made of NSC. By comparing the specimens made of HSC and NSC, it was demonstrated that the critical shear cracking was mostly governed by the strength of the web concrete, while the arching action mechanism strength depended on the strength of the slab concrete.
- Differential shrinkage in series DO did not have a significant influence on the vertical shear capacity of the composite beams without shear reinforcement. Although this conclusion cannot be generalized to other beam geometries and weather conditions, for which a more detailed study should be conducted, it is very important for this experimental programme, since it proves the validity of the experimental tests conducted. The results obtained in this test programme can be reference for further studies in this topic that analyse real concrete composite beams, in which normally the time elapsed between the precast beam fabrication and the cast-in-place concrete pouring is greater than 24 hours.

Finally, the current design codes predictions of vertical and horizontal shear strength were compared to the experimental results. This analysis was complemented with a deeper study on the safety of current shear formulations for beams without web reinforcement that was presented in the following conference paper:

- 4th paper: Rueda-García L, Bonet JL, Miguel Sosa PF, Fernández Prada MÁ. Safety assessment of shear strength current formulations for composite concrete beams without web reinforcement. In: Fédération Internationale du Béton (fib), editor. Proceedings for the 2021 fib Symposium. Concrete Structures: New Trends for Eco-Efficiency and Performance, Lisbon: 2021, p. 2305–14.

In this paper, the authors' experimental results were analysed together with 17 specimens taken from a previous study about composite elements by Kim *et al.* [1]. The vertical shear strength predictions were calculated in four ways: considering only the beam's shear strength and considering the entire composite beam's shear strength using the minimum compressive strength of the beam and slab concretes, the beam concrete compressive strength or the weighted average of the beam and slab compressive strengths, obtained from the area ratio of both concretes.

These research works concluded that:

- The existing formulations were more accurate when assessing the shear strength of the monolithic specimens than the composite specimens. Therefore, the need to incorporate a calculation methodology into design codes that adapts to composite concrete elements without web reinforcement was found.
- The formulations showed greater dispersion for the composite specimens made of different compressive strength concretes than for those made with equal compressive strength concretes. Thus, the formulations were not able to capture the effect of the beam concrete compressive strength on the shear strength of the elements.
- For the monolithic beams of this experimental programme, EC2 [2] provided unsafe estimations of the shear strength.
- When only the beam was considered to resist shear in the composite specimens, all the considered codes (EC2, EC2-20 D7 [3], MC-10 [4] and ACI 318-19 [5]) gave very safe results.
- When the entire composite effective depth was considered, EC2 provided unsafe estimations. The other codes gave in general safe estimations. Although the use of the entire effective beam depth and the beam concrete compressive strength is commonplace for calculating shear strength [6,7], and may be on the safety side if the beam's depth is much higher than that of the slab, this method proved slightly unsafe for the beams in this analysis when they were assessed with EC2-20 D7. Consequently, the best method for predicting the shear strength of composite beams without web reinforcement according to this analysis was the formulation of EC2-20 D7 with the entire composite beam's effective depth and the weighted average of the compressive strengths of the beam and slab concretes.
- Regarding the horizontal shear strength of the specimens, the codes highly underestimated the strength. Therefore, the required interface reinforcement to prevent horizontal shear failure is overestimated.

The results of this experimental programme on beams without web reinforcement are considered interesting in this field, given the limited number of experimental research on composite specimens without shear reinforcement. However, as observed above, further research should be conducted on beams with different dimensions and reinforcement ratios to delve in this study.

1.3. Concrete composite beams with web reinforcement

In this third phase of the experimental programme, which was the biggest in number of experimental tests and variables studied, specimens with web reinforcement were analysed.

1.3.1. Rectangular specimens

Given the large number of specimens tested at this stage, first the monolithic and composite specimens with rectangular cross-section were analysed. The experiments were described and studied in the following journal article:

- 5th paper: Rueda-García L, Bonet Senach JL, Miguel Sosa PF, Fernández Prada MA. Analysis of the shear strength mechanism of slender precast concrete beams with cast-in-place slab and web reinforcement. Engineering Structures 2021;246:113043. https://doi.org/10.1016/j.engstruct.2021.113043.

In this paper, 18 monolithic and composite rectangular specimens with web reinforcement, with equal and different cross-sectional depths, compressive strengths of the beam and slab's concretes, and different concrete ages, were experimentally tested. The specimens had the cross-sections A1, B1 and B2 defined in Fig. 7. Table 3 describes the main characteristics of the series of specimens analysed in this paper. A fixed shear reinforcement ratio of 0.22% was selected.

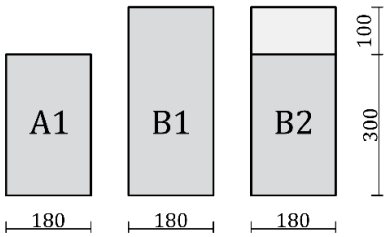

Fig. 7. Cross-section types of the rectangular specimens with web reinforcement (dimensions: mm).

Table 3. Series of the experimental programme of rectangular specimens with web reinforcement.

Series	Type of beam's concrete	Type of slab's concrete	Days between beam and slab's concrete pouring	Number of specimens per cross-sectional type		
				A1	B1	B2
NW	NSC	NSC	1	3	3	4
HW	HCS	NSC	1	2	2	2
DW	NSC	NSC	134	0	0	2

The shear strengths, shear-deflection relationships and instrumentation results were analysed. The crack patterns were carefully studied. Big differences were found in the crack patterns of monolithic and composite specimens, as shown in the examples of Fig. 8. In most specimens, the interface between concretes modified the crack pattern of the composite beams *versus* that of monolithic beams by forcing diagonal cracks to develop along the interface.

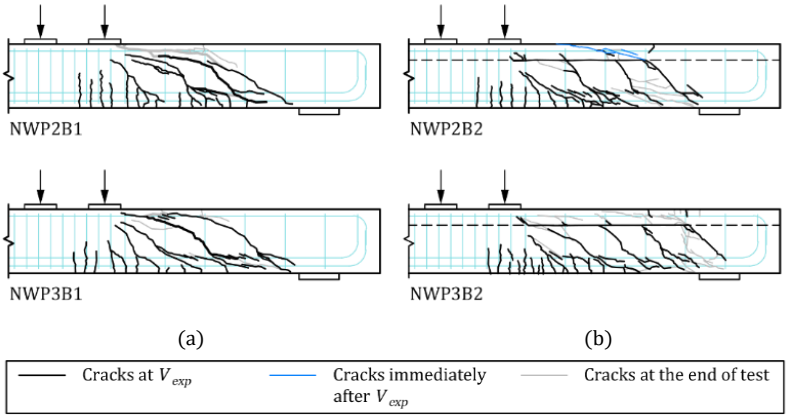

Fig. 8. Examples of crack patterns in rectangular beams with web reinforcement: (a) monolithic specimens; (b) composite specimens.

The effect of test parameters was analysed:

- Placing a cast-in-place slab on top of the precast beam increased the element's shear strength. However, this shear strength increase cannot be generalised to specimens of other dimensions and characteristics, since the contribution of the cast-in-place slab to shear strength depends on the horizontal shear strength of the interface.
- As indicated above, the interface modified the crack pattern, however, in specimens with similar concrete compressive strength in both the beam and slab the interface did not significantly modify the element's shear strength, regardless of the interface presenting more or less cracking. The composite beams with higher concrete compressive strength in the precast beam than in the slab showed lower shear strengths than their homologous monolithic specimens made with the same concrete as that of the precast beam.
- It was again verified that a marked differential shrinkage between concretes did not significantly modify the shear strength of the composite beams in this experimental programme in relation to that of those specimens with reduced differential shrinkage. Thus, as indicated in Section 2.2, the experimental tests of this test programme can be used as reference for further studies in this topic.

An important part in this paper was the analysis of the shear strength mechanisms. These mechanisms were captured in a strut-and-tie model for explaining the mechanical behaviour of the composite specimens with extended interface cracking (such as those shown in Fig. 8). The proposed strut-and-tie model was based on the crack patterns of the specimens and other experimental results like the shear-

deflection relationships, which showed abrupt or gradual load drops, and the strain gauges measurements, which measured strains at the reinforcement and the concrete surface.

The main characteristics of this preliminary model were:

- In the specimens with extended interface cracking of this experimental programme, shear was transmitted through two load paths: one through the precast beam; one through the cast-in-place slab. Consequently, the total shear resisted by the composite beam had two components: the shear resisted by the precast beam and the shear resisted by the cast-in-place slab. The transmission of horizontal forces between both load paths occurred through the interface crack due to the aggregate interlock at the crack and the dowel action of the transverse reinforcement crossing the crack.
- The mechanical model proposed to assess the shear strength of the composite elements in this experimental programme adapted to each specimen's crack pattern as shown in Fig. 9. Three possible variants of the strut-and-tie model (Variant A, B and C) were identified in the test specimens.
- The shear transmission through the precast beam was modelled using a double truss strut-and-tie model in which the failure criterion was the yielding of stirrups. The shear transmission through the cast-in-place slab was modelled by a simple truss strut-and-tie model without shear reinforcement in which two possible failures were considered: the slab bending failure due to the yielding of the slab longitudinal reinforcement or the slab shear failure when its concrete stresses reached the Kupfer's failure surface.
- Once known the variant of the strut-and-tie model for each specimen, the shear strength could be predicted. Very accurate results for the 6 specimens assessed with this model were obtained.

The formulation of this preliminary model can be checked in the 5th paper (Chapter 4). The proposed model presents multiple limitations for its use in specimens of other characteristics and reinforcement, since it was created to assess the specimens of this experimental programme. However, it lays the foundations for the further development of a shear formulation for composite elements, which was explained in Chapter 5 and will be discuss in Section 3 of this chapter.

To conclude with this paper, the shear strengths of the specimens were assessed with the current codes shear formulations. For beams with web reinforcement, the formulation of EC2 gave the most accurate result, similar to those given by the level III approximation of MC-10 and the formula (b) of ACI 318-19 when the weighted average of the compressive strengths of beam and slab concretes was used. Besides, the proposed mechanical model was used to predict the shear strength of the composite specimens considering the worst scenario (greatest interface cracking) since the interface crack extension is unknown, and provided very good estimations.

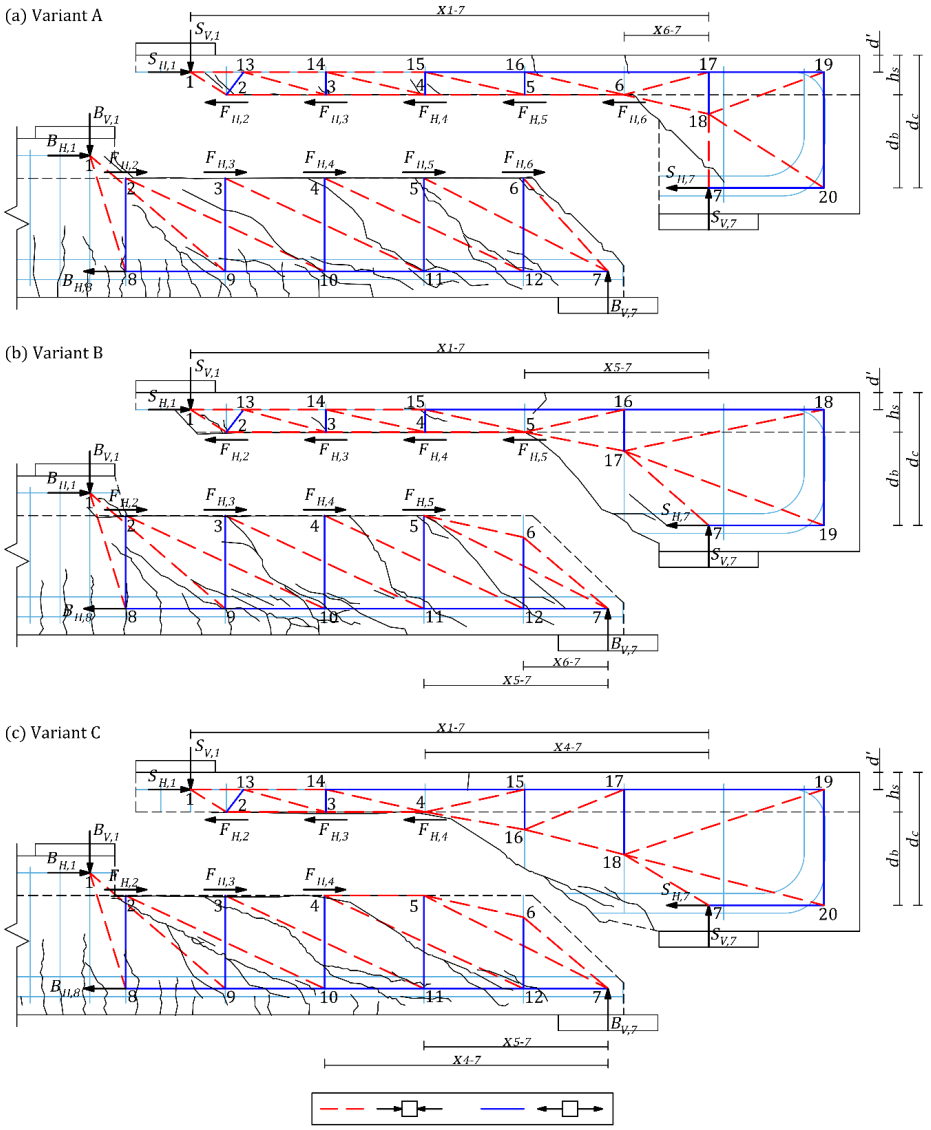

Fig. 9. Proposed strut-and-tie models for the precast beam and the cast-in-place slab separately: (a) Variant A (specimen NWP3B2); (b) Variant B (specimen NWP2B2); (c) Variant C (specimen NWP1B2).

This study marked the beginning of the development of a lower-bound plasticity-based model for predicting the shear strength of concrete composite elements. Although it was not among the initial objectives of the thesis, this analysis of shear

strength mechanisms by means of strut-and-tie models has greatly enriched this research.

1.3.2. T-shaped specimens

The specimens composed of a rectangular precast beam and a cast-in-place slab on top, forming composite T-shaped specimens, were studied in:

- 6th paper: Rueda-García L, Bonet Senach JL, Miguel Sosa PF, Fernández Prada MÁ. Experimental study on the shear strength of reinforced concrete composite T-shaped beams with web reinforcement. Engineering Structures 2022;255:113921. https://doi.org/10.1016/j.engstruct.2022.113921.

In this paper, 19 monolithic and composite T-shaped specimens were tested in shear with the following variable parameters: flange width, presence of an interface between concretes, and beam and slab's concrete strengths. The specimens had the cross-sections C1, C2, D1 and D2 defined in Fig. 10. Table 4 describes the main characteristics of the series of specimens analysed in this paper. The longitudinal and transverse reinforcement ratios and geometrical characteristics were fixed and equal to those of the previous tests to make them comparable.

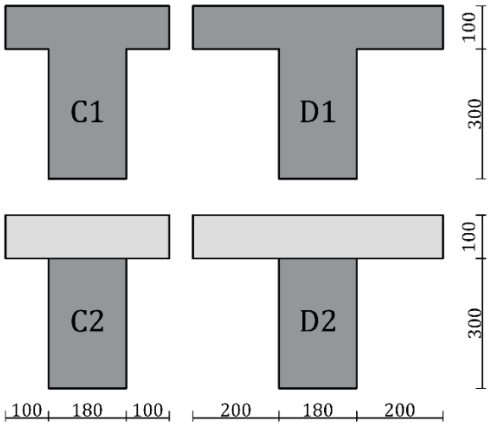

Fig. 10. Cross-section types of the experimental programme on T-shaped beams with web reinforcement (dimensions: mm).

Table 4. Series of the experimental programme on T-shaped beams with web reinforcement.

Series	Type of beam's concrete	Type of slab's concrete	Number of specimens per cross-sectional type			
			C1	C2	D1	D2
NW	NSC	NSC	3	3	2	3
HW	HCS	NSC	2	2	2	2

Following the procedure of the previous paper [8], the crack patterns were carefully analysed. As shown in the example of Fig. 11, both the cross-section width change plane in the monolithic T-beams and the interface in the composite T-shaped specimens deviated the diagonal cracks horizontally along them.

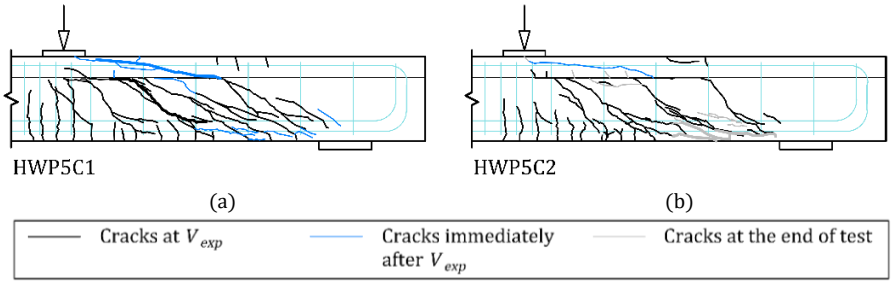

Fig. 11. Examples of crack patterns in T-shaped beams with web reinforcement: (a) monolithic beam; (b) composite beam.

By studying the crack patterns and other instrumentation results, an in-depth analysis of the shear strength mechanisms and failure modes of the specimens of this experimental programme was conducted by adapting to the specimens of this programme the mechanical model proposed in the previous paper [8], which explained the results obtained on the influence of the studied parameters. The adapted model accounted for the effect of flanges.

The horizontal crack at the cross-section width change derived in a shear strength mechanism similar to that of composite specimens. Thus, the model was also applied to monolithic T-shaped specimens.

By adapting the proposed model to T-shaped specimens an additional failure mode was defined, which was the interface failure, in which the maximum load was determined by the load that produced crack prolongation at the interface. The formulation for calculating this failure mode was also developed.

The 19 specimens were assessed with the proposed model by identifying first the variant of the strut-and-tie model (A, B or C) that better fitted them and calculating the shear strength of the slab given by the three failure modes: slab bending failure (BF), slab shear failure (SF) and interface failure (IF). The slab's shear strength was the minimum value between those obtained for the slab's three failure modes. The model gave excellent results at predicting the ultimate shear load: mean value of the relationship between the experimental and predicted shear strength of 1.02, with a coefficient of variation of 6.07%.

The test parameters were analysed by comparing specimens to one another, and also to the rectangular specimens of the previous study carried out by the authors in [8]. The main conclusions were:

- In the specimens with slab shear failure (all the monolithic specimens and some composite specimens), the presence of flanges increased shear strength. In this research work specimens, the shear strength increased in the same proportion as the shear-effective area increases when considering an effective slab width that equals the sum of the web width and flange depth (approx. 17%). This experimental observation was especially important for the future development of shear predictive models for T-shaped specimens.
- Most of the specimens with extended interface cracking, which were composite specimens in this test programme, showed slab bending failure, and flanges did not increase shear strength.
- The presence of an interface between concretes decreased the specimens' shear strength, since the greater interface cracking resulted in less resistant failure mechanisms, such as slab bending failure in the beams with extended interface cracking.
- The shear strength of the tested specimens that presented an extended interface cracking did not depend on the compressive strength of either the beam or slab's concrete, since, according to the proposed model, their shear strength is given by the yielding of the slab's longitudinal reinforcement. The shear strength of the specimens in which interface cracking was short depended on the compressive strength of the slab's concrete, since the shear strength is given by the slab failing in shear.

All these experimental conclusions agreed with the proposed mechanical model. Of course, the number of tests is reduced and therefore limitations must be taken into account, but having experimental evidence of the defined shear strength mechanisms is a step forward towards the development of a predictive model.

Current codes formulations for shear strength were also verified with the experimental results. EC2 gave the best result for the monolithic specimens, but still extremely safe as no code accounts for the flanges effect on shear strength. EC2, the level III approximation of MC-10 and equation (b) of ACI 318-19, using the weighted average of the beam and slab's concrete compressive strengths, offered the best estimations for composite T-shaped specimens, on the safety side. The shear strengths were also calculated with the proposed formulation, assuming the weakest shear strength mechanisms observed in the experimental tests since the crack extension is unknown prior to testing. The model gave the most accurate result for monolithic specimens and slightly better predictions than the current codes for composite specimens.

At the end of the paper, some basic recommendations for practice were given. First, the improvement of the interface shear strength of composite beams for increasing their shear strength. This will derive in the specimen having a slab shear failure. In this case, the slab width and the slab's concrete strength could be increased with the same purpose. If the interface shear strength cannot be improved, the composite specimen's shear strength can be safely predicted with the proposed model for beams with extended interface cracking. Nonetheless, it was highlighted that the results and the discussion of the experimental analysis were derived from the tested specimens' dimensions, reinforcement and concrete quality, and further research should be conducted to draw better recommendations for practice.

1.3.3. T-beams with cast-in-place slab

The last phase of the experimental programme consisted of testing T-beams covered by a cast-in-place slab. The test specimens and their results were described in:

- 7th paper: Rueda-García L, Bonet Senach JL, Miguel Sosa PF, Fernández Prada MÁ. Experimental analysis of the shear resistance of precast concrete T-beams with a top cast-in-place slab. 2022.

This experimental research was motivated by the knowledge that both the interface between concretes and the section width change modify the crack pattern and, thus, the shear strength mechanisms of the specimens. The aim of this paper was to study the contribution of the cast-in-place slab to shear strength in structures which have both weakness planes, like T-beams with a cast-in-place slab on top, since they are commonly used in precast construction. These reinforced concrete elements would be the last step before analysing precast prestressed girders with cast-in-place slab.

In this paper, 6 T-shaped specimens made of reinforced concrete with shear reinforcement and subjected to shear forces were experimentally tested. The following items that influence the shear strength were analysed by comparing different cross-section types and concrete qualities: the presence of a cast-in-place slab on top, the presence of an interface between concretes, the cast-in-place slab width and the compressive strength of the beam and slab concretes. The cross-sectional shapes showed in Fig. 12 were studied, made of normal-strength concrete (NSC) at both the beam and the slab, and with high-strength concrete (HSC) at the beam and NSC at the slab. Besides, the specimens were compared to the specimens C1 of the previous study to analyse the contribution of the cast-in-place slab to shear strength. The longitudinal and transverse reinforcement ratios were fixed and equal to those of the previous studies. The a/d ratio was also fixed and equal to that of the previous beams (4.0).

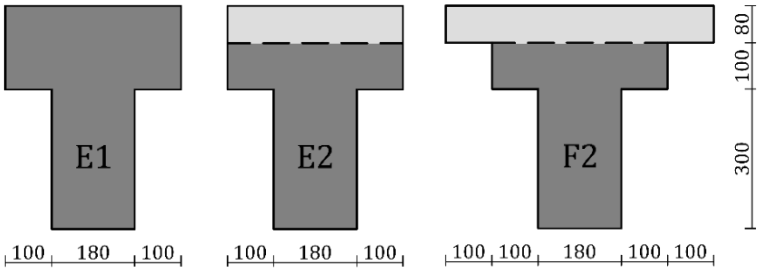

Fig. 12. Cross-section types of the experimental programme on T-beams with cast-in-place slab (dimensions: mm).

The crack patterns were analysed (see two examples in Fig. 13).

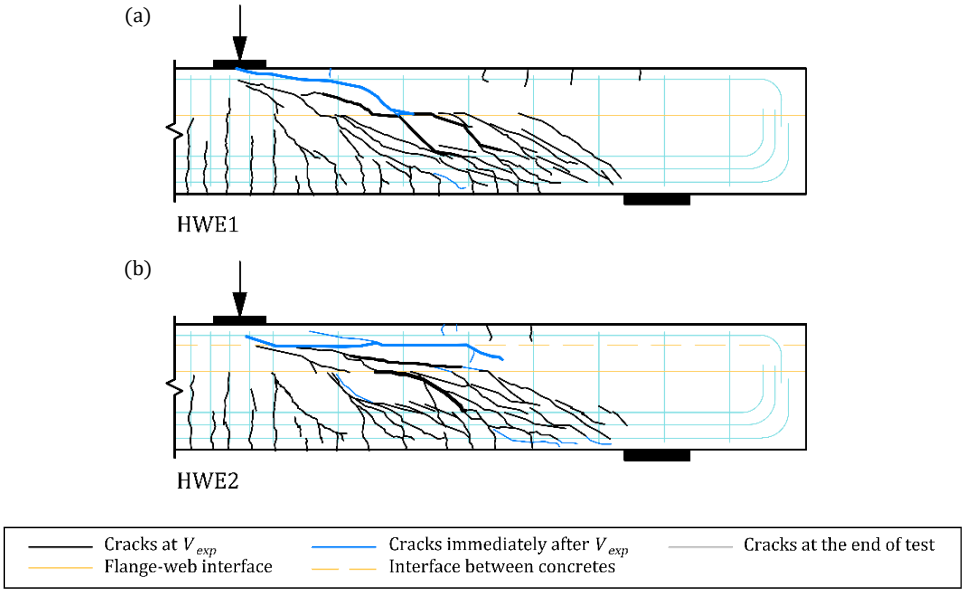

Fig. 13. Crack pattern examples of the T-beams in different test stages: (a) monolithic specimen; (b) composite specimen.

With the support of a similar strut-and-tie model to that previously proposed, the shear strength mechanisms were explained. In the monolithic T-shaped beams, the cross-section width change was a weakness plane that deviated the diagonal shear cracks along it and divided the shear transmission into two load paths: one through the beam web below the cross-section width change; one through the beam head or flanges. Failure occurred when the upper path, that at the flanges, reached its shear strength.

The T-shaped beams with cast-in-place slab on top (composite beams) had the same behaviour as the monolithic T-shaped beams until the maximum load. After that, the interface between the T-shaped beam and the slab cracked in the tested specimens. Thus, the failure occurred when the interface shear stress exceeded the interface shear strength.

Understanding properly the shear strength mechanisms was key to explain the influence of the variables considered on the shear strength of the specimens. These were the main conclusions:

- Regarding the contribution of the cast-in-place slab to shear strength, the experimental results showed that the shear strength of the composite specimen was an intermediate value between the shear strengths of the T-shaped specimen with no cast-in-place slab and the monolithic T-shaped specimen with the same depth as the composite specimen. The higher or lower strength was given by the interface shear strength.
- A wider cast-in-place slab did not increase the specimens' shear strengths. In fact, the specimens with a wider slab and made entirely with NSC showed a premature interface failure, which could be due to the rise in the neutral axis that made interface shear stresses increase. This conclusion was found very interesting. However, it was drawn from a limited number of experimental tests, so its generalisation is questionable.
- The use of high-strength concrete at the precast beam in composite specimens increased the shear strength. This observation was explained by means of the greater inclination of the compression struts at the beam web due to the better-quality concrete. The better concrete also decreased the interface shear stresses due to the higher location of the neutral axis, which postponed the interface failure. Again, this conclusion was found very important for the future development of a shear formulation for composite elements, but it should be proved in more experiments.

Finally, the test results were compared with the existing code provisions for shear strength. In this paper, three shear strength values were calculated for composite specimens: that which produces interface failure ($V_{pred,if}$); the shear strength of the precast beam alone ($V_{pred,pb}$); the shear strength of the entire composite specimen as if it were a monolithic beam ($V_{pred,mb}$). The predicted shear strength V_{pred} was taken as $V_{pred} = \min\{V_{pred,mb}; \max\{V_{pred,pb}; V_{pred,if}\}\}$, since it was considered the most appropriate interpretation of the design codes. The main finding was that the current codes give very safe results since the shear strength of flanges is neglected and the interface shear strength is underestimated. For these specimens, ACI 318-19 gave the most accurate result with a low coefficient of variation, which shows that the effect on shear strength of concrete compressive strength is well captured by this formulation.

Although some interesting findings were derived from these tests, the authors understand further research should be conducted on more specimens to consolidate these conclusions and develop a shear strength formulation for the shear assessment of these elements.

2. Mechanical model

During the analysis of the experimental tests, a strut-and-tie model for assessing the specimens' shear strengths was developed. This model had certain limitations:

- First, the model variant (A, B or C) must be known, since the formulae to calculate the shear components resisted by the precast beam and the slab depend on it and the crack pattern of the specimen at the maximum shear load must be known to determine the variant of the model.
- Second, the model is not generically applicable, since the formulae are exclusive for the strut-and-tie models proposed for the authors' specimens.

Consequently, the necessity of developing a generalized and simplified model based on the original model was found. This lower-bound plasticity-based model to predict the shear strength of concrete composite beams and monolithic T-shaped beams no longer needed the prior knowledge of the specimen's crack pattern. The development of this simplified model was explained in Chapter 5:

- 8th paper: Rueda-García L, Bonet Senach JL, Miguel Sosa PF, Fernández Prada MÁ. Shear strength prediction of slender reinforced concrete composite beams and monolithic T- and I-shaped beams with web reinforcement. 2022.

The model's concept is based on the cracking of the weakness plane, so that the shear strength of the beam is given by the sum of the shear strengths of the two transmission paths in which the interface crack divides the shear load: the shear strength of the precast beam or the web below the section width change, and the shear strength of the slab or the beam head.

The model includes the interface shear strength of the weakness plane in its formulation, which is a novel element with respect to the original model. The model takes into account the interface shear strength (by means of $cot\theta_{int}$) or the maximum concrete stress in the compression field (by means of $cot\theta_{str}$) to determine the shear strength of the precast beam (V_{pb}).

The maximum shear load is given by the slab failure. The model can distinguish different types of slab failure. When interface shear limits the shear strength of the precast beam, interface cracking is likely, so that the slab strength is given by the minimum of the shear forces resisted by the slab failing in bending ($V_{s,BF}$) and the slab failing in shear ($V_{s,SF}$). Otherwise, the slab is considered to fail in shear in T-

shaped beams ($V_{s,SF}$) or the specimen is treated as a monolithic specimen in composite rectangular beams (V_{pred} of EC2).

The guidelines for the application of the mechanical model are summed up in Table 5. The specific formulae are indicated in Table 6. For further explanations, see Chapter 5 of the thesis.

Table 5. Guidelines for the application of the proposed simplified mechanical model.

Requirement	Composite rectangular specimens	Monolithic and composite T- and I-shaped specimens
$cot\theta_{str}$ (1) < $cot\theta_{int}$ (2)	$V_{pred} = V_{pred}$ (EC2) using $f_{c,b}$	$V_{pred} = V_{pb}$ (4) + $V_{s,SF}$ (8-13)
$cot\theta_{str}$ (1) ≥ $cot\theta_{int}$ (2)	▪ If $A_{sl} > 0$, $V_{pred} = V_{pb}$ (4) + min{$V_{s,SF}$ (8-13), max{$V_{s,BF}$ (6); $V_{s,BF}$ (7)}} ▪ If $A_{sl} = 0$, $V_{pred} = V_{pb}$ (4) + min{$V_{s,SF}$ (8-13), $V_{s,BF}$ (7)}	

The formulae of Table 6 are indicated in brackets.

To verify the mechanical model, a database of 105 slender reinforced concrete specimens subjected to point loads and failing in shear with web reinforcement, obtained from 15 different groups of authors, was created in this paper: 24 composite rectangular specimens, 28 composite T-shaped specimens consisting of a rectangular precast beam with a cast-in-place slab on top and 53 monolithic T- and I-shaped specimens.

The proposed model was used to predict the shear strengths of those specimens. An assumption for applying the model to the specimens of the database was found necessary, which was the definition of a parameter α that multiplied the interface shear strength obtained from Eq. (3), as this formula, taken from EC2, highly underestimated the interface shear strengths.

To estimate this multiplier α, the 286 results of interface shear-transfer experiments from 13 different authors, collected in a database by Soltani and Ross [9], were assessed with the EC2 formulation for interface shear (Eq. (3)). A total of 38 specimens with a "smooth" interface, 184 with a "rough" interface and 64 specimens casted monolithically were used. The multiplier α was defined for the three interface roughness considered.

The proposed model gave good results for the mean value and coefficient of variation (CV) of the relationship between the experimental and the predicted shear strengths for the 3 specimen types analysed: a mean value of 1.24 and a CV of 12.00% for composite rectangular beams, 1.32 and 16.17% for composite T-shaped beams, and 1.07 and 10.46% for monolithic T- and I-shaped beams. The model results were also compared to those of the current design codes and gave better estimations in all cases.

Table 6. Formulae of the proposed simplified mechanical model.

Variable	Formula	
$cot\theta_{str}$	$1.0 \le \cot\theta_{str} = \sqrt{\frac{\upsilon \cdot f_{c,b}}{\rho_w \cdot f_{yw}} - 1} \le 2.5$	(1)
$cot\theta_{int}$	$\cot\theta_{int} = \frac{\tau_R \cdot b_w \cdot s}{T_w} \ge 1$	(2)
τ_R	$\tau_R = c \cdot f_{ct} + \rho_i \cdot f_{yw} \cdot \mu \le 0.5 \cdot \nu \cdot f_c$	(3)
V_{pb}	$V_{pb} = \frac{T_w \cdot d_b \cdot \min\{\cot\theta_{str}, \cot\theta_{int}\}}{s}$	(4)
R_H	$R_H = V_{pb} \cdot \frac{a - s}{d_b}$	(5)
$V_{s,BF}$	Yielding of the slab longitudinal reinforcement: $V_{s,BF} = \frac{R_H \cdot (h_s - d') \cdot d_b + T_l \cdot (h_s - d') \cdot (d_c - d')}{a \cdot d_b - s \cdot (d_c - d')}$	(6)
	Slab's most highly tensioned fibre reaches the tensile strength of the slab concrete: $V_{s,BF} = \frac{R_H \cdot (h_s - d') \cdot \left(d_c - \frac{h_s}{3}\right) + \frac{f_{ct,s}}{6} \cdot b_{eff,EC2} \cdot h_s^2 \cdot (d_c - d')}{a \cdot \left(d_c - \frac{h_s}{3}\right) - s \cdot (d_c - d')}$	(7)
$V_{s,SF}$	$N_s = \frac{V_{s,SF} \cdot a - R_H \cdot (h_s - d')}{d_c - d'}$	(8)
	$\sigma_x = -\frac{N_s}{b_{eff,s} \cdot h_s}$	(9)
	$\sigma_1 = \frac{\sigma_x}{2} + \sqrt{\left(\frac{\sigma_x}{2}\right)^2 + \tau^2} \le f_{ct,s}$	(10)
	$\sigma_2 = \frac{\sigma_x}{2} - \sqrt{\left(\frac{\sigma_x}{2}\right)^2 + \tau^2} \ge -f_{c,s}$	(11)
	$\sigma_1 = \lvert f_{ct,s} \rvert + 0.8 \frac{\lvert f_{ct,s} \rvert}{\lvert f_{c,s} \rvert} \sigma_2$; where τ is solved by substituting (10) and (11) in (12)	(12)
	$V_{s,SF} = 2/3 \cdot \tau \cdot b_{eff} \cdot h_s$	(13)

Notation:
ν is a strength reduction factor for concrete cracked in shear, calculated as $\nu = 0.6[1\text{-}f_{c,b}/250]$.
$f_{c,b}$ is the beam's concrete compressive strength.
$f_{c,s}$ is the slab's concrete compressive strength.
ϱ_w is the shear reinforcement ratio.
f_{yw} is yield strength of transverse reinforcement.
c and μ are factors which depend on the interface roughness.
f_{ct} is the tensile strength of concrete.
f_c is the minimum of the beam and slab concrete compressive strengths.
T_w is the tension force of web reinforcement when it reaches its yield strength, calculated as $T_w = A_{sw} \cdot f_{yw}$.
d_b is the precast beam's effective depth.
s is the stirrup spacing.

a is the length of the shear span.
h_s is the flange depth.
d' is the slab longitudinal reinforcement depth.
d_c is the entire composite beam's effective depth.
$f_{ct,s}$ is the tensile strength of slab concrete.
$b_{eff,EC2}$ is the slab effective width, which is taken as the effective flange width defined in Section 5.3.2.1 of EC2.
$b_{eff,s}$ is the effective shear width of the slab, equal to the sum of the web width and the flange depth in this model.

Given the accurate results and the characteristics of the database, it can be stated that the proposed formulation was verified for composite rectangular and T-shaped specimens and monolithic T- and I-shaped specimens made of reinforced concrete with web reinforcement, with concrete compressive strengths up to 60 MPa, h_s/h ratios below 0.30, in which the stirrups steel yields or is close to yielding.

Not only the model gave very good results, but also showed that with only one parameter (the multiplier α) the model could be better adjusted to the experimental results. This points out the model captures well the influence of the parameters. Notwithstanding, the model has a main weakness: the estimation of the interface shear strength, since it is an important aspect of the proposed model. There are multiple proposals in the literature for modifying the current codes interface shear formulations [10]. However, the current codes remain conservative since interface shear depends on many different variables. The study of the interface shear was not part of this research project, but the authors consider the accuracy of the proposed model may be improved in the future with a deeper interface shear study.

Moreover, the mechanical model proposed in this thesis is still in a basic stage and needs to be improved for its application in a wider range of specimen characteristics: dimensions, load states, reinforcements, geometries, etc. Nevertheless, the progress made is considered to be in accordance with the experimental results obtained and lays the foundations for future improvement.

3. Numerical model

In Chapter 6, some of the specimens tested in the experimental programme were numerically modelled with the IDEA StatiCa Detail (ISD) software. This chapter described the work developed during a 3-month stay abroad of the doctoral student at ETH Zurich (Switzerland).

Given the short duration of the stay and the complications during the work development, the scope of this phase did not cover the whole set of experimental tests of the thesis. The study could be extended in the future to conclude the

numerical modelling of all the specimens and to reach important conclusions on the modelling of an interface between concretes in the ISD software.

The Compatible Stress Field Method (CSFM) is a simplified non-linear finite element-based continuous stress field analysis procedure that is implemented in the software ISD. First, the assumptions of the CSFM were studied to understand the parameters of the numerical model that should be varied to get the proper modelling. Relevant aspects of the modelling were the material constitutive models, the compression softening law for concrete and the tension stiffening models for the reinforcement (Tension Chord Model (TCM) and Pull-Out Model (POM)).

Once the main assumptions of the CSFM and the ISD were known, the first group of experimental tests was modelled. The objective was to define basic aspects of the numerical modelling of the test specimens. To that aim, the most common structural elements of the test programme -monolithic rectangular beams with web reinforcement- were modelled before modelling more complex elements. The five specimens with cross-section shape B1 were modelled. The main aspects of this modelling to be solved were: the finite element mesh size, the compression softening model and the tension stiffening model.

Multiple finite element mesh sizes were defined: 5, 10, 15, 20, 25, 30 and 35 finite elements per smaller dimension. The ultimate shear loads predicted by those models, the shear-deflection curves, the computational cost and the failure modes, among others, were analysed. The models with a finite element size bigger than the concrete cover gave the best results. The model of 30 finite elements was chosen as the most suitable finite element mesh size for the following models given its accuracy and low computational cost.

Two compression softening models were analysed: the model implemented in ISD and the model of the Modified Compression Field Theory (MCFT) from Vecchio and Collins [11]. The model implemented in the software gave better results and was more compatible with the theoretical basis of the model than the MCFT.

Although the model gave very good estimations of the ultimate shear load for the five specimens, the experimental shear-deflection curves were much more flexible than the predicted curves. To solve this issue, different models of tension stiffening were considered in the tension longitudinal reinforcement and transverse reinforcement. However, the problems with the stiffness of the shear-deflection curve could not be solved, and the best results were given by the default options: TCM in the tension longitudinal reinforcement and POM in the stirrups. Further research should be conducted in the future to find out the way of better adapting the shear-deflection predicted curves to the experimental curves.

With the results derived from the modelling of the monolithic rectangular specimens, the monolithic T-shaped specimens were modelled. In this phase five

specimens with cross-section type C1 and four specimens with cross-section type D1 were analysed. The variable analysed in these specimens was the effective flange width.

Different effective flange widths were analysed. Although the predicted results were very similar, the best approximation was given by considering a flange width of 2/3 the flange depth in the specimens C1 and 8/6 the flange depth in the specimens D1. These flange widths were first estimated in a preliminary calculation of the compressive force transmitted through the flanges with strut-and-tie models (see Chapter 6 for more details). However, considering a flange width of 1/2 the flange depth, which was the effective shear width taken in the proposed mechanical model, gave also good estimations in C1 specimens, although much on the safety side in D1 specimens. In further studies, these flanges widths should be compared to the effective shear widths of the proposed mechanical model to find a general criterion.

The results for the rectangular and T-shaped specimens were compared to find that the model predicted very well the increase in shear strength provided by the flanges.

Finally, a preliminary numerical modelling of the rectangular composite specimens was carried out to find possible solutions for modelling the interface between concretes. The main conclusions of this prior analysis were that the proper way of numerically modelling the interface between concretes requires modifying the compression softening law of the interface concrete layer in the model, and that further research should be conducted to characterise the interface between concretes. This research should gather measurements of the crack openings, of the normal stresses at the interface, etc., to properly define the compression softening law.

Regarding the impact of the numerical modelling on the overall thesis, it should be noted that the numerical models performed on the monolithic T-shaped beams and the composite rectangular beams confirmed the observed shear strength mechanisms and the proposed mechanical model, through the visualisation of the stress fields provided by the software. Also the numerical model confirmed the failure mode of the specimens was related to the slab.

As explained above, a future line of research would be to conclude the numerical modelling of the test specimens by defining a suitable compression softening law to represent the weakness of the interface between concretes.

4. References

[1] Kim C-G, Park H-G, Hong G-H, Kang S-M. Shear strength of composite beams with dual concrete strengths. ACI Struct J 2016;113:263–74.

[2] CEN. EN 1992-1-1:2004. Eurocode 2: Design of concrete structures - Part 1-1: General rules and rules for buildings. 2004.

[3] CEN. prEN 1992-1-1-D7:2020 Eurocode 2: Design of Concrete Structures – Part 1-1: General rules – Rules for buildings, bridges and civil engineering structures. 2020.

[4] Fédération International du Béton (fib). Model Code 2010. Ernst & Sohn; 2012.

[5] ACI Committee 318. Building code requirements for structural concrete (ACI 318-19); and commentary (ACI 318R-19). Farmington Hills: American Concrete Institute; 2019.

[6] Runzell B, Shield C, French C. Shear Capacity of Prestressed Concrete Beams. 2007.

[7] Avendaño AR, Bayrak O. Shear strength and behaviour of prestressed concrete beams. Technical Report: IAC-88-5DD1A003-3, Texas Department of Transportation: 2008.

[8] Rueda-García L, Bonet Senach JL, Miguel Sosa PF, Fernández Prada MÁ. Analysis of the shear strength mechanism of slender precast concrete beams with cast-in-place slab and web reinforcement. Eng Struct 2021;246:113043. https://doi.org/10.1016/j.engstruct.2021.113043.

[9] Soltani M, Ross BE. Database evaluation of interface shear transfer in reinforced concrete members. ACI Mater J 2017;114:383–94. https://doi.org/10.14359/51689249.

[10] Duarte dos Santos PM. Assessment of the Shear Strength between Concrete Layers. 2009.

[11] Vecchio FJ, Collins MP. Modified Compression Field Theory for Reinforced Concrete Elements Subjected to Shear. J Am Concr Inst 1986;83:219–31.

Chapter 8. Conclusions and future work

The main conclusions of the doctoral thesis are listed in this chapter. In addition, recommendations for future research based on the limitations found during this research are given.

1. Conclusions

The work shown in the different chapters of the thesis was summarised in the "General discussion of the results" presented in Chapter 7. The main results of the experimental programme, the mechanical model and the numerical model were presented and discussed. In this section, the main conclusions derived from that discussion are listed.

From the experimental study for the characterisation of the interface between concretes the main finding was:

- The codes highly underestimate the interface shear strength of "smooth" and "very rough" interfaces. Therefore, the required interface reinforcement to prevent horizontal shear failure is overestimated. This was also experimentally proven in the rest of specimens tested during the research.

From the concrete composite specimens without web reinforcement:

- If the specimens are designed to avoid the horizontal shear failure as well as a monolithic behaviour, the interface will modify the direction of the diagonal shear crack by forcing the crack to propagate along this weakness plane. In T-shaped specimens, not only is the interface between concretes a weakness plane that deviates the trajectory of the diagonal crack but also the cross-section width change plane.
- The shear strength is reached when the critical shear crack forms. Afterwards, a higher shear strength can be reached if the critical shear crack leaves a wide enough depth of the compression chord intact to develop the arching action mechanism.
- As long as the interface shear strength is verified, the cast-in-place concrete slab increases the element's shear strength compared to the shear strength of only the beam, as the slab adds depth to the shear area. The contribution of the slab to the shear strength when the interface shear strength is not enough was not experimentally quantified, since none of the tests performed failed in horizontal shear.
- The interface between concretes had little influence on the shear strength of the composite specimens compared to monolithic specimens.
- The shear strength is governed by the shear transfer actions that occur at the beam's web, while the arching action mechanism strength depends on the strength of the slab concrete. This was deduced from the results of the rectangular and T-shaped specimens, that showed similar shear's first local maximums, and from comparing the specimens fabricated with normal-strength and high-strength concrete at the beam.

- Differential shrinkage did not have a significant influence on the vertical shear capacity of the composite beams of this experimental programme. This proves the validity of the experimental tests conducted, so the results obtained in this test programme can be reference for further studies in this topic that analyse real concrete composite beams, in which normally the time elapsed between the precast beam fabrication and the cast-in-place concrete pouring is greater than 24 hours.
- The existing shear formulations for beams without shear reinforcement are more accurate when assessing the shear strength of the monolithic specimens than the composite specimens. Therefore, the need to incorporate a calculation methodology into design codes that adapts to composite concrete elements without web reinforcement is found.
- The formulations show greater dispersion for the composite specimens made of different compressive strength concretes than for those made with equal compressive strength concretes. Thus, the formulations are not able to capture the effect of the beam concrete compressive strength on the shear strength of the elements.
- For the monolithic beams of this experimental programme, EC2 provides unsafe estimations of the shear strength.
- In the composite specimens, when the entire composite effective depth is considered, EC2 provides unsafe estimations. The other codes (EC2, EC2-20 D7, MC-10 and ACI 318-19) give in general safe estimations. The best method for predicting the shear strength of composite beams without web reinforcement is the formulation of EC2-20 D7 with the entire composite beam's effective depth and the weighted average of the compressive strengths of the beam and slab concretes.

From the concrete composite specimens with web reinforcement:

- In monolithic T-beams the cross-section width change plane is a weakness plane that modifies the trajectory of the diagonal cracks by forcing them to propagate along it.
- If the specimens are designed to avoid the horizontal shear failure as well as a monolithic behaviour, the interface between concretes modifies the crack pattern of the composite beams *versus* that of monolithic beams by forcing diagonal cracks to develop along the interface. Since the crack pattern of the specimens is modified by this horizontal crack, the shear strength mechanisms also change.
- When cracks develop at the interface between concretes in composite beams or at the cross-section width change plane in monolithic T-beams, shear is transmitted through two load paths: one through the precast beam; one through the cast-in-place slab. Consequently, the total shear resisted by the

composite beam has two components: the shear resisted by the precast beam and the shear resisted by the cast-in-place slab. The transmission of horizontal forces between both load paths occurs through the interface crack due to the aggregate interlock at the crack and the dowel action of the transverse reinforcement crossing the crack.

- The shear transmission through the precast beam may be limited by the yielding of the stirrups. The maximum shear resisted by the precast beam is reached before slab failure and it remains constant for increasing loads until the slab fails. Thus, the specimen's shear strength is reached when the slab fails. Three failure modes can occur in the slab or at the interface: slab bending failure due to the yielding of the slab longitudinal reinforcement (BF); slab shear failure when slab concrete stresses reach the Kupfer's failure surface (SF); interface failure when the interface shear strength is reached (IF).
- Placing a cast-in-place slab on top of the precast beam increases the element's shear strength as long as the interface shear strength is verified.
- In general, the presence of an interface between concretes decreases the specimens' shear strength, since the greater interface cracking results in less resistant failure mechanisms, such as slab bending failure in the beams with extended interface cracking.
- In the specimens with slab shear failure, the presence of flanges increases shear strength. In this research work specimens, the shear strength increased in the same proportion as the shear-effective area increases when considering an effective slab width that equals the sum of the web width and flange depth.
- The specimens with extended interface cracking usually show slab bending failure, and flanges do not increase shear strength.
- The shear strength of the rectangular and T-shaped specimens that presented an extended interface cracking did not depend on the compressive strength of either the beam or slab's concrete, since, according to the shear strength mechanism, their shear strength was mainly given by the yielding of the slab's longitudinal reinforcement. The shear strength of the specimens in which interface cracking was short depended on the compressive strength of the slab's concrete, since the shear strength was given by the slab failing in shear.
- In the T-beams with cast-in-place slab on top, the use of high-strength concrete at the precast beam increased the shear strength. This could be due to the higher inclination of the compression struts at the beam web given by the better-quality concrete. The better concrete also could decrease the interface shear stresses due to the higher location of the neutral axis, which postponed the failure.
- The same as in beams without web reinforcement, a marked differential shrinkage between concretes did not significantly modify the shear strength

of the composite beams in this experimental programme in relation to that of those specimens with reduced differential shrinkage.

- The formulation of EC2 provides the best estimation of shear strength for monolithic specimens. EC2, the level III approximation of MC-10 and equation (b) of ACI 318-19, using the weighted average of the beam and slab's concrete compressive strengths, offer the best estimations for composite specimens. However, the current codes are still very safe since the interface shear strength is underestimated and do not account for the flanges effect on shear strength in the T-shaped specimens.
- As a recommendation for practice, the improvement of the interface shear strength of composite beams is suggested for increasing their shear strength. This will derive in the specimen having a slab shear failure. In this case, the slab width and the slab's concrete strength could be increased with the same purpose.

From the proposed mechanical model:

- The shear strength of concrete composite specimens with rectangular or T-shaped cross-section and monolithic T-shaped specimens can be predicted with the proposed lower-bound plasticity-based model. The proposed model has a general and easy-to-use formulation based on a mechanical approach.
- The shear strength of the beam is given by the sum of the shear strengths of the two transmission paths in which the interface crack divides the shear load: the shear strength of the precast beam or the web below the section width change, and the shear strength of the slab or the beam head.
- The shear transmission through the precast beam can be modelled using a double truss strut-and-tie model in which the failure criterion is the yielding of stirrups. The shear transmission through the cast-in-place slab can be modelled by a simple truss strut-and-tie model without shear reinforcement in which two possible failures can occur: the slab bending failure due to the yielding of the slab longitudinal reinforcement or the slab shear failure when its concrete stresses reach the Kupfer's failure surface.
- The interface in composite beams or the plane in which section width changes in T-shaped beams is a weakness plane that limits the shear strength of the element. The proposed simplified model for predicting the shear strength of these elements includes the interface shear strength of the weakness plane in its formulation, which is a novel element.
- The interface shear strength or the maximum concrete stress in the compression field may limit the shear strength of the precast beam. The maximum shear load is given by the slab failure. The model can distinguish different types of slab failures. When interface shear limits the shear strength of the precast beam, interface cracking is likely, so that the slab strength is

given by the minimum of the shear forces resisted by the slab failing in bending and the slab failing in shear. Otherwise, the slab is considered to fail in shear in T-shaped beams or the specimen is treated as a monolithic specimen in composite rectangular beams.

- The model uses the interface shear formulation of a current code (EC2) to estimate the interface shear strength. The safe prediction of the interface shear strength given by the current codes' formulations have a negative impact in the accuracy of the proposed mechanical model for predicting the vertical shear strength of concrete composite elements.
- The interface shear strength can be adjusted with a multiplier α estimated with a database of 286 interface shear-transfer experiments with different interface roughness. The model can be well adjusted to the experimental results only varying this multiplier.
- The proposed model gives better results than the current design codes (EC2, MC-10 and ACI 318-19) when they are verified in a database of 105 slender reinforced concrete specimens subjected to point loads and failing in shear with web reinforcement (24 composite rectangular specimens, 28 composite T-shaped specimens consisting of a rectangular precast beam with a cast-in-place slab on top and 53 monolithic T- and I-shaped specimens). The mean value and coefficient of variation of the relationship between the experimental and the predicted shear strengths are, respectively, 1.18 and 16%.
- The effective shear width considered in this model for the specimens with flanges, equal to the sum of the web width and the flange depth, proved to derive in very good shear strengths estimations.
- Given the accurate results and the characteristics of the database, it can be stated that the proposed formulation was verified for composite rectangular and T-shaped specimens and monolithic T- and I-shaped specimens made of reinforced concrete with web reinforcement, with concrete compressive strengths up to 60 MPa, h_s/h ratios below 0.30, in which the stirrups steel yields or is close to yielding.

From the numerical model developed in IDEA StatiCa Detail:

- The modelling using the default settings for the material constitutive laws, the compression softening model for concrete and the tension stiffening in the reinforcement (Pull-Out Model in the stirrups and Tension Chord Model in the tension longitudinal reinforcement) gave the best results when using a finite element size for concrete bigger than the concrete cover thickness.
- One of the steps for modelling the interface between concretes with IDEA StatiCa Detail consists of modifying the compression softening law of the interface concrete layer.

- The stress fields and failure modes obtained with the numerical models confirm the observed shear strength mechanisms and the proposed mechanical model. The effective flange width considered in the mechanical model is also verified by means of the numerical model.

2. Recommendations for future research

Some limitations and problems were found during this research that show possible future research lines in the field of concrete composite structural elements. Some of these lines were pointed out in Chapter 7. "General discussion of the results" as these limitations were found. The recommendations for future research that are considered most remarkable are:

- In this thesis an extensive experimental study has been carried out. However, many parameters were fixed for all the specimens, such as the tension longitudinal reinforcement ratio, the transverse reinforcement ratio or the shear span-to-depth ratio. Consequently, experimental and numerical studies on composite beams with other dimensions and reinforcement ratios should be carried out to confirm the conclusions reached in this research.
- It has been shown that the interface shear strength is key in the shear strength of composite specimens. Therefore, it would be necessary to carry out an exhaustive study of the interface shear by searching existing experimental tests, of which there are extensive databases, and creating new experimental programmes, in order to define a more accurate interface shear equation than the existing ones.
- In the specimens without web reinforcement, no behaviour pattern was observed on the degradation level of the compression chord after the critical shear crack formation that allowed knowing prior to testing when the arching action mechanism was going to develop. Thus, it was not possible to know in advance if an over-strength would take place after the critical shear crack formation. In addition, the high tension longitudinal reinforcement ratio of the test specimens could influence this behaviour. Thus, testing beams with other reinforcement ratios and dimensions would be necessary to clarify this issue.
- In the specimens with web reinforcement, by comparing the results of rectangular and T-shaped beams and those of T-beams with slab, certain differences were observed in how the use of concrete of different qualities in the precast beam influences the shear strength, so that a general theory of its influence on the shear strength was not found. A larger number of tests should therefore be carried out focusing on the study of this variable in order to clarify this issue.

- Although the proposed model was verified in a database of experimental results, the number of existing tests in composite specimens is still very limited. Thus, further research should be conducted on beams with web reinforcement and with different dimensions and reinforcement ratios to delve in this study and extend the scope of application of the proposed mechanical model.
- Given the lack of information in the current design codes on the shear treatment of composite structural elements and the large number of existing structures of this type, a revision of the codes should be carried out to include in their formulation how these elements should be calculated.
- An in-depth study for the characterisation of the interface between concretes, with measurements of the crack openings, the normal stresses at the interface, etc., should be carried out to properly define the compression softening law for numerically modelling the interface concrete in the composite specimens.
- The main research line that would continue this thesis research would be the study of composite beams in which the precast beam is prestressed. This would be the most similar problem to reality and for which this thesis would be a basis.